HARD CONVEX BODY FLUIDS

M. P. ALLEN

H. H. Wills Physics Laboratory,
Tyndall Avenue Bristol BS8 1TL, UK

G. T. EVANS

Department of Chemistry, Oregon State University,
Corvallis OR 97331 USA

D. FRENKEL, B. M. MULDER

F.O.M. Institute for Atomic and Molecular Physics,
Kruislaan 407, 1098 SJ Amsterdam, The Netherlands

CONTENTS

Advances in Chemical Physics, Volume LXXXVI, Edited by I. Prigogine and Stuart A. Rice.
ISBN 0-471-59845-3

I. INTRODUCTION

The basis of our theoretical understanding of statistical mechanics of dilute gases dates back to the nineteenth century. The atomistic description of crystalline solids originated in the first half of the twentieth century. But the theoretical description of simple liquids in the framework of statistical

mechanics is of a much more recent origin. A possible reason for the slow development of a molecular theory of liquids is the following. The theory of dilute gases could be developed starting from the *ideal gas*, the properties of which could be evaluated analytically. Similarly, the theory of solids could be constructed starting from the *harmonic crystal*. But, for liquids, there is no corresponding *ideal liquid* model that can be solved exactly. As a consequence, much of the progress in the construction of a molecular theory of liquids had to await the advent of electronic computers that could generate essentially exact results for simple model liquids. During the past four decades, the numerical data on the hard-sphere fluid have provided us with a substitute for exact results on the *ideal liquid*. Much of the subsequent development of the theory of liquids, as described for instance in the book by Hansen and McDonald, [1] relies heavily on the insight gained from the numerical study of hard-sphere fluids.

The hard-sphere model is, however, not a good reference system for the description of molecular fluids consisting of nonspherical particles. This is particularly clear if one considers the possible phases of such molecular systems. Whereas hard spheres can only form an (isotropic) liquid phase and a crystalline solid phase, there are many nonspherical molecules in nature that can form so-called liquid crystalline phases, that is, phases that have a degree of order that is intermediate between the isotropic fluid and the crystalline solid (see, e.g., Ref. [2]). In fact, several dozens of distinct liquid-crystalline phases have been observed expereimentally. However, in the present review, we focus on the main classes of liquid crystals, i.e. the *nematic* phase, the *smectic-A* phase, the *columnar* phase and the *cholesteric* phase. Schematic drawings of the orientational and translational order characteristic of these phases are shown in Fig 1.1.

In order to extend the theory of simple atomic liquids to the more complex molecular liquids and, a fortiori, to liquid crystals, there is much need for 'exact' results on simple molecular reference fluids. Surprisingly, although there exists no exactly solvable model for atomic liquids, there does, in fact, exist an exactly solvable model for a (nematic) liquid crystal, viz. the Onsager model. [3] In the Onsager model, the liquid-crystal forming molecules are assumed to be infinitely thin, hard spherocylinders. The problem with the Onsager model is that, whereas many simple liquids are, to a first approximation, well described as an assembly of hard spheres, there are only a few liquid-crystal forming molecules with very long, thin hard rods. Once we try to extend our theoretical description of liquid-crystal forming fluids to molecules with less extreme shapes or, for that matter, to liquid-crystalline phases other than the nematic phase, we are again in need of numerical data on molecular "reference fluids" as a substitute for exact results.

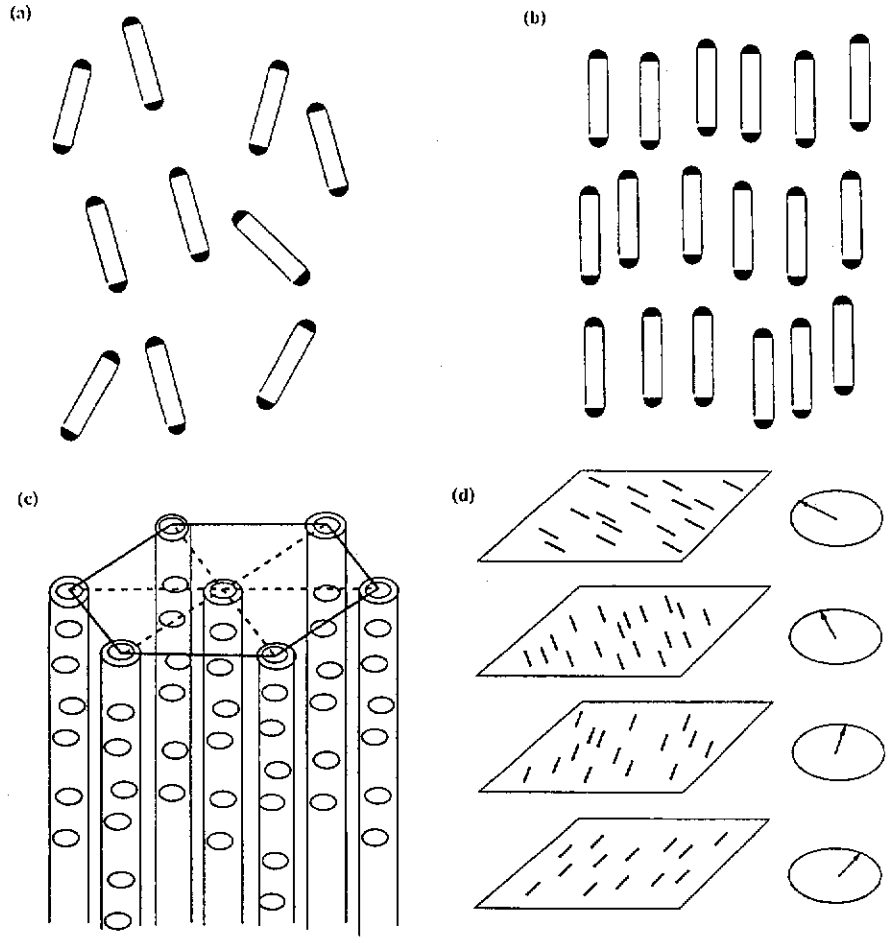

Figure 1.1. Snapshots of a typical molecular arrangement in the nematic (a), smectic-A (b), columnar (c) and cholesteric (d) phase.

Unfortunately, the choice of the appropriate molecular reference fluid is not unique. Even if we restrict our attention to rigid, nonspherical molecules, there are clearly many model systems that could be selected. However, our reference models should satisfy two important criteria: first, they should be sufficiently nontrivial to reproduce the most important classes of liquid crystals known to date, yet they should be sufficiently simple to ensure that they can be easily studied, both theoretically and numerically.

In this review, we discuss in considerable detail a particular class of

molecular "reference" systems that meet these criteria, namely *convex, hard-body fluids*. A body is convex if any line-segment connecting two points on the surface of that body is completely contained within that body. During the past decade there has been much progress both in the theoretical description and the numerical simulation of convex hard-body fluids. It is not our aim to give an exhaustive review of progress in this field of research. Rather, we wish to present a coherent overview of the theoretical and numerical techniques that are most widely used in this area of research. The choice of specific examples is, to a large extent, dictated by our own bias. Yet, we have tried as much as possible to refer to related work by other authors. We realize, however, that our review of the relevant literature will contain serious gaps and omissions. We apologize to all those whose contributions we have discussed either inadequately, or not at all.

The material presented in this review is organized in a way that emphasizes the complementary character of theory and simulation. This implies that on every topic we first have a section that discusses the relevant theory and then a section that deals with the appropriate simulation techniques. The latter section will typically contain a few numerical results that are of special interest in the context of the preceding discussion. In this way, we discuss first the static and dynamic properties of hard-core fluids in the isotropic phase, next phase transitions to (liquid)-crystalline phases, and finally some static and transport properties of the nematic liquid-crystalline phase. We do not discuss the dynamical properties of liquid-crystalline phases other than nematic, in view of the paucity of numerical data on such systems.

In this introduction, we give a brief preview of things to come, and explain the philosophy underlying much of the work presented in subsequent sections. For the benefit of the reader who is unfamiliar with computer simulations, we present a brief description of the role of numerical simulation in the study of liquids and liquid crystals. Next, we briefly preview the kind of hard-particle models that we are going to consider, the numerical techniques needed to study such systems, and the theories that are used to describe them.

A. Simulations

Computer simulations sit midway between experimental measurements and theories of condensed matter. Typically, the aim of a theory is to predict the properties of a system in terms of the interactions between molecules. However, these molecular interactions are themselves known only imperfectly, and must be modelled in some way. To test the accuracy of the molecular models separately from that of the theories, it is necessary

to obtain reliable "experimental" information about the models. This is accomplished using computer simulation. In recent years, progress has been made using both accurate, "realistic" models of specific molecular systems, and idealized models of wide applicability. In this review, we discuss recent work using models that fall into the latter category.

1. Simulation Strategies

The aim of a computer simulation of a (classical) many-body system is to compute "exactly" the static and dynamic equilibrium properties of the model system. In this context, "exactly" means "to any desired accuracy". There are two distinct factors that limit the accuracy of a simulation. First, simulations of models for bulk liquids or solids are usually performed on rather small systems ($\mathcal{O}(10^2$–$10^3)$ particles). Even though periodic boundary conditions are usually employed to minimize finite size effects, the properties of such relatively small systems do differ systematically from those of a truly macroscopic sample. In addition to this systematic error introduced in the numerical simulation, we are also faced with statistical fluctuations in the results of our numerical "measurements". In principle, the errors due to finite size effects can be suppressed by going to very large systems, while the statistical fluctuations can be suppressed by performing very long simulations. Clearly, if one is interested in the properties of a "family" of model systems over a wide range of densities, one should not invest all available computing time in one long simulation of one large system. It is even less advisable to plan short simulations of a very large system, in which case the statistical errors would be very much larger than the systematic errors. In general, one should select the model, the system size and the length of the simulations such that a reasonably complete set of simulations of acceptable accuracy can be performed within the available computing budget. In its generality, the preceding statement is vague to the extent of being almost meaningless. However, in the context of simulations of nonspherical, liquid-crystal forming molecules, we can be more precise. Typically, in order to map a phase diagram, one should study the equation of state of several model systems that belong to the same family. In addition, one or more free energy calculation may be required for every model system. As a result, one should expect to perform some 50 runs per model system. For a determination of a complete phase diagram, several hundred simulations will be required. Clearly, with this number of simulations, it is imperative that the individual simulations are "cheap". Again, "cheap" can only be used in the relative sense that any individual run should not consume more than, say, 1% of the available computing budget. As the power of computers continues to grow, much of what is not feasible today will most likely be feasible in a few years time. Yet, it is

fair to say that during the period covered by this review, systematic studies of the phase diagram were necessarily limited to rather simple model systems. We should stress, however, that most of the numerical techniques discussed below can be applied to more complex model systems.

B. Hard Particles

Since the 1950s, when computer simulation showed that the hard-sphere model provided a firm base for the study of the statistical mechanics of simple atomic liquids, [4,1], interest has steadily grown in the application of similar techniques to molecular fluids. The wealth of fluid phases found in nature has stimulated attempts to relate phase stability and properties to simple aspects of molecules and their interactions, beginning with elementary considerations of molecular size and shape. It has been known since the time of Onsager [3] that hard nonspherical particles can form an oriented fluid phase if the isotropic liquid is compressed, and that for sufficient elongation, this transition will occur before the system freezes. It is therefore surprising that significant progress in computer simulations of these phases has only been made in the last decade (although serious attempts have been made since the early 1970s [5,6]). The spherocylinder (see Fig. 1.2.a) was probably the first nonspherical hard shape to attract significant interest. This is a cylinder of length L, diameter D, with hemispherical caps of diameter D at each end. As we shall see, this model exhibits an isotropic fluid phase and a solid; for suitable values of L/D nematic and smectic-A liquid crystals can be seen.

A second shape of interest is the spheroid, with perpendicular semi-axes a, b and c. Most intensively studied have been hard ellipsoids of revolution, for which two of the axes are equal, but different in general from the third: $a \neq b = c$. This system forms isotropic fluid and fully ordered solid phases, and, for suitable values of the elongation $e = a/b$, also shows a nematic liquid crystal. Both rod-like (prolate, $e > 1$ see Fig. 1.2.b) and disk-like (oblate, $e < 1$ see Fig. 1.2.c) shapes are possible, and the nematic phases correspond to alignment of the long or short symmetry axes, respectively. An additional, biaxial phase may be exhibited by molecules having unequal axes $a \neq b \neq c$, thus being intermediate in shape between rods and disks.

Different oblate, or tablet-like, shapes can be obtained by slicing the top and bottom off a sphere using two parallel cuts. These "truncated sphere" (see Fig. 1.2.d) shapes may form nematic phases, and additionally can line up to give columnar phases. A further phase having cubic orientational symmetry has also been observed for these shapes. The relation between this "cubatic" phase and the cubatic phases that have been observed experimentally [7] is at this stage uncertain.

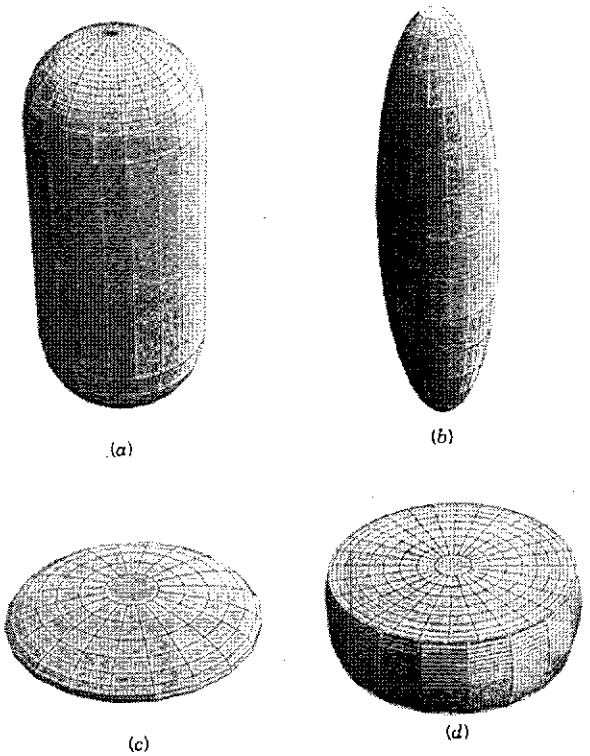

Figure 1.2. A few well-known hard convex bodies: (a) spherocylinder; (b) prolate ellipsoid of revolution; (c) oblate ellipsoid of revolution; (d) truncated sphere

C. Simulation Methods

Two classes of simulation are in common use: Monte Carlo and molecular dynamics.

In hard-particle Monte Carlo, trial moves are selected using a random number generator, accepted if they do not lead to particle overlap, and rejected if they do. This requires efficient evaluation of a pair overlap function: most usefully a function $F(\mathbf{r}_{ij}, \Omega_i, \Omega_j)$ of the orientations Ω_i and Ω_j and the relative position vector $\mathbf{r}_{ij}$ of a pair of molecules, which takes values $F < 1$ if they overlap, $F > 1$ if they do not, and $F = 1$ at contact. Efficient prescriptions exist [5,6,8,9] to determine F for both spherocylinders and spheroids, and we return to this in Section II.D.1.

The simple prescription of moving particles generates states sampled from the constant NVT ensemble where N is the number of particles, V the sample volume and T the temperature. For particles interacting

via infinite repulsive potentials, the configurational integral and all static configurational properties are independent of the temperature T. Extensions of the sampling prescription can be used to generate states from other ensembles, for example constant NPT, where P, the pressure, is prescribed. Again, in the special case of hard particles, configurational properties depend on the ratio P/T rather than on P and T separately.

In hard-particle molecular dynamics, Newton's equations are solved; the aim is to locate the next time of collision between a pair of particles. Between collisions, the configuration is advanced using free flight dynamics; each molecule moves with constant linear and angular momenta. At the point of collision, impulsive forces determined by the conservation laws and the contact condition (i.e., whether the colliding surfaces are rough or smooth) determine the postcollisional momenta. Both free flight and collision dynamics also depend on the choice of molecular masses and moments of inertia. The technique requires efficient evaluation of the pair overlap function F and its time derivative $\dot{F}$, so as to locate the exact time of collision by standard root-finding methods. Typically the constant NVE ensemble is probed, where E is the energy. For hard particles, kinetic energy and total energy are the same, and *static* configurational properties are independent of E. They also do not depend on the chosen mass and moment-of-inertia distribution. The *dynamical* properties, however, do depend on these values; the masses, moments of inertia and total energy determine translational and rotational time scales. It is possible to adapt the molecular dynamics algorithm to probe other ensembles. Intermittent velocity randomization can be included to give constant NVT sampling. A constant pressure form of dynamics has been described for hard particles [10] but a simpler procedure for sampling the constant NPT ensemble is to carry out intermittent volume changes according to the standard Monte Carlo prescription, in between periods of normal dynamics.

Further details of simulation techniques may be found elsewhere. [4,11] In all simulations of bulk phases, periodic boundary conditions are used to eliminate the effects of surfaces. There have been few systematic studies of the effects of periodic box size and shape on the stability and properties of phases, and this is of some concern when simulating systems that exhibit long-range correlations. The general rule seems to be to choose a box as large as possible, given the constraints of limited computer time, and for translationally disordered fluid phases to adopt one of the more nearly spherical geometries: truncated octahedral or rhombic dodecahedral shapes. For solids, or smectic liquid crystals, this may not be appropriate, and cuboidal boxes may be more suitable. In the simulations reported here, both cuboidal and truncated octahedral periodic boundary conditions have been employed. Typical system sizes are in the range

N =100–1000. In molecular dynamics simulations, typical production run lengths are $(0.5–1.6)\times10^6$ collisions in total, depending on density; this corresponds to run times $t_{run} \sim 2000–15,000t_c$, where t_c is the mean time between collisions per molecule. In Monte Carlo work, run lengths are of the order of $10^4–10^6$ moves per particle. These parameters are modest by today's standards; a typical run at one state point might take a few hours on a fast desktop workstation, or a few minutes on a supercomputer.

D. Theories

With such simple models, we are clearly going to be interested in comparing with theoretical predictions rather than experiment. Two major classes of theory are especially powerful when applied to hard-particle systems. Kinetic theories make specific predictions for transport coefficients and other dynamical properties in terms of collisional averages. Density functional theories, of which the approaches of van der Waals and Onsager may be considered special cases, are used to predict phase stability and properties, given an approximation scheme for the direct correlation function. Both methods have been extensively tested on the hard-sphere fluid, and their advantages and limitations in this area are well known. Their extension to nonspherical systems, however, has been very limited. In the following sections we attempt to give a perspective view of these theories, and the role of simulation in testing them out.

PART ONE: THE ISOTROPIC PHASE

II. STATIC PROPERTIES

A. Static Properties in the Isotropic Phase

Convexity is the central characteristic that makes hard convex body (HCB) fluids amenable to analysis. It is this property that allows a unique determination of the distance between two such particles. This in turn enables a relative simple description of the hard-core interactions in such systems. The simplest example of a HCB is of course the hard sphere and it should come as no surprise that most calculations of equilibrium thermodynamic properties of HCB systems such as free energies and pressures rest on the foundation provided by earlier analyses of hard spheres. [12] There are, however, features in the HCB systems that have no analog in hard-sphere (HS) systems and these pertain to the orientational degrees of freedom and their canonical momenta. Having said this, it should come as no sur-

prise that most of the successes in the analysis of fluids of HCBs have been obtained in studies of those properties that have a hard-sphere counterpart, such as pressure, chemical potential or the isotropic part of the pair correlation function at contact. Furthermore, most of the stumbling blocks have arisen in the calculation of properties that depend explicitly on the mutual orientation of HCBs, such as pair and direct correlation functions and structure factors. In this section, we summarize some of the progress made in the analysis of scalar properties (pressures, chemical potentials) and vector properties (orientational pair and direct correlation functions) in the theory of isotropic fluids of HCBs.

B. Theory

1. The System

We consider a system consisting of N HCBs in a container of volume V (at a number density $\rho = N/V$) and at a temperature T. The ith particle in the system has a mass m, a center of mass position vector, $\mathbf{r}_i$, a moment of inertia I, an orientation vector $\hat{\mathbf{u}}_i$ (for unaxial rotors) and Euler angles Ω_i (for biaxial or asymmetric tops), a center-of-mass velocity $\mathbf{v}_i$, linear momentum $\mathbf{p}_i$, angular velocity ω_i and angular momentum $\mathbf{L}_i$. Using conventional notation, one obtains a Helmholtz free energy

$$F_N(V,T) = -k_B T \ln Q_N(V,T) \tag{2.1}$$

with $Q_N(V,T)$ the canonical partition function

$$Q_N(V,T) = (N!)^{-1} \int d1 d2 \ldots dN \exp(-\beta \mathcal{H}) \tag{2.2}$$

and $\mathcal{H}$ the system Hamiltonian

$$\mathcal{H} = \sum_i \frac{1}{2}[m\mathbf{v}_i^2 + I\omega_i^2] + \sum_{i>j} U(\mathbf{r}_{ij}, \Omega_i, \Omega_j) \tag{2.3}$$

Here $\mathbf{r}_{ij}$ denotes the vector emanating from the mass center of particle i and extending to the mass center of particle j

$$\mathbf{r}_{ij} = \mathbf{r}_j - \mathbf{r}_i \tag{2.4}$$

The phase space volume di is taken to be

$$di = d\mathbf{r}_i \, d\mathbf{p}_i \, d\Omega_i \, d\mathbf{L}_i \tag{2.5}$$

and spans the translational and rotational degrees of freedom.

The hard-body potential energy $U(\mathbf{r}_{ij}, \Omega_i, \Omega_j)$ is given by

$$U(\mathbf{r_{ij}}, \Omega_i, \Omega_j) = \begin{cases} \infty, & \text{if } \mathbf{r}_{ij} \in V_{ex}(\Omega_i, \Omega_j) \\ 0, & \text{otherwise} \end{cases} \tag{2.6}$$

where $V_{ex}(\Omega_i, \Omega_j)$ is the volume excluded to particle i because of particle j (and vice versa).

Classical dynamics described by Eqs. (2.3) and (2.6) allow the particles to move freely subject to the constraint that particle overlap is forbidden. Since the Hamiltonian is separable into position and momentum components and the momentum is described by a homogeneous quadratic form, then $Q_N(T, V)$ reduces to

$$Q_N(V, T) = Z_N(T, V)[\mathcal{V}_T]^{-N}/N! \tag{2.7}$$

where $\mathcal{V}_T$ is the de Broglie volume as discussed in Appendix A.A, $Z_N(T, V)$ is the configurational integral

$$Z_N(T, V) = \int \prod_i d\mathbf{r}_i \, d\Omega_i \, \exp(-\beta U^N) \tag{2.8}$$

and U^N is the N particle potential energy. The microscopic structure of a fluid and the thermodynamic properties can also be expressed in terms of the pair correlation function (pcf), $g(1,2)$,

$$g(1,2) = V^2 \int d\mathbf{r}_3 \, d\Omega_3 \ldots d\mathbf{r}_N \, d\Omega_N \, \exp(-\beta U^N)/Z_N(T, V) \tag{2.9}$$

where 1 and 2 as arguments of $g(1,2)$ now pertain to the positional coordinates.

C. Thermodynamic Properties

The thermodynamic properties which characterize the HCB system are the internal energy ($E = (\frac{1}{2})Nk_BT(3 + r)$, for a system with r rotational degrees of freedom), the pressure P and the chemical potential μ . The derivation of the pressure and the chemical potential from the canonical ensemble is standard [13] and we merely present the results with a few words of clarification. The pressure can be given in a virial form

$$\beta P = \rho + (3V)^{-1} \sum_{i>j} \langle \mathbf{r}_{ij} \cdot \mathbf{F}_{ij} \rangle \tag{2.10}$$

where $\mathbf{F}_{ij}$ is the force on particle i due to particle j. For a system comprised of hard smooth particles, the force can be replaced by [14]

$$\beta \mathbf{F}_{12} = \hat{\mathbf{s}} \delta(s - 0^+) \tag{2.11}$$

where $\hat{\mathbf{s}}$ is the outward surface normal from particle 1 to particle 2 and s is the surface-to-surface separation measured along $\hat{\mathbf{s}}$. Accordingly, Eq (2.10) becomes

$$\beta P = \rho + (1/6)\rho^2 \int d\mathbf{r}_{12}\, d\Omega_1\, d\Omega_2 \mathbf{r}_{12} \cdot \hat{\mathbf{s}} \delta(s - 0^+) g(1,2) \tag{2.12}$$

All of the transport and most of the equilibrium properties to be discussed will involve the pcf at a distance infinitesimally removed (0^+) from the contact surface. We can take advantage of the ubiquitous presence of the contact surface by adopting a convex body coordinate system with coordinates s and $\hat{\mathbf{s}}$ in place of $\mathbf{r}_{12}$ and to this we now turn.

To change coordinates from the vector $\mathbf{r}_{12}$ to the unit vector $\hat{\mathbf{s}}$ and the surface-to-surface separation s, we begin by representing the center-to-center vector by

$$\mathbf{r}_{12}(\hat{\mathbf{s}}, s) = \xi_1(\hat{\mathbf{s}}) - \xi_2(-\hat{\mathbf{s}}) + s\hat{\mathbf{s}} \tag{2.13}$$

where $\xi_1(\hat{\mathbf{s}})$ and $\xi_2(-\hat{\mathbf{s}})$ emanate from the mass center of particles 1 and 2, respectively. The radius vector ξ_j for a general convex body can be written in terms of the support function [15]

$$h_j = \hat{\mathbf{s}} \cdot \xi_j(\hat{\mathbf{s}}) \tag{2.14}$$

and by means of the support function, all the geometric properties of the convex body can be derived (see Appendices A.B, A.C and A.D for details). The geometry of the situation is illustrated in Fig. 2.1

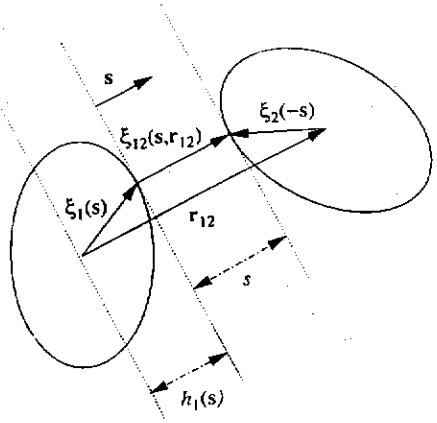

Figure 2.1. The geometry of two convex bodies. The symbols are explained in the text.

The Jacobian for the transformation from $\mathbf{r}_{12}$ to $\hat{\mathbf{s}}$ and s is

$$\begin{aligned} d\mathbf{r}_{12} &= |\,(\partial\mathbf{r}_{12}/\partial s)\cdot(\partial\mathbf{r}_{12}/\partial\theta)\times(\partial r_{12}/\partial\phi)\,|\;ds\,d\theta\,d\phi \\ &= |\,\hat{\mathbf{s}}\cdot(\partial\mathbf{r}_{12}/\partial\theta)\times(\partial\mathbf{r}_{12}/\partial\phi)\,|\;ds\,d\theta\,d\phi \\ &= S^{12}(\mathbf{s},\Omega_1,\Omega_2)\sin\theta\,ds\,d\theta\,d\phi = S^{12}(s,\Omega_1,\Omega_2)\,d\mathbf{s} \end{aligned} \tag{2.15}$$

where θ and ϕ are the polar and azimuthal angles that $\hat{\mathbf{s}}\,(\mathbf{s}=s\hat{\mathbf{s}})$ makes with respect to a fixed but otherwise arbitrary coordinate system. The abbreviated notation $d\mathbf{s}$ denotes $ds\,d\hat{\mathbf{s}}$. Equation (2.15) is a crucial result as it relates the volume element $d\mathbf{r}_{12}$ on a spherical contour to the contours appropriate for a general convex body. If we now return to Eq. (2.12) we can write directly

$$\beta P = \rho + (2\pi/3)\rho^2 \int d\Omega_1\,d\Omega_2 h_{12} G(s=0,\Omega_1,\Omega_2) \tag{2.16}$$

with

$$h_{12} = h_1 + h_2 \tag{2.17}$$

and

$$G(s,\Omega_1,\Omega_2) = S^{12}(s,\Omega_1,\Omega_2)g(s,\Omega_1,\Omega_2) \tag{2.18}$$

An exact expression for the chemical potential of HCBs can be derived by considering the reversible work required to insert a particle in a hard-body fluid [13,16,17] and the result is

$$\beta\mu = \ln\rho\mathcal{V}_T + 4\pi\rho\int_{q_{\min}}^{1} dq\,d\Omega_1\,d\Omega_2 h_1 G_q(s=0,\Omega_1,\Omega_2) \tag{2.19}$$

where $\mathbf{r}_{12}(\hat{\mathbf{s}},s) = q\xi_1(\hat{\mathbf{s}}) - \xi_2(-\hat{\mathbf{s}}) + s\hat{\mathbf{s}}$. Note that G_q depends on the scaling parameter, q, of particle 1 through $g(1,2)$ and S_q^{12}. The lower bound to the scaling variable corresponds to the ratio of axes lengths for the scaled particle: $q_{\min}$ = -long axis/short axis. Both Eqs. (2.16) and (2.19) reduce to the hard- sphere (HS) limit when we take $h_{12} = \sigma$ (the HS diameter) and $S^{12} = \sigma^2$. To proceed further with our analysis of HCBs, we need to be more explicit about the pcf.

1. Relationship of Pair Correlation Functions to Thermodynamic Properties

In 1963, Steele [18] suggested that $g(1,2)$ be expressed as a spherical harmonic expansion

$$g(1,2) = 4\pi\sum_{j,j',m} g_{jj'm}(r)Y_{j,m}(\Omega_1)Y_{j',-m}(\Omega_2) \tag{2.20}$$

where $r = |\mathbf{r}_{12}|$ and with Ω_1,Ω_2 being measured with respect to $\mathbf{r}_{12}$. Equa-

tion (2.20) can also be expressed as an invariant or scalar product of $\mathbf{r}$ and the orientations $\hat{\mathbf{u}}_1$ and $\hat{\mathbf{u}}_2$, as suggested by Blum. [19–21] For hard-body systems, the expansion coefficients $g_{jj'm}(r)$ of Eq. (2.20) have been determined by integral equation methods [22,23] and by computer simulation [24,25–27]. Although the direct approach afforded by Eq. (2.20) has the advantage of clarity, the convergence characteristic are particularly poor [26,28] as the short range correlations are explicit functions of the surface-to-surface separation and not the center-to-center distance. To improve the convergence properties of the expansion of $g(1,2)$, several modifications have been made.

In an application to the Gaussian overlap approximation for hard ellipsoids, Kabadi and Steele [29,30] represented $g(1,2)$ with a distance variable scaled by the orientation dependent ellipsoid diameter. For fluids of hard spherocylinders Kabadi and Steele [31] devised a center-to-center separation coordinate which reflected the mutual orientation of a pair of molecules. Ghazi and Rigby [32] continued this line of inquiry and found that the convergence of the Kabadi expansion for hard spherocylinders was greatly accelerated from that achieved by Eq. (2.20) when another orientation dependent coordinate was used.

For a system comprised of a hard ellipse in a fluid of hard disk, Kumar et al. [33] expanded the ellipse-disk pcf as

$$g(1,2) = \sum_j g_j(s) P_j(\hat{\mathbf{u}} \cdot \hat{\mathbf{s}}) \tag{2.21}$$

where $P_j(\hat{\mathbf{u}} \cdot \hat{\mathbf{s}})$, the Legendre polynomials, were a function of the orientation of ellipse ($\hat{\mathbf{u}}$) with respect to the surface normal ($\hat{\mathbf{s}}$). However, the Legendre polynomials, $P_j(\hat{\mathbf{u}} \cdot \hat{\mathbf{s}})$ were nonorthogonal as the surface integrations were taken over the convex surfaces described by the addition of a disc to an ellipse and the weight function which accompanies this integration was $S^{12}(s, \hat{\mathbf{u}} \cdot \hat{\mathbf{s}})$. When one orthogonalizes the Legendre polynomials with respect to the weight function, one finds that the first anisotropic contribution to $g(1,2)$ vanishes at zero density and is directly proportional to the particle nonsphericity: the desired properties. But the set of orthogonalized polynomials representing $g(1,2)$ depend explicitly on $\hat{\mathbf{s}}$ (since the integrations are taken over nonspherical surfaces whose nonsphericity changes with $\hat{\mathbf{s}}$). The selection of $\hat{\mathbf{s}}$-dependent orthogonal basis functions was a possibility for simple systems such as an infinitely dilute solution of a single HCB, but it is not practical for the case where several orientation angles are required.

To avoid these complications, Kumar et al. [33] and Talbot et al. [34] followed the suggestion of Kabadi and Steele [31] and expressed $S^{12}(s, \Omega_1, \Omega_2)$ $g(1,2)$ (or G of Eq. (2.18)) in a set of spherical harmonics, $Y_{jm}(\Omega)$,

$$G(s,\Omega_1,\Omega_2) = 4\pi \sum_{j,j',m} G_{jj'm}(s) Y_{j,m}(\Omega_1) Y_{j',-m}(\Omega_2) \tag{2.22}$$

For simplicity we have restricted attention to $C_{\infty v}$ molecules (with two rotational degrees of freedom). The orientation angles in Eq. (2.22) are expressed with respect to the surface normal directed along the minimum surface-to-surface separation. A disadvantage of the method of Eq. (2.22) is that G is anisotropic even in the limit of zero density, but to its credit, the expansion functions are the familiar spherical harmonics and are independent of $\hat{\mathbf{s}}$.

The motivation for the orthogonal function expansion of $G(s,\Omega_1,\Omega_2)$ is in part subjective. Both Eqs. (2.16) and (2.19) suggest that to determine structural properties for HCB systems, surface integrals of the pcf are required. But in the case of the pressure, the integral of $\hat{\mathbf{g}}$ is weighted by the excluded volume Jacobian $h_{12}S^{12}$ so that the pressure is related to the excluded volume average of g. This, in turn, suggests that perhaps one should expand $h_{12}G(1,2)$ in spherical harmonics rather than $G(1,2)$ alone. To this we counter that in the theory of transport properties, the prefactor of $h_{12}G(1,2)$ does not generally arise and it is $G(1,2)$ that is common to most transport coefficient integrands. [35] As our concerns are with both thermodynamic and dynamic properties, the expression of the pcf will reflect our subjective choice toward surface area averaging as opposed to volume averaging.

By means of Eq. (2.22) and the remarks of the previous paragraph, one defines the isotropic surface-averaged pcf [33]

$$g_{\mathrm{iso}}(s) = \frac{\int d\Omega_1\, d\Omega_2 G(s,\Omega_1,\Omega_2)}{\int d\Omega_1\, d\Omega_2 S^{12}(s,\Omega_1,\Omega_2)} = \frac{G_{000}(s)}{S^{12}(s)} \tag{2.23}$$

and as a result, one can express any surface average as

$$< B\delta(s-s^*) >= 4\pi \int d\Omega_1\, d\Omega_2 G(s,\Omega_1,\Omega_2) B = 4\pi g_{\mathrm{iso}}(s^*) S^{12}(s^*) < B >_{s^*} \tag{2.24}$$

i.e., the product of the isotropically averaged pcf $g_{\mathrm{iso}}(s^*)$, the isotropically averaged surface area $S^{12}(s^*)$ and a conditional average $< B >_{s^*}$ on the convex surface $s = s^*$, thus,

$$< B >_{s^*} = \frac{\int d\Omega_1\, d\Omega_2 G(s,\Omega_1,\Omega_2) B(s,\Omega_1,\Omega_2)}{\int d\Omega_1\, d\Omega_2 G(s,\Omega_1,\Omega_2)} \tag{2.25}$$

The pressure, Eq. (2.16), can be expressed in these terms

$$\beta P/\rho = 1 + (2\pi/3)\rho < h_{12} >_c g_c S_c \tag{2.26}$$

where the subscript "c" on $< h_{12} >_c g_c$ $(= g_{\text{iso}}(s = 0))$ and S_c denotes the average on the contact $s = 0$ surface.

In contrast, certain equilibrium properties such as the isothermal compressibility, κ_T, and the static orientational correlation factor g_2 (i.e., the parameter that determines the integrated intensity of depolarized light scattering due to collective orientational fluctutaions), are expressed in terms of the *full* pcf rather than its *contact value*. Starting from the familiar relationships [13,36]

$$\rho k_B T \kappa_T = 1 + \rho \int d\mathbf{r}\, d\Omega_1\, d\Omega_2\, [g(\mathbf{r}, \Omega_1, \Omega_2) - 1] \tag{2.27}$$

$$g_2 = 1 + \rho \int d\mathbf{r}\, d\Omega_1\, d\Omega_2\, P_2(\hat{\mathbf{u}}_1 \cdot \hat{\mathbf{u}}_2)[g(\mathbf{r}, \Omega_1, \Omega_2) - 1] \tag{2.28}$$

one can apply the convex body coordinates to convert these two equations to

$$\begin{aligned} \rho k_B T \kappa_T = {} & 1 + 4\pi\rho \int d\Omega_1\, d\Omega_2 \int_0^\infty ds S^{12}[g(1,2) - 1] \\ & -(4\pi/3)\rho \int d\Omega_1\, d\Omega_2 S^{12}(s = 0, \Omega_1, \Omega_2) h_{12} \end{aligned} \tag{2.29}$$

$$\begin{aligned} g_2 = {} & 1 + 4\pi\rho \int d\Omega_1\, d\Omega_2 \int_0^\infty ds P_2(\hat{\mathbf{u}}_1 \cdot \hat{\mathbf{u}}_2) S^{12}[g(1,2) - 1] \\ & -(4\pi/3)\rho \int d\Omega_1\, d\Omega_2 P_2(\hat{\mathbf{u}}_1 \cdot \hat{\mathbf{u}}_2) S^{12}(s = 0, \Omega_1, \Omega_2) h_{12} \end{aligned} \tag{2.30}$$

Both Eqs. (2.29) and (2.30) consist of two parts: a long range term reflecting the decay of the s-dependent pcf and a short range contact term arising from excluded volume considerations. The isothermal compressibility simplifies further to represent this explicit separation

$$\rho k_B T \kappa_T = 1 - \rho V_{12} + 4\pi\rho \int_0^\infty ds S^{12}(s)[g_{\text{iso}}(s) - 1] \tag{2.31}$$

where V_{12} is the excluded volume for a pair of HCBs.

The general remarks made so far do not bring us appreciably closer to the calculation of equilibrium properties of the systems of HCBs. Analytical techniques have had little success in providing the full angle dependence of the pcf for a fluid of HCBs as only the contact orientational pcf

for a single HCB in a HS fluid has been determined to date. [17] Most of the work to date on HCB systems in the isotropic phase has focussed on the scalar properties (such as virial coefficients) and the contact properties (such as the pressure and the isotropic pcf) [12] rather than the anisotropic pcf.

2. *Scalar Properties*

a. Virial Coefficients. The virial coefficients of HCB systems, even of single component fluids, increase rapidly in complexity as the number of particles in each cluster increases. Whereas B_2 is particularly straightforward,

$$\begin{aligned} B_2 &= (2\pi/3)\int d\Omega_1\, d\Omega_2 h_{12} S^{12}(s=0,\Omega_1,\Omega_2) \\ &= (1/2)V_{12} \end{aligned} \tag{2.32}$$

B_3 is more complicated and numerical procedures are needed for its evaluation. [37–41]For example,

$$\begin{aligned} B_3 = \int \lambda^2\, d\lambda \eta^2\, d\eta\, d\Omega_1\, d\Omega_2\, d\Omega_3 \\ \times h_{12} S^{12}(s_{12}=0,\{\Omega\}) h_{13} S^{13}(s_{13}=0,\{\Omega\}) \chi(2,3) \end{aligned} \tag{2.33}$$

where $\mathbf{r}_{23} = \lambda \mathbf{r}_{12}(\hat{\mathbf{s}}_{12}) - \eta \mathbf{r}_{13}(\hat{\mathbf{s}}_{13})$ is the center-to-center separation for the λ -scaled 1,2 surface and the η -scaled 1,3 surface. $\chi(2,3)$ is unity if bodies 2 and 3 overlap and zero otherwise. Evaluation of B_4 and B_5 requires numerical methods. [37,38,40] For elongated prolate ellipsoids, B_4 is negative. In contrast, the first seven virial coefficients of hard spheres are known to be positive. Values of B_2 for various ellipsoids have been collected by Boublik. [12] Certainly the most important property of the virial coefficients of prolate HCBs is

$$\lim_{\text{shape anisotropy} \to \infty} B_n/(B_2^{n-1}) \to 0 \tag{2.34}$$

This point is discussed in more detail in Section II.D.4.

b. Equations of State. Approximate equations of state have been derived on the basis of Scaled Particle Theory (SPT) [12,14,42–45] and re-summed virial expansions [46–48]. Both of these approaches begin with an assumption as to how the solution should behave. In SPT one guesses how the pcf depends on the scaling length whereas in the virial expansion re-summations, one guesses at the density dependence of the pressure or the contact pcf. Exact constraints, such as virial coefficients or other limiting

behaviors, fix the constants in the assumed equation of state (or isotropic contact **g**). The philosophy behind the scaled-particle theory is explained in more detail in the context of phase transitions in hard-core fluids (Section IV.A.2). A reasonably up to date account of scaled-particle theory in the context of isotropic hard-core fluids can be found in Ref. [12]. Boublik and Nezbeda have played a significant role in the development of the equations of state of HCBs and their work has been complemented by Wojcik and Gubbins, [46] Naumann et al. [47] and Song and Mason. [48] From the standpoint of accommodating data on many systems, the approach of Song and Mason appears to be most successful. However, none of the "phenomenological" approaches provides insight into the nature of a first order isotropic to nematic transition and, in that sense, no "first principles" equation of state is available.

The studies of pressures (by analytical approximate means) have also led to theories of the contact pcf and in particular, its volume average

$$g_{\text{vol}} = (4\pi/3) \int d\Omega_1 \, d\Omega_2 G(s = 0, \Omega_1, \Omega_2) h_{12}/V_{12} \tag{2.35}$$

rather than the surface averaged pcf of Eq. (2.23). For the purpose of forming a perspective on the basic algebraic forms of the isotropic pcfs, we sketch the SPT approach used by Boublik, [14] who found the pressure and g_{vol} to be

$$\beta P/\rho = [1 + 3\alpha y + 3\alpha^2 y^2] \frac{1}{1 - \rho^*} \tag{2.36}$$

$$g_{\text{vol}} = \left[1 + \frac{3\alpha y}{1 + 3\alpha} + \frac{3\alpha^2 y^2}{1 + 3\alpha}\right] \frac{1}{1 - \rho^*} \tag{2.37}$$

Here y is the Barboy–Gelbart [49–51] density variable

$$y = \rho^*/(1 - \rho^*) \tag{2.38}$$

which is discussed in more detail in Section IV.A.2, and α the nonsphericity parameter

$$\alpha = 4\pi R_1 S_1/(3V_1) \tag{2.39}$$

where R_1 and S_1 are, respectively, $1/4\pi$ times the mean curvature and the surface area of a single body and V_1 is the volume. (For spheres $\alpha = 1$.)

The goal of Boublik's SPT was to determine the contact pcf, which was related to the reversible work (i.e., the chemical potential) for the insertion of a q-scaled particle in a fluid. For a point particles, the PV work is related to the probability of finding a point cavity and this, in turn, is

related to the free volume ($= V - NV_1 = V(1 - \rho^*)$). By means of the exact relationships between the contact pcf and the work to insert a point particle in a fluid, exact conditions are placed on the volume average of both $g(q = 0)$ and $dg(q)/dq|_{q=0}$. A third exact condition follows from the work necessary to increase the volume of a macroscopic HCB from V_q to $V_q + dV_q$. This third condition links the pressure to $g(q = \infty)$. When these three conditions are incorporated into an assumed functional of the scaling parameter, Boublik obtained Eqs. (2.36) and (2.37). Equation (2.36) reduces to the Percus–Yevick [52] (PY) result (i.e., obtained via the compressibility relation) [13] when $\alpha = 1$, viz.,

$$(\beta P(\mathrm{HS})/\rho)_{\mathrm{PY}-c} = \frac{(1 + \rho^* + \rho^{*2})}{(1 - \rho^*)^3} \tag{2.40}$$

For small anisotropies ($\alpha \simeq 1$) and low densities, Eqs. (2.36) and (2.37) are useful. Heuristic modifications of Boublik's results for highly nonspherical HCBs (5:1 particles), based on the Carnahan–Starling hard sphere limiting result [53], improved the accuracy but the HCB equations of state and contact pcfs prove to be less accurate than their HS analogues. [38–40] At present, the most accurate equation of state and contact pcf are due to Song and Mason [48] who found that

$$g_{\mathrm{vol}} = \frac{1 - \gamma_1\rho^* + \gamma_2\rho^{*2}}{(1 - \rho^*)^3} \tag{2.41}$$

where

$$\gamma_1 = 3 - \frac{1 + 6\alpha + 3\alpha^2}{1 + 3\alpha} \tag{2.42}$$

and

$$\gamma_2 = 3 - \frac{1 + 2.6352\alpha + 7\alpha^2}{1 + 3\alpha} \tag{2.43}$$

Although the isotropic contact pcfs of fluids of HCBs can be estimated with some accuracy using the Song and Mason result, this area of research is by no means closed, as systematic and accurate first principle results are not at hand.

3. *Vector Properties*

a. Virial Coefficients. Ordinarily, the virial coefficients are not considered to be vector properties. However, in the context of the liquid crystal work to be presented in the following sections, we can anticipate some

reinterpretations. B_2, B_3 as well as all the higher virial coefficients depend on the mutual orientation of the bodies. This dependence could have been anticipated from Eq. (2.32) since we expressed B_2 as an integral over an orientation dependent integrand,

$$B_2 = \int d\Omega_1 \, d\Omega_2 B_2(\Omega_1, \Omega_2) \tag{2.44}$$

with

$$B_2(\Omega_1, \Omega_2) = (2\pi/3) h_{12} S^{12}(s = 0, \Omega_1, \Omega_2) \tag{2.45}$$

The angle dependence of B_2 was first derived by Onsager [3] for spherocylinders and by Isihara [54] for ellipsoids. Mulder [55] determined $B_2(\Omega_1, \Omega_2)$ analytically for spheroplatelets (a biaxial spherocylinder). Tjipto-Margo and Evans used orthogonal function expansions to express $B_2(\Omega_1, \Omega_2)$ and $B_3(\Omega_1, \Omega_2, \Omega_3)$ for uniaxial ellipsoids [41] and $B_2(\Omega_1, \Omega_2)$ for biaxial ellipsoids. [56]

b. Contact Orientational Correlations. She et al. [17,57] employed SPT to find the dependence of the contact pcf on the orientation of the solvent (taken to be a HS of radius a) with respect to a solute (a single but arbitrary HCB). The contact pcf for a fully scaled (q = 1) HCB was found to be function of $\hat{\mathbf{s}}$ (the HCB-atom contact surface normal), the solvent packing fraction and various measures of the geometry of the HCB. Specifically,

$$g(s = 0, x) = 1 + 4\rho^* g_{\mathrm{HS}} + \sum_{j=1}^{3} a_j(x)/(1 + h(x)/a)^j \tag{2.46}$$

where

$$x = \hat{\mathbf{u}} \cdot \hat{\mathbf{s}} \tag{2.47}$$

and the $a_j(x)$ coefficients are given elsewhere. [57] Equation (2.46) was derived using a SPT with four exact conditions: $g(s = 0, \hat{\mathbf{s}}, q = 0)$, $(dg(s = 0, \hat{\mathbf{s}}, q)/dq)|_{q=0}$, $(d^2 g(s = 0, \hat{\mathbf{s}}, q)/dq^2)|_{q=0}$ and $g(s = 0, \hat{\mathbf{s}}, q = \infty)$. Only the second derivative term introduces orientation dependence into $g(s = 0, \hat{\mathbf{s}}, q)$. All theories based on constraints for $g(\mathbf{s}, q = 0)$ and $dg(\mathbf{s}, q = 0)/dq$ will predict the pcf to be isotropic on the contact surface.

When the scaled particle is allowed to become spherical, the contact pcf and the pressure can be derived for the HS fluid within the context of the four-condition SPT described above, thus [33,57]

$$g_{HS} = \frac{1 - (1/4)\rho^* + (1/2)\rho^{*2} - (1/8)\rho^{*3}}{(1-\rho^*)^2(1 - (3/4)\rho^* + (1/2)\rho^{*2})} \tag{2.48}$$

and

$$(\beta P_{HS}/\rho)_{SPT} = 1 + 4\rho^* g_{HS} \tag{2.49}$$

This four-condition SPT provides the exact isotropic and anisotropic second viral coefficient and at low density g_{HS} has the expansion

$$g_{HS} \simeq 1 + 2.5\rho^* + 4.3755\rho^{*2} \tag{2.50}$$

Equation (2.50) is in disagreement with the findings of Tully-Smith and Reiss, [58] who find that a similar four-condition SPT predicts incorrect second and third virial coefficients. The resulting contact properties of the four-condition SPT are close to but not identical to that derived from the PY theory using the pressure equation [13]

$$(\beta P_{HS}/\rho)_{SPT} \simeq (\beta P_{HS}/\rho)_{PY-\rho} = \frac{1 + 2\rho^* + 3\rho^{*2}}{(1-\rho^*)^2} \tag{2.51}$$

Basically, an n-condition SPT and the PY theory have no formal equivalence; although the calculated equations of state are similar, this is more fortuitous than substantive. SPT in itself does not suggest any particular method of closure of the hierarchy (say by means of the choice of an appropriate length scaling functional) and so to this exent there is no unique SPT. Clearly the exact conditions are unique, however. At present, SPT has yet to provide a theory for the direct correlation function or for that matter, for a simple theory of the pcf. Reiss and Casberg [59] have calculated the HS pcf using the ideas of SPT but this version of SPT bears little resemblance to the original SPT. Certainly much remains to be done in the utilization of SPT to understand the properties of fluids of HCBs.

4. Integral Equation Methods

The pcf $g(1,2)$ and its companion, the total correlation function $h(1,2)$

$$h(1,2) = g(1,2) - 1 \tag{2.52}$$

(not be confused with the support function, h_{12}) can be approximated as a solution to an integral equation. The integral equations and the approximations for $g(1,2)$ are succinctly stated in terms of the direct correlation function $c(1,2)$, defined by the Ornstein–Zernike equation

$$h(1,2) = c(1,2) + \rho \int d3h(1,3)c(2,3) \tag{2.53}$$

For fluids of HCBs, the PY approximation is

$$c(1,2) = y(1,2)\chi(1,2) \tag{2.54}$$

and this is to be compared with the HNC approximation

$$c(1,2) = y(1,2)f(1,2) + y(1,2) - 1 - \ln y(1,2) \tag{2.55}$$

where we have introduced $y(1,2)$, the background correlation function

$$y(1,2) = \exp(+\beta U(1,2))g(1,2) \tag{2.56}$$

and $f(1,2)$ the Mayer f-bond

$$f(1,2) = \exp(-\beta U(1,2)) - 1 \tag{2.57}$$

In the HS system, $c(1,2)$ has been found to have a small positive tail outside the hard core for the HNC theory whereas $c(1,2)$ vanishes outside the hard core for the PY theory.

Methods of solution of the integral equations for the anisotropic pcf of nonspherical molecules are given by Gray and Gubbins. [60] Stemming from the work of Chen and Steele, [22] a considerable literature is now developing regarding the spherical harmonic expansion of $g(1,2)$. No reported calculations of $g(1,2)$ take advantage of the explicitly convex nature of the particles and hence the techniques presented in the preceding pages. That which is known about the expansion properties of $g(1,2)$ and $c(1,2)$ prior to 1988 is summarized by Nezbeda et al. [61] More recently Labik et al. [62] compared the $g_{jj'm}(r)$ expansion functions for hard dumbbells obtained from integral equation theories (PY, HNC and Bridge function methods). Talbot et al. [24] also compared the results of HNC and PY closures on the $g_{jj'm}(r)$ for hard ellipsoids. Generally all the integral equation predictions of $g_{jj'm}(r)$ are in basic agreement with each other and with MD simulations. Although the PY theory was less accurate than the HNC and Bridge function theories, one might argue that the selection amongst theories could be based on practicality, which would, in turn, would always favor the use of the PY theory.

A more sensitive measure of orientational correlations than the $g_{jj'm}(r)$ is required to discriminate between the growing assortment of integral equations. One such measure involves the expansion coefficients $c_{jj'm}(r)$ of $c(1,2)$

$$c(1,2) = \sum_{j,j',m} c_{jj'm}(r) C_{j,m}(\Omega_1) C_{j',-m}(\Omega_2) \tag{2.58}$$

Perera et al. [25] calculated the volume integral of the Legendre polynomial parts of $c(1,2)$

$$\begin{aligned} c_{jj0} &= 4\pi \int_0^\infty dr r^2 \, d\hat{\mathbf{u}}_1 \, d\hat{\mathbf{u}}_2 P_j(\hat{\mathbf{u}}_1 \cdot \hat{\mathbf{u}}_2) c(1,2) \\ &= 4\pi \int_0^\infty dr r^2 c_{jj0}(r) \end{aligned} \tag{2.59}$$

In the PY approximation for 3:1 hard ellipsoids, Perera [25] found that $c_{000}(r)$ behaved like the corresponding HS function; for $j \geq 2$, c_{jj0} was nearly density independent and in marked contrast with the strong density dependence from the HNC findings. Furthermore, the PY predictions for c_{jj0} $(j \geq 2)$ displayed less density dependence than that derived from the two term virial expansion for $c(1,2)$. [63] This decided difference between the anisotropies in $c(1,2)$ has a profound influence on the issue of liquid crystal formation in the context of PY and HNC theories. The anisotropy in $c(1,2)$, derived by the PY theory, is so weak that the PY theory fails to predict a liquid crystal transition at any realizable density. Thus, the PY theory, broadly accepted as a good indicator of radial correlations in the HS fluids [12,60] shows a serious breakdown in the analysis of orientational correlations in fluids of HCBs.

D. Simulations

In this section, we discuss numerical simulations of hard-body fluids in the isotropic phase. The material in this section is organized as follows. First, we discuss those aspects of simulation techniques that are peculiar to hard-body systems, or otherwise not completely standard. We devote considerable attention to a systematic description of the various tests that can be used to detect a hard-core overlap of two (convex) bodies, mainly because, in the existing literature, the discussion of this subject is quite fragmented. Next, we briefly summarize the essential features of the computation of the first few virial coefficients and the equation of state of hard-body fluids. Following this technical introduction, we review the results that have been obtained using these techniques. In view of the large amount of numerical data on hard-body fluids that have been reported in the literature, we focus the discussion of the simulation results on those features that are, in some sense, peculiar to hard-body fluids.

1. Overlap Criteria

The first step in a computer study of a model system for a liquid crystal forming substance, is the selection of the actual model. As was explained

in the Introduction, we prefer to study models that are computationally "cheap". At the same time, the model should be sufficiently rich to give rise to a nontrivial phase diagram. And finally, it is obviously attractive if the model belongs to a "family" of models that includes, as special or limiting cases, systems about which much is already known. For example, hard spheres can be considered as a special case of both hard ellipsoids and of hard spherocylinders. Similarly, the exactly solvable Onsager model of thin, hard rods, is again a limiting case of both models.

In this review, we consider several families of model systems, viz. hard ellipsoids (both uni-axial and bi-axial), hard spherocylinders, hard platelets (truncated spheres) and hard fused spheres. As we shall see below, all these model systems exhibit interesting static or dynamic behavior. In this section, we show that these models are all convenient from a computational point of view. As we are discussing hard-core models, the computation of the potential energy of the system can be reduced to a series of tests for overlap between pairs of molecules i and j with orientations Ω_i and Ω_j, at a relative distance $\mathbf{r}_{ij}$.

Usually, the test for overlap between two particles can be reduced to a test of the sign of one, or several, functions of the relative coordinates of a pair of particles. The choice of these functions is, in general, not unique but is dictated by computational convenience. For instance, we shall find that for ellipsoids there are (at least) two, quite different tests for overlap that are best used in combination. Below we discuss the overlap criteria that have been used for the model systems decribed in this review. In addition, we briefly refer to some other model systems.

We should, however, first explain that we are really only discussing a *subclass* of all possible hard-core interactions. In the most general case, one can construct a hard-core model by simply defining a pair potential-energy function $u(\mathbf{r}_{ij}, \mathbf{\Omega}_i, \mathbf{\Omega}_j)$ to be infinite for some finite, connected domain of coordinate values and zero elsewhere. Once this function is specified, we can construct the excluded volume of a pair of particles. In general, this excluded volume will not be convex. More importantly, in general it will not be meaningful to speak about the *shape* of the individual hard-core particles. In other words, although the *excluded volume* of a pair of particles can be visualized as an object in space, the individual particles cannot. It should be stressed that the idea that individual particles have a shape of their own, is a classical one that has little meaning at the molecular level. Hence, there is nothing wrong with a hard-core model that cannot be interpreted in terms of the overlap of two well-defined geometrical objects. In fact, a popular example of such a nondecomposable model is the Gaussian hard-core model [39,64]. However, in this review, we limit ourselves to hard-core models where the individual particles have

a well defined shape. The reason for restricting ourselves to such models is two-fold: first, it is easier to develop a mental picture of the factors that determine the static and dynamic behavior of hard-body systems, if we can visualize that system. Second, in nature, hard-core systems are most closely approximated by colloidal particles. For these particles, that can often be *seen* by electron microscopy, it is not unreasonable to attribute a shape to individual particles. Finally, for most of the models that we discuss, the shape of the individual particles is convex. This choice is motivated only by the fact that the theoretical description of both static and dynamic properties is often much simpler for convex than for nonconvex hard particles.

a. Spheres and Composite Particles. It is convenient to start our description of overlap criteria with the simplest case, namely hard spheres. Two hard spheres of radius R_1 and R_2, respectively overlap if the distance r_{12} between the centers of these spheres is less than $\sigma_{12} \equiv R_1+R_2$. In a simulation, we usually do not compare r_{12} with σ_{12}, but r_{12}^2 with σ_{12}^2, because the latter test is computationally cheaper. For future reference, it is important to note that the hard-sphere overlap test can be considered as a sequence of tests for *nonoverlap*. The test could be broken down into three steps namely $\Delta_1^2 \equiv \sigma_{12}^2 - x_{12}^2 < 0$, $\Delta_2^2 \equiv \Delta_1^2 - y_{12}^2 < 0$, and $\Delta_3^2 \equiv \Delta_2^2 - z_{12}^2 < 0$. Only if all three tests are *not satisfied* do we have overlap between the two spheres. In fact, as any pair of particles that fails the final test must also fail the previous two, it may be computationally cheaper to carry out only the final test. However, that is not the issue here. What we wish to show is that it is possible to break up our test into subtests that allow us to decide, at an early stage, whether a given pair of particles does *not* overlap. Later, on when we consider more complex overlap tests, we will see that it is advisable to have a cheap test for nonoverlap as the first "filter" in the test sequence.

As a specific example of such a screening, consider a composite particle consisting of several hard spheres. Such fused hard sphere models have been used to model rod-like mesogens. [65] Let us assume that we wish to know if two molecules, both consisting of n identical hard spheres, are overlapping. Clearly, the test for overlap between these two composite molecules can be broken down into n^2 hard-sphere tests (for convenience, we assume that we do not have to worry about intra-molecular overlaps). Now, we see that the nature of the subtests is different from the hard-sphere case. As soon as we find overlap between *any* pair of hard spheres, we know that the two molecules overlap and we can terminate the test sequence. However, in order to make sure that the two molecules do not overlap, we have to run through the complete sequence of n^2 tests.

However, if the two molecules are sufficiently far apart, it is possible to tell in advance that there can be no overlap. For instance, one could construct for every molecule a circumscribed sphere that contains all spheres in that molecule. Clearly, no overlap between the two molecules is possible if the circumscribed spheres of these molecules do not overlap. Thus, we can obviate n^2 overlap tests by one "nonoverlap" test. This example illustrates the respective role of overlap and nonoverlap tests. *Nonoverlap* tests are used to ensure that we do not perform expensive overlap tests on molecules that are far apart. But once we know that we really must carry out the complete test, then it is better to have a series of *overlap* tests, because this sequence can be terminated as soon as any such test is satisfied.

In many cases, this combination of nonoverlap and overlap tests is not applied to a single pair of molecules, but to all neighbors of a given moleucle that has undergone a trial displacement. First, we "short-list" the possible overlap partners by using a nonoverlap test. Next, we apply the overlap test on the short-listed neighbors. As soon as an overlap is detected, we know that we can reject the trial move. In this sense, the construction of the well-known Verlet neighborlist [66] is simply an example of a short-list produced by a nonoverlap filter. For anisometric hard-core molecules, the corresponding nonoverlap tests are used to construct a "nonspherical" Verlet list.

b. Spherocylinders. Let us now consider a slightly more complex hard-core model, namely the spherocylinder. Just as a sphere can be defined as the set of points that are within a distance R from a given origin (namely the center of the sphere), so the spherocylinder can be thought of as the set of points that are within a distance R from a line segment of length L. Clearly, we can draw around every point on this line segment a sphere of radius R that contains all points that are within a distance R from that point. Hence, a spherocylinder can be considered as the union of all spheres around points on a line segment L. We can thus consider a spherocylinder as the volume that is swept out by a sphere of radius R that is moved along a line segment of length L. The test for overlap between two spherocylinders can be constructed by computing the shortest distance between the two line segments that form the "core" of the spherocylinders. If this distance of closest approach is less than $D_{12} \equiv R_1 + R_2$, the two spherocylinders overlap. This distance of closest approach is therefore the central quantity to be computed in an overlap test for spherocylinders. In fact, some of the steps needed to compute the distance of closest approach between two spherocylinders, are also needed in the construction of other overlap criteria to be discussed below. We therefore

break down the construction of the overlap test for spherocylinders into a number of elementary steps, namely:

1. the construction of the point of closest approach between two lines;
2. the construction of the perpendicular distance-vector between two lines;
3. the determination of the distance of closest approach between two line segments in a plane.

Although the overlap test for spherocylinders usually skips the second step, it is useful to include it, both for future reference and because it makes the whole procedure more transparent. Step 1 is sufficient to determine the overlap of line segments in two dimensions. Combined with step 3, it allows us to test for overlap between two-dimensional spherocylinders. Steps 1 and 2 will turn out to be useful in the test for overlap between hard platelets in three dimensions.

POINT OF CLOSEST APPROACH BETWEEN TWO LINES. Our aim is to determine the minimum distance between two finite line-segments i and j, with orientations $\hat{\mathbf{u}}_i$ and $\hat{\mathbf{u}}_j$ and centers $\mathbf{r}_i$ and $\mathbf{r}_j$. Let us first consider the minimum distance between these two segments, in the limit that their length is infinite. In that case, we can describe any point on line i parametrically as

$$\mathbf{r}_i(\lambda) = \mathbf{r}_i + \lambda\hat{\mathbf{u}}_i$$

while line j is given by

$$\mathbf{r}_j(\mu) = \mathbf{r}_j + \mu\hat{\mathbf{u}}_j$$

The vector distance between these two points is given by

$$\mathbf{r}_{ij}(\lambda, \mu) = (\mathbf{r}_i - \mathbf{r}_j) + \lambda\hat{\mathbf{u}}_i - \mu\hat{\mathbf{u}}_j \tag{2.60}$$

Next, we wish to determine those values of λ and μ for which the distance r_{ij} is minimal. A simple method to find these values of λ and μ is the following. Construct the dot product of $\mathbf{r}_{ij}(\lambda, \mu)$ with both $\hat{\mathbf{u}}_i$ and $\hat{\mathbf{u}}_j$. The shortest distance vector must be perpendicular to both $\hat{\mathbf{u}}_i$ and $\hat{\mathbf{u}}_j$. Hence, we should solve the following simultaneous equations:

$$\begin{aligned}(\mathbf{r}_i - \mathbf{r}_j)\cdot\hat{\mathbf{u}}_i &= -\lambda\hat{\mathbf{u}}_i\cdot\hat{\mathbf{u}}_i + \mu\hat{\mathbf{u}}_j\cdot\hat{\mathbf{u}}_i \\ (\mathbf{r}_i - \mathbf{r}_j)\cdot\hat{\mathbf{u}}_j &= -\lambda\hat{\mathbf{u}}_i\cdot\hat{\mathbf{u}}_j + \mu\hat{\mathbf{u}}_j\cdot\hat{\mathbf{u}}_j\end{aligned} \tag{2.61}$$

Solving these equations for λ and μ, we obtain

$$\begin{pmatrix} \lambda_0 \\ \mu_0 \end{pmatrix} = \frac{1}{1-(\hat{\mathbf{u}}_i \cdot \hat{\mathbf{u}}_j)^2} \begin{pmatrix} -\hat{\mathbf{u}}_i \cdot \mathbf{r}_{ij} + (\hat{\mathbf{u}}_i \cdot \hat{\mathbf{u}}_j)(\hat{\mathbf{u}}_j \cdot \mathbf{r}_{ij}) \\ +\hat{\mathbf{u}}_j \cdot \mathbf{r}_{ij} - (\hat{\mathbf{u}}_i \cdot \hat{\mathbf{u}}_j)(\hat{\mathbf{u}}_i \cdot \mathbf{r}_{ij}) \end{pmatrix} \tag{2.62}$$

where we have used the shorthand notation $\mathbf{r}_{ij} \equiv \mathbf{r}_{ij}(\lambda = 0, \mu = 0)$. We have assumed that the line segments i and j are not parallel. In fact, the parallel case is simpler, and is discussed separately. The above expression for λ_0 and μ_0 allows us to carry out a testing for overlap between two line segments of length L_i and L_j in two dimensions. In that case, we simply have to verify that $|\lambda_0| \leq L_i/2$ and $|\mu_0| \leq L_j/2$.

PERPENDICULAR DISTANCE VECTOR BETWEEN TWO LINES. We wish to know the shortest distance between two line-segments in three dimensions. We can decompose this vector in a component perpendicular to $\mathbf{u}_i$ and $\hat{\mathbf{u}}_j$ and a component in the plane of $\mathbf{u}_i$ and $\hat{\mathbf{u}}_j$. By varying λ and μ, we can only change the latter distance. Hence, our problem reduces to the computation of the fixed perpendicular distance between the lines i and j and of the minimal in-plane distance between the two line segments. For future reference, it is convenient to construct the perpendicular distance vector as follows. From the unit vectors $\hat{\mathbf{u}}_i$ and $\hat{\mathbf{u}}_j$, we construct three orthogonal unit vectors $\hat{\mathbf{u}}_+$, $\hat{\mathbf{u}}_-$ and $\hat{\mathbf{u}}_\perp$, defined as

$$\hat{\mathbf{u}}_+ \equiv \frac{1}{\sqrt{2}} \frac{\hat{\mathbf{u}}_i + \hat{\mathbf{u}}_j}{(1+(\hat{\mathbf{u}}_i \cdot \hat{\mathbf{u}}_j))^{1/2}} \tag{2.63}$$

$$\hat{\mathbf{u}}_- \equiv \frac{1}{\sqrt{2}} \frac{\hat{\mathbf{u}}_i - \hat{\mathbf{u}}_j}{(1-(\hat{\mathbf{u}}_i \cdot \hat{\mathbf{u}}_j))^{1/2}} \tag{2.64}$$

$$\hat{\mathbf{u}}_\perp \equiv \hat{\mathbf{u}}_+ \times \hat{\mathbf{u}}_- \tag{2.65}$$

The perpendicular vector distance between lines i and j is then given by

$$\mathbf{r}_{ij}^\perp \equiv (\mathbf{r}_{ij} \cdot \hat{\mathbf{u}}_\perp)\hat{\mathbf{u}}_\perp \tag{2.66}$$

DISTANCE OF CLOSEST APPROACH BETWEEN TWO LINE SEGMENTS IN A PLANE. Finally, we must compute the distance of closest approach between two line segments in a plane. Of course, if both $|\lambda_0| \leq L_i/2$ and $|\mu_0| \leq L_j/2$, the two line segments intersect, and the in-plane distance is zero. In that case, the total distance is given by $|\mathbf{r}_{ij}^\perp|$. However, we have to consider the more general case that the in-plane distance between the line segments is nonzero. For this purpose, it is convenient to take as the origin of our (two-dimensional) coordinate frame, the intersection point between the lines i and j projected in a plane spanned by $\hat{\mathbf{u}}_i$ and $\hat{\mathbf{u}}_j$. In this frame, the center of segment i is located at $-\lambda_0\hat{\mathbf{u}}_i$ and the center of segmenty j is at $-\mu_0\hat{\mathbf{u}}_j$. The squared distance between two arbitrary points on the lines given by $\gamma\hat{\mathbf{u}}_i$ and $\delta\hat{\mathbf{u}}_j$, is

$$(r_{ij}^{\parallel}(\gamma,\delta))^2 = \gamma^2 + \delta^2 + 2\gamma\delta(\hat{\mathbf{u}}_i \cdot \hat{\mathbf{u}}_j) \tag{2.67}$$

The curves of the constant in-plane distance are ellipses with major axes along the lines $\gamma = \delta$ and $\gamma = -\delta$. Figure 2.2 shows a contour plot of the (squared) in-plane distance in the (γ, δ)-plane. When computing the shortest distance between two line segments, we should search for the minimum of the parabolic function shown in the figure, subject to the conditions $|\gamma + \lambda_0| \leq L_i/2$ and $|\delta + \mu_0| \leq L_j/2$. This constraint defines a rectangle in the (γ, δ)-plane. The procedure to find the distance of closest approach is now as follows.

1. If the origin is contained in the rectangle, the line segments intersect and the in-plane distance is zero.
2. Otherwise, find the allowed values of γ and δ that are closest to the origin: $\gamma_{\min}$ and $\delta_{\min}$. As, in the present case, the origin does not correspond to an allowed (γ, δ)-combination, either $|\gamma_{\min}|$ or $|\delta_{\min}|$, or both, are not equal to zero. Without loss of generality, we assume that $|\gamma_{\min}| \geq |\delta_{\min}|$ (otherwise, we simply relabel γ and δ). We now fix γ at the value $\gamma_{\min}$. Next, we minimize $(r_{ij}^{\parallel}(\gamma_{\min}, \delta))^2$ with respect to δ. From Eq. (2.67) it follows that the minimum distance is reached for $\delta'_{\min} = -2\gamma_{\min}(\hat{\mathbf{u}}_i \cdot \hat{\mathbf{u}}_j)$.

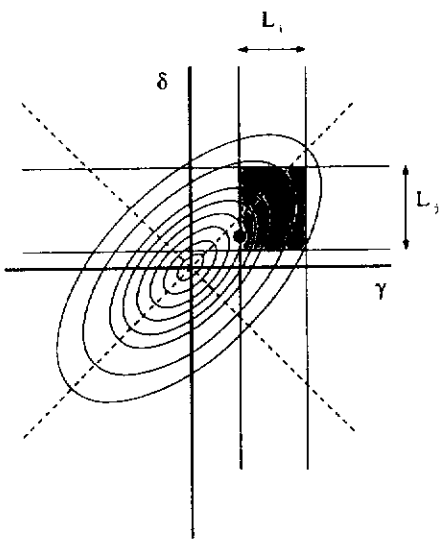

Figure 2.2. Contour lines of equal distance between two line segments of length L_i and L_j in a plane. The geometrical interpretation of this figure is discussed in the text

3. We now test if $|\delta'_{\min} + \mu_0| \leq L_j/2$. If so, we have found the value of δ that minimizes the in-plane distance. Otherwise, we choose the allowed value of δ that is closest to $\delta'_{\min}$.

Using Eq. (2.67), we can now simply evaluate the squared, in-plane distance. As we have already computed the (squared) perpendicular distance, we know the distance of closest approach of the two line segments i and j.

c. Platelets. We can use many of the results obtained in the previous section to construct a test for overlap between two infinitely thin platelets with radii R_i and R_j. In what follows, we denote the coordinate of the center of either disk by $\mathbf{r}_i$ (or $\mathbf{r}_j$), while the unit vectors $\hat{\mathbf{u}}_i$ and $\hat{\mathbf{u}}_j$ give the orientation of the symmetry axes of the disks.

As in the previous section, we define $\hat{\mathbf{u}}_\perp$, the unit vector perpendicular to both $\hat{\mathbf{u}}_i$ and $\hat{\mathbf{u}}_j$. If we project both disks on a plane normal to $\hat{\mathbf{u}}_\perp$, all points in the plane of disk i project onto a line with direction

$$\mathbf{v}_i \equiv \hat{\mathbf{u}}_\perp \times \hat{\mathbf{u}}_i$$

Similarly, the plane of disk j projects onto a line with direction

$$\mathbf{v}_j \equiv \hat{\mathbf{u}}_\perp \times \hat{\mathbf{u}}_j$$

The projections of disks i and j are line segments with a length $2R_i$ and $2R_j$ respectively. Clearly, a necessary (but not sufficient) condition for overlap of the two disks is that these line segments cross. But the problem of the intersection of two line segments in a plane was already discussed in Section II.D.1 above. In the present case, it is more convenient to express λ (μ), the distance between the center of disk i (j) and the intersection-line of the planes of disk i and j, in terms of the unit vectors $\hat{\mathbf{u}}_i$ and $\hat{\mathbf{u}}_j$, rather than the auxiliary vectors $\mathbf{v}_i$ and $\mathbf{v}_j$, defined above. It is easy to show that

$$\begin{pmatrix} \lambda^2 \\ \mu^2 \end{pmatrix} = \frac{1}{1 - (\hat{\mathbf{u}}_i \cdot \hat{\mathbf{u}}_j)^2} \begin{pmatrix} (\hat{\mathbf{u}}_j \cdot \mathbf{r}_{ij})^2 \\ (\hat{\mathbf{u}}_i \cdot \mathbf{r}_{ij})^2 \end{pmatrix} \tag{2.68}$$

If either $\lambda^2 > R_i^2$ or $\mu^2 > R_j^2$, no overlap is possible. Otherwise, the plane of disk j intersects disk i over a line segment of length

$$\Delta_i = \sqrt{R_i^2 - \lambda^2}$$

and

$$\Delta_j = \sqrt{R_j^2 - \mu^2}$$

Clearly, in order to have overlap between disks i and j, we must satisfy the following condition:

$$\Delta_i + \Delta_j < |\mathbf{r}_{ij} \cdot \hat{\mathbf{u}}_\perp| \tag{2.69}$$

This concludes our test for overlap between two infinitely thin hard platelets. In practice, this overlap criterion is rewritten in such a way that the "expensive" computation of square roots is avoided. For details, see Ref. [67].

d. Truncated Spheres. A convenient convex hard-core model for platelike molecules with a finite thickness is obtained by taking a sphere of diameter D and slicing off the top and the bottom at a distance $\pm L/2$ from the equatorial plane. In the limit $L/D \to 0$, the truncated sphere reduces to an infinitely thin, hard platelet whereas, in the limit $L \to D$, we obtain a hard sphere. At first sight, the truncated sphere would appear to be a needlessly complex model for a disk-like molecule. It would seem more natural to model such particles by short cylinders. However, from a computational point of view, truncated spheres are more convenient because the test for overlap between two such particles can be decomposed into a finite sequence of simple subtests. For cylinders the corresponding tests appear to be less simple, except when the cylinders are parallel. This may explain why only approximate simulations of freely rotating, hard cylinders have been reported in the literature. [68]

Although the test for overlap between truncated spheres consists of simple steps, the test as a whole is rather elaborate. The reason is that different tests are needed to detect overlap of the two spherical rims, of the two flat circular faces, and of a flat face and a circular rim. Below, we discuss all these tests in succession. In addition, the procedure also includes a few tests that allow us to ascertain, at an early stage, either that i and j *cannot* overlap, or that they *must* overlap.

As before, we consider two particles i and j, at positions $\mathbf{r}_i$ and $\mathbf{r}_j$ and with orientations $\hat{\mathbf{u}}_i$ and $\hat{\mathbf{u}}_j$. For convenience, we assume that the truncated spheres have the same diameter D and the same thickness L. The generalization of the overlap tests to dissimilar truncated spheres is straightforward. Below, we go through the sequence of overlap tests, step by step.

1. *Sphere test.* We first test if particles i and j are close enough to overlap. A necessary conditions is

$$r_{ij}^2 < D^2$$

Only if this test is satisfied do we proceed with further overlap tests.

2. *Rim-rim test.* Next, we consider the cosine of the angle that $\mathbf{r}_{ij}$ makes with $\hat{\mathbf{u}}_i$. If the absolute value of this cosine is less than L/D, the $\mathbf{r}_{ij}$ *must* intersect the spherical rim of particle i. Similarly, if the abolute value of the cosine of the angle that $\mathbf{r}_{ij}$ makes with $\hat{\mathbf{u}}_j$ is less than L/D, then $\mathbf{r}_{ij}$ *must* intersect the spherical rim of particle j. If both conditions are satisfied, the test for overlap between the truncated spheres i and j reduces to a test for overlap between two spheres of diameter d. However, this test was already performed in the previous step. Hence, if

$$\text{Max}[(\mathbf{r}_{ij}.\hat{\mathbf{u}}_i)^2, (\mathbf{r}_{ij}.\hat{\mathbf{u}}_j)^2] < r_{ij}^2(L/D)^2$$

then i and j must overlap

3. *Too close or too far?* Next, we consider $\cos\theta_{ij} \equiv \hat{\mathbf{u}}_i.\mathbf{u}_j$. We distinguish between the case $|\cos\theta_{ij}| < (L/D)$ and $|\cos\theta_{ij}| > (L/D)$. We can easily compute $r_{\min}(\theta_{ij})$, the shortest possible distance that i and j can approach one another without overlapping. If $|\cos\theta_{ij}| < (L/D)$, then $r_{\min}(\theta_{ij}) = L/2 + D/2$. Hence if $|\mathbf{r}_{ij}|$ is less than $r_{\min}(\theta_{ij})$, then the particles *must* overlap. Conversely, if the distance between the center of one particle and the equatorial plane of the other is larger than $r_{\min}(\theta_{ij})$, then the particles *cannot* overlap. Next, consider the case where $|\cos\theta_{ij}| > (L/D)$. In that case, the smallest possible distance between two nonoverlapping particles is

$$r_{\min}(\theta_{ij}) = L/2(1 + |\cos\theta_{ij}|) + \sqrt{D^2 - L^2}/2|\sin\theta_{ij}|$$

Again, the particles *must* overlap if

$$|\mathbf{r}_{ij}| < r_{\min}(\theta_{ij})$$

and they *cannot* overlap if

$$\text{Max}[(|\mathbf{r}_{ij}.\hat{\mathbf{u}}_i|), |(\mathbf{r}_{ij}.\hat{\mathbf{u}}_j)|] > r_{\min}(\theta_{ij})$$

4. *Circular faces overlap?* If we have passed all the tests thus far, two tests remain. The first is a test for overlap between one of the (circular) faces of particle i with one of the faces of particle j. As we have already discussed the test for overlap between two infinitely thin disks, we do not repeat the criteria that have been derived in Section II.D.1.

5. *Face-rim overlap?* The only kind of overlap that we have not yet excluded is between the circular face of one platelet and the spherical rim of the other. To derive the criterion for such an overlap, let us first consider the intersection of a *sphere* of diameter D around $\mathbf{r}_i$ with a circular disk of radius $R_f \equiv \sqrt{D^2 - L^2}/2$ that constitutes the nearest face of particle j. The distance between $\mathbf{r}_i$ and the plane of this face is $d_\perp = |\mathbf{r}_{ij} \cdot \mathbf{u}_j| -$

$L/2$. The sphere around j intersects the plane in a circle of radius $R_c = \sqrt{(D/2)^2 - d_\perp^2}$. The distance between the center of this circle and the axis of particle j is $\sqrt{r_{ij}^2 - (\mathbf{r}_{ij}.\mathbf{u}_j)^2}$. Overlap between the sphere and the circular disk is only possible if the latter distance is less than $R_f + R_c$. Now we take into account that particle i is a truncated sphere rather than a full sphere. This imposes an additional constraint on the overlap criterion, namely that at least some points of the intersection between the sphere around $\mathbf{r}_i$ and the nearest circular face of j must be within a distance $L/2$ from the equatorial plane of i. In fact, this test can be simplified because we have already eliminated overlap between the circular faces of i and j. This means that if *any* point in the intersection of the sphere and the platelet is contained between the top and bottom faces of i, then *all* points in the intersection must satisfy the same criterion, because otherwise the circular faces of i and j must intersect. The choice of the point on which to apply the test is then merely a matter of convenience. In practice, we take the projection of $\mathbf{r}_i$ on the plane of j, unless this point is outside the radius of the circular face of j. In the latter case, we take the point where the perimeter of the circular face of particle j intersects the projection of $\mathbf{r}_{ij}$ in the plane of this face. This test is performed to test if the rim of i intersects the face of j or vice versa.

This completes our description of the test for overlap between two truncated spheres. This test demonstrates how tests for overlap and for non-overlap can be combined in a systematic manner.

e. Ellipsoids. We discuss two different approaches towards the determination of overlap between ellipsoidal hard particles. The first is due to Vieillard-Baron. [5,69] The second is due to Perram and Wertheim. [9] The reason for including both techniques is the fact that it is computationally attractive to use them in combination as explained below.

THE VIEILLARD-BARON CRITERION. The starting point of the Vieillard-Baron criterion (VB) is the equation describing the locus of points on the surface of an ellipsoid

$$F_A(\mathbf{r}) = (\mathbf{r} - \mathbf{r}_A) \cdot \mathbf{A}^{-1} \cdot (\mathbf{r} - \mathbf{r}_A) - 1 = 0 \tag{2.70}$$

where $\mathbf{r}_A$ is the location of the center of the ellipsoid A, and $\mathbf{A}$ is the matrix $\mathbf{A} = \sum_{i=1}^{3} R_i^2 \hat{\mathbf{a}}_i \otimes \hat{\mathbf{a}}_i$, where R_i is half the length of the ith axis and $\{\hat{\mathbf{a}}_i\}_{i=1,2,3}$ is a set of unit vectors along the axes. Introducing so-called homogeneous projective coordinates $x_\mu \quad \mu = 0, 1, 2, 3$, through $r_\nu = x_\nu / x_0, \quad \nu = 1, 2, 3$, the ellipsoid equation can be written as

$$\sum_{\mu=0}^{3}\sum_{\nu=0}^{3}\mathcal{A}_{\mu\nu}x_\mu x_\nu = 0 \tag{2.71}$$

where the 4×4 matrix $\mathcal{A}$ is defined by

$$\begin{aligned}
\mathcal{A}_{00} &= -1 - \mathbf{r}_A \cdot \mathbf{A}^{-1} \cdot \mathbf{r}_A \\
\mathcal{A}_{0j} &= (\mathbf{r}_A \cdot \mathbf{A}^{-1})_j, & j &= 1,2,3 \\
\mathcal{A}_{i0} &= (\mathbf{A}^{-1} \cdot \mathbf{r}_A)_i, & i &= 1,2,3 \\
\mathcal{A}_{ij} &= \mathbf{A}^{-1}_{ij}, & i,j &= 1,2,3
\end{aligned} \tag{2.72}$$

Given two ellipsoids A and B in the above-mentioned representation, we can construct the so-called pencil of conics passing through them, defined by the equation

$$\sum_{\mu=0}^{3}\sum_{\nu=0}^{3}(\mathcal{A}_{\mu\nu} + \lambda\mathcal{B}_{\mu\nu})x_\mu x_\nu = 0, \quad \lambda \in \mathbb{C} \tag{2.73}$$

This pencil contains four (possibly multiply) degenerate conics, for those λ such that

$$P(\lambda) \equiv \det(\mathcal{A} + \lambda\mathcal{B}) = 0 \tag{2.74}$$

The properties of these degenerate conics determine whether A and B have any real points in common. These properties in turn follow from the roots of $P(\lambda)$. We can now state the relevant rule: A and B do *not* have any real points in common (i.e., do *not* intersect) if and only if all roots of $P(\lambda)$ are real and *not* all are negative.

We thus need a root determination scheme. There are several choices available but we prefer the one given in the classical algebra text by Weber. [70] Given a normalized fourth degree polynomial,

$$N(\lambda) = \lambda^4 + n_3\lambda^3 + n_2\lambda^2 + n_1\lambda + n_0 \tag{2.75}$$

we can convert into the canonical form by the substitution $\lambda = \tau - \frac{1}{4}n_3$, yielding

$$C(\tau) = \tau^4 + c_2\tau^2 + c_1\tau + c_0 \tag{2.76}$$

with

$$\begin{aligned}
c_2 &= -\frac{3}{8}n_3^2 + n_2 \\
c_1 &= \frac{1}{8}n_3^3 - \frac{1}{2}n_3n_2 + n_1 \\
c_0 &= -\frac{3}{256}n_3^4 + \frac{1}{16}n_3^2n_2 - \frac{1}{4}n_3n_1 + n_0
\end{aligned} \tag{2.77}$$

The discriminant D of the canonical polynomial is given by

$$27D = 4\left(c_2^2 + 12c_0\right)^3 - \left(2c_2^3 - 72c_2c_0 + 27c_1^2\right)^2 \tag{2.78}$$

The necessary conditions for the reality of the roots are

(i) $D > 0$
(ii) $c_2 < 0$
(iii) $c_2^2 - 4c_0 > 0$

while the condition that not all roots are negative is met when

(iv) *at least* one of the coefficients $\{n_3, n_2, n_1\} < 0$

The only input needed for the application of the overlap criterion are thus the coefficients $\{n_k\}$ of the normalized charcateristic polynomial $P(\lambda)$ for the specific ellipsoidal particles in question. Here we will give the explicit results for two cases:(i) nonisomorphic ellipsoids of revolution; (ii) isomorphic general ellipsoids.

(i) *Nonisomorphic ellipsoids of revolution.* For ellipsoids of revolution, it is useful to define the matrices

$$\mathbf{A}^{-1} = \alpha\mathbf{1} + \gamma\hat{\mathbf{a}}\otimes\hat{\mathbf{a}}, \qquad \mathbf{B}^{-1} = \beta\mathbf{1} + \delta\hat{\mathbf{b}}\otimes\hat{\mathbf{b}} \tag{2.79}$$

where

$$\begin{aligned} \alpha &= R_{A,1}^{-2}, & \gamma &= R_{A,3}^{-2} - R_{A,1}^{-2} \\ \beta &= R_{B,1}^{-2}, & \delta &= R_{B,3}^{2} - R_{B,1}^{-2} \end{aligned} \tag{2.80}$$

and $\hat{\mathbf{a}}$ and $\hat{\mathbf{b}}$ are unit vectors along the major symmetry axis of the two particles.

Defining $\mathbf{r} = \mathbf{r}_B - \mathbf{r}_A$, $\Delta_A = \det \mathbf{A}^{-1}$ and $\Delta_B = \det \mathbf{B}^{-1}$ and introducing the auxiliary terms

$$\begin{aligned} P_A &= -2\alpha\beta\delta - \beta\gamma\delta + \beta\gamma\delta(\hat{\mathbf{a}}\cdot\hat{\mathbf{b}})^2 - 3\alpha\beta^2 \\ &\quad -\beta^2\gamma + \alpha\Delta_B r^2 - \Delta_B + \gamma\Delta_B(\mathbf{r}\cdot\hat{\mathbf{a}})^2 \\ P_B &= -2\alpha\beta\gamma - \alpha\gamma\delta + \alpha\gamma\delta(\hat{\mathbf{a}}\cdot\hat{\mathbf{b}})^2 - 3\alpha^2\beta \\ &\quad -\alpha^2\delta + \beta\Delta_A r^2 - \Delta_A + \delta\Delta_A(\mathbf{r}\cdot\hat{\mathbf{b}})^2 \\ P_{AB} &= \alpha\beta\gamma\delta\left\{r^2 - r^2(\hat{\mathbf{a}}\cdot\hat{\mathbf{b}})^2 + 2(\mathbf{r}\cdot\hat{\mathbf{a}})(\mathbf{r}\cdot\hat{\mathbf{b}})(\hat{\mathbf{a}}\cdot\hat{\mathbf{b}})\right\} \\ &\quad +\alpha\beta^2\gamma r^2 + \alpha\beta^2\gamma(\mathbf{r}\cdot\hat{\mathbf{a}})^2 - \alpha\Delta_B r^2 \\ &\quad +\alpha^2\beta\delta r^2 + \alpha^2\beta\delta(\mathbf{r}\cdot\hat{\mathbf{b}})^2 - \beta\Delta_A r^2 \\ &\quad +\Delta_A + \Delta_B + 2\alpha^2\beta^2 r^2 - \gamma\Delta_B(\mathbf{r}\cdot\hat{\mathbf{a}})^2 - \Delta_A(\mathbf{r}\cdot\hat{\mathbf{b}})^2 \end{aligned} \tag{2.81}$$

The coefficients of the normalized characteristic polynomial are then given by

$$\begin{aligned} n_3 &= -P_A/\Delta_B \\ n_2 &= -(P_A + P_B + P_{AB})/\Delta_B \\ n_1 &= -P_B/\Delta_B \\ n_0 &= \Delta_A/\Delta_B \end{aligned} \tag{2.82}$$

(ii) *Isomorphic general ellipsoids.* For the isomorphic, but general (i.e., $R_1 \neq R_2 \neq R_3$) ellipsoids, the results can be given in a more compact form. Defining $l_i = R_i^{-2}$, ϵ_{ijk} the totally antisymmetric three-tensor and assuming summation over repeated Cartesian indices, we get

$$\begin{aligned} n_0' &= -l_1 l_2 l_3 \\ n_1' &= l_1 l_2 l_3 \, l_i (\mathbf{r} \cdot \hat{\mathbf{b}}_i)^2 - l_1 l_2 l_3 - \frac{1}{2} l_i l_j l_k (\hat{\mathbf{b}}_i \cdot \hat{\mathbf{a}}_j \wedge \hat{\mathbf{a}}_k)^2 \\ n_2' &= l_1 l_2 l_3 \, l_i \mid \epsilon_{ijk} \mid (\mathbf{r} \cdot \hat{\mathbf{a}}_j \wedge \hat{\mathbf{b}}_k)^2 + \frac{1}{2} l_i^2 l_j^2 \mid \epsilon_{ijk} \mid (\mathbf{r} \cdot \hat{\mathbf{a}}_k \wedge \hat{\mathbf{b}}_k)^2 \\ &\quad - \frac{1}{2} l_i l_j l_k (\hat{\mathbf{a}}_i \cdot \hat{\mathbf{b}}_j \wedge \hat{\mathbf{b}}_k)^2 - \frac{1}{2} l_i l_j l_k (\hat{\mathbf{b}}_i \cdot \hat{\mathbf{a}}_j \wedge \hat{\mathbf{a}}_k)^2 \\ n_3' &= l_1 l_2 l_3 \, l_i (\mathbf{r} \cdot \hat{\mathbf{a}}_i)^2 - l_1 l_2 l_3 - \frac{1}{2} l_i l_j l_k (\hat{\mathbf{a}}_i \cdot \hat{\mathbf{b}}_j \wedge \hat{\mathbf{b}}_k)^2 \end{aligned} \tag{2.83}$$

where the primed coefficients are related to the normalized ones through the relation

$$n_k = n_k'/n_0', \quad k = 1, 2, 3 \tag{2.84}$$

THE PERRAM–WERTHEIM CRITERION. Given two ellipsoids A and B, we form the family of interpolating functions

$$F(\mathbf{r}, \lambda) = \lambda F_A(\mathbf{r}) + (1 - \lambda) F_B(\mathbf{r}) + 1 \tag{2.85}$$

using the definition (2.70) for the equations defining the surface of an ellipsoid. Introduce

$$F(A, B) = \max_{\lambda \in [0,1]} \min_{\mathbf{r}} F(\mathbf{r}, \lambda) \tag{2.86}$$

The following property of the quantity $F(A, B)$ is now proposed to hold

$$F(A, B) = \begin{cases} > 1, & A \text{ and } B \text{ are } \textit{non}\text{overlapping} \\ 1, & A \text{ and } B \text{ are exteriorly tangent} \\ < 1, & A \text{ and } B \text{ overlap} \end{cases} \tag{2.87}$$

A sketch of the proof of this, at first sight remarkable property runs as follows. The minimum over all space of $F(\mathbf{r}, \lambda)$ is found by solving

$$2\nabla F(\mathbf{r}, \lambda) = \lambda \mathbf{A}^{-1} \cdot (\mathbf{r} - \mathbf{r}_A) + (1 - \lambda) \mathbf{B}^{-1} \cdot (\mathbf{r} - \mathbf{r}_B) = 0 \tag{2.88}$$

We can easily solve for this minimum, which we denote by $\mathbf{r}(\lambda)$

$$\mathbf{r}(\lambda) - \mathbf{r}_A = (1-\lambda)\mathbf{A}\cdot\mathbf{C}\cdot\mathbf{r}_{AB} \quad \text{or} \quad \mathbf{r}(\lambda) - \mathbf{r}_B = -\lambda\mathbf{B}\cdot\mathbf{C}\cdot\mathbf{r}_{AB} \tag{2.89}$$

where $\mathbf{r}_{AB} = \mathbf{r}_B - \mathbf{r}_A$ and

$$\mathbf{C} = (\lambda\mathbf{B} + (1-\lambda)\mathbf{A})^{-1} \tag{2.90}$$

We can now eliminate $\mathbf{r}(\lambda)$ to find

$$\min_{\mathbf{r}} F(\mathbf{r},\lambda) = F(\mathbf{r}(\lambda),\lambda) = \lambda(1-\lambda)\mathbf{r}_{AB}\cdot\mathbf{C}\cdot\mathbf{r}_{AB} \tag{2.91}$$

Consider the path $\wp(\lambda) = \{\mathbf{r}(\lambda) \mid \lambda \in [0,1]\}$. This path runs from $\mathbf{r}_0 = \mathbf{r}_B$ to $\mathbf{r}_1 = \mathbf{r}_A$ (cf. 2.89), the interpolating function vanishing at these endpoints, that is, $F(\mathbf{r}_B,0) = F(\mathbf{r}_A,1) = 0$. The following cases can now be distinguished:

- If A and B do *not* overlap, the path $\wp$ passes through the region *outside* both A and B, where F_A and F_B are both > 0. Since F is a convex combination of F_A and F_B it follows that $F(\mathbf{r}(\lambda),\lambda) > 1$ in this region and hence $F(A,B) > 1$, as proposed.
- If A and B overlap then, inside the region of overlap $A\cap B$, $F(\mathbf{r},\lambda) < 1$ independent of λ, since both F_A and F_B are less than zero there. This implies that $F(\mathbf{r}(\lambda),\lambda) < 1$ for all λ and hence $F(A,B) < 1$.
- Finally, if A and B touch exteriorly at $\mathbf{r}^*$, we have that $F(\mathbf{r}^*,\lambda) = 1$ for all λ as $F_A(\mathbf{r}^*) = F_B(\mathbf{r}^*) = 0$, so $F(\mathbf{r}(\lambda),\lambda) \le 1$. This precludes the path from going outside both A and B and hence there must be a λ^* such that $\mathbf{r}(\lambda^*) = \mathbf{r}^*$ so that $F(A,B) = F(\mathbf{r}^*,\lambda^*) = 1$.

The only implicit assumption we still have to prove is that $F(A,B)$ is in fact unique. This is easily accomplished by twice differentiating

$$\frac{d^2}{d\lambda^2}F(\mathbf{r}(\lambda),\lambda) = -2\mathbf{r}_{AB}\cdot\mathbf{C}\cdot\left(\lambda\mathbf{A}^{-1} + (1-\lambda)\mathbf{B}^{-1}\right)\cdot\mathbf{C}\cdot\mathbf{r}_{AB} < 0 \tag{2.92}$$

The inequality follows because all the matrices in the expression are positive definite. We have now shown that $F(\mathbf{r}(\lambda)\lambda)$ is indeed concave on the interval $[0,1]$ hence the maximum $F(A,B)$ is unique.

We now turn to the explicit calculation of $F(\mathbf{r}(\lambda)\lambda)$ which involves the computation of the matrix $\mathbf{C}$. Define

$$\mathbf{\Gamma} = \mathbf{C}^{-1} = \lambda\mathbf{A} + \mu\mathbf{B} \tag{2.93}$$

where we have introduced the shorthand $\mu = 1-\lambda$. We make use of the fact that Γ is a root of its own characteristic equation

$$Q(\xi) = \det\mathbf{\Gamma} - \xi\mathbf{1} = -\xi^3 + w_2\xi^2 - w_1\xi + w_0 \tag{2.94}$$

allowing us to find

$$\mathbf{C} = \mathbf{\Gamma}^{-1} = \frac{1}{w_0}\left\{\mathbf{\Gamma}^2 - w_2\mathbf{\Gamma} + w_1\mathbf{1}\right\} \tag{2.95}$$

The algebra involved in computing the coefficients w_j is much simpler than in the Vieillard-Baron case and we can give the result for two arbitray ellipsoids. Writing $A_j = R_{A,j}^2$ and $B_j = R_{B,j}^2$, we have

$$\begin{aligned}
w_0 &= \lambda^3 B_1 B_2 B_3 + \lambda^2\mu\left(\frac{1}{2}B_i B_j A_k(\hat{\mathbf{b}}_i \wedge \hat{\mathbf{b}}_j \cdot \hat{\mathbf{a}}_k)^2\right) \\
&\quad + \lambda\mu^2\left(\frac{1}{2}A_i A_j B_k(\hat{\mathbf{a}}_i \wedge \hat{\mathbf{a}}_j \cdot \hat{\mathbf{b}}_k)^2\right) + \mu^3 A_1 A_2 A_3 \\
w_1 &= \lambda^2(B_1B_2 + B_1B_3 + B_2B_3) \\
&\quad + \lambda\mu\left\{(A_1 + A_2 + A_3)(B_1 + B_2 + B_3) - A_iB_j(\hat{\mathbf{a}}_i \cdot \hat{\mathbf{b}}_j)^2\right\} \\
&\quad + \mu^2(A_1A_2 + A_1A_3 + A_2A_3) \\
w_2 &= \lambda(B_1 + B_2 + B_3) + \mu(A_1 + A_2 + A_3)
\end{aligned} \tag{2.96}$$

Using Eq. (2.91), $F(\mathbf{r}(\lambda), \lambda)$ is now easily calculated. Its maximization still has to be carried out numerically, but given the concavity of this function, an ultrafast routine like the Brent method [71] can be used.

OPTIMIZING THE OVERLAP TEST. It turns out to be computationally efficient to mix the two overlap criteria in such a manner that nonoverlaps are detected as economically as possibly. The following three-stage process is designed to do just this.

1. Test for overlap of the circumscribed spheres. If these do not overlap accept the move. Else
2. Evaluate the function $F(\mathbf{r}(\frac{1}{2}), \frac{1}{2})$ from the Perram–Wertheim criterion. If this is larger than unity we know that the ellipsoids do not overlap and can accept the move. Else
3. Perform the Vieillard-Baron test, which with its four subcriteria is the most involved.

The first two tests are "nonoverlap" tests, while the third is an "overlap" test.

f. Parallel Hard Particles. In a number of cases, it is of interest to study the properties of model systems with restricted orientations. Most common among these restricted orientation models are systems of parallel (hard) particles. Such model systems can be thought of as a limiting case of a system of freely rotating particles in a strong aligning field. The main

reason to study systems of parallel particles is that both the theoretical analysis and the numerical simulation of such systems is usually simpler than that of their freely rotating counterparts. This is particularly clear in the case of aligned ellipsoids. Any configuration of a system of aligned ellipsoids can be transformed into a configuration of hard spheres via a simple affine transformation. For instance, spheroids with an axial ratio α that are aligned along the z-axis, can be transformed to the corresponding hard-sphere system via the affine transformation $z \to z' = z/\alpha$. All systems of aligned ellipsoids (both uni-axial and bi-axial) are therefore equivalent to the hard-sphere system. Hence, the behavior of any system of aligned ellipsoids can be deduced from the behavior of the hard-sphere system at the same packing fraction.

However, for hard particles with other shapes, the aligned system is not trivially related to some known reference system. Here, we briefly review the overlap criteria for two model systems consisting of aligned particles.

ALIGNED SPHEROCYLINDERS. Consider a system of sphero-cylinders aligned along the z-axis. For convenience, we assume that all particles have the same diameter D, while the cylindrical part has a length L. In order to test whether two particles i and j overlap, we first compute z_{ij}, their distance in the z-direction, and $r_{ij}^{\perp}$, their distance in the xy-plane. Overlap between i and j is only possible if the following conditions are both satisfied:

$$z_{ij} < L + D \quad \text{and} \quad r_{ij}^{\perp} < D$$

Let us assume that these conditions are indeed satisfied. Then, if

$$z_{ij} < L$$

the cylindrical parts must overlap. In fact, if we study hard, parallel right cylinders (i.e., cylinders without a hemi-spherical cap), this is our final test. For spherocylinders, however, if $z_{ij} > L$, then we must test if the hemi-spherical caps overlap. The corresponding test is

$$(r_{ij}^{\perp})^2 + (z_{ij} - L)^2 < D^2$$

Clearly, the test for overlap between aligned spherocylinders is considerably simpler than the corresponding test for freely oriented spherocylinders.

ALIGNED TRUNCATED SPHERES. Next, consider truncated spheres with diameter D and thickness L, aligned along the z-axis. The test for overlap is extremely simple. If

$$z_{ij} > L$$

no overlap is possible. Otherwise, we simply apply the test for overlap between two spheres, that is,

$$r_{ij}^2 < D^2$$

g. Other Shapes. Finally, we briefly review a few other convex hard-core models that have been discussed in the literature. Although some of these bodies appear to have a simpler shape than the models discussed above, the test for overlap may be more involved.

RIGHT CYLINDERS. A case in point is a model consisting of right cylinders of length L and diameter D. The test for overlap between two such particles can be decomposed into several subtests. The first test is similar to the computation of the distance of closest approach between two spherocylinders. However, we can only use this test if the shortest vector between the axes of the two cylinders intersects both cylinders. Otherwise, we must test if the flat faces of the cylinders overlap (see Section. II.D.1). In the final test, we check if the flat face of one cylinder intersects the cylindrical part of the other. This test can be reduced to an overlap between coplanar ellipses (see Section. II.D.1). Clearly, this sequence of tests is feasible. However, it is more complex than the test for overlap between two spherocylinders.

OBLATE SPHEROCYLINDERS. An oblate model that could serve as an alternative to the truncated sphere is the so-called oblate spherocylinder. [46] This shape is obtained by moving the center of a sphere with diameter L over a circular disk with diameter D. In this case, the time-consuming step in the overlap test is the computation of the distance of closest approach between the toroidal rims of two oblate spherocylinders. Wojcik and Gubbins solve this problem by using an iterative minimization scheme. [46] Although such a scheme may be quite efficient in practice, we have limited ourselves to test schemes that are guaranteed to terminate in a finite number of steps.

"UFOs". Siders and co-workers [72,73] have considered an alternative model for an oblate molecule, namely the intersection volume of two equal hard spheres at a distance $r < D$ (where D is the diameter of the spheres). This object, called UFO by Siders et al., might, in some cases, serve as an alternative for oblate spheroids. The tests for overlap between UFOs are fairly straightforward.

GAUSSIAN CORE. Thus far, we have only considered models in which the individual particles have a well-defined geometry. However, as mentioned

earlier, this is a subclass of all hard-core interactions. The use of hard-core interaction that cannot be interpreted in terms of the "shape" of the individual particles has advantages and disadvantages. The advantage is that it is often possible to write very simple expressions for the potential energy function. The disadvantage is that much of our intuitive understanding of local packing effects is lost if we use a model in which individual particles do not have a "shape". Best known among these nongeometrical hard-core models is the so-called Gaussian-core model. [39,64] In this model, the form of the potential energy function is similar to that of hard spheres, that is,

$$u(r_{12}) = \begin{cases} 0, & r_{12} > \sigma_0 \\ \infty & r_{12} < \sigma_0 \end{cases}$$

But, unlike the hard-sphere case, σ_0 now depends on the orientations ($\hat{\mathbf{u}}_1$ and $\hat{\mathbf{u}}_2$) of the molecules, and the orientation of the vector $\mathbf{r}_{12}$ joining the centers of mass of the molecules:

$$\sigma(\mathbf{r}_{12}, \hat{\mathbf{u}}_1, \hat{\mathbf{u}}_2) = \sigma_0 \left(1 - \frac{\chi}{2}\left[\frac{(\hat{\mathbf{r}}_{12}\cdot\hat{\mathbf{u}}_1 + \hat{\mathbf{r}}_{12}\cdot\hat{\mathbf{u}}_2)^2}{1+\chi\hat{\mathbf{u}}_1\cdot\hat{\mathbf{u}}_2} + \frac{(\hat{\mathbf{r}}_{12}\cdot\hat{\mathbf{u}}_1 - \hat{\mathbf{r}}_{12}\cdot\hat{\mathbf{u}}_2)^2}{1-\chi\hat{\mathbf{u}}_1\cdot\hat{\mathbf{u}}_2}\right]\right)^{-1/2} \tag{2.97}$$

where χ is a measure of the nonsphericity of the molecule. For two parallel molecules lying side by side, $\sigma_\perp = \sigma_0$. If the same molecules are positioned end to end, $\sigma_\parallel = \sigma_0[(1+\chi)/(1-\chi)]^{1/2}$. Conversely, if we *define* the aspect ratio of the molecule as $\kappa \equiv \sigma_\parallel/\sigma_\perp$, then

$$\chi = \frac{\kappa^2 - 1}{\kappa^2 + 1}$$

For two parallel Gaussian hard-core molecules, the excluded volume is identical to that of parallel ellipsoids with the same aspect ratio. However, the Gaussian hard-core interaction and the hard ellipsoid interaction are not identical for nonparallel molecules. In fact, Perram et al. [74] have shown that the Gaussian hard-core model has a simple interpretation in terms of the function $F(\mathbf{r}, \lambda)$ defined in Eq. (2.85). Namely, that the overlap criterion in the Gaussian hard-core model corresponds to the criterion $F(\mathbf{r}, 1/2) = 1$. We recall that the latter criterion is the "quick" Perram–Wertheim test described in Section II.D.1. From the analysis below Eq. (2.85), it then follows immediately that the Gaussian overlap criterion is always an *upper bound* to the ellipsoid overlap criterion. Moreover, Perram et al. show that the difference between the two models becomes more pronounced with increasing nonsphericity of the molecules or, in the case of unlike molecules, when the molecules become more dissimilar. In fact, the available simulation data on hard-ellispoids and hard Gaussian-overlap models [39,64,75] appear to pass this test.

2. *Virial Coefficients*

Once the criterion for hard-core overlap between two convex hard bodies has been specified, we are in a position to study the properties of the model under consideration by computer simulation. Such simulations (either MC or MD) are usually performed on a model consisting of several hundreds to several thousands of particles. First, however, we briefly discuss a few-body calculation, namely the numerical evaluation of the virial coefficients of the system. The virial coefficients B_n with $n = 1, 2, 3, \ldots$, are the expansion coefficients of the compressibility factor $Z = PV/Nk_BT$ in powers of the number density $\rho \equiv N/V$:

$$Z = 1 + B_2\rho + B_3\rho^2 + \cdots \tag{2.98}$$

where we have used the fact that $B_1=1$. Clearly, knowledge of the first few virial coefficients would allow us to predict the equation of state of the model system at moderately low densities. This is important, because it provides an independent test of our MC or MD calculations, in which the equation of state is computed in a completely different fashion. The virial coefficients can be expressed in terms of sums of (multidimensional) integrals of the Mayer f-functions (see, e.g. Ref. [1]). Ree and Hoover [76] have shown that, for hard-core particles, the number of "diagrams" can be greatly reduced and that the resulting expressions lend themselves to numerical (Monte Carlo) evaluation. Although we do not discuss the Ree–Hoover scheme in any detail, we wish to point out that different implementations of the MC scheme are possible. In order to clarify this point, we need to know only one thing about the Ree–Hoover scheme to compute B_n, namely that the quantity that must be sampled is a function of the coordinates of n molecules and that a necessary (although not sufficient) condition for this function to be nonzero is that particle i overlaps with j, j with k , ... and l with i, where $i, j, k, \ldots, l$ is any permutation of $\{1, 2, 3, \ldots, n\}$. The schemes to compute the B_n are based on an algorithm to generate, in an unbiased way, configurations where 1 overlaps with 2,2 with 3 , ..., $n-1$ with n. The contribution of this configuration to the nth virial coefficient can then be evaluated by a series of tests for overlap (e.g., between n and 1) and nonoverlap, that are described in Ref. [76]. We only wish to point out that there are two distinct ways of generating the "open chain" configuration $1 - 2 - \cdots - n$. The simplest (and most common) is a dynamic scheme in which normal "Metropolis" sampling is performed on the coordinates of all n particles. Whenever a trial move "breaks" the chain from 1 to n, it is rejected. Although this scheme is simple, it has the disadvantage that there is appreciable correlation between successive configurations and, more importantly, the sampling becomes less efficient as

the molecules become more anisometric. The second scheme, which does not suffer form these drawbacks, is the "static" scheme. Here, a new, random chain conformation is generated from scratch at every step. In order to achieve this, one must be able to generate, with the correct probability, all configurations of molecule k that overlap with $k-1$. For extremely elongated molecules, the static scheme is, to our knowledge, the only feasible method to compute the higher virial coefficients. In order to explain the difference between the static and the dynamic schemes, consider the computation of the third virial coefficient of line segments in two dimensions. The third virial coefficient can be computed from the probability that line segment 3 overlaps with 1, given that 1 overlaps with 2 and 2 with 3. In the dynamic scheme, we would prepare the three lines such that the pairs 1–2 and 2–3 overlap. Next, we would perform a random trial displacement or rotation of one of the particles. If that trial moves maintains the 1–2 and the 2–3 overlap, it is accepted. Otherwise it is rejected. Of course, subsequent configurations are rather strongly correlated. Hence, there is not much point in testing for overlap between 3 and 1 after *every* trial move. In the static scheme, we fix particle 1. Next, we generate a trial orientation for particle 2 with a probability that is proportional to the pair-excluded volume of 1 and 2 for that particular orientation. Finally, we place the center of mass of 2 anywhere in this excluded volume. This procedure guarantees that 1 and 2 overlap and also that all overlapping configurations are generated with the correct statistical weight. We repeat the same procedure to insert particle 3 in such a way that it overlaps with 2. Finally, we test for overlap between 1 and 3. In this static scheme, there are no correlations between subsequent configurations. When comparing the static and dynamic schemes, we should bear in mind that the dynamic scheme is easier to implement than the static scheme. In particular, care should be taken in the static scheme that all trial configurations are generated with the correct weight. In contrast, in the dynamic scheme, a simple test for overlap suffices to accept or reject a trial configuration.

3. *Equation of State*

There exist several techniques to compute the pressure in a hard-core system. Although these techniques are, in principle, equivalent, they appear rather different. In molecular dynamics simulations, the most convenient starting point for computation of the pressure is based on the virial. This expression is based on the observation that, in a bounded N-particle system,

$$\sum_{i=1}^{N} \mathbf{p}_i \cdot \mathbf{r}_i$$

is bounded, where $\mathbf{p}_i$ is the momentum of particle i and $\mathbf{r}_i$ denotes the center of mass position of that particle. As the virial itself is bounded, its average time derivative is zero. This condition yields an expression that relates the average collisional momentum transfer along the line joining the center of mass of two collision partners to the pressure in the system:

$$P/(\rho k_B T) = 1 + \frac{1}{d} < \Delta\mathbf{P}_{ij} \cdot \mathbf{r}_{ij} > \tag{2.99}$$

where $\Delta\mathbf{P}_{ij}$ denotes the collisional momentum transfer between particles i and j, while $\mathbf{r}_{ij}$ denotes the vector joing the centers of mass of these particles and d is the dimensionality of the system. The angular brackets denote time averaging. In a hard-core molecular dynamics program, as the collisional momentum transfer has to be computed anyway, the computation of the pressure requires very little overhead. For more details, see Ref. [77].

Clearly, the above method to measure the pressure cannot be used in Monte Carlo simulations. A convenient technique to measure the pressure in such simulations is based on the fact that pressure is equal to (minus) the volume derivative of the Helmholtz free energy F

$$P = -(\partial F/\partial V)_{NT} \tag{2.100}$$

We can approximate the pressure by a ratio of finite differences:

$$P \approx -(\Delta F/\Delta V)_{NT} \tag{2.101}$$

Equation. (2.101) is a convenient starting point for a numerical scheme to measure P. To this end, we must compute the free energy difference between a system at volume V and the same system at a smaller volume $V' = V + \Delta V$. The free energy of a system of N molecules at volume V is given by $F = -k_B T \ln Q(N, V, T)$, with

$$Q(N, V, T) = \frac{q^N(T) V^N}{N!} \int_0^L \cdots \int_0^L d\mathbf{r}^N \, d\boldsymbol{\Omega}^N \exp(-\beta U(\mathbf{r}^N, \boldsymbol{\Omega}^N)) \tag{2.102}$$

where $\mathcal{V}_T$ is the part of the partition funtion that results from integration over the momenta (see Appendix A.A). It is convenient to rewrite Eq. (2.102) in a slightly different way. Let us assume that the system is contained in a cubic box with diameter $L = V^{1/3}$. We now define scaled coordinates $\mathbf{s}^N$, by

$$\mathbf{r}_i = L\mathbf{s}_i$$

for $i = 1,2,\ldots,N$. If we now insert these scaled coordinates in Eq. (2.102) we obtain

$$Q(N,V,T) = \frac{V^N}{V_T^N N!} \int_0^1 \cdots \int_0^1 d\mathbf{s}^N \, d\boldsymbol{\Omega}^N \, \exp(-\beta U(\mathbf{s}^N, \boldsymbol{\Omega}^N; L)) \quad (2.103)$$

In Eq (2.103), we have written $U(\mathbf{s}^N, \boldsymbol{\Omega}^N; L)$ to indicate that U depends on the *real* rather than the *scaled* distances between the particles. The expression for the Helmholtz free energy of the system is

$$\begin{aligned} F(N,V,T) &= -k_B T \ln Q \\ &= -k_B T \ln\left(\frac{V^N}{V_T^N N!}\right) \\ &\quad -k_B T \ln\left(\int d\mathbf{s}^N \, d\boldsymbol{\Omega}^N \, \exp(-\beta U(\mathbf{s}^N, \boldsymbol{\Omega}^N; L))\right) \end{aligned} \quad (2.104)$$

It is now straighforward to write down the expression for the pressure given in Eq. (2.101):

$$\begin{aligned} -\frac{\Delta F}{\Delta V} &= \frac{k_B T}{\Delta V} \ln(Q(V')/Q(V)) \\ &= \frac{k_B T}{\Delta V} \ln\left(\frac{V'^N \int d\mathbf{s}^N \exp(-\beta U(\mathbf{s}^N, \boldsymbol{\Omega}^N; V'))}{V^N \int d\mathbf{s}^N \exp(-\beta U(\mathbf{s}^N, \boldsymbol{\Omega}^N; V))}\right) \end{aligned} \quad (2.105)$$

or

$$P = P_{\text{id}} - \frac{k_B T}{\Delta V} \ln < \exp(-\beta \Delta U(\mathbf{s}^N)) > , \quad (2.106)$$

where $\Delta U \equiv U(\mathbf{s}^N, \boldsymbol{\Omega}^N; V) - U(\mathbf{s}^N, \boldsymbol{\Omega}^N; V')$. Equation. (2.106) may be interpreted as the acceptance probability of a *virtual* Monte Carlo move in which the volume is decreased from V to V'. Equation. (2.106) is valid if *all* nonoverlapping configurations of a system with volume V' correspond to nonoverlapping configurations of the system with the larger volume V. For convex hard bodies, this is indeed the case. For nonconvex hard bodies, one should measure the acceptance ratio of virtual volume changes from V to V', and vice versa. For more details, see Ref. [67].

An alternative scheme to determine the equation of state of a hard-body fluid in a Monte Carlo simulation, is to perform such simulations at constant pressure, [78,79] rather than at constant volume. If the pressure of a system of N particles is fixed at P, then the probability density to find that system in a particular configuration of the N molecules (as specified by $\mathbf{s}^N, \boldsymbol{\Omega}^N$) *and* a given volume V is given by

$$\mathcal{P}(V;\mathbf{s}^N,\boldsymbol{\Omega}^N) = \frac{V^N \exp(-\beta PV)\exp(-\beta U(\mathbf{s}^N,\boldsymbol{\Omega}^N;L))}{\int_0^\infty dV' V'^N \exp(-\beta PV')\int d\mathbf{s}^N d\boldsymbol{\Omega}^N \exp(-\beta U(\mathbf{s}^N,\boldsymbol{\Omega}^N;L'))}$$

We can carry out Metropolis sampling on the reduced coordinates $\mathbf{s}^N, \boldsymbol{\Omega}^N$ *and* on the volume V, with a weight function $\rho(\mathbf{s}^N, V)$ proportional to

$$\exp(-\beta\{U(\mathbf{s}^N,\boldsymbol{\Omega}^N;V) + PV - N\beta^{-1}\ln V\})$$

In the constant N, P, T MC method, V is simply treated as an additional coordinate, and trial moves in V must satisfy the same rules as trial moves in $\mathbf{r}$ (in particular, we should maintain the symmetry of the underlying Markov chain). Let us assume that our trial moves consist of an attempted change of the volume from V to $V' = V + \Delta V$, where ΔV is a random number uniformly distributed between over the interval $[-\Delta V_{\max}, +\Delta V_{\max}]$. In the Metropolis scheme, such a random, volume changing move will be accepted if

$$\exp(-\beta[U(\mathbf{s}^N,\boldsymbol{\Omega}^N;V') - U(\mathbf{s}^N,\boldsymbol{\Omega}^N;V) + P(V'-V) - N\beta^{-1}\ln(V'/V)]) > \mathcal{R} \tag{2.107}$$

where $\mathcal{R}$ is a random number, uniformly distributed over the interval $[0, 1]$.

4. *Some Results*

It is not our aim to review the large amount of numerical data that have been gathered on the static properties of isotropic hard-body fluids. In fact, several papers exist that discuss the comparison of the numerical results for virial coefficients and for equations of state of such fluids with various approximate theories. In particular, the excellent review by Boublik and Nezbeda [12] contains a compilation of the first five virial coefficients of prolate and oblate spherocylinders and ellipsoids, and of the first seven virial coefficients of hard spheres. Subsequently, several papers have appeared that discuss the equation of state or virial coefficients (of other hard-body fluids [38,39,64,80,81]. There are fewer systematic studies of the structure of hard-body fluids. However, a useful compilation of some of the numerical data can be found in a paper by Nezbeda et al.[61]

a. Virial Coefficients of Spherocylinders. Onsager's model plays a unique role in the theory of liquid crystals, because it is the only exactly solvable model with full translational and orientational degrees of freedom which exhibits a transition to the nematic phase. However, as explained in Section IV.A.2, the Onsager theory is only valid in the limit $L/D \to \infty$,

while most thermotropic liquid crystals have effective L/D ratios of 3 to 5. The reason why the Onsager theory cannot be used to describe molecular systems with such "small" L/D values is the following: an essential assumption in its derivation is that, in the expansion of the free energy in powers of the density, all virial coefficients B_n with $n > 2$ may be neglected. This condition is satisfied if $B_n/B_2^{n-1} \ll 1$. Onsager gave a qualitative argument to show that for large L/D, $B_3/B_2^2 \sim (D/L)\ln(L/D)$. Hence, in the limit $L/D \to \infty$, the reduced third virial coeffient does indeed vanish. Onsager made the plausible assumption that the higher virial coefficients can also be neglected in the same limit. Of course, the question arises if this assumption about the higher virial coefficients is indeed correct, and if so, how large L/D must be to observe this asymptotic behavior. Unfortunately, the virial coefficients compiled in Ref. [12] are limited to particles with a length to width ratio between 10 and 0.1. We therefore computed the third through fifth virial coefficient of hard spherocylinders as a function of L/D, for L/D between 1 and 10^5, [82,83] using the techniques described in Section II.D.2.

Figure 2.3 shows the L/D dependence of B_3/B_2^2, B_4/B_2^3 and B_5/B_2^4 for hard spherocylinders with L/D between 1 and 10^5. As can be seen from Fig. 2.3, the computed virial coefficients do indeed become small for large L/D. However, for B_4 and B_5 this decrease only sets in at rather large L/D values. This effect is seen more clearly by dividing the reduced virial coefficients by a factor proportional to the value that one should expect if the asymptotic L/D dependence was valid for all L/D; that is, $(D/L)\ln(L/D)$ for B_3 and D/L for B_4 and B_5. The resulting "scaled" virial coefficients are shown in Fig. 2.4. Apparently, for B_3 the asymptotic behavior already sets in for small L/D. Not so for B_4 and

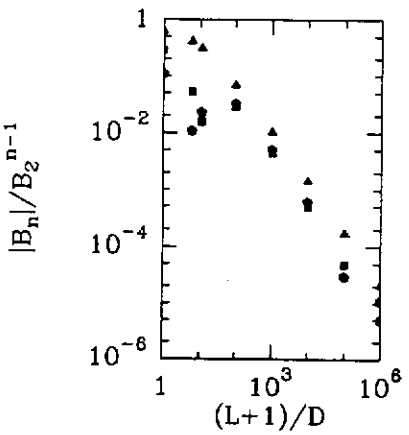

Figure 2.3. Virial coefficients spherocylinders. Filled triangles, B_3/B_2^2, filled squares, $|B_4|/B_2^3$ and filled pentagons, B_5/B_2^4. For $L/D \to \infty$, B_3 and B_5 are positive while B_4 is negative. For $L/D \to 0$, all three virial coefficients are positive.

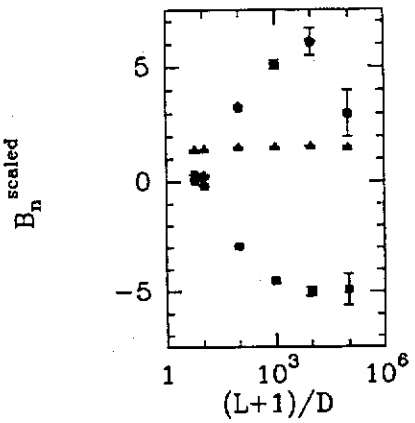

Figure 2.4. Scaled virial coefficients spherocylinders. To show the approach of the virial coefficients of hard spherocylinders to their asymptotic behavior, we plot $B_3/B_2^2 \times (L/D)/\ln(L/D)$ (▲), $B_4/B_2^3 \times (L/D)$ (■) and $B_5/B_2^4 \times (L/D)$ (⬟). As $L/D \to \infty$, these "scaled" virial coefficients are all expected to approach a constant value.

B_5. As can be seen from Fig. 2.4, the approach to the asymptotic behavior is only observed beyond $L/D = \mathcal{O}(10^2)$. The reason is that, whereas only one (positive) cluster integral contributes to B_3, B_4 and B_5 contain several contributions from diagrams of different sign and different asymptotic L/D dependence. The partial cancellation of these contributions is responsible for the behavior of B_4 and B_5 for small L/D. In the limit $L/D \to \infty$, only the leading diagram survives. This diagram is positive for odd n and negative for even n. Almost identical behavior is observed for the virial coefficients of hard ellipsoids. [84,85].

E. Structure

The pair structure of the hard ellipsoid fluid has been examined by Talbot and co-workers. [24,34] Here the interest lies in spherical harmonic expansions of the orientation dependence of $g(r, \mathbf{e}_1, \mathbf{e}_2)$, the success or otherwise of theories in fitting to the simulation results, and the use of alternative expansions, for example in the surface–surface distance. The surface–surface distance is calculated by a procedure due to Wertheim and Talbot. [86] For completeness we sketch it here.

1. Surface–Surface Distance for Ellipsoids

Consider two ellipsoids of revolution, with centre of mass positions $\mathbf{r}_i$ and $\mathbf{r}_j$ and with unit vectors along the symmetry axes $\mathbf{e}_i$ and $\mathbf{e}_j$. Both ellipsoids have semi-axes a and b. The surface of i is defined by

$$(\mathbf{r} - \mathbf{r}_i) \cdot \mathbf{A}_i^{-1} \cdot (\mathbf{r} - \mathbf{r}_i) = 1$$

where

$$\mathbf{A}_i = b^2 \mathbf{1} + (a^2 - b^2)\mathbf{e}_i \mathbf{e}_i \tag{2.108}$$

$$\mathbf{A}_i^{-1} = b^{-2}\mathbf{1} + (a^{-2} - b^{-2})\mathbf{e}_i\mathbf{e}_i \tag{2.109}$$

At any point $\mathbf{r}$ on the surface, the outward unit normal $\mathbf{n}_i$ lies in the direction $\mathbf{A}_i^{-1} \cdot (\mathbf{r} - \mathbf{r}_i)$. The point on the surface having a prescribed normal $\mathbf{n}_i$ is given by

$$\xi_i = \mathbf{r} - \mathbf{r}_i = \mathbf{A}_i \cdot \mathbf{n}_i / \sqrt{\mathbf{n}_i \cdot \mathbf{A}_i \cdot \mathbf{n}_i}$$

Similar expressions apply for j. The problem of finding the shortest distance between two ellipsoids reduces to finding three vectors, $\xi_{ij} = \mathbf{r}_{ij} + \xi_i - \xi_j, \mathbf{n}_j$ and $-\mathbf{n}_i$ all parallel. These vectors are shown in Fig. 2.1.

This suggests several iterative schemes, all based on an initial guess ξ_{ij} at the surface–surface vector. One simple approach is to calculate new values of ξ_i and ξ_j from

$$\xi_i' = -\frac{\mathbf{A}_i \cdot \xi_{ij}}{\sqrt{\xi_{ij} \cdot \mathbf{A}_i \cdot \xi_{ij}}} \quad \text{and} \quad \xi_j' = \frac{\mathbf{A}_j \cdot \xi_{ij}}{\sqrt{\xi_{ij} \cdot \mathbf{A}_j \cdot \xi_{ij}}} \tag{2.110}$$

that is, the surface points on each ellipsoid that would have ξ_{ij} as a normal. Then a new estimate $\xi_{ij}' = \mathbf{r}_{ij} + \xi_i' - \xi_j'$ would be mixed with the old ξ_{ij} in some proportion for the next iteration. In other words, we are iteratively solving the equation

$$\mathbf{C} \cdot \xi_{ij} = \mathbf{r}_{ij} \quad \text{with} \quad \mathbf{C} = \mathbf{1} + \frac{\mathbf{A}_i}{\sqrt{\xi_{ij} \cdot \mathbf{A}_i \cdot \xi_{ij}}} + \frac{\mathbf{A}_j}{\sqrt{\xi_{ij} \cdot \mathbf{A}_j \cdot \xi_{ij}}} \tag{2.111}$$

for ξ_{ij} given that $\mathbf{r}_{ij}$, $\mathbf{A}_i$, and $\mathbf{A}_j$ are fixed. An alternative approach is to write the equation as $\xi_{ij} = \mathbf{C}^{-1}\mathbf{r}_{ij}$ and solve this by iteration, setting at each stage $\xi_{ij}' = \mathbf{C}^{-1}(\xi_{ij}) \cdot \mathbf{r}_{ij}$. This seems to be slow to converge.

Starting from an initial guess at ξ_{ij} and the outward normals $\mathbf{n}_i = -\mathbf{n}_j = -\xi_{ij}/|\xi_{ij}|$, calculate revised values ξ_i' and ξ_j' from Eq. (2.110). From this, compute $\xi_{ij}' = \mathbf{r}_{ij} + \xi_i' - \xi_j'$ and new values $\mathbf{n}_i' = -\mathbf{n}_j' = -\xi_{ij}'/|\xi_{ij}'|$. The mixing factor for the next iteration is determined as follows. Construct the matrix

$$\mathbf{R} = \frac{\mathbf{A}_i - \xi_i\xi_i}{\sqrt{\mathbf{n}_i \cdot \mathbf{A}_i \cdot \mathbf{n}_i}} + \frac{\mathbf{A}_j - \xi_j\xi_j}{\sqrt{\mathbf{n}_j \cdot \mathbf{A}_j \cdot \mathbf{n}_j}}$$

and from it the matrix

$$\mathbf{K} = \frac{\mathrm{Tr}(\mathbf{R})(\mathbf{1} - \mathbf{n}_i\mathbf{n}_i) - \mathbf{R}}{\mathrm{Tr}(\mathrm{Cof}(\mathbf{R}))}$$

where Tr stands for trace and Cof($\mathbf{R}$) is the matrix of cofactors of $\mathbf{R}$. Then the old and new normals are mixed together in proportion $\mathbf{n}_i + \chi\mathbf{n}_i'$ where

$$\chi = \frac{|\xi_{ij}'|\xi_{ij}' \cdot \mathbf{K} \cdot \xi_{ij}'}{\xi_{ij}'^2 - (\xi_{ij}' \cdot \mathbf{n}_i)^2}$$

for the next iteration.

Talbot et al. [24] investigated the expansion of $g(r, \mathbf{e}_1, \mathbf{e}_2)$ in rotational invariants, discussed in Section II.C.1, for a range of ellipsoid shapes and densities. They compared their results with the standard theories of liquid structure, hypernetted chain (HNC) and Percus–Yevick (PY). A general result was that both these theories seem to give reasonable descriptions of the first few expansion functions for prolate ellipsoids with $e = 2, 3, 5$, with HNC being slightly superior. Moreover, the accuracy of the theories at a given packing fraction did not depend strongly on the elongation of the molecules, an encouraging and perhaps surprising result. The most stringent test is at high packing fraction, and for $e = 2$ the fluid phase extends at least up to $\rho/\rho_{cp} = 0.8$, well above the freezing point for the hard-sphere fluid. Indeed, at this density, solutions to the HNC equations could not be obtained. Nonetheless, agreement with PY is still fair for most of the expansion functions. The exception is the function $g_{222}(r)$, which seems to be very sensitive to inaccuracies in the theory, especially at short range.

For oblate ellipsoids with $e = \frac{1}{3}$, at the single density studied, $\rho/\rho_{cp} = 0.5$, the HNC theory is once more in reasonable agreement with simulation results. PY, however, is rather poor for this case for several of the expansion functions.

A disadvantage of expanding $g(r, \mathbf{e}_1, \mathbf{e}_2)$ is that the higher coefficients do not decrease quickly in magnitude, that is, the expansion does not converge very well. Talbot et al. [34] investigated the consequences of expanding the function $G(s, \mathbf{e}_1, \mathbf{e}_2)$ discussed in Section II.C.1, where s is the surface–surface distance. This seems to bring the expected benefits of more rapid convergence. Moreover, once the (exactly calculable) effects of the surface Jacobian $S(s)$ are taken into account, the expansion functions seem to be quite short-ranged in s. This breakdown succeeds in highlighting certain physical features of the packing in dense liquids, such as the preference for prolate ellipsoids to pack side by side. Various properties characterizing pairs in contact, such as the pressure and the collision rate, are easily related to the appropriate functions in the limit $s \to 0$. This approach also leads to a description of the structure in terms of the isotropically averaged pair distribution function $g_{iso}(s)$, which, at least at short distances, is very similar to the hard-sphere pair distribution function for the same packing fraction and molecular volume. Finally, in this study, the use of surface–surface functions as a route to the orientational correlation parameter g_2 was examined. It was shown that the function $g_2(s)$ can be separated into a short-range excluded volume component and a longer range term. There

is a substantial contact contribution to g_2. However, it was also evident that, in both centre–centre and surface–surface decompositions, the longer range component makes a significant contribution to the integrated value g_2 measured, for example, in depolarized light scattering experiments. For details, we refer the reader to Ref. [34].

III. DYNAMICAL PROPERTIES

A. Transport Phenomena in Isotropic Phases

The time evolution of a dynamical quantity in a system comprised of HCBs arises from the action of free streaming (uninterrupted translation and rotation) and collisions. Free streaming is implemented into the dynamics by operators akin to the infinitesimal generators of free translation and rotation. In hard-particle systems, collisions are strictly two-body events and for convex bodies, the colliding bodies touch at only one point at any instant. The effect of a collision on a property is represented by binary collision operators and owing to the nature of impulsive force laws, the physical content of a binary collision operator is exceedingly simple. The binary collision operator determines if two particles are approaching and are at a contact separation. If these conditions are satisfied, then the incoming particle momenta are replaced by the restituting momenta, derived on the basis of the conservation laws for linear and angular momentum and kinetic energy. Since the colliding bodies are smooth and convex, the collisional impulse is directed along the surface normal at the point of impact.

The development of a kinetic theory of rigid convex bodies was due to Curtiss and his co-workers [87–96]. Equations of motion, BBGKY hierarchies and collision operators derived by the Curtiss school were natural extensions of the Chapman–Enskog hard-sphere kinetic theory. [97,98] Much of the progress in the calculation of dynamical properties of HCB systems has resulted from exploiting the analogies with hard-sphere systems. Even the accommodation of the angular momentum and the orientational angles appropriate to HCB collisions has been influenced by the techniques developed for hard spheres. As a result of these efforts, transport coefficients and spectra of fluids of HCBs can be obtained nearly to the same level of rigor as that for hard-sphere systems. The development of HCB transport theory has not been greatly influenced by the adoption of special coordinate systems which restrict analysis to a certain shape (e.g., an ellipsoid or a spherocylinder). Rather the techniques developed by Curtiss, Dahler and Hoffman allow transport properties, for hard spheres and for HCBs of arbitrary shape, to be treated on the same footing.

The HCB kinetic theory has several basic ingredients:

1. the definition of the Liouville operator (hereafter called the pseudo-Liouville operator since it will prove to be non self-adjoint); [99]
2. a systematic method for the derivation of formal [100] and at the same time operational [101] expressions that permit the computation of transport coefficients and time correlation functions;
3. an exact way to perform the collision integrals over the momentum and orientational angles decribing the phase space for a two body encounter. [95]

B. Time Evolution Operators

The time evolution of HCB systems was cast in a binary collision operator formalism by Cole et al. [99] and here we begin with a summary of their findings. Consider the time evolution of an arbitrary dynamical variable, $A(\Gamma)$ where Γ denotes the phase space coordinates of the N particle system. By Liouville's theorem, $A(\Gamma)$ evolves in time according to

$$\begin{aligned} A(\Gamma;t) &= \exp(iLt)A(\Gamma;0) \\ &= A(\exp(iLt)\Gamma) = A(\Gamma(t)) \end{aligned} \tag{3.1}$$

When the potentials are soft and differentiable, the operator iL is a linear differential operator and Eq. (3.1) generates a series expansion in time. However, when the forces are impulsive, there is no meaning to an expansion of Eq. (3.1) in terms of the spatial derivatives of delta function forces. Instead one must reinterpret the formal time evolution operator and separate iL into a free streaming, iL_0, and an interaction $(iL - iL_0)$ part. Likewise, the dynamics are to be treated using this same separation,

$$\exp(iLt) = \exp(iL_0t) + \int_0^t d\tau \exp(iL\tau)(iL - iL_0) \exp(iL_0(t - \tau)) \tag{3.2}$$

where the streaming operator (for rotor and spherical tops) is given by

$$iL_0 = \sum_j (\mathbf{v} \cdot \nabla_{\mathbf{r}} + (\omega \times \hat{\mathbf{u}}) \cdot \nabla_{\hat{\mathbf{u}}})_j \tag{3.3}$$

Next, we "coarse-grain" time, that is, we divide time into bins of width ϵ, and stipulate that it is during the interval ϵ that a collision occurs. In this view, one replaces the collection of terms in the $(iL - iL_0)$ part of Eq. (3.2) with three terms: first, a free propogation operator, $\exp(iL_0(t - \tau))$, which places the system at the beginning of the desired time bin; second, an operator which constructs the difference between the post- and precollision values of the system during the time interval ϵ; and third,

an operator $\exp(iL\tau)$ which propagates the system under the influence of the full Liouvillian. The explicit time evolution operator satisfying these conditions is

$$\exp(iL(\epsilon)t) = \exp(iL_0 t) + \int_0^t d\tau \exp(iL\tau)T(\epsilon) \exp(iL(t-\tau)) \quad (3.4)$$

where

$$T(\epsilon) = \delta\left(s - \frac{1}{2}|ds/dt|\epsilon\right)|ds/dt|H(-ds/dt)(\mathbf{b} - 1) \quad (3.5)$$

s is the surface-to-surface separation of two bodies measured along $\hat{\mathbf{s}}$, the surface normal. ds/dt is the velocity along $\hat{\mathbf{s}}$ (to be given explicitly later) and $\mathbf{b}$ is an operator which converts precollision momenta to their post-collision values and vice versa. The binary collision operator, $T(\epsilon)$, registers a collision provided the particles are approaching (negative ds/dt) and reside infinitestimally outside the contact surface. [102] The curious $\frac{1}{2}\epsilon$ in Eq. (3.5) arises as a consequence of the mean value theorem which specifies that one locate the collision to be half-way through the coarse-grained time period ϵ. Finally, the Liouville operator is given by the $\epsilon \to 0$ limit. We suppress ϵ in all the equations to follow but note that the ϵ limit must be taken at the end of the calculation rather than at the outset.

Equation (3.4) defines an expansion of the system evolution operator which allows one to evaluate time correlation functions of the form

$$< B(0)|A(t) >= \int d\Gamma f^N(\Gamma)B(\Gamma) \exp(iLt)A(\Gamma) \quad (3.6)$$

where $f^N(\Gamma)$ is the N particle equilibrium distribution function. For soft potentials, a parts integration of Eq. (3.6) yields

$$< B(0)|A(t) >= \int d\Gamma A(\Gamma) \exp(-iLt)f^N(\Gamma)B(\Gamma) \quad (3.7)$$

and both Eqs. (3.6) and (3.7) are equivalent. To make hard particles abide by Eqs. (3.6) and (3.7), some effort is needed and this issue has been discussed on several occasions by Ernst et al. [102,103] for spherical systems. The complication for hard-body systems arises because of the combined effect of the streaming operators and the discontinuous nature of f^N. When two particles overlap, $f^N = 0$, whereas at a separation infinitesimally exterior to the excluded volume surface, f^N is nonzero.

The action of iL_0 on f^N is to introduce delta functions that have the appearance of terms in the collision operator. In other words, when we derive a result equivalent to Eq. (3.7) for HCB systems, the binary collision

operator will have to be altered. Provided that the f^N function is to the left of iL, no infinities are produced by the action of iL_0. In order to retain the property of Eq. (3.7), we must replace $\exp(-iLt)f^N(\Gamma)$ by its Hermitian adjoint, (denoted by †), defined through the relation

$$\int d\Gamma B(\Gamma)X(\Gamma)A(\Gamma) = \int d\Gamma (X(\Gamma)B(\Gamma))^\dagger A(\Gamma) \tag{3.8}$$

where $X(\Gamma)$ is an arbitrary operator and $A(\Gamma)$ and $B(\Gamma)$ two arbirtrary functions of the phase space coordinates.

To construct the adjoint of the hard body Liouville operator, consider the $< B|iL|A >$ matrix element. First we integrate the streaming operator,

$$\int d\Gamma f^N(\Gamma)B(\Gamma)iLA(\Gamma)$$
$$= \int d\Gamma(-A(\Gamma)iL_0(B(\Gamma)f^N(\Gamma)) + f^N(\Gamma)B(\Gamma)TA(\Gamma)) \tag{3.9}$$

and we note that [99]

$$\int d\Gamma f^N(\Gamma)B(\Gamma)TA(\Gamma) = \int d\Gamma A(\Gamma)T^\dagger B(\Gamma)f^N(\Gamma) \tag{3.10}$$

where

$$T^\dagger = (ds/dt)\delta(s)(H(ds/dt)\mathbf{b} + H(-ds/dt)) \tag{3.11}$$

Combining Eqs. (3.9), (3.10) we find

$$\int d\Gamma f^N(\Gamma)B(\Gamma)iLA(\Gamma) = \int d\Gamma A(\Gamma)(iL(f^N(\Gamma)B(\Gamma)))^\dagger \tag{3.12}$$

so that the adjoint of iL is given by

$$(iL)^\dagger = -iL_0 + T^\dagger \tag{3.13}$$

and accordingly

$$< B(0)|A(t) > = \int d\Gamma f^N(\Gamma)B(\Gamma)\exp(iLt)A(\Gamma)$$
$$= \int d\Gamma A(\Gamma)\exp((-iL_0 + T^\dagger)t)[f^N(\Gamma)B(\Gamma)]^\dagger \tag{3.14}$$

A consequence of Eq. (3.14) is that the time evolution of the distribution function is described by a Liouville operator different from that used to

describe the time evolution of a dynamical variable and this difference is reflected directly in the equations of motion for a dynamical variable

$$dA(\Gamma;t)/dt = (iL_0 + T)A(\Gamma;t) \tag{3.15}$$

and for the full N particle distribution function $f^N(\Gamma;t)$

$$(\partial/\partial t)f^N(\Gamma;t) = (-iL_0 + T^\dagger)f^N(\Gamma;t) \tag{3.16}$$

It then follows that the first member of the BBGKY hierarchy, $f(1;t)$, the singlet distribution function obeys

$$(\partial/\partial t)f(1;t) = -iL_0 f(1;t) + \int_0^t d2T_{12}^\dagger f(1,2;t) \tag{3.17}$$

where $f(1,2;t)$ is the pair distribution function. Here the reduced distribution functions are defined by

$$f(1,2,...n;t) = (N!/(N-n)!)\int d(n+1)...dN f^N(\Gamma;t) \tag{3.18}$$

This completes our analysis of the time evolution of an arbitrary dynamical variable and the phase space distribution function.

C. Time Correlation Functions

There are several ways to calculate a general transport coefficient in the Enskog (uncorrelated collision) approximation. Broadly, these procedures are based on a linear response theory in which the "disturbance" is a shear gradient, a temperature gradient or a concentration gradient and the response is a momentum, energy or a diffusion current, respectively. [97,98] For the specific case of a linear response theory for the shear viscosity, one would calculate the stress tensor as a consequence of the imposed shear gradient and the coefficient relating stress to strain is the shear viscosity. The "Enskog" method for the calculation of a transport coefficient or more generally those appproaches based on the use of the distribution function were shown by Ernst et al. [102,104,105] to be equivalent to the flux–flux time correlation function approaches. All of the usual facets of Enskog kinetic theory (basis functions expansions, the factorization ansatz of the precollisional $f(1,2;t)$) [106] also arise in the analysis of flux–flux time correlation functions.

Some of the vestiges of distribution function Enskog kinetic theory can be avoided and the resulting calculations simplified by the use of a Mori projection operator. In this approach, practiced by Forster, [107] Mazenko, [108] Mazenko and Yip, [109] Evans [101] and summarized suc-

cinctly by Hansen and McDonald, [1] one applies the Mori method (with one or two primary variables) to derive a generalized Langevin equation for the flux–flux time correlation function. Apart from some simple thermodynamic functions, the decay rates for the flux–flux time correlation function are the transport coefficients. We will illustrate this method by the calculation of a few single particle properties, hydrodynamic collective properties and purely position dependent orientational properties.

From the above paragraphs, it would appear that there are two distinct schools of thought: those involved with the construction of BBKGY hierarchies for the singlet and pair distribution function (motivated by the desire to derive improved Boltzmann–Enskog equations of motion) and those concerned with the derivation of generalized Langevin equations for the flux time correlation functions. Sung and Dahler [110–112] have taken a middle road and have derived generalized Langevin equations for the tagged particle distribution function and the untagged members of the surrounding fluid. The Mori techniques used by Sung and Dahler are precisely the same techniques that we use here. It seems to us that the transport theory is both simpler to use and to understand if one takes a limited description and focusses attention on the flux time correlation functions rather than on the phase space distribution function. We illustrate this method by the calculation of a few single particle properties, hydrodynamic collective properties and purely position dependent orientational properties.

1. Single Particle Properties

The simplest transport properties to understand for a fluid of nonspherical molecules are the self diffusion coefficient D_s

$$D_s = (1/3)\int_0^\infty dt < \mathbf{v}(0)\cdot\mathbf{v}(\mathbf{t}) >= \int_0^\infty dt C_v(t) = k_B T/(mf_s) \qquad (3.19)$$

and the rotational diffusion coefficient D_ω

$$D_\omega = (1/2)\int_0^\infty dt < \omega(0)\cdot\omega(\mathbf{t}) >= \int_0^\infty dt C_\omega(t) = k_B T/(If_\omega) \qquad (3.20)$$

where $C_v(t)$ and $C_\omega(t)$, are the linear and angular momentum time correlation functions, respectively. Accompanying the diffusion coefficients are the friction coefficients f_s and f_ω which are also used in the preceding two equations.

We illustrate the Mori method by a calculation of f_ω. The choice of f_ω rather than f_s was made in order to demonstrate the role of nonsphericity which clearly governs angular momentum relaxation but is only

of secondary importance for linear momentum relaxation. The Mori method allows one to derive an exact generalized Langevin equation for $C_\omega(t)$ [113,114]

$$(\partial/\partial t)C_\omega(t) = -f_\omega^E C_\omega(t) - \int_0^t d\tau \nu_\omega(\tau) C_\omega(t-\tau) \tag{3.21}$$

In the parlance of Hansen and MacDonald, [1] f_ω^E is the direct term,

$$f_\omega^E = - < \omega \cdot |T|\omega > / < \omega^2 > \tag{3.22}$$

also the single variable Enskog friction, and $\nu_\omega(\tau)$ is the indirect term

$$\nu_\omega(\tau) = - < \omega \cdot |T \exp(iQ_\omega L Q_\omega \tau) Q_\omega T|\omega > / < \omega^2 > \tag{3.23}$$

with

$$Q_\omega = 1 - |\omega > [I/(2\beta)] < \omega| \tag{3.24}$$

and is a measure of the correlations usually ignored in Enskog theory. By means of Eqs. (3.21)–(3.24), one can associate the total friction with the sum of the direct and the indirect terms

$$f_\omega = f_\omega^E + \int_0^\infty dt \nu_\omega(t) \tag{3.25}$$

The Enskog (or direct) term f_ω^E involves a single binary collision operator, whose matrix elements can be determined easily. This term measures the uncorrelated impulses on the surface of the tagged particle as weighted by the anisotropic pair correlation function of the system.

The indirect term, $\nu_\omega(t)$, is more complex as it contains both the dilute gas and the dense gas/liquid classes of correlations. The gas phase correlations omitted from a single variable Enskog theory and contained in $\nu_\omega(t)$ reflect two effects: (1) that ω is not an exact eigenfunction of T and T couples ω (fortunately only weakly) to higher Sonine polynomials of ω and $\mathbf{v}$ (see Refs. [115,116]) and (2) that a colliding pair may suffer a chattering collision. [99,117] A chattering collision arises when a particular trajectory has more than one impulsive encounter. In the context of a binary collision expansion, the chattering sequences arise from products of T operators such as $T_{12} \exp(iL_0 t) T_{12}$, that is, an initial 1,2 impact with the hard core, free propagation for a time t, followed by another 1,2 impact. It is precisely this class of collisions that are eliminated from all hard-sphere binary collision expansions [118,119] although these same col-

lision sequences are particularly important for rotational energy relaxation cross sections. [117] Neither the Sonine nor the chattering corrections to f_ω alters the density dependence from its Enskog value.

The liquid phase correlations present in $\nu_\omega(t)$ reflect the role of solvent induced recollisions of a specific pair of molecules [113,114,120] and this process has a direct influence on the density dependence of f_ω. To incorporate some of the solvent induced correlated collisions in $\nu_\omega(t)$, one must represent the resolvent $\exp(iQ_\omega LQ_\omega t)$ (alias the recollision operator) with basis functions having the same symmtery as $T\omega$. One such function is ϕ_ω,

$$\phi_\omega = \mathbf{r}_{12} \times \hat{\mathbf{s}}\Delta(s) \tag{3.26}$$

where the "delta" function has the property that

$$\Delta(s) = \begin{cases} 1, & \text{if } 0 < s < d \\ 0, & \text{otherwise} \end{cases} \tag{3.27}$$

and d is a small (but noninfinitesimal) distance. ϕ_ω is square normalizable function that behaves like a torque exerted by the solvent on the contact surface of the tagged particle. Using the time reversal properties of T, one can show that

$$\nu_\omega(\tau) = [< \omega \cdot |iL|\phi_\omega > / < (\phi_\omega)^2 >]^2 < \phi_\omega(0) \cdot \phi_\omega(t) > / < \omega^2 > \tag{3.28}$$

where all of the static matrix elements can be determined exactly and $< \phi_\omega(0) \cdot \phi_\omega(t) >$ can be approximated using diffusional (Smoluchowski) modelling. [113,114] Thus, the rotational friction follows from Eq. (3.25) where f_ω^E is given by Eq. (3.22) and $\nu_\omega(t)$ from Eq. (3.28) The predictions of Enskog theory and the utility of the recollision corrections to the rotational friction will be assessed in subsequent sections.

2. *Collective Properties*

There are many transport coefficients for polyatomic fluids [121] and in principle all of these should be determined. For the present purposes, we will demonstrate how the Mori, generalized Langevin method described in the previous section provides a mechanism for the calculation of the shear viscosity η and the thermal conductivity λ of a pure fluid of HCBs. [101]

Several methods have been applied to the calculation of the transport properties of fluids of HCBs. Theodosopulu and Dahler, [122–124] Jagannathan, et al. [125] and Cole et al., [126] Cole and Evans, [35] and Evans [101] have provided distinct means for the determination of transport coefficients. In the work of the Dahler group, kinetic equations were

derived for the phase space density and these equations were solved by moment methods developed by Grad. [127] In the Cole, Evans and Hoffman works, [35] the transport properties were expressed as a time correlation function and the method of Ernst (developed for hard spheres) [104,105] was applied to transform the time correlation function expressions into distribution function schemes so that the usual Enskog factorizations and expansions could be made. For both the Dahler and the Ernst methods, the operating expressions for the evaluation of the transport coefficients are complicated and in the end, the relationship of the computed transport coefficients to the hard-sphere limit is not always clear. A direct time correlation function approach, [1,101] based on the Mori method is, in our opinion, simpler and leads to results of some generality. Cole et al. [126] Cole and Evans, [35] and Theodosopulu and Dahler [122–124] found that "new" collisional integrals arose in the transport coefficient calculations which incorporated the nonlocal nature of the collision event. In the present approach, these non-local corrections follow as matrix elements of the binary collision operator.

We begin with a calculation of the shear viscosity, η. Accordingly we introduce the collective variable whose decay defines η : the $\mathbf{k}$-space current density [1]

$$\mathbf{v}(\mathbf{k},t) = \sum_i \mathbf{v}_i(t)\, \exp(i\mathbf{k}\cdot\mathbf{r}_i(t)) \tag{3.29}$$

along with its transverse part,

$$\mathbf{J}(\mathbf{k},t) = i\mathbf{k}\times\mathbf{v}(\mathbf{k},t) \tag{3.30}$$

From linear response theory, the time correlation function of the fluctuating current density obeys a phenomonological decay law

$$m\rho(\partial/\partial t) < \mathbf{J}(-\mathbf{k},0)\cdot\mathbf{J}(\mathbf{k},t) >= -\eta k^2 < \mathbf{J}(-\mathbf{k},0)\cdot\mathbf{J}(\mathbf{k},t) > \tag{3.31}$$

with a decay rate of $k^2\eta/(m\rho)$. So, to calculate η one must derive an analogous but microscopic equation for the time correlation function of the fluctuating current density and associate the decay rate with $k^2\eta/(m\rho)$.

In the Mori, generalized Langevin method, one writes the kinetic equation for the transverse momentum density time correlation function as [128]

$$(\partial/\partial t)C(\mathbf{k},t) = -\nu_1 C(\mathbf{k},t) - \int_0^t d\tau \nu_2(\tau) C(\mathbf{k},t-\tau) \tag{3.32}$$

with

$$\nu_1(\mathbf{k}) = - < \mathbf{J}(-\mathbf{k})|iL|\mathbf{J}(\mathbf{k}) > /C(\mathbf{k}) \tag{3.33}$$

$$\nu_2(\mathbf{k},\tau) = - < \mathbf{J}(-\mathbf{k})|iL \exp(iQLQ\tau)iQL|\mathbf{J}(\mathbf{k}) > /C(\mathbf{k}) \quad (3.34)$$

$$C(\mathbf{k}) = C(\mathbf{k}, t = 0) \quad (3.35)$$

$$Q_J = 1 - |\mathbf{J}(\mathbf{k}) > [C(\mathbf{k})]^{-1} < \mathbf{J}(-\mathbf{k})| \quad (3.36)$$

and

$$C(\mathbf{k},t) =< \mathbf{J}(-\mathbf{k},0) \cdot \mathbf{J}(\mathbf{k},t) > \quad (3.37)$$

By comparison of the phenomonological decay law, Eq. (3.31), with the generalized Langevin result, Eq. (3.32), one obtains

$$\eta = \lim_{k,z\to 0} \eta(k,z)$$

$$\eta(k,z) = m\rho(\nu_1(\mathbf{k}) + \int_0^\infty dt \exp(-zt)\nu_2(\mathbf{k},t))/k^2 \quad (3.38)$$

where η is the zero frequency ($z = 0$), zero wave vector ($k = 0$) limit of the k, z dependent shear viscosity. For soft potentials, $\nu_1(\mathbf{k})$ vanishes and $\nu_2(\mathbf{k}, t)$ is the wave vector dependent time correlation function of the fluctuating part of the stress tensor. For hard bodies, $\nu_1(\mathbf{k})$ is a nonvanishing, positive definite collisional term (the "direct" part of η) which can be determined exactly. $\nu_2(\mathbf{k}, t)$, the "indirect" part of $\eta(k, z)$, can be determined by approximating the resolvent operator and we do this in the spirit of traditional kinetic theory methods (such as in Grad's method of moments [127] or early Enskog theory [97,98]).

The simplest approach to unravel the memory function is to represent the projected time evolution operator, $\exp(iQ_JLQ_Jt)$, by a single basis function, $\phi(\mathbf{k})$,

$$\phi(\mathbf{k}) = iL_0\mathbf{J}(\mathbf{k}) \quad (3.39)$$

which is the convective derivative of the flux in question. In this single Hermite polynomial, Enskog approximation, appropriate at dilute gas densities, $\nu_2(\mathbf{k}, t)$ becomes

$$\nu_2(\mathbf{k},t) = < \mathbf{J}(-\mathbf{k})|iL|\phi(\mathbf{k}) >< \phi(-\mathbf{k})|\exp(iQLQt)|\phi(\mathbf{k}) > \times < \phi(-\mathbf{k})|iQL|\mathbf{J}(\mathbf{k}) > /(\Omega^4(\mathbf{k})C(\mathbf{k})) \quad (3.40)$$

where

$$\Omega^2(\mathbf{k}) =< \phi(-\mathbf{k})|\exp(iQLQt)|\phi(\mathbf{k}) > \quad (3.41)$$

Since $\mathbf{J}(\mathbf{k})$ and $\phi(\mathbf{k})$ have different time reversal symmetries, then

$$< \mathbf{J}(-\mathbf{k})|iL|\phi(\mathbf{k}) >= - < \phi(\mathbf{k})|iQL|\mathbf{J}(\mathbf{k}) >^* \tag{3.42}$$

and if the projected time dependence of $\phi(\mathbf{k})$ is dominated by collisional relaxation rather than by convection, then

$$< \phi(-\mathbf{k})|\exp(iQLQt)|\phi(\mathbf{k}) > \simeq < \phi(-\mathbf{k})|\exp(Tt)|\phi(\mathbf{k}) > \tag{3.43}$$

On this basis, $\nu_2(\mathbf{k}, t)$ becomes

$$\begin{aligned} \nu_2(\mathbf{k}, t) &= |< \phi(-\mathbf{k})|iL|\mathbf{J}(\mathbf{k}) >|^2 \\ &\quad \times < \phi(-\mathbf{k})|\exp(Tt)|\phi(\mathbf{k}) > /[\Omega^4(\mathbf{k})C(\mathbf{k})] \\ &= [1 + q_\eta(\mathbf{k})]^2 < \phi(-\mathbf{k})|\exp(Tt)|\phi(\mathbf{k}) > /C(\mathbf{k}) \end{aligned} \tag{3.44}$$

with

$$q_\eta(\mathbf{k}) = < \phi(-\mathbf{k})|T|\phi(\mathbf{k}) > /\Omega^2(\mathbf{k}) \tag{3.45}$$

To complete the reduction of $\nu_2(\mathbf{k}, t)$, we represent the inverse of T by a single function, $\phi(\mathbf{k})$ itself, so that

$$\int_0^\infty dt\, \exp(-zt) < \phi(-\mathbf{k})|\exp(Tt)|\phi(\mathbf{k}) >= \Omega^2(\mathbf{k})/(z + \nu_3(\mathbf{k})) \tag{3.46}$$

with

$$\nu_3(\mathbf{k}) = |< \phi(-\mathbf{k})|T|\phi(\mathbf{k}) >|/\Omega^2(\mathbf{k}) \tag{3.47}$$

and finally [101]

$$\int_0^\infty dt\, \exp(-zt)\nu_2(\mathbf{k}, t) = [(1 + q_\eta(\mathbf{k}))\Omega(\mathbf{k})]^2/[C(\mathbf{k})(z + \nu_3(\mathbf{k}))] \tag{3.48}$$

Thus, the shear viscosity follows from the Eq. (3.38) as the sum of the direct part, given by Eq. (3.33) and the indirect part, given by Eq. (3.48).

The thermal conductivity, λ, is determined by precisely the same approach as used for the shear viscosity. [101] Now we associate $\mathbf{J}(\mathbf{k}, t)$ with the local kinetic energy density, $\mathbf{J}_E(\mathbf{k}, t)$

$$\mathbf{J}_E(\mathbf{k}, t) = \sum_i \left(\frac{1}{2}\right)[mv_i^2 + I\omega_i^2 - 5k_BT]\, \exp(i\mathbf{k} \cdot \mathbf{r}_i(t)) \tag{3.49}$$

which obeys a linear transport equation

$$m\rho C_v(\partial/\partial t) < \mathbf{J}_E(-\mathbf{k}, 0)\cdot\mathbf{J}_E(\mathbf{k}, t) >= -k^2\lambda < \mathbf{J}_E(-\mathbf{k}, 0)\cdot\mathbf{J}_E(\mathbf{k}, t) > \tag{3.50}$$

As a result of an analysis completely analogous to that applied to the shear

viscosity, we find that λ is the zero frequency, zero wave vector limit of the full $\lambda(k,z)$, thus

$$\lambda = \lim_{k,z\to 0} \lambda(k,z)$$

$$\lambda(k,z) = m\rho C_v(\nu_1(\mathbf{k}) + \int_0^\infty dt\, \exp(-zt)\nu_2(\mathbf{k},t))/k^2 \qquad (3.51)$$

where $\nu_1(\mathbf{k})$ is given by Eq. (3.33) and $\nu_2(\mathbf{k},t)$ by Eq. (3.48) with $\mathbf{J}_E$ replacing $\mathbf{J}$. The shear viscosity and the thermal conductivity obtained from this procedure are summarized in a subsequent section.

3. *Positional and Orientational Properties*

Both the single particle and collective transport properties discussed in the previous sections were derived from time correlation functions of momentum variables which changed as a consequence of collisions. When dealing with time correlation functions of collisionally conserved dynamical variables, such as positions and orientations, another version of the Mori method is needed and this version uses two rather than one primary variable. [129,130]

Consider a time correlation function of the form

$$C_A(t) = < A(0)|A(t) > / < A|A > \qquad (3.52)$$

where A is a positional collisional invariant. If two primary variables, A and its first derivative, $iL_0A \equiv \dot{A}$, are employed in a Mori analysis, one obtains an identity for a frequency component of $C_A(t)$ in the form of a two term continued fraction

$$C_A(z) = \int_o^\infty dt\, \exp(-zt)C_A(t)$$

$$= 1/[z + \Omega^2/(z + \nu_1 + \nu_2(z))] \qquad (3.53)$$

Here

$$\Omega^2 = < \dot{A}^2 > / < A^2 > \qquad (3.54)$$

$$\nu_1 = - < \dot{A}|T|\dot{A} > / < \dot{A}^2 > \qquad (3.55)$$

$$\nu_2(z) = < \dot{A}|iL[z - iQ_2LQ_2]^{-1}iQ_2L|\dot{A} > / < \dot{A}^2 > \qquad (3.56)$$

and

$$Q_2 = 1 - |A > [< A^2 >^{-1}] < A| - |\dot{A} > [< \dot{A}^2 >^{-1}] < \dot{A}| \qquad (3.57)$$

The correlation time τ_A associated with the dynamical variable A is the zero frequency ($z = 0$) part of $C_A(z)$ and this is

$$\tau_A = (\nu_1 + \nu_2(z = 0))/\Omega^2 \tag{3.58}$$

Equation (3.58) has the precisely the same form as the equations for the hydrodynamic transport coefficients, Eqs. (3.38) and (3.51), and the friction coefficient, Eq. (3.25).

By means of the Mori-generalized Langevin formalism presented above, one can calculate the orientational correlation times for a fluid. [131] Specifically, consider the orientational correlation time τ_2 associated with the decay of a second rank Legendre polynomial $P_2(\hat{\mathbf{u}} \cdot \hat{\mathbf{z}})$ (or P_2 for short) specifying the orientation $\hat{\mathbf{u}}$ of a rotor-like molecule with respect to $\hat{\mathbf{z}}$, an arbitrarily chosen laboratory frame. To perform this calculation, we associate A in Eq. (3.53) with P_2 and $\dot{A}$ with its time derivative

$$\dot{A} = iL_0 P_2 = \omega \cdot (\hat{\mathbf{u}} \times \nabla_u) P_2 \tag{3.59}$$

If we wish to represent the effects of free precession in the ν_2 term, we express the resolvent operator in terms of the projected convective derivative of $\dot{A}$,

$$B = Q_2 \ddot{A} \tag{3.60}$$

and so

$$\tau_2 = (I/6k_B T)(\nu_1 + \nu_2(z = 0)) \tag{3.61}$$

where

$$\nu_1 = f_\omega^E \tag{3.62}$$

$$\nu_2(z = 0) = |<\dot{A}|iL|B>|^2/[<B|T|B><\dot{A}^2>] \tag{3.63}$$

Equation (3.61) is applied to the calculation of the single particle and collective orientational correlation times in the following sections.

4. *Collision Integrals*

In the previous section, we summarized procedures in which transport properties were cast in the form of collision integrals (or matrix elements of binary collision operators). Fortunately, the momentum portions of the binary collision integrals can be performed exactly as shown by Hoffman. [95] Actually the method espoused by Hoffman applies to matrix elements adjoint of the collision operator (and to the so-called Chapman–

Cowling bracket integrals [97] $[A, B]$ which are related to the binary collision operator by the identity [35]

$$[A, B] = - < A(1)|T_{12}^{\dagger}|(B(1) + B(2)) > = < (B(1) + B(2))|T_{12}|A(1) > \tag{3.64}$$

That a method exists for the exact calculation of the momentum integrals is crucial to the development of the kinetic theory. For without Hoffman's procedure, our general collision integrals would require numerical methods for their evaluation. Hoffman's procedure has been applied (and amplified) elsewhere. [132] Here we merely summarize its essentials.

Consider a collision of two smooth HCBs in which each HCB possesses three linear and two angular momentum degrees of freedom. Only one velocity component plays a crucial role in the dynamics of the combined ten dimensional momentum space and that component is ds/dt, the relative velocity of the contact points

$$ds/dt = \hat{\mathbf{s}} \cdot \mathbf{g} \tag{3.65}$$

with

$$\mathbf{g} = \mathbf{v}_2 + \omega_2 \times \xi_2 - (\mathbf{v}_1 + \omega_1 \times \xi_1) \tag{3.66}$$

ξ_j is a vector that emanates from the mass center of particle j and extends to the contact point on its surface. After the collision, the component of $\mathbf{g}$ along $\hat{\mathbf{s}}$, the surface normal at the contact point, changes sign from its negative precollisional value $(\hat{\mathbf{s}} \cdot \mathbf{g}^*)$ to its positive postcollisional value $(\hat{\mathbf{s}} \cdot \mathbf{g})$

$$\mathbf{g} = \mathbf{g}^* - 2\hat{\mathbf{s}}\hat{\mathbf{s}} \cdot \mathbf{g}^* \tag{3.67}$$

When the set of ten momenta are expressed in an orthogonal coordinate system in which $(\hat{\mathbf{s}} \cdot \mathbf{g})$ is a member, the effect of the collision is to reverse one component (ds/dt) and to leave all the remaining nine momentum variables unchanged. Recall that when one deals with hard-sphere collisions, the velocity coordinates are normally taken to be the center of mass $(\frac{1}{2})(\mathbf{v}_1 + \mathbf{v}_2)$ and the relative velocity $\mathbf{v}_r \equiv (\mathbf{v}_2 - \mathbf{v}_1)$ and it is $\mathbf{v}_r$ which plays the role of $\mathbf{g}$. For nonspherical molecules, Hoffman expressed all the momentum dependent functions in terms of the nine orthogonal but otherwise arbitrary coordinates and the one special ds/dt coordinate. Integrations over the nine momentum degrees of freedom could be executed freely (i.e., independent of collision details) and the one special coordinate remained for integration subject to the particular constraints (e.g., a restricted integration over the pre- or postcollisional hemisphere).

After having performed the momentum integrals exactly, one is left with various orientation integrals over the excluded volume surface, $d\hat{\mathbf{u}}_1 d\hat{\mathbf{u}}_2$

$d\mathbf{r}_1 d\mathbf{r}_2$, and these remaining integrations are conducted in the manner discussed in Section II.C. On the basis of these remarks, all the collision integrals can be reduced to surface integrals weighted by the contact pair correlation function. This completes our summary of the kinetic theory of polyatomic fluids.

D. Applications of Enskog Theory

In this section, we summarize a few transport coefficients for a pure fluid of convex bodies and an infinitely dilute solution of a single convex body in a fluid of spheres. The entries were chosen either for their simplicity or for their importance to transport processes in dense fluids.

1. Pure Fluids of HCBs

The simplest transport coefficients are the self-diffusion coefficients for the particle translation and rotation, D_s and D_ω, respectively. These two transport coefficients can be expressed in terms of the friction coefficients which are collisional matrix elements in the Enskog approximation

$$f_s^E = | < \mathbf{v}_1 \cdot |T_{12}|\mathbf{v}_1 > |/ < v_1^2 > \tag{3.68}$$

$$f_\omega^E = | < \omega_2 \cdot |T_{12}|\omega_1 > |/ < \omega_1^2 > \tag{3.69}$$

After some algebra, one obtains

$$f_s^E = \rho g_c v_r \sigma_v \tag{3.70}$$

$$f_\omega^E = \rho g_c v_r \sigma_\omega \tag{3.71}$$

Here $g_c (\equiv g_{iso}(s = 0))$ is the surface averaged contact pair correlation function discussed in Section II, v_r is the relative thermal speed,

$$v_r = [8k_B T/(\pi\mu)]^{1/2} \tag{3.72}$$

μ is the reduced mass for the pair of HCBs ($= m/2$) and σ_v and σ_ω are the linear and angular momentum cross sections, given explicitly by

$$\sigma_v = (2/3)\pi S_c < 1/D >_c \tag{3.73}$$

$$\begin{aligned}\sigma_\omega &= 2\pi(\mu/I)S_c < (\xi_1 \times \hat{\mathbf{s}})^2/D >_c \\ &= 2\pi(\mu/I)S_c < (1 - x^2)(h'(x))^2/D >_c\end{aligned} \tag{3.74}$$

where S_c is the average surface area on the contact surface and

$$D^2 = 1 + (\mu/I)[(\xi_1 \times \hat{\mathbf{s}})^2 + (\xi_2 \times \hat{\mathbf{s}})^2] \tag{3.75}$$

Roughly, $1/D^2$ and $(D^2 - 1)/D^2$ measure the fractional participation of

linear and angular momentum in the collision, respectively. Both the linear and the angular momentum friction coefficient and cross sections are related to the collision frequency per particle Z (and the total cross section σ_{tot}) by means of an Enskog sum rule:

$$Z = (3/4)f_v + (1/2)f_\omega = (1/2)\rho g_c v_r \sigma_{\text{tot}} \tag{3.76}$$

$$\sigma_{\text{tot}} = \pi S_c < D >_c \tag{3.77}$$

Z contains a factor of one-half in order to avoid counting the 1–2 and 2–1 collisions as two events.

The frequency dependent shear viscosity and thermal conductivity can be determined by our methods of Section III.C.2 and we obtain in the $k = 0$ limit,

$$\eta(z) = \eta_0(z)(1 + q_\eta)^2 + \eta_1 \tag{3.78}$$

$$\lambda(z) = \lambda_0(z)(1 + q_\lambda)^2 + \lambda_1 \tag{3.79}$$

For the shear viscosity, one has

$$\eta_0 = \lim_{z \to 0} \eta_0(z)$$

$$= (15/16)[mk_BT/\pi]^{\frac{1}{2}}/g_c S_c < 5/D - 2/D^3 >_c \tag{3.80}$$

$$\eta_0(z) = \rho k_B T/(z + \nu_3) \tag{3.81}$$

$$\nu_3 = (4\pi/15)\rho v_r g_c S_c < 5/D - 2/D^3 >_c \tag{3.82}$$

$$\eta_1 = (4\pi/15)[mk_BT/\pi]^{\frac{1}{2}}\rho^2 g_c S_c < (2r^2 - (\mathbf{r} \cdot \hat{\mathbf{s}})^2)/D >_c \tag{3.83}$$

$$q_\eta = (4\pi/15)\rho g_c S_c < h_{12}/D^2 >_c \tag{3.84}$$

and for the thermal conductivity,

$$\lambda_0 = \lim_{z \to 0} \lambda_0(z)$$

$$= (49/32)[mk_B^3 T/\pi]^{\frac{1}{2}}/g_c S_c < Q_0/D >_c \tag{3.85}$$

$$\lambda_0(z) = (9k_B/2)\rho k_B T/(z + \nu_4) \tag{3.86}$$

$$\nu_4 = (36\pi/49)\rho v_r g_c S_c < Q_0/D >_c \tag{3.87}$$

$$\lambda_1 = (2\pi/3)k_B[mk_BT/\pi]^{\frac{1}{2}}.\rho^2 g_c S_c < Q_1 >_c \tag{3.88}$$

$$q_\lambda = (2\pi/7)\rho g_c S_c < h_{12}(2 + D^{-4} - 2D^{-2}) >_c \tag{3.89}$$

with

$$\mathbf{a}_i = (\mu/I)^{1/2}\hat{\mathbf{s}} \times \xi_i \tag{3.90}$$

$$Q_0 = D^2 + (1/3)(a_1/D)^2 - 2(a_1^4/D^2) + (9/8)(a_1^2 - a_2^2)^2/D^4 \tag{3.91}$$

$$Q_1 = r^2[1 + 2a_2^2(1 + 2a_2^2)/D^2]/D \tag{3.92}$$

The algebraic form of the derived transport coefficients is identical to that found by Jagannathan et al. [125] Each transport coefficient has a frequency independent plateau (arising from the "direct" terms) and a Maxwell model [133,134] relaxing term (arising from the "indirect terms"). In a dilute gas, the transport coefficients are given by $\eta_o(z)$ and $\lambda_o(z)$. Equations (3.78) and (3.79) were written in a form to emphasize the similarities to those for hard-sphere fluids.

Not all dynamical properties of fluids of HCBs necessarily map smoothly onto those of hard spheres. Consider the spherical limit approached by allowing the HCB to become spherical ($D = 1, \mathbf{r} = \hat{\mathbf{s}}\sigma, S_c = \sigma^2, g_c = g_{HS}, \mathbf{a}_i = 0$). In this limit, the shear viscosity, Eq. (3.78) for the fluid of HCBs reduces to that of a hard-sphere fluid. However, the same situation does not prevail for the thermal conductivity. Bodies with a vanishingly small nonsphericity can still transmit angular kinetic energy and thus there is a discontinuous change in λ from that of an atom,

$$\lambda(\mathrm{HS})/\rho = (mk_B^3 T\sigma^2/\pi)^{1/2}[(75/64)(1 + (2\pi/5)X)^2/X + (2\pi/3)X] \quad (3.93)$$

to that of a spherical diatom,

$$\lambda(\mathrm{HCB})/\rho = (mk_B^3 T\sigma^2/\pi)^{1/2}[(49/32)(1 + (2\pi/7)X)^2/X + (2\pi/3)X] \quad (3.94)$$

with the same dimensions of the atom. Here $X(\equiv \rho\sigma^3 g_{HS})$ is a dimensionless contact density. The difference between λ(HS) and λ(HCB) (in the spherical limit) arises trivially from the differing heat capacities of hard spheres and HCBs and nontrivially from dynamical corrections.

This difference between the thermal conductivities of a spherical HCB and a hard sphere is largest at low density (when $X = 0$ and $\lambda(\mathrm{HCB})/\lambda(\mathrm{HS}) = 1.31$) and decreases monotonically at high densities (when $X \to \infty$ and $\lambda(\mathrm{HCB})/\lambda(\mathrm{HS}) = 0.85$). Evidence for this trend can be found in the MD simulations of Murad et al. [135] on a fused hard sphere model of Cl_2.

The molecular dynamics of rotation in condensed phases is sampled by the single particle and the collective second rank orientational correlation functions, whose integrals give, respectively, the single particle and colllective correlation times

$$\tau_2^s = \int_0^\infty dt < P_2(\hat{\mathbf{u}}(0) \cdot \hat{\mathbf{u}}(t) > \quad (3.95)$$

$$\tau_2^c = \sum_{i,j} \int_{J_0}^\infty dt < P_2(\hat{\mathbf{u}}_j \cdot \hat{\mathbf{u}}_i(t) > / \sum_{i,j} < P_2(\hat{\mathbf{u}}_j \cdot \hat{\mathbf{u}}_j) > \quad (3.96)$$

τ_2^s and τ_2^c are related by the Kivelson–Keyes [131] equation

$$\tau_2^c/\tau_2^s = g_2/j_2 \tag{3.97}$$

where g_2 is the static second rank pair correlation factor (see Eq. (2.28)) and j_2 is the dynamical equivalent of g_2. τ_2^s can be calculated by the procedures of Section III.C.3 and we obtain

$$\tau_2^s = f_\omega^E I/(6k_B T) + (4/3)(1/f_\omega^E)\Lambda \tag{3.98}$$

where

$$\Lambda = 1/(2 - < a_1^4/D^3 >_c / < a_1^2/D >_c) = [0.5, 0.9) \tag{3.99}$$

Equation (3.98) depicts a high density branch in which τ_2^s is proportional to the friction ($\simeq \rho g_c$) and a low density branch in which τ_2^s is inversely proportional to friction ($\simeq 1/(\rho g_c)$). The convective upswing in τ_2^s reflects the result that without collisions the second rank projection of the molecular orientation does not relax. Kinetic theory with its hard potentials does not predict a density independent term in τ_2^s which we might interpret as an intercept in a plot of τ_2^s versus $\rho g_c (\simeq \eta/\rho)$ in contrast to the situation involving soft forces. [136] Note that Eq. (3.98) differs from that reported by Cole [35] in two ways: (1) we find no intercept; and (2) the coefficient of the convective term is (4/3) rather than the (5/3) originally quoted. The values for Λ remain the same.

Kinetic theory methods can be directly applied to determine collective properties such as τ_2^c and this calculation can be reduced to a few matrix elements, specifically [132]

$$\tau_2^c = [< \dot{P}_2^c(\hat{\mathbf{u}} \cdot \hat{\mathbf{z}}) | T | \dot{P}_2^c(\hat{\mathbf{u}} \cdot \hat{\mathbf{z}}) > / < (P_2^c(\hat{\mathbf{u}} \cdot \hat{\mathbf{z}})^2 >] g_2 I/(6k_B T) \tag{3.100}$$

where

$$P_2^c(\hat{\mathbf{u}} \cdot \hat{\mathbf{z}}) = \sum_i P_2(\hat{\mathbf{u}}_i \cdot \hat{\mathbf{z}}) \tag{3.101}$$

After performing the matrix elements in Eq. (3.100) and comparing the result with the Kivelson–Keyes relation, we can identify

$$j_2 = 1/(1 + dj) \tag{3.102}$$

with

$$dj = 2(\mu/I)\pi < h'(x)h'(x_2)[\hat{\mathbf{u}} \cdot \hat{\mathbf{u}}_2(1 - 2x^2 - 2x_2^2 + 2xx_2 \hat{\mathbf{u}} \cdot \hat{\mathbf{u}}_2) + xx_2]/D >_c / \sigma_\omega \tag{3.103}$$

where $x_2 = \hat{\mathbf{s}} \cdot \hat{\mathbf{u}}_2$ and $h'(x) = dh(x)/dx$. This completes our summary of the orientational properties.

2. *Infinitely Dilute Solution*

The fluid of HCBs with the simplest static and dynamic properties is the infinitely dilute solution comprised of a hard-sphere solvent and a single HCB solute particle. For this case, the macroscopic shear viscosity and thermal conductivity of the fluid is that appropriate to a hard-sphere fluid and the single particle and collective orientational correlation times are identical. The tagged particle friction coefficients (and accompanying cross-sections) for the linear and angular momentum and rotational kinetic energy differ slightly those of single component fluids of HCBs and are [113,114]

$$f_i = \rho v_r g_c \sigma_i \tag{3.104}$$

with $i = v, \omega$, and r, the velocity, angular momentum and rotational energy, respectively. v_r is the relative thermal speed of the hard sphere with respect to the HCB. Cross-sections derived on the basis of Enskog theory are

$$\sigma_v = (4\pi/3)(\mu/m) \int_0^1 dx\, G(s=0,x)/(D(x)g_c) \tag{3.105}$$

$$\sigma_\omega = 2\pi \int_0^1 dx\, G(s=0,x)(D^2(x)-1)/(D(x)g_c) \tag{3.106}$$

$$\sigma_r = 4\pi \int_0^1 dx\, G(s=0,x)(D^2(x)-1)/(D^3(x)g_c) \tag{3.107}$$

with $x = \hat{\mathbf{u}} \cdot \hat{\mathbf{s}}$,

$$G(s=0,x) = g(s=0,x)S^{12}(s=0,x) \tag{3.108}$$

$g(s=0,x)$ the orientation dependent contact pair correlation function, $S^{12}(s=0,x)$ the surface area element on the HS-HCB excluded volume surface and $D^2(x)$ the HS-HCB translational-to-rotational energy transfer function

$$D^2(x) = 1 + (\mu/I)(\xi_i \times \hat{\mathbf{s}})^2 = 1 + (\mu h'^2(x)/I)(1-x^2) \tag{3.109}$$

For a uniaxial convex body with a specified support function, we can calculate Enskog approximations to the three cross sections given above using the SPT orientation dependent contact pair correlation function, Eq. (2.46) and the surface area element S^{12} appropriate to a HCB-sphere surface (see Appendix A.D). Furthermore, by means of the recollision kinetic theory summarized earlier, that is, incorporating the single function given by Eq. (3.26), the rotational friction coefficient can be extended

beyond the uncorrelated binary collision approximation. The recollision correlations take the form [113,114]

$$f_\omega \simeq f_\omega^E(1 + \rho^* \exp(5\rho^*)) \tag{3.110}$$

f_ω includes a positive definite enhancement to the friction based on the influence of "caging" recollisions, which were analyzed using a Smoluchowski equation to describe diffusion in a hard-sphere potential of mean force.

If the convex body is slightly aspherical, then σ_v, σ_ω and σ_r can be determined analytically. For simplicity, consider an ellipsoidal HCB with semi-major axis a and semi-minor axis b in a fluid of hard spheres with diameter σ. We obtain

$$\sigma_v \simeq (4\pi/3)(\mu/m)S_c \tag{3.111}$$

$$\sigma_\omega \simeq (16\pi/15)S_c\mu(a-b)^2/I \tag{3.112}$$

$$\sigma_r \simeq 2\sigma_\omega \tag{3.113}$$

with $S_c = (a + (1/2)\sigma)^2$. For pure fluids of HCBs, these results undergo small changes ($\mu \to m/2, \sigma \to a$) and the distinction between single particle and collective orientational relaxation times becomes important. In the case of slightly aspherical prolate ellipsoids, j_2 becomes

$$1/j_2 \simeq 1 + (2/5)\exp(-[(b/a)^2 - 1]/10) \tag{3.114}$$

and thus j_2 is less than unity in an Enskog approximation for ellipsoids. Spherocylinders show similar behavior and those results have been given elsewhere. [35,137] This completes our brief summary of transport properties.

E. Simulations

1. *Translational and Rotational Diffusion*

Translational and rotational motion in the isotropic phase have been investigated for ellipsoids of revolution with $e = 2, 3, \frac{1}{3}$. [34,138] Translational and rotational diffusion coefficients are calculated by integrating the linear and angular velocity autocorrelation functions, respectively:

$$D_T = \frac{1}{3}\int_0^\infty \mathrm{d}t\ \langle \mathbf{v}_i(0)\cdot\mathbf{v}_i(t)\rangle$$

$$D_R = \frac{1}{2}\int_0^\infty \mathrm{d}t\ \langle \boldsymbol{\omega}_i(0)\cdot\boldsymbol{\omega}_i(t)\rangle$$

In doing this, it is important to check that any slow long-time decay is correctly included. In the case of translational diffusion, it is possible to check the numerical procedure by measuring the limiting gradient of the mean-square displacement with respect to time; this should equal $6D$. Additional checks were carried out in this study, to compare with the well-known diffusion coefficients of hard spheres at similar system sizes. It should be borne in mind that D_T depends significantly on system size, so like must be compared with like.

A major aim of this study was to compare with the predictions of Enskog theory, which is based on the independent binary collision model. As was explained in Section III.D, the Enskog predictions are simply obtained by averaging appropriate geometrical functions for pairs at contact. [35] The results of this study [138] are shown in Figs. 3.1 and 3.2, and several interesting features are present. Firstly, as for hard spheres, D_T/D_T^E first rises, then falls, as density increases. The high density decrease is well understood; caging effects in the dense liquid produce a rapid decay of the velocity autocorrelation function, and indeed a negative rebound region at the highest densities, which cause D_T to be much less than the simple kinetic theory would predict. The same observation applies to ro-

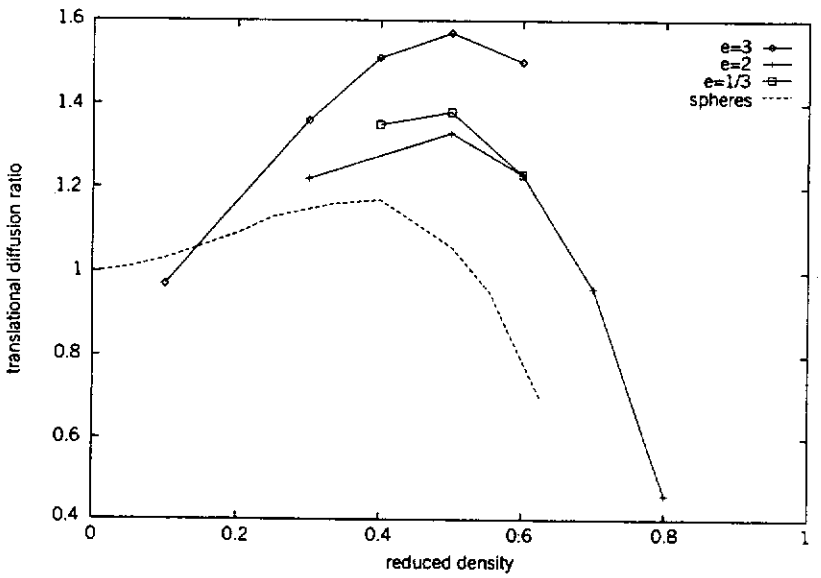

Figure 3.1. Ratio of translational diffusion coefficient to Enskog value, D_T/D_T^E, for ellipsoids of axial ratio $e = 3$, 2, 1/3 and 1 (hard spheres), plotted as a function of reduced density ρ/ρ_{cp} where ρ_{cp} is the close-packed density. The results for hard spheres are taken from Ref. [139].

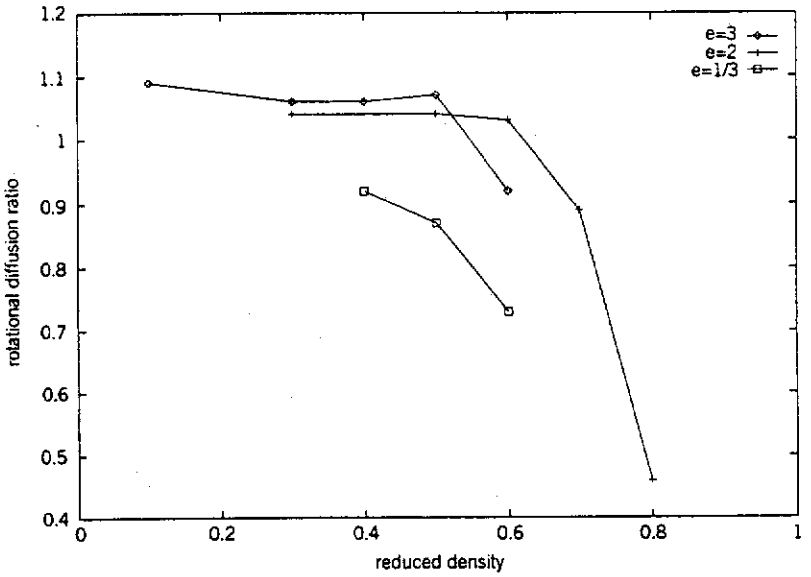

Figure 3.2. Ratio of rotational diffusion coefficient to Enskog value, D_R/D_R^E, for ellipsoids of axial ratio $e = 3$, 2 and 1/3, plotted as a function of reduced density ρ/ρ_{cp} where ρ_{cp} is the close-packed density.

tational diffusion; caging dominates. Further study of caging phenomena in these systems [24] has raised some puzzling features, however. For both $\langle \mathbf{v}_i(0) \cdot \mathbf{v}_i(t) \rangle$ and $\langle \omega_i(0) \cdot \omega_i(t) \rangle$, a minimum in the function is reached after quite a large number of binary collision times, typically 20–30$\times t_c$. This time is much longer than what is typically observed in a dense fluid of hard spheres and is not really compatible with the idea of a rapid reversal of velocity following a single "rattle" in a cage. Reference [24] discusses the various factors that may contribute to this effect.

At low densities, for hard spheres, D_T approaches its Enskog value, since the independent binary collision model becomes correct in the dilute gas. This is manifestly not true for the ellipsoid systems, although the deviations from unity amount to, at most, 10% for the systems studied in the limit $\rho \to 0$. The translational diffusion coefficient is systematically lower than would be predicted by theory. At the same time, the rotational diffusion coefficient is slightly higher. These discrepancies occur because, even when the density is sufficiently low that molecules meet as isolated pairs, each such event may consist of several correlated collisions. This "chattering" phenomenon was discussed in Section III.C.1. Although chattering collisions are not accounted for by the simplest version of Enskog theory, a more sophisticated version [99] predicts these effects. A qualitative explanation can easily be put forward, referring to Fig. 3.3.

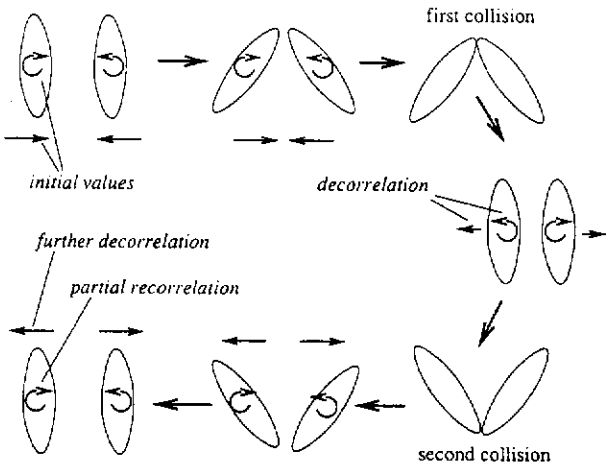

Figure 3.3. Double collision between two hard bodies, illustrating correlating and decorrelating effects on linear and angular velocities (schematic).

Here we focus on the "double-hit" collisions, the ones that provide the largest correction to the simple Enskog prediction. Many of these will involve a side-by-side geometry, as shown in the figure, and we take as an example a near-symmetrical case with both molecules approaching each other at similar speeds. The effect of the first collision is to reverse both the indicated linear and angular velocities. This contributes to the decorrelation effects seen as the initial decay of both $\langle \mathbf{v}_i(0) \cdot \mathbf{v}_i(t) \rangle$ and $\langle \omega_i(0) \cdot \omega_i(t) \rangle$. This part is correctly given by simple Enskog theory. However a second collision modifies both linear and angular velocities further. The effect on the linear velocity is to enhance the results of the first collision; the velocities become *more* decorrelated with their original values, on average. The effect on the angular velocities is to partially negate the results of the first collision, and to *restore* some of the original correlation. Consequently, $\langle \mathbf{v}_i(0) \cdot \mathbf{v}_i(t) \rangle$ decays at long times more quickly than expected, giving $D_T < D_T^E$, while $\langle \omega_i(0) \cdot \omega_i(t) \rangle$ decays at long times more slowly than expected, giving $D_R > D_R^E$. This description is, of course, qualitative. In reality, there will be a complete range of geometries and initial conditions in three dimensions, over which an average must be taken.

The most interesting feature in Fig. 3.1, however, is the rise of D_T/D_T^E above unity at intermediate densities. In the hard-sphere case, this is associated with the celebrated $t^{-3/2}$ algebraic long-time tails in the velocity autocorrelation function [139–141] arising from coupling with hydrodynamic vortex modes. It seems likely that another effect is operating in the case of the ellipsoids, swamping the vortex coupling, since the enhancement in

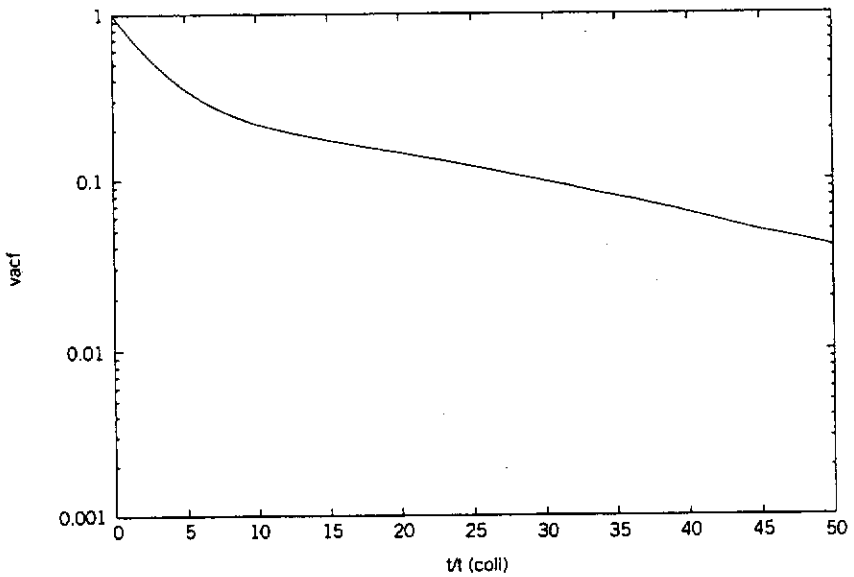

Figure 3.4. Translational velocity autocorrelation function (log scale) for prolate ellipsoids with $e = 10$ at a reduced density $\rho/\rho_{cp} = 0.2$. Time is measured in units of the mean time between collisions per particle.

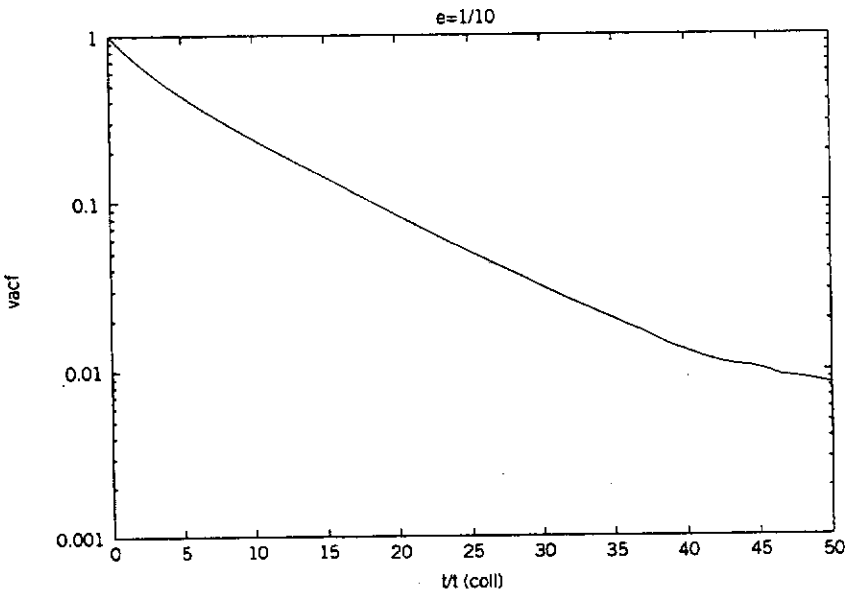

Figure 3.5. Translational velocity autocorrelation function (log scale) for oblate ellipsoids with $e = 1/10$ at a reduced density $\rho/\rho_{cp} = 0.2$. Time is measured in units of the mean time between collisions per particle.

D_T/D_T^E is much larger. Certainly, no evidence of algebraic decay is seen in the systems studied (in any case, it would be difficult to obtain direct evidence of this in the modest system sizes used). What is seen, especially in the prolate case, is a two-exponential decay in time (see Figs. 3.4, 3.5), indicating some coupling of the velocity with other degrees of freedom, possibly reorientation. A detailed theory of this phenomenon is still lacking, but related, and even more dramatic, effects are seen in isotropic fluids of thin hard needles [142–144] and in liquid crystalline phases of disklike molecules. [145] In the latter context (see Section VI), we briefly sketch a possible mechanism that can lead to such large deviations from the Enskog theory.

2. *Pretransitional Collective Rotation*

A key feature of the I→N transition is the appearance of pretransitional effects in molecular reorientation in the isotropic phase. Allen and Frenkel [146] compared single particle and collective rotation, in the isotropic phase near to the ordering transition, with a view to identifying these pretransitional fluctuations. The crucial theoretical prediction is the Kivelson–Keyes equation of Section (3.D.1) [131,147] where the single particle second-rank correlation time τ_2^s and its collective counterpart τ_2^c are calculated in the simulation as time integrals of appropriate time correlation functions, and the static second-rank Kirkwood factor g_2 is computed as a sum over pairs. In the simulations (for the $e = 3$ prolate ellipsoid system), collective rotation was seen to slow down dramatically near the I→N transition, but

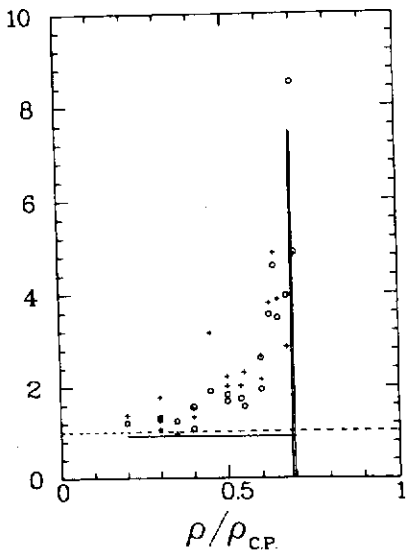

Figure 3.6. Density dependence of g_2 (open circles) and τ_2^c/τ_2^s (pluses) for ellipsoids with $e = 3$. The horizontal line is the best estimate for j_2, assuming the latter quantity to be independent of density. The dotted line marks a value of unity. The vertical lines mark the estimated boundaries of the $I - N$ coexistence region for this system size.

the effect is mostly explained by the divergence of the static factor g_2. There is little evidence for any dramatic variation in j_2, which seems to be just less than unity in agreement with (low density) kinetic theory (see Fig. 3.6) [35] (see Section III.D.1) and with the (scant) experimental evidence. [148,149] Indeed, in the absence of information to the contrary, j_2 had long been assumed to be essentially unity, and the simulations seem to provide some justification for this. However, for spherocylinders the situation is not so simple. [77] The low density theoretical prediction is again that j_2 is slightly less than unity, and this is confirmed by simulation. However, at higher densities, j_2 appears to rise to more than 1.5.

Throughout, one must remember that the I→N transition is weakly first order, rather than continuous, so actually it preempts the complete divergence of g_2 and τ_2^c/τ_2^s. Also, it is important to bear in mind the limitations of small system sizes and modest simulation run lengths, when discussing collective reorientational degrees of freedom near a phase transition.

PART TWO: THE LIQUID-CRYSTALLINE PHASE

IV. PHASE TRANSITIONS

A. Theory

In order to describe phase transitions in liquid-crystalline systems,[1] we need a statistical mechanical formalism capable of dealing with spontaneous symmetry breaking. The formalism based on the canonical partition function employed in the section on the isotropic phase is not up to this task. We therefore introduce the general framework of density functional theory (DFT), with which one can give a unified description of all phase transition phenomena in continuous systems. Next we give an overview of the diverse approximations that have been proposed to obtain workable functionals for the description of liquid-crystalline phase transitions in HCB fluids. Finally, we review the application of these ideas to specific transitions.

[1] In the compilation of this section, we were able to make use extensively of the in-depth review by Vroege and Lekkerkerker *Phase Transitions in Lyotropic Colloidal and Polymer Liquid Crystals* [150]. We are grateful to these authors for supplying a preprint version of their review.

1. *Density Functional Formalism*

The density functional formalism is in essence just a variational formulation of the classical statistical mechanics of many-particle systems. It has, however, several advantages with respect to other approaches. First, variational problems are well understood and there exists a large body of mathematical knowledge concerning their solution. Secondly, the quantity being varied is a function of the degrees of freedom of a single particle only, so that we are shielded from the complexities of n-particle distributions. In fact, it is a deep and surprising result of the theory that there is a one-to-one correspondence between the single particle distribution function and the full N-particle probability density. Finally, the formalism can deal with spontaneous symmetry breaking in a direct and natural way, making it an ideal tool for the study of symmetry related phase transitions. To our knowledge the first application of density functional techniques to liquid crystals is due Workman and Fixman. [151]

In order to state the the theory, we first need to define the one-particle distribution function (ODF)

$$\rho^{(1)}(\xi) = \left\langle \sum_{i=1}^{N} \delta(\xi - \xi_i) \right\rangle \tag{4.1}$$

where $\xi = (\mathbf{r}, \Omega)$ is shorthand for the degrees of freedom of a single particle, being, for the HCBs we are considering, the position of the center of mass $\mathbf{r}$ and the orientation Ω with respect to a fixed reference frame. The sum on the right hand side of Eq. (4.1) runs over all the N particles in the system and the angular brackets denote equilibrium averaging. Note that the ODF so defined is normalized to the number of particles, that is,

$$\int_V d\xi \rho^{(1)}(\xi) = N \tag{4.2}$$

where the integration runs over the finite volume V of our system.

The full statement of density functional theory for classical many particle systems [152] is the assertion that there exists a functional $\mathcal{W}[\rho^{(1)}]$ of the ODF with the following properties:

1. For any arbitrary ODF $\rho^{(1)}$, the following inequality holds: $\mathcal{W}[\rho^{(1)}] \geq \mathcal{W}[\rho_{\text{eq}}^{(1)}]$ where ${\rho^{(1)}}_{\text{eq}}$ is the equilibrium distribution.
2. $\mathcal{W}[\rho_{\text{eq}}^{(1)}] = \mathcal{W}_{\text{eq}}$ where $\mathcal{W}_{\text{eq}}$ is the thermodynamic equilibrium value of the grand canonical potential.

As such, this statement is entirely nonconstructive: We are told that the functional exists, but not how to construct it. As we shall see, the actual

construction involves approximations, which in final analysis can only be tested through comparison with simulation data. Nevertheless, the general structure of the functional can be analyzed somewhat further. First, recalling the thermodynamic relation $W = F - \mu N$ relating the grand canonical potential W to the free energy F, the chemical potential μ and the number of particles N, we can write

$$\mathcal{W}[\rho^{(1)}] = \mathcal{F}[\rho^{(1)}] - \mu \int_V d\xi \rho^{(1)}(\xi) \tag{4.3}$$

which introduces the functional $\mathcal{F}[\rho^{(1)}]$ representing the Helmholtz free energy of the system. This free energy functional can be split into an ideal and an excess part, the latter containing all contributions due to the interactions between the particles.

$$\beta\mathcal{F}[\rho^{(1)}] = \int d\xi \rho^{(1)}(\xi)\{\ln \mathcal{V}_T \rho^{(1)}(\xi) - 1\} - \Phi[\rho^{(1)}] \tag{4.4}$$

where $\mathcal{V}_T$ is the thermal de Broglie volume discussed in Appendix A.A and we have introduced the functional $\Phi[\rho^{(1)}] = -\beta\mathcal{F}_{\text{excess}}[\rho^{(1)}]$ that serves as a generating functional for the n-particle direct correlation functions

$$c^{(n)}(\xi_1, \xi_2, ..., \xi_n; [\rho^{(1)}]) = \frac{\delta^n \Phi[\rho^{(1)}]}{\delta\rho^{(1)}(\xi_1)\delta\rho^{(1)}(\xi_2)\cdots\delta\rho^{(1)}(\xi_n)} \tag{4.5}$$

Historically, the first approach to the actual construction of the functional is in terms of a diagram expansion obtained by re-summing the diagrams in an expansion of the grand canonical potential in terms of an external field, which is eliminated in favor of the ODF through a topological reduction technique. [153] The result is the following identity:

$$\Phi[\rho^{(1)}] = \begin{cases} \text{Sum of all connected, irreducible diagrams with } \rho^{(1)} \text{ vertices and Mayer function bonds:} \\ f(\xi_i, \xi_j) = e^{-\beta v(\xi_i, \xi_j)} - 1 \end{cases} \tag{4.6}$$

For hard particles the Mayer function is just the negative of the characteristic function χ of the mutual excluded volume of the particles,

$$f(\xi_i, \xi_j) = -\chi(\xi_i, \xi_j) = \begin{cases} -1, & \text{if } i \text{ and } j \text{ overlap} \\ 0, & \text{if } i \text{ and } j \text{ do } \textit{not} \text{ overlap} \end{cases} \tag{4.7}$$

One can also use the definition (4.5) to relate the excess part Φ to some properties of a reference state $\rho_0^{(1)}$ through a double functional integration. Consider an arbitrary one parameter family of ODFs $\rho_\alpha^{(1)}$ interpolating smoothly between a reference system at $\rho_0^{(1)}$ and a final state at $\rho_1^{(1)}$ as a

parameter α goes from 0 to 1. Since the functionals are unique, the final result will *not* depend on the path of integration. [154] A first integration yields

$$\begin{aligned}\Phi[\rho_1^{(1)}] - \Phi[\rho_0^{(1)}] &= \int_0^1 d\alpha \frac{d}{d\alpha}\Phi[\rho_\alpha^{(1)}] \\ &= \int_0^1 d\alpha \int d\xi \frac{\delta\Phi[\rho_\alpha^{(1)}]}{\delta\rho^{(1)}(\xi)} \frac{\partial\rho_\alpha^{(1)}(\xi)}{\partial\alpha} \\ &= \int_0^1 d\alpha \int d\xi c^{(1)}(\xi, [\rho_\alpha^{(1)}]) \frac{\partial\rho_\alpha^{(1)}(\xi)}{\partial\alpha} \end{aligned} \tag{4.8}$$

One can now repeat such an integration to eliminate the one-particle direct correlation function in favor of a description in terms of the two-particle direct correlation function.

$$c^{(1)}(\xi, [\rho_\alpha^{(1)}]) = c^{(1)}(\xi, [\rho_0^{(1)}]) + \int_0^\alpha d\alpha' \int d\xi' c^{(2)}(\xi, \xi', [\rho_{\alpha'}^{(1)}]) \frac{\partial\rho_{\alpha'}^{(1)}(\xi')}{\partial\alpha'} \tag{4.9}$$

Putting these two results together yields

$$\begin{aligned}&\Phi[\rho_1^{(1)}] = \\ &\quad \Phi[\rho_0^{(1)}] + \int_0^1 d\alpha \int d\xi c^{(1)}(\xi, [\rho_0^{(1)}]) \frac{\partial\rho_\alpha^{(1)}(\xi)}{\partial\alpha} \\ &\quad + \int_0^1 d\alpha \int_0^\alpha d\alpha' \int d\xi d\xi' c^{(2)}(\xi, \xi', [\rho_{\alpha'}^{(1)}]) \frac{\partial\rho_\alpha^{(1)}(\xi)}{\partial\alpha} \frac{\partial\rho_{\alpha'}^{(1)}(\xi')}{\partial\alpha'} \end{aligned} \tag{4.10}$$

This expression, which can be used to relate the excess free energy of a system to the structural properties of a (possibly simpler) reference phase, is the starting point for many approximations considered.

In order to locate the equilibrium ODF of our system, we have to minimize the grand canonical functional. This leads first of all to the necessary (but not yet sufficient) criterion that the functional be stationary to variation in the equilibrium ODF,

$$\left.\frac{\delta\mathcal{W}[\rho^{(1)}]}{\delta\rho^{(1)}(\xi)}\right|_{\rho^{(1)}=\rho_{eq}^{(1)}} = 0 \tag{4.11}$$

Inserting the explicit forms (4.3) and (4.4) and using the definition (4.5), we find the following equation for the ODF:

$$\rho^{(1)}(\xi) = \frac{1}{\mathcal{V}_T} e^{\beta\mu} \exp c^{(1)}(\xi, [\rho^{(1)}]) \tag{4.12}$$

The chemical potential μ can be eliminated from this equation by using the normalisation condition (4.2). One can look on this equation as a non-linear self-consistency relation for the ODF, the one-particle direct correlation function $c^{(1)}$ playing the role of an effective field that acts on a particle due to interactions with the rest of the system.

To ensure that a stationary distribution satisfying the condition (4.11) is indeed a minimum, we need the following condition to be met for arbitrary variations $\Delta\rho^{(1)}$:

$$\int d\xi d\xi' \frac{\delta \mathcal{W}[\rho^{(1)}]}{\delta\rho^{(1)}(\xi)\delta\rho^{(1)}(\xi')} \Delta\rho^{(1)}(\xi)\Delta\rho^{(1)}(\xi') > 0 \tag{4.13}$$

It should be stressed that this condition is necessary but not always sufficient to determine the stability of the phase in question. This becomes apparent when calculating phase coexistence at constant pressure where the Gibbs free energy is the relevant thermodynamic potential. This necessitates a separate calculation of the pressure of each potential phase.

A useful technique for analyzing nonlinear equations like the stationarity condition (4.11) in the neighborhood of phase transitions, where, as a rule, coexisting solutions to the equations occur, is bifurcation analysis. This technique probes new solutions to the equations that branch off from a known reference solution by making a parametric expansion around the branch or bifurcation point. In our case, a reference solution would be a locally stable phase $\rho_0^{(1)}$ that exists in a given range of densities. The procedure starts by assuming the following form for a solution close to the reference solution at the density n_0:

$$\begin{aligned} \rho_\epsilon^{(1)} &= \rho_0^{(1)} + \epsilon\rho_1^{(1)} + \epsilon^2\rho_2^{(1)} + \cdots \\ n_\epsilon &= n_0 + \epsilon n_1 + \epsilon^2 n_2 + \cdots \end{aligned} \tag{4.14}$$

These expansions are inserted into the stationarity equation (4.11) and a solution is constructed order by order in the arbitrary parameter ϵ. The first order equation is usually called the bifurcation equation and provides information both about the location of the bifurcation, that is, the density at which it occurs, and the nature of the new solution (symmetry). It takes the form of a generalized eigenvalue problem

$$\rho_1^{(1)}(\xi) = \rho_0^{(1)}(\xi) \int d\xi' c^{(2)}(\xi, \xi', [\rho_0^{(1)}])\rho_1^{(1)}(\xi') \tag{4.15}$$

One can successively solve the higher order equations in the hierarchy generated by these expansions, thus constructing approximations to the bifurcating solution that are valid at ever increasing distances (in the solution space) from the reference solution.

2. *Specific Approximations*

a. The Onsager Approximation. Historically, the first and, undoubtably, the most influential approach to ordering phenomena in HCBs is that proposed by Onsager in 1949. Although derived from first principles using the theory of mixtures, it is in fact a density functional theory avant la lettre. In terms of the expansion (4.6), it consists of neglecting all higher order diagrams, keeping just the lowest order single bond diagram. The explicit expression for this diagram is given by

$$\Phi_2[\rho^{(1)}] = \frac{1}{2}\int d\xi d\xi' f(\xi,\xi')\rho^{(1)}(\xi)\rho^{(1)}(\xi') \tag{4.16}$$

Considering for a moment just spatially homogeneous phases for which the ODF factorizes $\rho^{(1)}(\mathbf{r},\Omega) = n\psi(\Omega)$, where n is the number density and ψ a normed orientational distribution function, we can simplify to

$$\Phi_2[\psi] = -\frac{1}{2}Nn\int d\Omega\, d\Omega' \mathcal{E}(\Omega,\Omega')\psi(\Omega)\psi(\Omega') \tag{4.17}$$

where we have introduced the mutual excluded volume of two HCBs at fixed orientations,

$$\mathcal{E}(\Omega,\Omega') = \int d\mathbf{r}'\chi(\mathbf{r}-\mathbf{r}',\Omega,\Omega') \tag{4.18}$$

Onsager justified his approximation by arguing that in the isotropic phase of a system of extremely elongated rods, this diagram dominates all higher order ones. More recently, it was shown that the same holds true for d-dimensional generalizations of HCB fluids in the limit that the dimensionality is very high. [155] Especially this latter observation seems to indicate that the Onsager approximation is the hard-particle analog of the mean field approach for long-range interactions, which is also exact in the infinite dimensionality limit. Moreover, the stationarity equations obtained within the approximation are also formally equivalent to the mean field one, the pair excluded volume playing the role of the potential and the number density that of the inverse temperature. An added advantage of the approximation is that the pair excluded volume at fixed relative orientation has been determined analytically for a number of convex bodies

(ellipsoids of revolution, spherocylinders, spheroplatelets, right circular cylinders) allowing detailed calculations to be made.

A natural extension of the Onsager approximation is,of course, the consideration of higher order diagrams in the virial expansion. Here one meets with severe difficulties due to the complexity of the integrals involved. The only head on attempt to face this problem was made by Tjipto-Margo and Evans [41] who expanded the kernel of the third virial coefficient of hard ellipsoids into a set of invariant functions. The lower order coefficients in this expansion could be determined through a Monte Carlo procedure. These results were then used both in a straightforward extension of the original Onsager theory as well as a y-expansion approach (to be discussed below). The results are a definite improvement over the original second-virial coefficient based theories.

A related approach, originally proposed by Barboy and Gelbart, [49–51], is the so called y-expansion, where the diagram expansion for a homogeneous fluid is re-summed in terms of the reduced density variable

$$y = \frac{\eta}{1 - \eta} \tag{4.19}$$

where we introduce the packing fraction $\eta = nv_0$, with v_0 the proper volume of the HCB. The idea behind this expansion is to exploit similarity with the exact solution of the Percus–Yevick equation for hard spheres, which suggests that all relevant quantities can be expressed as short power series in the variable y. For a homogeneous phase, the free energy per particle can be expressed as an expansion in the number density n

$$\frac{\beta\mathcal{F}[\psi]}{N} = \int d\Omega\psi(\Omega) \ln \psi(\Omega) + \ln \mathcal{V}_T n + \sum_{k=2}^{\infty} \frac{B_k[\psi]}{k-1} n^{k-1} \tag{4.20}$$

where the B_k are the generalized virial coefficients

$$B_k = -\frac{k-1}{V} \sum \begin{pmatrix} \text{Connected diagrams with} \\ k\ \psi\text{-vertices and } f\text{-bonds} \end{pmatrix} \tag{4.21}$$

Eliminating the number density in favor of the variable y, we find

$$\frac{\beta\mathcal{F}[\psi]}{N} = \int d\Omega\psi(\Omega) \ln \psi(\Omega) + \ln \frac{\mathcal{V}_T}{v_0} + \ln y + \sum_{k=2}^{\infty} \frac{C_k[\psi]}{k-1} y^{k-1} \tag{4.22}$$

where the coefficients $C_k[\psi]$ are expressed in terms of the generalized virial coefficients of order k and lower.

$$C_k[\psi] = (k-1)\sum_{j=2}^{k}\binom{-j+1}{k-j}\frac{B_j[\psi]v_0^{j-1}}{j-1} + (-)^{j-1} \tag{4.23}$$

b. Scaled Particle Theory. Scaled particle theory (SPT), originally developed in the context of the hard sphere fluid, [42] was extended by several authors to apply to fluids of non-spherical particles. [156–161] SPT is based on the intriguing and original approach to calculate the amount of reversible work needed to add a scaled copy of the original particles to the fluid. The most elaborate version of the theory as applied to nonspherical particles is the one presented in Ref. [158] which considers hard spherocylinders and allows both the length and the breadth of the particles to be considered as independent scaling parameters. This approach, however, is effective only for spherocylinders, due to the special form of the pair excluded volume as a function of the particle's dimensions. [161] Here, for simplicity, we present the theory with a single scaling parameter. We do, however, follow Cotter [160] in her perscription for achieving consistent thermodynamics, which was lacking in the earlier applications of the theory.

Consider an HCB fluid to which we add a single scaled copy of the other particles. The size of the inserted particle is governed by the scaling parameter λ. When λ is taken to be zero, we are adding a point particle to the fluid, when $\lambda = 1$, the inserted particle is identical in size to the other particles, and when $\lambda \gg 1$, we are effectively creating a particle-shaped macroscopic cavity in the fluid. The main assumption of SPT is that the reversible work W done to insert the scaled particle smoothly interpolates between the limits $\lambda \ll 1$ and $\lambda \gg 1$. Denoting by $v_0(\lambda)$ the proper volume of the particle as a function of the scaling parameter, we can easily calculate the work for the case that the inserted particle is macroscopic in size,

$$W(\Omega|\lambda) \sim Pv_0(\lambda) = \lambda^3 Pv_0 \tag{4.24}$$

where P is the equilibrium pressure. The fact that the particle volume, and hence this contribution to the work, scales as the third power in the scaling parameter suggests that if we can calculate the contribution of adding a very small particle up to second order in λ, we can by adding these two together obtain an expression that works well in both limits and so allow us to interpolate to $\lambda = 1$. For the case of a homogeneous but possibly orientationally ordered fluid, where the ODF has the form $\rho^{(1)}(\mathbf{r}, \Omega) = n\psi(\Omega)$ the expansion to second order in λ can be calculated from a generalization of the expansion, originally derived by Reiss et al. [42]

$$-\beta W(\Omega|\lambda) = \ln \sum_{k=0}^{\infty} \frac{(-)^k}{k!} n^k F^{(k)}(\Omega|\lambda) \tag{4.25}$$

where the $F^{(k)}$ are related to the equilibrium k-particle distribution functions through

$$F^{(k)}(\Omega|\lambda) = \prod_{j=1}^{k} \int d\Omega_j \psi(\Omega_j) \int_{\chi(\mathbf{r}_j,\Omega,\Omega_j|\lambda)=1} d\mathbf{r}_j g^{(k)}(\mathbf{r}_1\Omega_1, \ldots, \mathbf{r}_k\Omega_k, [\psi]) \tag{4.26}$$

The spatial integrations run over all configurations where the fluid particles overlap with the scaled particle, which is inserted at the origin. Note that in an orientationally ordered phase, the work done depends on the orientation of the inserted particle with respect to a fixed reference frame. The k-particle distribution functions that appear are generalizations of the well-known two-particle radial distribution function and are defined through the relation

$$\begin{aligned} \rho^{(k)}(\xi_1, \ldots, \xi_k, [\rho^{(1)}]) &= \left\langle \sum_{i_1 \neq i_2 \neq \ldots \neq i_k}^{N} \delta(\xi_1 - \xi_{i_1}) \ldots \delta(\xi_k - \xi_{i_k}) \right\rangle \\ &\equiv \left(\prod_{i=1}^{k} \rho^{(1)}(\xi_i) \right) g^{(k)}(\xi_1, \ldots, \xi_k, [\rho^{(1)}]) \end{aligned} \tag{4.27}$$

Since the k-particle distribution functions are identically zero in any configuration where two or more particles overlap each other (the probability of these configurations being zero), we can write down the expansion (4.25) in the case where the scaled particle is so small that no three particles can overlap with the scaled particle without also overlapping which each other:

$$\begin{aligned} e^{-\beta W(\Omega|\lambda)} = 1 &- n \int d\Omega_1 \psi(\Omega_1) \int_{\chi(\Omega,\Omega_1|\lambda)=1} d\mathbf{r}_1 \\ &+ \frac{1}{2} n^2 \int d\Omega_1 \psi(\Omega_1) \int d\Omega_2 \psi(\Omega_2) \\ &\times \int_{\chi(\Omega,\Omega_1|\lambda)=1} d\mathbf{r}_1 \int_{\chi(\Omega,\Omega_2|\lambda)=1} d\mathbf{r}_2 g^{(2)}(\mathbf{r}_1\Omega_1, \mathbf{r}_2\Omega_2, [\psi]) \end{aligned} \tag{4.28}$$

One can even reduce this expression further by using exact constraints on the pair distribution function to show that the second term does not contribute to second order in λ. One is thus left with

$$e^{-\beta W(\Omega|\lambda)} = 1 - n \int d\Omega_1 \psi(\Omega_1) \mathcal{E}(\Omega, \Omega_1|\lambda) \tag{4.29}$$

where we have introduced the excluded volume at fixed orientations between the scaled particle and one of the system particles. Recalling Eqs. (2.15) and (2.32) from Section II and the results from Appendix A.D, we can express this excluded volume explicitly as

$$\mathcal{E}(\Omega, \Omega_1|\lambda) = v_0(1 + \lambda^3) + \lambda(1 + \lambda)\left(\frac{1}{2}\mathcal{E}(\Omega, \Omega_1) - v_0\right) \tag{4.30}$$

Performing the expansion to second order in λ and adding the cubic term, we arrive at our final approximation for the average reversible work needed to add the scaled particle:

$$-\beta\bar{W} = \ln(1 - nv_0) - yW_2[\psi]\lambda - \frac{1}{2}\left(2W_2[\psi]y + W_3[\psi]y^2\right)\lambda^2 - \beta P v_0 \lambda^3 \tag{4.31}$$

where the parameter $y = nv_0/(1 - nv_0)$ is the one also introduced in the previous subsection and the functionals W_k are defined by

$$W_2[\psi] = \int d\Omega \int d\Omega' \psi(\Omega)\psi(\Omega')\mathcal{C}(\Omega, \Omega') \tag{4.32}$$

$$W_3[\psi] = \int d\Omega \int d\Omega' \int d\Omega'' \psi(\Omega)\psi(\Omega')\psi(\Omega'')\mathcal{C}(\Omega, \Omega')\mathcal{C}(\Omega, \Omega'') \tag{4.33}$$

with the kernel $\mathcal{C}$ is given by

$$\mathcal{C}(\Omega, \Omega') = \left(\frac{1}{2v_0}\mathcal{E}(\Omega, \Omega') - 1\right) \tag{4.34}$$

All the necessary ingredients have now been collected. The contact with thermodynamics is made through the obeservation that the excess chemical potential of the fluid is related to the average reversible work needed to create a cavity of the same size as the original particles, hence

$$\mu_{ex} = \int d\Omega \psi(\Omega) W(\Omega|\lambda = 1) \tag{4.35}$$

The equation of state can now be found by integrating the Gibbs–Duhem relation

$$\frac{\partial P}{\partial n} = 1 + n\frac{\partial \mu_{ex}}{\partial n} \tag{4.36}$$

The free energy is now easily calculated by using the relation $G = \mu N = F + PV$,yielding as our final result

$$\beta\mathcal{F}[\psi]/N = \ln \mathcal{V}_T v_0 + \ln y + \int d\Omega \psi(\Omega)(\ln \psi(\Omega) - 1) + W_2[\psi]y + \frac{1}{6}W_3[\psi]y^2 \tag{4.37}$$

This result looks identitical in structure to the y-equation result (Eq. 4.20) if one keeps terms up to second order in y. Indeed upon closer inspection, one finds that W_2 is in fact identical to C_2. The coefficient W_3, however, differs from the corresponding C_3, [161] except in the case of hard spheres where both approaches lead to the same result, which is also identitical to the one obtained from the exact solution to the Percus–Yevick equation [1] using the compressibility route for the equation of state.

It should be pointed out that the method of implementing SPT outlined above and followed, with minor variations, by all the papers cited, is not the optimal way of doing it. Tully-Smith and Reiss [58] have devised a more general scheme, based on the same ideas, that removes the limitation of expanding the work function just to third order in the scaling parameter and replacing it by an asymptotic expansion of the kernel of the work function in inverse powers of the scaling parameter. The coefficients in this expansion are then fixed by maximally exploiting a number of exact constraints.

c. Direct Correlation Function Approaches. In this section, we discuss the approaches to the problem of constructing a free energy functional for the nonisotropic HCB fluid that take the expansion about a reference fluid (4.10) as a starting point. We will take the reference fluid to be both isotropic and homogeneous, that is, $\rho_0^{(1)} = n_0/8\pi^2$ and at the same number density as the system, that is, $n_1 = n_0$. Since the free energy is a true functional, the path of the functional integration can be freely chosen to be of the simple form $\rho_\lambda^{(1)} = \rho_0^{(1)} + \lambda\Delta\rho^{(1)}$ where $\Delta\rho^{(1)} = \rho_1^{(1)} - \rho_0^{(1)}$. Using the fact that the one-particle direct correlation in the reference phase does not depend on the particle's coordinates, we arrive at

$$\Phi[\rho^{(1)}] = \Phi[\rho_0^{(1)}] + \frac{1}{2}\int d\xi d\xi' c^{(2)}(\xi, \xi, [\rho_0^{(1)}])\Delta\rho^{(1)}(\xi)\Delta\rho^{(1)}(\xi') \tag{4.38}$$

We now need to specify the two-particle direct correlation function in the reference phase. The various approaches discussed below distinguish themselves by the way in which they deal with this problem.

First, and as an aside, it is instructive to see that the previously described

Onsager approximation is recovered, if we replace the direct correlation by the first term in its low density expansion

$$c^{(2)}(\xi, \xi', [\rho_0^{(1)}]) = f(\xi, \xi'), \quad n_0 \ll 1 \tag{4.39}$$

where f is the Mayer function.

The most direct route to obtaining $c^{(2)}$ in the isotropic phase was followed by Patey and co-workers [23,25,162] who used results from the numerical solution of the various liquid state integral equations for the isotropic HCB fluid. In this scheme, one obtains a set of density dependent coefficients in an invariant expansion of the direct correlation function which can be used as input to the functional expansion. This is of necessity a rather involved procedure. Many authors therefore take the simplifying step of mapping the problem onto the direct correlation function for hard spheres, for which we possess an approximation in analytical form through the solution to the Percus–Yevick equation as well as several semi-empirical extensions thereof. Given the scarcity of hard information, these approximations are all, to a greater or a lesser degree, inspired guesses.

A first proposal, originally suggested by Pynn, [163,164] is to model the direct correlation function by the hard-sphere one, artificially made orientation dependent by scaling the interparticle distance with the distance of closest approach between the two HCBs $\sigma(\hat{\mathbf{r}}, \Omega, \Omega')$, where $\hat{\mathbf{r}}$ is the unit vector along the line connecting the centers of the two particles,

$$c^{(2)}(\mathbf{r}, \Omega, \Omega', [\rho_0^{(1)}]) = c_{\mathrm{HS}}^{(2)}(r/\sigma(\hat{\mathbf{r}}, \Omega, \Omega'), n_0) \tag{4.40}$$

This expression of course reduces to the correct expression for hard spheres. Since in this approach the influence of relative orientation is decoupled from the influence of interparticle distance, the name decoupling approximation is appropriate. It has the defect, first noticed by Lado, [165] that for $r \to 0$ the direct correlation function is predicted to be isotropic, contrary to reality.

Another proposal, due to Baus et al. [166] who formulated it with ellipsoids of revolution in mind, is the following:

$$c^{(2)}(\mathbf{r}, \Omega, \Omega', [\rho_0^{(1)}]) = \frac{\mathcal{E}(\Omega, \Omega')}{v_0} c_{\mathrm{HS}}^{(2)}(r/\sigma_{\mathrm{eff}}, n_{\mathrm{eff}}) \tag{4.41}$$

where in the simplest case the effective hard-sphere diameter is determined by the equal volume rule $4\pi\sigma_{\mathrm{eff}}^3/3 = v_0$ and the effective density n_{eff} is taken equal to the reference density n_0. By construction, this expression does not have the deficiency of being isotropic at short distances.

One can go one step further by assuming that one can use the expression (4.41) to describe an approximate direct correlation of an orientationally ordered phase. This new reference phase will already contain some of the effects of orientational order but still posses a rotationally invariant direct correlation function. To correct for the fact that there is on average less interaction between the partially aligned particles at a given density as compared to the isotropic fluid of the same density, the pseudonematic reference state should have a lower effective density. This effective density can be fixed by requiring the same value at contact of the direct correlation function in the purely isotropic case and in the effective nematic case, where the average contact distance in the latter case should be reduced in order to take into account the ordering of the particles. The perscription suggested by Colot et al. is the following

$$c^{(2)}_{\mathrm{HS}}(r/\sigma_{\mathrm{eff}} = 1, n_0) = c^{(2)}_{\mathrm{HS}}(r/\sigma_{\mathrm{eff}} = x, n_{\mathrm{eff}}) \tag{4.42}$$

where x is a factor that accounts for the reduced average contact distance. For ellipsoids, Colot et al. [167] unfortunately chose $x = b/a$ where a and b are the lengths of the major and minor axes, respectively. This implies an average contact distance *smaller* than the minor axis of the ellipsoids, which is of course unphysical.

d. Weighted Density Approximations. Next, we briefly discuss a class of methods for the construction of density functionals for HCB fluids, the so-called weighted density approximations (WDA), all traceable to the ideas originally suggested by Tarazona and Evans [168,169] and Curtin and Ashcroft [170,171] in their work on the inhomogeneous hard-sphere fluid. Consider our general expression for the density functional (4.10) in the case that the reference state is the zero density state, that is, $\Delta\rho^{(1)}(\xi) = \rho^{(1)}(\xi)$. In that case, the excess free energy functional can be written as

$$\Phi[\rho^{(1)}] = \int d\xi \rho^{(1)}(\xi) \Delta\psi(\xi, [\rho^{(1)}]) \tag{4.43}$$

where $\Delta\psi(\xi, [\rho^{(1)}])$ is a nonlocal functional of the ODF. The idea of the WDA is to replace this nonlocal functional by a *function* $\Delta\phi(\bar{\rho}^{(1)}(\xi))$ of a suitably chosen *local* density $\bar{\rho}^{(1)}(\xi)$. This local density is then taken to be some kind of weighted average of the true ODF over a neigborhood surrounding the point in question. In practice, the effective density is taken to depend only on the position and the orientational effects are included in an effective way through the averaging procedure. The usual form of this averaging is therefore

$$\bar{n}(\mathbf{r}) = \int d\mathbf{r}' \, d\Omega \, d\Omega' w(\mathbf{r} - \mathbf{r}', \Omega, \Omega') \rho^{(1)}(\mathbf{r}', \Omega') \tag{4.44}$$

The approximated excess free energy functional will then take the form

$$\Phi[\rho^{(1)}] = \int d\mathbf{r} n(\mathbf{r}) \Delta\phi(\bar{n}(\mathbf{r})) \tag{4.45}$$

where we have introduced

$$n(\mathbf{r}) = \int d\Omega \rho^{(1)}(\mathbf{r}, \Omega) \tag{4.46}$$

The two inputs of a specific WDA are thus the form of the weight function $w(\mathbf{r} - \mathbf{r}', \Omega, \Omega')$ and the explicit form of the function $\Delta\phi$.

The proposal put forward by Poniewierski and Holyst [172,173] is to take the following definition for the averaged local density:

$$\bar{n}(\mathbf{r}) = \int d\Omega \int d\mathbf{r}' \, d\Omega' \frac{1}{2B_2^{\text{iso}}} \chi(\mathbf{r} - \mathbf{r}', \Omega, \Omega') f(\mathbf{r}, \Omega) \rho^{(1)}(\mathbf{r}', \Omega') \tag{4.47}$$

where the orientational distribution function $f(\mathbf{r}, \Omega)$ is defined as

$$f(\mathbf{r}, \Omega) = \rho^{(1)}(\mathbf{r}, \Omega) / \int d\Omega' \rho^{(1)}(\mathbf{r}, \Omega') \tag{4.48}$$

and the isotropic second virial coefficient is introduced to obtain a proper normalization:

$$\int d\mathbf{r} \, d\Omega \, d\Omega' \chi(\mathbf{r} - \mathbf{r}', \Omega, \Omega') = \int d\Omega \, d\Omega' \mathcal{E}(\Omega, \Omega') \equiv 2(8\pi^2)^2 B_2^{\text{iso}} \tag{4.49}$$

Given the fact that the effective local density is independent of orientation so that the system is effectively sphericalized, it is natural to select an effective excess free energy density related to the hard sphere system. Poniewierski and Holyst chose

$$-\Delta\phi(n) = nB_2 + \left(\frac{\beta F_{\text{CS}}^{\text{excess}}}{N}(\eta) - 4\eta \right) \tag{4.50}$$

which is the Carnahan–Starling expression for the excess free energy per particle of the hard-sphere fluid in terms of the packing fraction η (see Ref. [1]) corrected to give the proper second virial coefficient for the non-spherical particles in the isotropic phase.

$$-\frac{\Delta\phi^{\text{CS}}(\eta)}{N} \equiv \frac{\beta F_{\text{CS}}^{\text{excess}}}{N}(\eta) = \frac{\eta(4 - 3\eta)}{(1 - \eta)^2} \tag{4.51}$$

A related approach is the one introduced by Somoza and Tarazona [174, 175]. They base their analysis on a mapping onto the system of parallel

hard ellipsoids (PHE) rather than onto the the hard-sphere fluid. In this way, they hope to include more of the anisotropic structure of the full HCB fluid into the reference system. Moreover, in the case of PHEs, one is able to make use of the fact that this system can be related to the hard sphere fluid using an affine scale changing transformation. [176] Their procedure is as follows. First select the equivalent PHE system through the rule that the volume of the PHE is equal to that of the HCB in question and that the the average moments of inertia of the HCB are proportional to those of the PHE, that is,

$$\langle \mathbf{I}_{\mathrm{HCB}} \rangle = \int d\Omega f(\mathbf{r}, \Omega) \mathbf{I}_{\mathrm{HCB}}(\Omega) \propto \mathbf{I}_{\mathrm{PHE}} \tag{4.52}$$

Then use a scaled version of the weighting function applied to the inhomogeneous hard-sphere fluid, [177] the scaling given by the mapping between the HS and PHE, to obtain the effective local density $\bar{n}(\mathbf{r})$ of the PHE. Finally, construct the WDA excess free energy functional for the PHE with an extra factor that corrects for the second virial coefficient of the HCB in a manner similar to that of the phenomenological Parsons approach.

$$\Phi[\rho^{(1)}] = \int d\mathbf{r}\, d\Omega \rho^{(1)}(\mathbf{r}, \Omega) \Delta\phi_{\mathrm{HPE}}(\bar{n}(\mathbf{r})) \frac{\int d\mathbf{r}'\, d\Omega' \rho^{(1)}(\mathbf{r}', \Omega') \chi_{\mathrm{HCB}}(\mathbf{r} - \mathbf{r}', \Omega, \Omega')}{\int d\mathbf{r}'\, d\Omega' \rho^{(1)}(\mathbf{r}', \Omega') \chi_{\mathrm{PHE}}(\mathbf{r} - \mathbf{r}')} \tag{4.53}$$

e. Empirical Approaches Finally, we discuss some of the more empirical approaches to the construction of theories for phase transitions in HCB fluids. In all cases an attempt is made to somehow incorporate nonsphericity into known results on the hard sphere system.

One of the first such theories is due to Flapper and Vertogen [178,179] who argued that the packing fraction η for hard spheres of diameter σ can also be interpreted as

$$\eta = \frac{\pi}{6}\sigma^3 n = \frac{1}{8} V_{\mathrm{excl}} n \tag{4.54}$$

where V_{excl} is the excluded volume of two spheres. They therefore proposed to identify the effective packing fraction for nonspherical particles (in a homogeneous, e.g., nematic phase) as

$$\eta_{\mathrm{eff}}[\psi] = \frac{1}{8} n \langle \mathcal{E}[\psi] \rangle = \frac{1}{8} n \int d\Omega\, d\Omega' \psi(\Omega) \psi(\Omega') \mathcal{E}(\Omega, \Omega') \tag{4.55}$$

The equation of state for the HCB fluid is then postulated to be the one for the HS fluid, but with the above effective packing fraction. Choosing

for instance the Carnahan–Starling relation [53] to model the HS behavior, we can construct the approximate free energy functional

$$\frac{\beta\mathcal{F}[\psi]}{N} = \int d\Omega\psi(\Omega)\ \ln\ \psi(\Omega) + \ln\ \mathcal{V}_T n + \frac{\eta[\psi](4-3\eta[\psi])}{(1-\eta[\psi])^2} \tag{4.56}$$

In a similar vein we have the "scaling" approach introduced by Lee. [180,181] Here the excess free energy of the Carnahan–Starling HS equation is rather arbitrarily multiplied by a scaling function that contains the dependence on the orientational distribution

$$\beta\mathcal{F}^{\text{excess}}[\psi] = \frac{\langle\mathcal{E}[\psi]\rangle}{8v_0}\left(\frac{\eta(4-3\eta)}{(1-\eta)^2}\right) \tag{4.57}$$

As was pointed out by Vroege and Lekkerkerker, [150] this result coincides with that of the so called decoupling approximations, both the direct correlation version discussed in Section. IV.A.2 above as well as one based on the radial distribution function discussed by Parsons. [182]

3. *Specific Transitions*

In this section we presents the results of the theoretical approaches described above as they are applied to the various liquid crystalline phase transitions thatoccur in HCBs.

a. Isotropic–Nematic Transition. The most studied transition occurring in HCB fluids is, of course, the isotropic–nematic transition. As is observed in the computer simulations, HCBs that are sufficiently nonspherical undergo a weakly first order transition from the low density isotropic phase to the uniaxially symmetric nematic phase. The first order nature of the transition is correctly captured by all theories. They differ, however, in their predictions about the strength and the location of the transition. Key quantities to compare are therefore the packing fractions η_{iso} and η_{nem} of the coexisting phases, the coexistence pressure P_{coex} conveniently expressed in dimensionless units as $P^* = \beta P v_0$ and the jump in the nematic order parameter $< P_2 >_c$ at the transition.

For ellipsoids of revolution, the most detailed comparisons can be made for particles with a length-to-width ratio $x = 3$. The results are summarized in Table I.

From these results it is clear that most theories *under*estimate the coexistence densities and probably *over*estimate the jump in the order parameter.[2] The scaling approach of Lee[181] seems incredibily accurate

[2]No reliable results are quoted for this quantity in the literature, but it is generally believed to be of the order of $< P_2 > \approx 0.35$

TABLE I
Comparisons of Results for the Isotropic–Nematic Transition of Several Theories with MC Data for the Case of Hard Ellipsoids at $x = 3$

Method	Source Reference	η_{iso}	η_{nem}	P^*_{coex}	$< P_2 >_c$
Monte Carlo	[183]	0.507	0.517	9.79	–
y-expansion true B_3	[41]	0.465	0.481	8.107	0.641
y-expansion approx. B_3	[160]	0.420	0.438	5.31	0.568
Integral equations	[25]	0.418	0.436	—	0.657
Decoupling approximation	[184]	0.493	0.494	–	0.017
Decoupling + partial $c^{(3)}$	[185]	0.314	0.335	–	0.547
Structural mapping	[167]	0.472	0.494	7.76	0.561
Structural mapping + decoupling	[186]	0.475	0.494	–	0.547
Weighted density	[173]	0.454	0.474	4.68	0.485
Scaling approach	[181]	0.508	0.517	10.00	0.533

as far as the densities and the pressure are concerned but this might be fortuitous since it does less well at length-to-breadth ratio $x = 2.75$ (although it might be argued that that is in fact a much harder case since we are close to the isotropic-nematic-solid triple point). In the light of the recent results from more extended simulations with larger number of particles at $x = 3$, [187] which indicate that the true transition densities are probably even higher than the ones quoted here, we should be careful to draw definite conclusions about the relative merit of these theories based on the numbers given.

We now turn to spherocylinders where we make a comparison at length-to-breadth ratio $x = 5$ in Table II The same general picture already apparent from the results on the ellipsoids is also evident here. The phenomenology of the transition is well captured, the numbers seem to be of the right order of magnitude but it is unclear whether they represent a *systematic* approximation to the the actual values. We return to these questions in the concluding remarks of this section.

The question of what happens to the isotropic–nematic transition if the particles are no longer uniaxially symmetric has a history dating back to Freiser's observation [189] that one could even imagine the formation

TABLE II
Comparisons of Results for the Isotropic–Nematic Transition of Several Theories with MC Data for the Case of Hard Spherocylinders at $x = 5$

Method	Source Reference	η_{iso}	η_{nem}	P^*_{coex}	$< P_2 >_c$
Monte Carlo	[188]	0.40	0.40	4.9	–
Integral equations	[25]	0.325	0.338	–	0.635
Weighted density	[173]	0.38	0.41	2.9	0.59
Scaling	[180]	0.400	0.418	5.36	0.667

of a biaxial nematic phase, that is, a phase where both a major and the minor axes of the molecule are orientationally ordered. In the context of hard particle fluids, the theoretical approaches were at first confined to systems of rectangular slabs that were only allowed a discrete set of orthogonal orientations. [193,190–193]. More progress was made with the analytical solution of the excluded volume problem at arbitrary relative orientations of a biaxial generalization of the spherocylinder, the so-called spheroplatelet, which allows, for example, the Onsager theory to applied to such a system. [55] Using the methods of bifurcation analysis, Mulder [194] was later able to clarify the distinct features of the phasediagram in the Onsager approximation for all hard particles having the same symmetry as rectangular slabs (symmetry group D_{2h}). The most important feature in this phase diagram, depicted schematically in Fig. 4.1, is the occurrence of a so-called Landau bicritical point as one continuously deforms a prolate particle into an oblate particle. This bicritical point is the end point of two

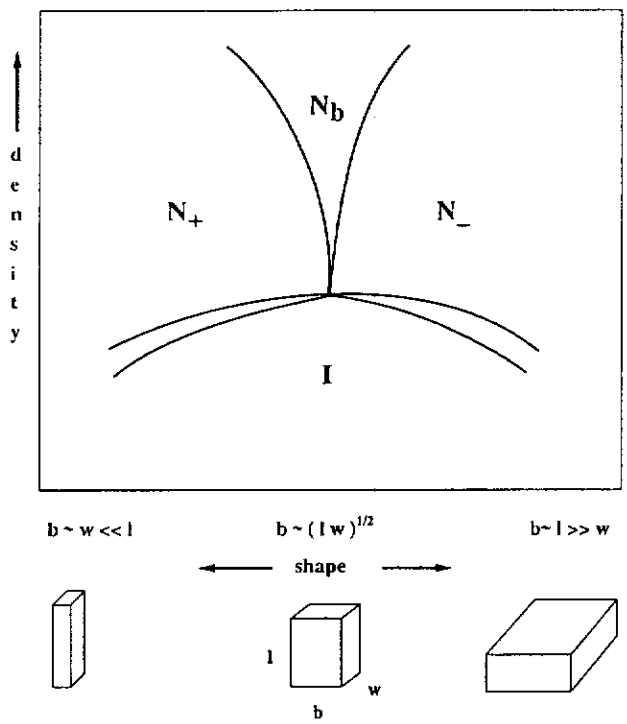

Figure 4.1. Schematic phasediagram for hard biaxial particles. On the horizontal axis the shape of the particle is varied by changing one of its characteristic lengths so that particles ranging from elongated rods to flat disks are obtained

first order transition lines to the rod-like (N_+) and plate-like (N_-) nematic phases formed by the rather prolate particles and rather oblate particles, respectively. The intermediate case is a particle which is neither distinctly rod-like nor platelike and undergoes a second order phase transition to a biaxial nematic (N_b) phase. The theory of Ref. [194] gives an analytical expression for determining this intermediate particle shape in terms of moments of the pair-excluded volume. If we characterize the particle by three distinct dimensions *l*ength $\leq$ *b*readth $\leq$ *w*idth then the "bicritical" shape is given approximately by the intuitively reasonable result

$$b_{\text{bi-cr}} = \sqrt{lw} \tag{4.58}$$

that is, the middle dimension is the geometric mean of the outer two. Hołyst and Poniewierski [195] considered the same type of system using their version of the weighted-density approximation as well as an adapted version of the scaling theory of Lee. [180] Although this involves more elaborate free energy functionals than the Onsager approximation, the results for the bicritical shape were nevertheless the same as in Ref. [194], a fact which can be explained by an application of formal methods [196] showing how relatively *in*sensitive results concerning the symmetry properties of phase diagrams are to the type of approximations employed. In fact the predictions of the theory are well borne out by the results of simulations performed by Allen [197] (see Section IV.B.3) on a system of hard biaxial spheroids.

A very recent result concerns the isotropic–cholesteric transition in a HCB fluid. By applying a torsional deformation to a biaxial spheroid, Evans [198] was able to construct a chiral HCB (this construction is explained in Appendix A.C). Employing a version of the Parsons–Lee [180] scaling approach, he was able to determine the pitch of the cholesteric helix which,for a realistic choice of molecular size and chirality, turns out to be a visible wavelength as is also observed in experiments.

b. Nematic-Smectic Transition. The fact that particles with purely repulsive interactions would be able to form a smectic would have been actively dismissed by most workers in the field until just a couple of years ago. Nevertheless, the possibility had been clearly demonstrated by Hosino et al. [199] as early as 1979. They considered a fluid of hard rods with their long axis constrained to point in a chosen preferential direction thus forming a "nematic" by design. Using an approximate method to locate a possible instability of such a phase to a density wave along the preferred direction, they were able to give predictions in the Onsager approximation for the packing fraction at which a smectic phase would set in and the initial

wavelength of the density modulation. Later on they showed [200] that the smectic phase even occurred in their model when the rods were allowed to point in three mutually orthogonal directions.

Since the first observation of the actual formation of a smectic phase in a system of parallel hard cylinders by Stroobants et al. [201] most theoretical work has concentrated on sytems of aligned rods. Interestingly enough, one of the simplest HCBs, the ellipsoid of revolution, does not show a smectic phase for the perfectly aligned system. This fact is easily understood on the basis of the observation made by Lebowitz and Perram [176] that a system of aligned ellipsoids can be mapped onto the hard sphere fluid by a global change of scale. Since hard-sphere fluids do not possess a smectic phase neither do the aligned ellipsoids. Theories have therefore concentrated on hard right circular cylinders and spherocylinders. We can compare their results by looking at their predictions for the critical packing fraction η_c and the wavelength λ_c of the smectic density modulation at the transition. In Table III, we collect the results on parallel cylinders which undergo a continuous transition, as is correctly predicted by all theoretical approaches. For hard spherocylinders the situation is somewhat more complex since the results depend on the length-to-width ratio $x = L/D$ of the particles. In the limit that $x \to \infty$, the results should coincide with those on the cylinders since in that limit the influence of the hemi-spherical caps becomes negligible. In Table IV we compare some results for $x = 3$.

By considering oblique cylinders or parallelepipeds, a number of authors have also studied smectic phases where the density wave is not parallel to the direction of molecular alignment thereby modelling the so-called smectic-C phase. [199,208]

A number of authors have also considered the possibility of the formation of a columnar phase in these systems [205,204,207,209] but since

TABLE III

Comparisons of Results for the Nematic–Smectic Transition of Several Theories with MC Data for the Case of Parallel Hard Cylinders. (Note That the Critical Wavelength Scales with the Length L of the Cylinder

Method	Source Reference	η_c	λ_c/L
Monte Carlo	[201]	0.35	1.27
Onsager	[202]	0.58	1.40
Onsager+B_3	[202]	0.36	1.35
Onsager+B_3+B_4	[202]	0.37	1.34
Effective free energy	[203]	0.35	1.28
Weighted density	[204]	0.28	1.40

TABLE IV
Comparisons of Results for the Nematic–Smectic Transition of Several Theories with MC Data for the Case of Parallel Hard Spherocylinders with Length-to-Breadth Ratio $x = 3$

Method	Source Reference	η_c	λ_c/L
Monte Carlo	[201]	0.43	≈ 1.6
Cell model	[205] [1]	≈ 0.5	≈ 1.6
Integral equation	[206]	≈ 0.38	≈ 1.5
Decoupling	[207]	0.36	1.65
Weighted density	[208]	0.42	1.6

[1] This theory predicts a first order N–S transition

the recent simulation results indicate that the stability of this phase is questionable [210] (see Section IV.B.4), we will not discuss this point in detail.

A final result on the nematic–smectic transition in aligned sytems worth mentioning is the recent work by Hołyst. [211] He considers parallel particles built up from a thinner and a thicker cylindrical segment, that is, particles that are not up-down symmetric. In a fluid where half of the particles points up and the other half down, he finds in the Onsager approximation a transition to a smectic phase with a double modulation of the density. The smallest wavelength is due to the tendency of the fluid to form closely coupled alternating layers with the molecules pointing up and down, respectively. These bilayers themselves are at a typical distance from each other given by the second, larger wavelength. This phase is commonly known as a smectic A_d phase.

The problem of the nematic–smectic transition for the case of freely rotating particles has also been considered by several authors: Poniewierski and Hołyst [172,212,213] using the weighted density approximation (see Eq. (4.47)) and Somoza and Tarazona [175,208,214] using their density functional theory with the aligned ellipsoids of revolution fluid as a reference system (see Eq. (4.53)). In both cases, the particles considered were sphero-cylinders. Unfortunately there exists only a single set of simulation data on this system for the case $x = 5$ making quantitative comparisons next to impossible. Nevertheless one notes major differences in the results of the two approaches. A key factor determining these differences is their respective predictions for the location of the tricritical point on the nematic–smectic transition line. For very elongated rods the theory predicts a continuous transition which is consistent with the idea that these systems at the typical N–S transition densities are almost fully orientation-

ally ordered and thus should behave like their perfectly aligned counterparts. [3] At a finite length-to-width ratio x_{tri} the transition is predicted to become first order. In the Poniewierski–Holyst theory this critical aspect ratio is predicted to be $x_{tri} = 5.9$ [213] while the Somoza–Tarazona result is $x_{tri} = 50$. The nature of this large discrepancy is at present not understood. Moreover, there is no indications from the simulation data at $x = 5$ that the transition is first order. Both theories do agree on the location of the isotropic-nematic-smectic triple point at $x \approx 3$.

Taylor and Herzfeld [216] applied scaled particle theory to a system of hard spheroplatelets with a view on determining the role of particle biaxiality on the nature and location of the smectic phase. They restricted themselves, however, to discrete orientations for the molecules. New features in their work are the appearance of a biaxial smectic phase and a near complete suppression of the biaxial nematic phase in favor of the smectic phase.

Finally, Evans [217] studied the question of how the shape of a particle influences the propensity to form smectic phases. He introduces a particle intermediate between the ellipsoid of revolution and the spherocylinder, the "ellipocylinder" which allows one to study a one-parameter family of shapes ranging from the ellipsoid of revolution, which does not form a smectic phase, to a spherocylinders that does. Using the Parsons–Lee "scaling" approach, he determines the phase diagrams of the different sytems. The main result is that the freely rotating "ellipocylinders" do form a smectic phase indicating that the ellipsoids of revolution are indeed a singular case.

c. Mixtures. Theoretical work on mixtures of hard particles has been very limited, although most of the theoretical approaches discussed here can in principle be generalized to treat multicomponent systems. Lekkerkerker and co-workers [218,219] considered binary mixtures of rods of different length in the Onsager approximation. The results show a host of new phenomena of which we mention (i) fractionation effects; the concentration of the longer rods is enhanced in the nematic phase; (ii) widening of the coexistence region; the density of the isotropic phase at coexistence may be substantially smaller than that of the nematic phase; (iii) re-entrancy; on

[3] Recent work by Poniewierski [215] who analyzed the behavior of spherocylinders in the limit $L/D \to \infty$ shows that this is a rather subtle question. In fact there are non-zero contributions to the free energy due to the rotational freedom of the particles even in the limit. This shows that one can not simply identify the infinitely long rods with the aligned system as had been tacitly assumed by most workers

the increace of density some mixtures can undergo a re-entrant transition from a nematic phase to an isotropic phase.

Another system of interest is a mixture of rod-like and plate-like particles. Alben [220] predicted on the basis of a lattice model that such a mixture might form a biaxial nematic phase at certain compositions. In fact the phase diagram of this mixture as a function of composition should be isomorphic to the one shown in Fig. 4.1. Rabin et al. [221] and Stroobants and Lekkerkerker [219] later considered this question for hard particles in the Onsager approximation and essentially confirmed Alben's predictions. A later paper by Palffy-Muhoray et al. [222], albeit dealing with a mean field description, raised the question whether phase separation between a rod-like and plate-like nematic phase would not be thermodynamically more favourable. To our knowledge, this is still an open question.

d. Two-Dimensional Nematics. Two-dimensional liquid crystals are very different from their three-dimensional counterparts. This can be clearly demonstrated by considering the isotropic–nematic transition in two dimensions. On basis of the Landau theory of phase transitions, we expect that the isotropic nematic transition in two dimensions should be of second order. Density functional theory [223] predicts the same. However, the actual situation is much more subtle than that. The point is that two-dimensional nematics are very similar to the two-dimensional Heisenberg system ("2D-xy model") and hence there is a possibility that topological defects have a pronounced effect on the nature of the phase transitions. [224] In order to see this, we should consider the change in free energy of a two-dimensional nematic, due to distortions of the director field. In fact, in Section V.A.4, we discuss the so-called Frank distortion free energy of a 3D nematic liquid crystal in some detail. Here we simply "borrow" the expression for the distortion free energy of a $3D$ nematic (Eq. 5.8) and adapt it to the 2D case under consideration. We choose the average director along the y-axis. We denote the angle between the average director and the instantaneous local director by θ. By analogy to the three-dimensional case, [2] the expression for the deformation free energy is of the form

$$\begin{aligned} F_D &= \frac{1}{2}K_1(\partial_x n_x)^2 + \frac{1}{2}K_3(\partial_y n_x)^2 \\ &= \frac{1}{2}K_1(\partial_x \theta)^2 + \frac{1}{2}K_3(\partial_y \theta)^2 \end{aligned} \tag{4.59}$$

where K_1 and K_3 are the "splay" and "bend" elastic constants discussed in Section V.A.4. In the last line of Eq. (4.59), we have assumed that θ

is small. We shall simply postulate that the deformation free energy of a 2D nematic is given by Eq. (4.59). Moreover, we shall assume for the sake of convenience that $K_1 = K_3$. In that case, we obtain a very simple expression for the deformation free energy density;

$$F_D = \frac{1}{2}K(\nabla\theta)^2 \tag{4.60}$$

Using this expression, it is easy to compute the elastic contribution to the free energy of a single π-disclination in a 2D nematic. Consider a circular path (circumference $2\pi r$) around the disclination core. Along this path, the director rotates over an angle π. Hence $(\nabla\theta)^2 = (1/2r)^2$. If we insert this expression in Eq. (4.60) and integrate from the disclination core (radius a_0, say) to L (the linear dimension of the system), then we find that the elastic energy of an isolated disclination is

$$F_{\text{el}} = \frac{1}{2}K\int_{a_0}^{L}\frac{2\pi r}{4r^2}\,dr = \frac{\pi K}{4}\log(L/a_0) \tag{4.61}$$

Clearly, $F_{\text{el}} \to \infty$ if $L \to \infty$. This would seem to suggest that no free disclinations are possible in a $2D$ nematic. However, we should also consider the "configurational entropy" of a single disclination, that is, the entropy $k \log \Omega$ associated with the number of distinct ways in which we can place a disclination in a two-dimensional area L^2. If we use a_0 as our unit of length, then the configurational entropy is given by $k \log(L/a_0)^2$ (where we have neglected an additional constant, independent of system size). Combining this expression for the configurational entropy with our expression for the elastic free energy (Eq. 4.61), we obtain the following expression for the total free energy of a single disclination in a 2D nematic:

$$F_{\text{total}} = \left(\frac{\pi K}{4} - 2kT\right)\log(L/a_0) \tag{4.62}$$

Equation (4.62) suggests that if $kT < (\pi K/8)$, no free disclinations are possible, whereas for $kT > (\pi K/8)$, spontaneous generation of free disclinations may take place. However, if a nematic contains a finite concentration of free disclinations, orientational correlations are destroyed over distances longer than the characteristic separation of the free defects and the resulting phase is an isotropic fluid. This simple version of the Kosterlitz–Thouless scenario for defect mediated phase transitions predicts that the nematic phase cannot be stable above a critical temperature $kT^* = (\pi K/8)$. At that temperature, there is a continuous phase transition (of "infinite" order) from the nematic to the isotropic phase. However,

there is an alternative possibility: namely that the I–N transition is simply first order. But if the I–N transition is of first order, then this transition must occur *before* the nematic phase has reached the point where it becomes unstable with respect to the formation of free disclinations; that is, at a first order I–N transition, the following inequality *must* hold:

$$K > \frac{8kT}{\pi}$$

This condition also follows from the more rigorous version of the KT-theory.

Note that our discussion of the disclination-mediated I–N transition was based on the assumed from of the Frank free energy (Eq. 4.59). It should be stressed that this form of the deformation free energy has quite drastic consequences for the nature of orientational order in 2D nematics. In particular, it implies that there exists no true long-ranged orientational order in such systems. We define the ℓth orientational correlation function as

$$g_\ell(r) \equiv < \cos 2\ell(\theta(0) - \theta(r)) > = \mathrm{Re} < \exp[-2i\ell(\theta(0) - \theta(r))] > \quad (4.63)$$

Using the fact that the free energy (Eq. 4.60) is quadratic in $\theta(\mathbf{k})$, it is easy to show that $g_\ell(r)$ has the following form:

$$g_\ell(r) = \left(\frac{r}{a_0}\right)^{-2\ell^2 kT/\pi K} \equiv \left(\frac{r}{a_0}\right)^{-\eta_\ell} \quad (4.64)$$

where the last term on the right-hand side of Eq. (4.64) defines the exponent η_ℓ. Note that this equation implies that, provided that Eq. (4.59) is valid, there is no true long-range orientational order in a 2D nematic, but algebraic or "quasi long-range" order. Similarly, it can be shown that the order parameter $< \cos 2\theta >$ also vanishes algebraically with increasing system size:

$$< \cos 2\theta > \propto \left(\frac{L}{a_0}\right)^{-kT/\pi K} \quad (4.65)$$

Now recall that a 2D nematic is only expected to be stable against the spontaneous generation of free disclinations, when K is larger than $\pi/(8kT)$. Hence, at the K–T transition, the orientational correlation functions and the nematic order parameter must satisfy the following relations:

$$g_\ell(r) = \left(\frac{r}{a_0}\right)^{-\ell^2/4} \quad (4.66)$$

$$< \cos 2\theta > \propto \left(\frac{L}{a_0}\right)^{-1/8} \tag{4.67}$$

Two points should be stressed: (1) if the I–N transition is first order, then at the transition the exponents of g_ℓ and $< \cos 2\theta >$ must be less than the critical values given by Eq. (4.66); (2) the above arguments rest on the assumption that the deformation free energy is of the form given by Eq. (4.60). If this expression is valid, 2D nematics can only have algebraic orientational order. However, it has thus far only been possible to prove the absence of true long-range orientational order for a certain class of short-ranged potentials called *separable*. [225] A pair-potential is called separable if the interaction energy of two molecules at fixed center-of-mass separation $\mathbf{r}_{ij}$ depends only on the relative orientation of the two molecular axes $\mathbf{u}_i \cdot \mathbf{u}_j$, but not on $\mathbf{r}_{ij} \cdot \mathbf{u}_i$ or $\mathbf{r}_{ij} \cdot \mathbf{u}_j$. Realistic pair-potentials are hardly ever separable. We come back to this point in Section IV.B.5.

4. Critical Discussion

After having reviewed the various approaches to the theory of phase transitions in HCB fluids it seems fitting to comment on what has been achieved so far. On the one hand we observe that, more or less, all theories are able to reproduce the phenomenology of the phase transitions in question. It is worth pointing out that one does not need an elaborate density functional to achieve this goal. In fact most of the transitions that occur can be understood on the basis of the Onsager approximation alone. For the class of functionals that do not explicitly contain a three particle contribution, this observation can even be given a formal justification, [196] at least as far as transitions from the isotropic phase are concerned.

As far as the quantitative predictions of the various theories are concerned the situation is less clear. In many cases, reasonable to good results (as compared to simulations) are obtained. However, one is at a loss to understand why a specific choice of functional performs well or not. Moreover it is not evident that one can systematically improve on the proposals given here. The techniques based on series expansions of the free energy functional (generalized Onsager and y-expansion) are liable to suffer from convergence problems even if the difficulties of obtaining higher order contributions was surmounted. Scaled particle theory should in principle be extensible but its quantitative predictions at the level where we are able to use it are not encouraging. The direct correlation function approaches are even harder to generalize. In the case of the integral equations, one first of all has to deal with the unknown influence of the choice of the closure equation. Next, in order to deal with true breaking of symmetry, one should really solve a coupled set of equations involving both the ODF and

a correlation function, rather than study the instabilities of the isotropic phase. This has not been attempted so far. The approaches based on the idea of a local weighted density are burdened by the fact that the choice of weighting function is essentially arbitrary and that it is unclear whether the hard-sphere equation of state is indeed the proper reference system for the thermodynamics of nonspherical particles.

At a more general level, one should keep in mind that constructing a density functional also implies certain approximations for the correlation functions. Since density functionals are usually employed to study the thermodynamics of the systems involved, this is not often discussed. It remains to be seen whether the approximate correlation functions bear any resemblance to the real ones for these systems. Probably the theory of HCB fluids still has a long way to go before it achieves the level of simultaneous prediction of both the structure and the equation of state that is obtained in the current theories of the hard-sphere fluid.

B. Simulations

1. Phase Transitions and Free Energy

In order to map the "phase diagram" of a hard-core model system by computer simulation, we must be able to accurately locate all phase transitions. In this section, we section we discuss the special techniques that are required to locate first-order phase transitions.

The most direct way to study first order phase coexistence in a computer simulation would be to simply change the temperature or pressure of the system under study until a phase transformation occurs. In the real world, it is often (although by no means always) possible to ensure that such a phase change takes place reversibly. The coexistence point is defined as the point where the reversible phase transformation occurs. At coexistence, the temperature and pressure of the coexisting phases are equal. In addition, the chemical potential of every individual species α must have the same value in every phase.

$$P_{\mathrm{I}} = P_{\mathrm{II}}, \qquad T_{\mathrm{I}} = T_{\mathrm{II}}, \qquad \mu_{\mathrm{I}}^{\alpha} = \mu_{\mathrm{II}}^{\alpha} \tag{4.68}$$

Although it is usually not possible to locate a phase transition in a simulation by direct observation of the coexistence of two phases, much progress has been made during the past few years in the simulation of phase coexistence of moderately dense fluid phases. The so-called Gibbs-ensemble method of Ref. [226] relies on the fact that it is possible to satisfy the conditions for coexistence between two bulk phases (or, to be more precise, homogeneous phases with periodic boundary conditions)

by allowing them to exchange both volume and molecules. Unfortunately, such a direct simulation method is of limited value in computer simulations of transitions involving dense phases that have some translational order. The reason why the Gibbs-ensemble method breaks down under those circumstances is twofold. First, pronounced hysteresis effects are usually observed in computer simulations of a strong first order phase transition, such as melting. This implies that it is difficult for the molecules in the system to spontaneously rearrange from a configuration belonging to the "old" phase, to one that corresponds to the "new" phase. But even if the two different phases have somehow been prepared, it is usually impossible to exchange particles between them. As a consequence, we cannot ensure the equality of the chemical potential in the two phases.

Under those circumstances, it is still possible to locate the point where the two phases coexist. But in order to do so, we must explicitly compute the chemical potential of the homogeneous phases at the same temperature and pressure and find the point where the two μ's are equal. Below, we describe several techniques that can be used to compute the chemical potential (or, equivalently, the Helmholtz free energy) of particles in dense phases.

a. The Natural Way. When discussing techniques to measure free energies, it is useful to recall how such quantities are measured experimentally. In the real world, free energies cannot be obtained from a single measurement either. What can be measured, however, is the derivative of the free energy with respect to volume V and temperature T:

$$\left(\frac{\partial F}{\partial V}\right)_{NT} = -P \tag{4.69}$$

and

$$\left(\frac{\partial F/T}{\partial 1/T}\right)_{NV} = E \tag{4.70}$$

Here P is the pressure and E the energy of the system. The trick is now to find a reversible path that links the state under consideration to a state of known free energy. The change in F along that path can then simply be evaluated by integration of Eqs. (4.69) and (4.70). In the real world, the free energy of a substance can only be evaluated directly for a very limited number of thermodynamic states. One such state is the ideal gas phase, the other is the perfectly ordered ground state at $T = 0$K. In computer simulations, the situation is quite similar. In order to compute the free energy of a dense liquid, one may construct a reversible path to the very dilute gas

phase. It is not really necessary to go all the way to the ideal gas. But at least one should reach a state that is sufficiently dilute that the free energy can be computed accurately, either from knowledge of the first few terms in the virial expansion of the compressibility factor PV/Nk_BT, or that the chemical potential can be computed by other means (see Ref. [227] and Section IV.B.2 below). For the solid, the ideal gas reference state is less useful (although techniques have been developed to construct a reversible path from a dense solid to a dilute (lattice-) gas [228]). The obvious reference state for solids is the harmonic lattice. Computing the absolute free energy of a harmonic solid is relatively straightforward, at least for atomic and simple molecular solids. However, for hard-core models, the crystalline phase is never harmonic. Hence, other techniques are required to compute the free energy of hard-core solids.

b. Artificial Reversible Paths. Fortunately, in computer simulations we do not have to rely on the presence of a "natural" reversible path between the phase under study and a reference state of known free energy. If such a path does not exist, we can construct an artificial path (see e.g. Ref. [1]). It works as follows: consider a case where we need to know the free energy $F(V,T)$ of a system with a potential energy function U_1, where U_1 is such that no "natural" reversible path exists to a state of known free energy. Suppose now that we can find another model system with a potential energy function U_0 for which the free energy *can* be computed exactly. Now let us define a generalized potential energy function $U(\lambda)$, such that $U(\lambda = 0) = U_0$ and $U(\lambda = 1) = U_1$. The free energy of a system with this generalized potential is denoted by $F(\lambda)$. Although $F(\lambda)$ itself cannot be measured directly in a simulation, we can measure its derivative with respect to λ:

$$\left(\frac{\partial F}{\partial \lambda}\right)_{NVT\lambda} = \left\langle \frac{\partial U(\lambda)}{\partial \lambda} \right\rangle_{NVT\lambda} \tag{4.71}$$

If the path from $\lambda = 0$ to $\lambda = 1$ is reversible, we can use Eq. (4.71) to compute the desired $F(V,T)$. We simply measure $(< \partial U/\partial \lambda >$ for a number of values of λ between 0 and 1. Typically, 10 quadrature points will be sufficient to get the absolute free energy per particle accurate to within $0.01k_BT$. However, it is important to select a reasonable reference system. For solids, one of the safest approaches is to choose as a reference system an Einstein crystal with the same structure as the phase under study. [229] This choice of reference system makes it improbable that the path connecting $\lambda = 0$ and $\lambda = 1$ will cross an (irreversible) first order phase transition from the initial structure to another, only to go back to its

original structure for still larger values of λ. Nevertheless, it is important that the parametrization of $U(\lambda)$ be chosen carefully. Usually, a linear parametrization (i.e., $U(\lambda) = \lambda U_1 + (1 - \lambda)U_0$) is quite satisfactory. But for hard particles, such a λ-parametrization leads to problems because one cannot continuously switch off a hard-core potential using a *linear* parametrization. In Appendix B.A, we briefly sketch how to compute the Helmholtz free energy of the crystalline state of a system of non-spherical hard particles. More details about such free energy computations can be found in Refs. [81,227,230,231].

2. *Phase Transitions in Liquid Crystals*

Let us consider how the techniques sketched in the previous section can be applied to first order phase transitions in liquid crystals. At the outset, it should be stressed that it is often not trivial to construct a reversible path that will link a liquid-crystalline phase to a state of known free energy. Usually, the liquid-crystalline phase of interest will be separated by first order phase transitions from both the dilute gas and the low temperature (harmonic) solid. In the case of the nematic phase, this problem has been resolved by switching on a strong ordering field. In the presence of such a field, the first order isotropic–nematic transition is suppressed and a reversible expansion to the dilute gas becomes possible. [75] However, this approach has one obvious disadvantage: in order to compute the (very small) difference in the free energy of the isotropic and the nematic phase, we subtract two large numbers. The first is the change in (excess) free energy of the isotropic phase upon compression from the dilute gas to the I–N transition. The second is the change in free energy associated with (**a**) the alignment of the dilute gas in a strong field, (**b**) the compression of this aligned fluid to the density of the nematic phase and (**c**) the switching off of the aligning field at this density. Usually, the free energy change in step (**a**) is evaluated analytically. However, the other steps all require numerical integration. As a consequence, our estimate of difference in free energy of the isotropic and nematic phases is usually rather inaccurate. In this respect, the method is similar to the one used to locate the liquid–vapour transition by integrating around the critical point. It also suggests that the solution of this problem may be similar; rather than constructing a long "physical" integration path, it may be advantageous to construct a short "artificial" path. For instance, it is in principle straightforward to compute the reversible work needed to transform the isotropic phase directly into the nematic phase along a "reaction path" where we constrain the nematic order parameter to take on values intermediate between isotropic and nematic. In a different context, this approach has been explored by van Duijneveldt and Frenkel. [232]

a. Particle Insertion Method. An alternative method that can be used to compute the free energy of a fluid phase (including the nematic phase) is the so-called particle insertion method of Widom. [16] The statistical mechanics that is the basis for this method is quite simple. Consider the definition of the chemical potential μ_α of a species α. From thermodynamics, we know that μ is defined as

$$\mu = \left(\frac{\partial F}{\partial N}\right)_{VT} \tag{4.72}$$

where F is the Helmholtz free energy of the N-particle system. If we express the Helmholtz free energy of an N-particle system in terms of the partition function Q_N (Eq. 2.104), then it is obvious from Eq. (4.72) that, for sufficiently large N the chemical potential is given by $\mu = -kT \ln(Q_{N+1}/Q_N)$. If we use the explicit form (Eq. 2.104) for Q_N, we find

$$\begin{aligned}\mu &= -kT \ln(Q_{N+1}/Q_N) \\ &= -kT \ln\left(\frac{q(T)V}{N+1}\right) - kT \ln\left(\frac{\int d\mathbf{s}^{N+1} \exp(-\beta U(\mathbf{s}^{N+1}))}{\int d\mathbf{s}^N \exp(-\beta U(\mathbf{s}^N))}\right) \\ &= \mu_{\text{id}}(V) + \mu_{\text{ex}} \,.\end{aligned} \tag{4.73}$$

In the last line of Eq. (4.73), we have indicated the separation in the ideal gas contribution to the chemical potential, and the excess part. As $\mu_{\text{id}}(V)$ can be evaluated analytically, we focus on μ_{ex}. We now separate the potential energy of the $(N+1)$-particle system into the potential energy function of the N-particle system, $U(\mathbf{s}^N)$, and the interaction energy of the $(N+1)$th particle with the rest: $\Delta U \equiv U(\mathbf{s}^{N+1}) - U(\mathbf{s}^N)$. Using this separation, we can write μ_{ex} as

$$\mu_{\text{ex}} = -kT \ln < \int d\mathbf{s}_{N+1} \exp(-\beta \Delta U) >_N \tag{4.74}$$

where $< \cdots >_N$ denotes canonical ensemble averaging over the configuration space of the N-particle system. The important point to note is that Eq. (4.74) expresses μ_{ex} as an ensemble average that can be sampled by the conventional Metropolis scheme. This last integral can be sampled as follows: we carry out a constant NVT Monte Carlo simulation on the system of N particles. At frequent intervals during this simulation we randomly generate a coordinate $\mathbf{s}_{N+1}$, uniformly over the unit cube. With this value of $\mathbf{s}_{N+1}$, we then compute $\exp(-\beta \Delta U)$. By averaging the latter quantity over all generated trial positions, we obtain the average that appears in Eq. (4.74). So, in effect, we are computing the average of the Boltzmann factor associated with the random insertion of an additional

particle in an N-particle system, but we never accept any such trial insertions, because then we would no longer be sampling the average needed in Eq. (4.74). The Widom method is a very powerful method to compute the chemical potential of (not too dense) atomic and simple molecular liquids. Its main advantage is its great simplicity, and the fact that it can be added onto an existing constant NVT MC program, without any modifications to the original sampling scheme; we are simply computing one more thermal average.

The Widom method was first applied to the evaluation of the free energy of the isotropic and nematic phases of infinitely thin platelets by Eppenga and Frenkel. [67] The particle insertion scheme is well suited for the latter system, as the method works best for strongly anisometric molecules at low density. In fact, in Ref. [67] it is shown that, in the case of nematics, the scheme can be made more efficient by inserting particles that are aligned with the nematic direction. For details, we refer the reader to Ref. [67].

b. Free Energies of Smectic and Columnar Phases. For the calculation of free energies of smectic and columnar phases, other techniques have to be used. The situation is simplest if the transition from the nematic to smectic phase is continuous (or, at least, free of hysteresis). In that case, the "natural" thermodynamic integration of Eq. (4.69) may be used to compute the free energy of the smectic phase, assuming that we know the free energy of the nematic phase. This approach was, for instance, followed in Refs. [201,233]. Often, however, the smectic phase cannot be expanded or compressed reversibly into a phase of known free energy. In such cases, we should construct an artificial path to a phase of known free energy. For instance, in the study of the phase behavior of freely rotating spherocylinders, a smectic phase was observed that was separated by first order phase transitions from both the isotropic and the solid phase. [234] However, in the corresponding system of *parallel* spherocylinders, the smectic phase could be expanded reversibly to the dilute gas reference state. In this case, it was possible to compute the free energy of the smectic phase of freely rotating molecules, by computing the (excess) reversible work required to align the spherocylinders.

Even if such a convenient reference system is not at hand, there exist fairly robust schemes to compute the free energy of an arbitrary smectic or, for that matter, columnar phase. In the case of a smectic, we can exploit the fact that a smectic phase can be considered as a one-dimensional solid stacking of 2D fluid (S_A) *or* solid (S_B) layers. Similarly, a columnar phase resembles a 2D crystal of 1D fluid columns. In Ref. [230], a technique is described that makes it possible to reversibly decompose such smectic (columnar) phases into isolated fluid layers (columns). However, this ap-

proach has, to our knowledge, not yet been applied to such liquid crystals. It should be stressed that such absolute free energy calculations need not be repeated for *every* model that we may care to study. For instance, if we have computed the absolute free energy of one state point in the smectic phase of rod-like molecules with an aspect ratio of 5 (say), then we can compute the free energy of the smectic phase of similar molecules with another aspect ratio simply by computing the reversible work needed to change the shape of our model particles from the initial aspect ratio to the desired value. [235] Such an approach has been followed by Allen in his study of biaxial ellipsoids. [197]

c. Alternatives to Free Energy Calculations. Up to this point, we have discussed various techniques that allow us to locate a first order phase transition in a computer simulaion. Sometimes, however, such calculations may result in a less accurate estimate of the phase transition than can be obtained from other criteria. This is of particular relevance in the case of weak first order phase transitions, such as the one separating the isotropic fluid from the nematic phase. In the latter case, the coexistence point is bracketed by a rather narrow pressure (or temperature) range where hysteresis occurs. Clearly, if our free energy calculations result in an inaccuracy in the coexistence pressure that exceeds the range where hysteresis occurs, we might as well have estimated the location of the phase transition directly from the equation of state data. Another, less well founded but quite convenient, criterion to locate the I–N transition is to use the equivalent of the Lindemann rule for the I–N transition. Experimentally, it is known that, at the isotropic–nematic transition, the order–parameter in the nematic phase has a value of 0.35 ± 0.15. It would seem that such an ill-defined "melting rule" cannot possibly provide us with a very accurate estimate of the I–N transition. However, in the vicinity of the I–N transition, the nematic order parameter varies quite steeply. As a consequence, the above rule of thumb usually yields an estimate of the density of the I–N transition that is as least as good as the one obtained by free energy calculations.

3. *Results: Spheroids*

Computer simulations of hard-core models for two-dimensional liquid crystals were pioneered by Vieillard-Baron in the early 1970s. [5] Vieillard-Baron also made much progress towards the study of three-dimensional model systems, [6] but did not observe spontaneous nematic ordering in 3D. The first systematic simulation study of a three-dimensional hard-core nematogen was performed by Frenkel and Mulder [75] who studied a system of hard ellipsoids of revolution for a number of length-to-width ratios between 1/3 and 3.

The shape of hard ellipsoids of revolution is characterized by a single parameter, x, the ratio of the length of the major axis ($2a$) to that of the minor axis ($2b$): $x = a/b$ (in the literature, both e and x are used to denote the ratio a/b). Prior to the simulations reported in Ref. [75], the phase behavior of hard spheroids was only known for a few special values of x, viz. $x = 1$: hard spheres, which freeze at 66% of close packing. [236] $x \to \infty$: thin hard needles, because this limit is equivalent to the Onsager's model. The latter system has a transition to the nematic phase at vanishing volume fraction. And $x \to 0$: thin hard platelets, which also form a low density nematic. [67] The simulations of Ref. [75] were performed on a system containing $\sim 10^2$ particles and for values of x between 3 and 1/3. In order to locate all phase transitions, the absolute free energy of all phases was computed. Figure 4.2 shows how the stability of the different phases of hard ellipsoids depend on their length-to-width ratio. Four distinct phases can be identified, namely the low density isotropic fluid, an intermediate density nematic liquid-crystalline phase, which is only stable if the length-to-width ratio of the ellipsoids is larger than 2.5 or less than 0.4, and a high density orientationally ordered solid phase. In the case of weakly anisometric ellipsoids, an orientationally disordered solid

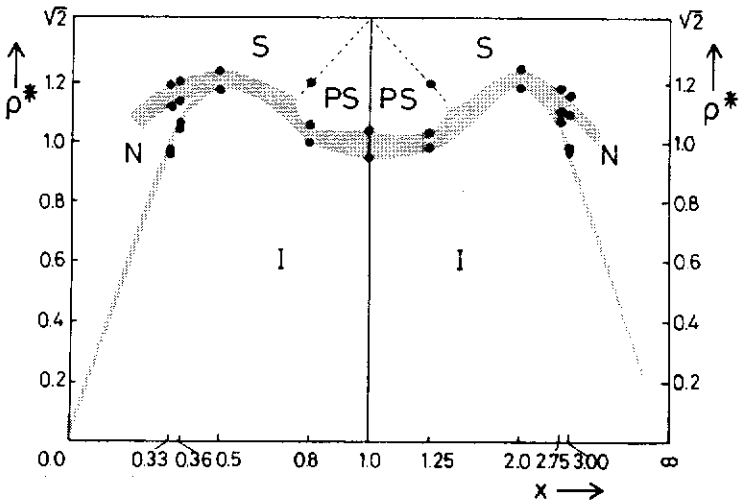

Figure 4.2. "Phase diagram" of a system of hard ellipsoids of revolution. [75] The ratio of the length of the semi-major to the semi-minor axis is denoted by x. The reduced density ρ^* is defined such that the density of regular close packing is equal to $\sqrt{2}$ for all x. The shaded areas indicate two-phase regions associated with a first order phase transition. The following phases can be distinguished: **I**; isotropic fluid, **S**; orientationally ordered crystalline solid. **PS**; orientationally disordered ("plastic") crystal, and **N**; nematic liquid-crystalline phase. The densities of coexisting phases at a first order phase transition (black dots) were computed in a free-energy calculation. Note that no stable nematic is possible for $0.4 < x < 2.5$.

phase was also observed. One thing to note about the phase transitions in the hard-ellipsoid system is that for particles with $3 \geq x \geq (1/3)$ the relative density-jump at the I–N transition is much smaller than for the Onsager model. Typically, the density changes only by some 2% at the I–N transition. Hence the very large density discontinuity at the I–N transition in the Onsager model (more than 20%) is peculiar to long rods and not to hard-core models in general. Recent simulations of Zarragoicoechea et al. [187] indicate that, although the nematic phase is stable in a system of $\mathcal{O}(100)$ ellipsoids with an axial ratio $x = 3$, the nematic phase becomes unstable for systems of 256 ellipsoids. This result is surprising in view of the fact that Allen and Frenkel found an (apparently) stable nematic phase for a system consisting of up to 216 particles. It seems likely that the very weakly first order isotropic nematic transition is more sensitive to finite-size effects than a strong first order transition, such as freezing. In any event, the findings of Ref. [187] suggest that the isotropic–nematic transition line may have a slightly larger slope than indicated in Fig. 4.2. It seems unlikely that this will affect the qualitative features of the phase diagram. However, when we speak about "the" phase diagram of hard ellipsoids of revolution, the reader should bear in mind that the results that we discuss were obtained for system sizes of the order of 100 particles.

Perhaps the most striking feature of the phase diagram in Fig. 4.2 is the near symmetry between the behavior of oblate and prolate ellipsoids with inverse length-to-width ratios. Prolate-oblate ($x \rightarrow 1/x$) symmetry of ellipsoids is to be expected at *low* densities because the second virial coefficient $B_2(x)$ equals $B_2(1/x)$. However, no such relation holds between the third and higher virial coefficients. To give a specific example: in the limit $x \rightarrow \infty$ (the Onsager limit), $B_3/B_2^2 \rightarrow 0$, whereas for $x \rightarrow 0$ (hard platelets [67]) $B_3/B_2^2 \rightarrow 0.4447(3)$. Hence there is no reason to expect any exact symmetry in the phase diagram of hard ellipsoids of revolution. For larger anisometries than studied in the simulations of Ref. [75] one should expect to see asymmetric behavior in the location of the isotropic–nematic transition. In fact, Allen has performed simulations of ellipsoids with aspect ratios 5, 10, 0.2 and 0.1. [237] These simulations show that, as the molecular anisometry increases, the isotropic–nematic transition continues to shift to lower densities. This is to be expected in view of the known limiting behavior of infinitely thin hard platelets and infinitely thin hard rods (see above). However, in Ref. [237] the exact location of the isotropic–nematic transition is not computed.

Even though we expect to see appreciable prolate-oblate asymmetry in the location of the isotropic–nematic transition for highly anisometric spheroids, it is doubtful if the near symmetry of the melting line will be much affected. Strongly aligned rods and platelets follow the same

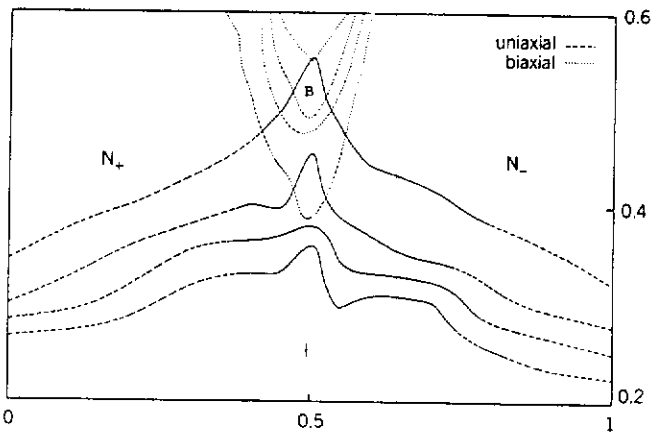

Figure 4.3. $\rho/\rho_{\text{close-packed}}$ of a system of biaxial ellipsoids with axial ratio $c/a = 10$, while b/a varies between 1 (prolate limit) and 10 (oblate limit). In this figure, b/a is represented on a logarithmic scale with base 10. The dashed curves separate state points belonging to the different phases: I denotes the isotropic phase, N_+ the "rod-like" nematic phase, N_- the "platelike" nematic phase and B the biaxial phase. The drawn curves connect the measured state-point data within one phase at a given reduced density . Note that the biaxial phase ends in a Landau bi-critical point at an aspect ratio $a/b \approx \sqrt{10}$. This behavior is in agreement with the theoretical predictions of Mulder. [194]

equation of state ($P = 3\rho$) and a simple estimate of the melting point of very anisometric ellipsoids [238] suggests that in the limit $x \to \infty$, the symmetry between oblate and prolate ellipsoids is still present.

More recently, Allen has studied the effect of molecular biaxiality on the mesogenic properties of hard ellipsoids. [197] In particular, Allen studied the nature of the liquid-crystalline phase as a prolate spheroid was made increasingly biaxial and was finally transformed into an oblate spheroid. In this case it was found that the rod-like and plate-like nematic phases are separated by a biaxial phase. Figure 4.3 shows how the stability of the different liquid-crystalline phases depends on the molecular biaxiality.

4. Beyond Nematics

The existence of a nematic phase in a system of hard-core molecules is not surprising. In fact, the earliest analysis of any statistical-mechanical model for a liquid-crystalline phase, that is, Onsager's study of a system of thin hard rods, shows that this simple hard-core system *must* form a nematic phase at sufficiently high density. It would, of course, be nice if there existed something like the Onsager model for smectics: an exactly solvable model system that exhibits a transition to the smectic-A phase. Unfortu-

nately, no such model is known. Hence the only way to test approximate "molecular" theories of the smectic phase is to compare with computer simulations. In the spirit of Section IV.B.3 we look for the simplest possible model that will form a smectic phase. In the case of nematics, convex hard-core models were the natural candidates because these constituted the natural generalization of the Onsager model. However, for smectics it is not obvious that hard-core models will work. In fact, in the existing textbooks on liquid-crystal physics the possibility of a hard-core smectic is not even discussed. The only presimulation article discussing the possibility of hard-core smectics is a paper by Hosino et al. [239] The "traditional" approach was to ascribe smectic ordering to attractive interactions between the molecular cores or, alternatively, to the change in packing entropy of the flexible tails of the mesogenic units. [240–243]

a. Parallel Molecules. Whereas essentially *any* fluid of sufficiently nonspherical convex hard bodies will form a nematic phase, nonsphericity alone is not enough to from a smectic phase. This is best demonstrated by the following simple example. We know from experiment that in many smectic phases, the orientational order parameter $S \approx 1$. Let us therefore first consider the possibility of forming a smectic phase in a fluid of *perfectly aligned* molecules ($S = 1$). We know that sufficiently nonspherical hard ellipsoids can form a nematic phase (see Section IV.B.3). It is natural to ask whether a perfectly aligned nematic of hard ellipsoids can transform into a smectic phase. The answer to this question is *no*. The reason is quite simple. Consider a fluid of ellipsoids with length-to-width ratio a/b, all aligned along the z-axis (say). Now we perform an affine transformation that transforms all z coordinates into coordinates z', such that $z' = (b/a)z$. At the same time we transform to new momenta in the z-direction: $p'_z = (a/b)p_z$. Clearly, this transformation does not change the partition function of the system, and hence all thermodynamic properties of the system are unchanged. However, the effect of this affine transformation is to change a fluid of parallel ellipsoids into a system of hard spheres. But, as far as we know, hard spheres can only exist in two phases; fluid and crystal. Hence parallel ellipsoids can only occur in the (nematic) fluid phase and in the crystalline solid phase. In particular, no smectic phase is possible. This makes it extremely improbable that a fluid of nonparallel ellipsoids will form a stable smectic. Such a phase is only expected in the unlikely case that the orientational fluctuations would *stabilize* smectic order. This example demonstrates that we should be careful in selecting possible models for a hard-core smectics. Surprisingly (and luckily) it turned out that another very simple hard-core model system, namely a system of parallel hard spherocylinders, does form a

smectic phase. [201,233] A stable smectic phase is possible for length-to-width ratios $L/D \geq 0.5$. In addition, we find that another phase appears at high densities and larger L/D values. In small systems, the phase appeared to be columnar, [201] but in larger systems the range of stability of the columnar phase shrinks (see Fig. 4.4) and is largely replaced by a hexagonal solid phase. In order to tell whether the latter phase is indeed truly solid or, for example, smectic-B, would require simulations on systems that contain many more particles than the 1000–2000 that we were thus far able to study systematically. It should be noted that, although the present evidence suggests that there may not be a columnar phase in a system of *pure* parallel spherocylinders, very recent work of Stroobants [244] indicates that, in a binary mixture of parallel spherocylinders of unequal length, the columnar phase reappears.

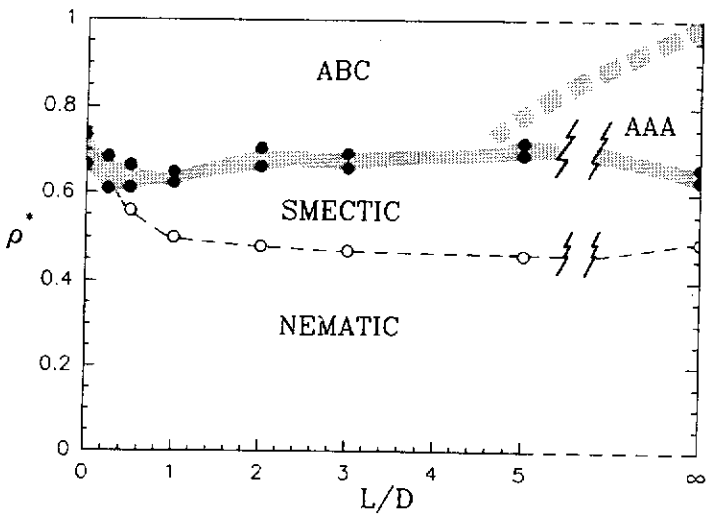

Figure 4.4. Schematic "phase diagram" of a system of parallel hard spherocylinders as obtained by computer simulation. [210] The abcissa indicates the length-to-width ratio L/D. The ordinate measures the density referred to the density at regular close packing.The dashed area indicates the two-phase region at the first order freezing transition. For $L/D < 5$, the solid consists of "ABC"-stacked triangular planes. For larger values of L/D, we find evidence for a hexagonal ("AAA") stacking of the molecules (i.e., triangular lattices stacked on top of one another. At very high densities and large L/D values we find a pocket where the system appears to form a columnar phase. However, the range of stability of this phase is strongly dependent on the size of the system studied. Although we still observed this columnar phase for a system of 1080 particles, it is conceivable that this phase will disappear altogether in the thermodynamic limit. The dashed curve indicates the nematic–smectic transition.

b. The Effect of Rotation. Of course, a model system consisting of *parallel* spherocylinders is rather unphysical. It is therefore of considerable interest to know if a system of freely rotating hard-core molecules can form a smectic phase. This question is of some practical interest, in view of the experimental evidence that smectic [245] and columnar [246] ordering may take place in concentrated solutions of rod-like DNA molecules.

Simulations of a system of freely rotating spherocylinders with length-to-width ratio $L/D = 5$ [188,247] revealed the presence of a stable smectic phase, in addition to the expected isotropic, nematic and solid phases. This work was recently extended to other aspect ratios by Veerman and Frenkel. [234] These authors show that the smectic phase disappears at $L/D = 3$. At this aspect ratio, the nematic phase is no longer (meta)-stable. Figure 4.5 shows a tentative phase diagram of freely rotating hard spherocylinders.

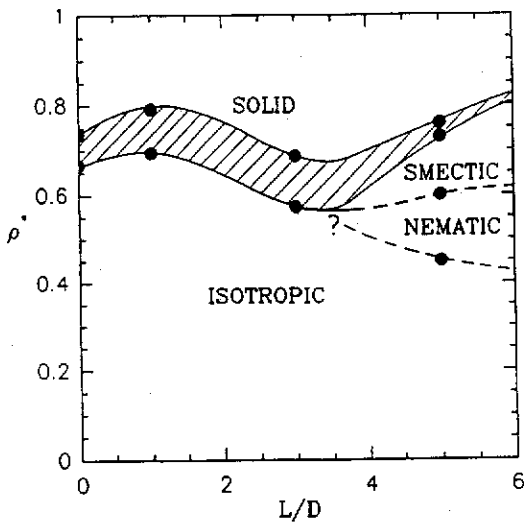

Figure 4.5. Phase diagram of a system of freely rotating spherocylinders as a function of the ratio between the length of the cylindrical part (L) and the diameter (D). The ordinate ρ^* measures the density divided by the density at regular close packing. The grey (dashed) area is the two-phase region separating the densities of the coexisting solid and fluid phases. The black dots indicate computed phase-coexistence points. The nematic-smectic transition is indicated by a dashed curve, as is the isotropic-nematic transition. Although the latter transition is expected to be of first order, the resolution of the current simulations was insufficient to determine the density discontinuity at this transition. The location of the isotropic-nematic-smectic triple point can only be estimated approximately and is indicated in the figure by a question mark.

c. Columnar Phases If hard-core models exhibit smectic phases, one may wonder if excluded volume effects can also induce the formation of the even more ordered, columnar phase. In this case, it is natural to look for a convex, plate-like molecule. Oblate ellipsoids are not expected to form columnar phases. The argument why this should be so is essentially the same as the one that "explains" why prolate ellipsoids should not form smectic phases. Rather, we should look for the oblate equivalent of the spherocylinder.

For ellipsoids, the transition from prolate to oblate shapes is controlled by a single parameter (the axial ratio a/b). In contrast, spherocylinders cannot be changed into oblate particles simply by changing L/D (unless we allow for the possibility of negative L/D). It turns out that a particularly convenient "oblate spherocylinder" model is the so-called *truncated sphere* [248] discussed in Section II.D.1

At high densities, truncated spheres can be stacked in a regular close-packed lattice. The volume fraction at regular close packing is

$$\eta_{cp} = (\pi/6)\sqrt{3 - (L/D)^2}$$

Note that for $L/D = 1$ (hard spheres), this reduces to the well-known hard-sphere result $\eta_{cp} = \pi/\sqrt{18}$. For $L/D \to 0$ (flat, cylindrical platelets), we obtain the $2D$ hard-disk value $\eta_{cp} = \pi/\sqrt{12}$.

Veerman and Frenkel [81] have reported Monte Carlo simulations on a system of truncated spheres with L/D=0.1, 0.2 and 0.3, over a range of densities between dilute gas and crystalline solid [81,248]. Surprisingly, it turned out that all three model systems behaved completely differently.

For the system with $L/D = 0.1$, it was observed that the system spontaneously ordered to form a nematic phase at a reduced density of 0.335 (i.e., at 33.5% of regular close packing). At a density corresponding to 49% of regular close packing, this nematic phase undergoes a strong first-order transition to a columnar phase (at a reduced density $\rho^* = 0.534$. The columnar–crystalline transition occurs at much higher density ($\rho^* > 0.80$). Surprisingly, the columnar phase is not present in systems of *aligned* truncated spheres. [249]

Next, we turn to the system of platelets with $L/D = 0.2$. At first sight, the behavior of this system looks quite similar to that observed for the thinner platelets. In particular, the equation of state for truncated spheres with $L/D = 0.2$ looks similar to the one corresponding to $L/D = 0.1$. However, we do not find a nematic phase in the dense fluid, close to freezing. In particular, if we measure the orientational correlation function $g_2(r) \equiv < P_2(\mathbf{u}(0) \cdot \mathbf{u}(r)) >$ of the dense fluid, we find that it decays to zero within one molecular diameter, even at the highest densities of the "fluid"

branch (see Fig. 4.6). In a nematic phase, $g_2(r)$ should tend to a finite limit: $g_2(r) \to S^2$ as $r \to \infty$, where S is the nematic order parameter. It should be stressed that the absence of nematic order in the $L/D = 0.2$ system is not a consequence of the way in which the system was prepared. Even if we started with a configuration at a reduced density $\rho/\rho_{cp} = 0.50$ with all the molecules initially aligned, the nematic order would rapidly dissapear. In other words, at that density the nematic phase is *mechanically* unstable. If we had to base our analysis exclusively on Fig. 4.6, we would have concluded that truncated spheres with $L/D = 0.2$ freeze from the *isotropic* phase.

The surprise comes when we consider the higher order orientational correlation function $g_4(r) \equiv < P_4(\mathbf{u}(0) \cdot \mathbf{u}(r)) >$. Usually, when $g_2(r)$ is short-ranged, the same holds a fortiori for $g_4(r)$. However, Fig. 4.7 shows that for densities $\rho/\rho_{cp} > 0.55$, $g_2(r)$ is much longer ranged than $g_2(r)$. This suggests that the system has a strong tendency towards orientational order with *cubic* symmetry ("cubatic", not to be confused with cubic, which refers to a system that also has *translational* order). In computer simulations one should always be very suspicious of any spontaneous order-

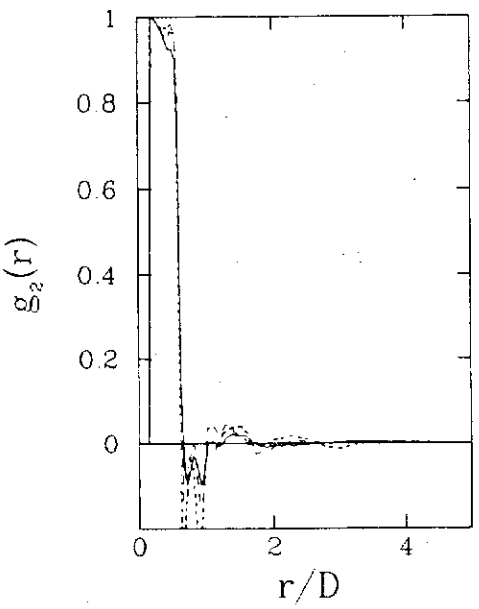

Figure 4.6. Density dependence of the orientational correlation function $g_2(r) \equiv < P_2(\mathbf{u}(0) \cdot \mathbf{u}(r)) >$ in a system of hard truncated spheres with a length-to-width ratio L/D=0.2. Drawn curve; $\rho/\rho_{cp} = 0.51$; long dashes; $\rho/\rho_{cp} = 0.57$, short dashes; $\rho/\rho_{cp} = 0.63$. Note that even at the highest densities studied, $g_2(r)$ is short ranged.

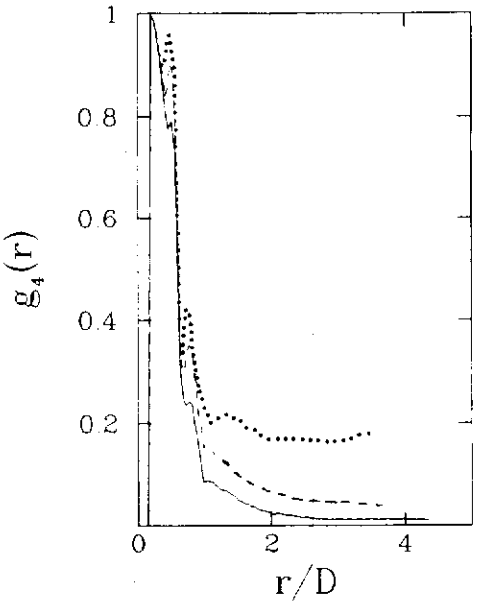

Figure 4.7. Density dependence of the orientational correlation function $g_4(r) \equiv < P_4(\mathbf{u}(0)\cdot\mathbf{u}(r)) >$ in a system of hard truncated spheres with a length-to-width ratio L/D=0.2. Symbols as in Fig. 4.6. Note that, unlike $g_2(r)$, $g_4(r)$ appears to be long-ranged at high densities.

ing with cubic symmetry, because such ordering could be induced by the (cubic) periodic boundary conditions. In order to test if the boundary conditions were responsible for the cubatic order, we did a number of long simulations with systems of up to 2048 particles. These simulations strongly suggest that the onset of cubatic orientational order is not an artifact of the boundary conditions. Another indication that the boundary conditions are not the cause of the observed ordering is that still higher order correlations (g_6 and g_8) that could also be induced by the periodic boundaries, are in fact rapidly decaying functions of r. If we make a log–log plot of $g_4(r)$ in the large system for several densities between $\rho = 0.51$ and $\rho = 0.63$ (see Fig. 4.8), it appears that the cubatic order is not truly long-ranged but quasi-long-ranged, that is, $g_4(r) \sim r^{-\eta}$, where η depends on the density ρ. This observation should, however, be taken with a large grain of salt, as the range over which linear behavior in the log–log plot is observed corresponds to less than one decade in r.

Finally, for truncated spheres with L/D=0.3, both the nematic and the "cubatic" phase are absent. We have summarized our knowledge of the phase behavior of the truncated-sphere system [81] in a tentative phase

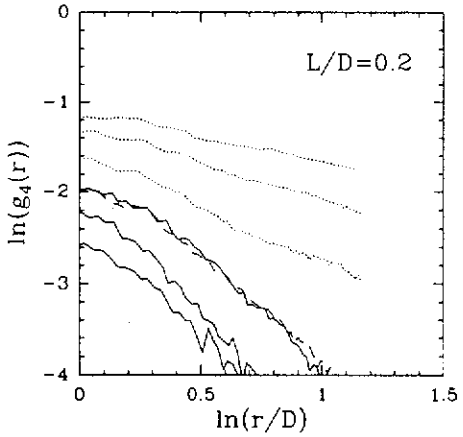

Figure 4.8. Log–log plot of the orientational correlation function $g_4(r) \equiv < P_4(\mathbf{u}(0) \cdot \mathbf{u}(r)) >$ in a system of hard truncated spheres with a length-to-width ratio L/D=0.2 as a function of density. With increasing density, the amplitude of this correlation function goes up. The lowest curve corresponds to $\rho^* = 0.51$. The following drawn curves to $\rho^* = 0.54$ and $\rho^* = 0.56$. The long-dashed curve corresponds to $\rho^* = 0.57$. At higher densities ρ^*=0.58, 0.60 and 0.63 (long-dashed curves), $g_4(r)$ appears to decay algebraically over the narrow range of distances ($1 < r/D < 3.2$) where we could observe monotonic decay of $g_4(r)$.

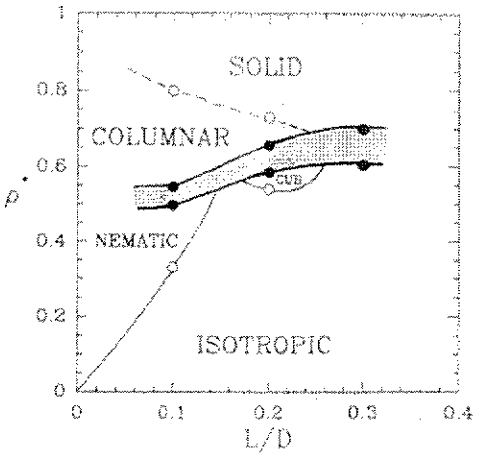

Figure 4.9. Tentative phase diagram of cut spheres with an aspect ratio L/D between 0.1 and 0.3. The high density solid/columnar phase is separated by a first order phase transition from the low density fluid phase. The densities of the coexisting phases are indicated by black dots. The open circles indicate the approximate location of phase transitions that have been estimated using techniques other than free energy calculations. The isotropic–nematic transition is weakly first order. The same appears to be the case with the isotropic–cubatic transition. In our simulations, the transition between the solid and the columnar phases appeared to be continuous.

diagram (Fig. 4.9). In fact, we know a few features of this phase diagram for both larger and smaller values of L/D. In particular, we know that for $L/D=1$ (hard spheres), the two-phase region is located between $\rho^*=0.67$ and $\rho^*=0.74$. For $L/D \to 0$, the isotropic–nematic transition occurs at $\rho^*=0$.

5. *Simulation of 2D Nematics*

In Section IV.A.3, we discussed the peculiar nature of the nematic phase in two-dimensional systems. The discussion in that section suggests that there are two obvious questions about 2D nematics that one could try to answer by simulation. (1) If the pair potential is nonseparable, do we find algebraic or true long-range order? (2) If we find algebraic order, do we observe a first order I–N transition or a continuous one of the Kosterlitz–Thouless type. For the first question, a good starting point would be to choose a pair potential that is as nonseparable as possible. An obvious

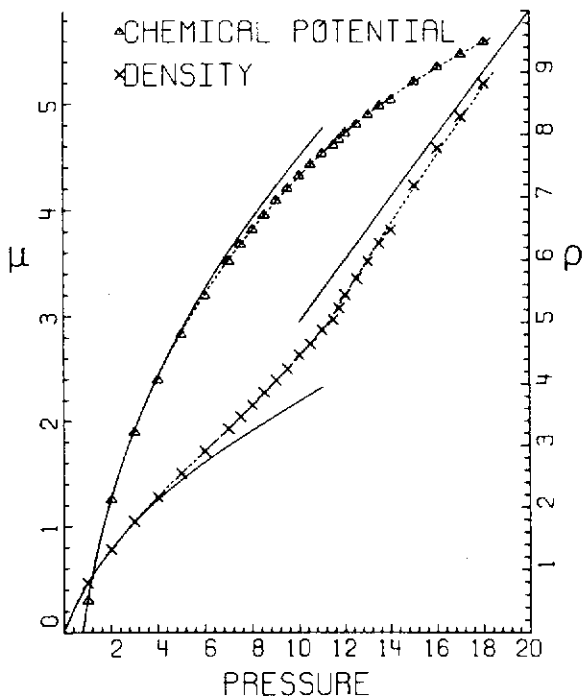

Figure 4.10. Equation of state of two-dimensional fluid of infinitely thin hard needles of length 1. Note that in this figure the reduced pressure is the independent variable. The reduced density (ρL^2) is indicated by crosses, the chemical potential μ by triangles. The drawn curves at low pressure were computed using a 5-term virial series.

candidate is a two-dimensional model of infinitely thin hard needles, [250] that is, a two-dimensional hard-body fluid. This pair potential is very non-separable in the sense that, at fixed $|r_{ij}|$ and fixed $\mathbf{u}_i.\mathbf{u}_j$ the pair potential is *not* constant, but may vary between 0 and ∞. The equation of state of this system is shown in Fig. 4.10. According to the bifurcation analysis of the corresponding Onsager limit, [251] a second order isotropic–nematic transition is expected at a density $\rho L^2 = (3\pi/2) = 4.712\cdots$ and a pressure$PL^2 = 11.78\cdots$. At first sight this seems to be quite a reasonable estimate of the I–N transition, because very close to this point the equation of state appears to exhibit a change of slope. However, analysis of the long-range behavior of the orientational correlation functions and of the system-size dependence of the order parameter $< \cos 2\theta >$ indicate that the higher density phase is not a stable nematic. The orientational correlation functions decay either exponentially (see Fig. 4.11) or with an

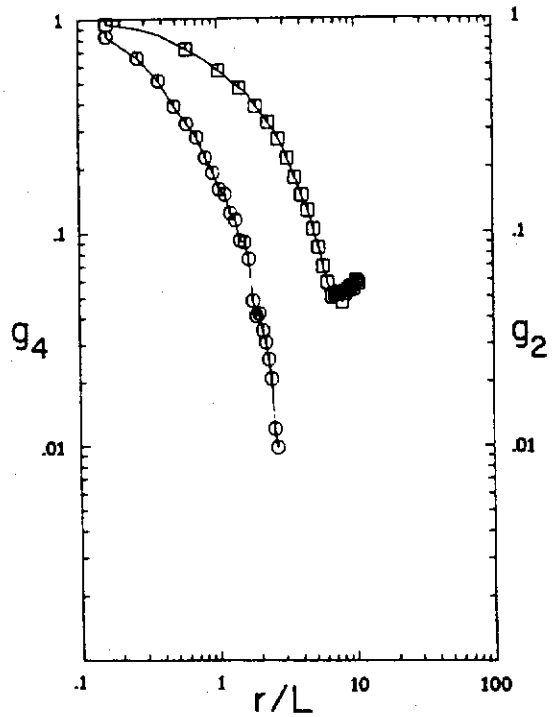

Figure 4.11. Orientational correlation functions $g_2(r) \equiv< \cos 2(\phi(0) - \phi(r)) >$ and $g_4(r) \equiv< \cos 4(\phi(0) - \phi(r)) >$ for a two-dimensional system of hard needles of length L=1. This figure shows that at a reduced density ρL^2=6.75, the orientational order decays exponentially. In other words: the phase is isotropic.

apparent algebraic exponent that is larger than the critical value given in Eq. (4.66). Only at a density that is almost twice the Onsager transition point does the observed behavior conform to what is expected for a stable nematic with algebraic order (see Fig. 4.12). However, at this density, the equation of state is completely featureless. Such behavior is to be expected of the I–N transition and is in fact of the K–T type.

Subsequently, Cuesta and Frenkel [223] have studied the isotropic to nematic transition in a system of 2D hard ellipses with aspect ratios 2, 4 and 6. It is found that in all cases where a stable nematic phase is found (aspect ratios 4 and 6), this phase exhibits algebraic orientational order. However, whereas the I–N transition appears to be of the K–T type for aspect ratio 6 (and larger), the transition is found to be of first order

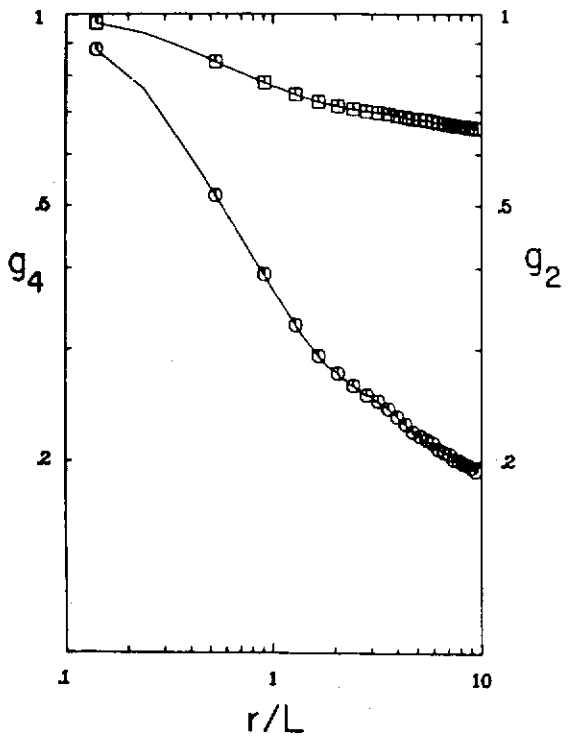

Figure 4.12. Orientational correlation functions $g_2(r) \equiv < \cos 2(\phi(0) - \phi(r)) >$ and $g_4(r) \equiv < \cos 4(\phi(0) - \phi(r)) >$ for a two-dimensional system of hard needles of length L=1. This figure shows that at a reduced density $\rho L^2 = 8.75$, the orientational order decays algebraically. From the values of the algebraic exponents η_2 and η_4 the effective Frank elastic constant can be computed. At $\rho = 8.75$, this Frank constant is large enough to make the 2D nematic stable with respect to disclination unbinding.

for aspect ratio 4. This implies that in the latter case, the 2D nematic undergoes a first-order transition *before* it has reached the point where it becomes absolutely unstable with respect to diclination unbinding. A very puzzling feature is the nature of the high density phase of 2D ellipses. A snapshot of such a phase is shown in Fig. 4.13. This phase does not appear to have true crystalline order, nor for that matter, smectic order.

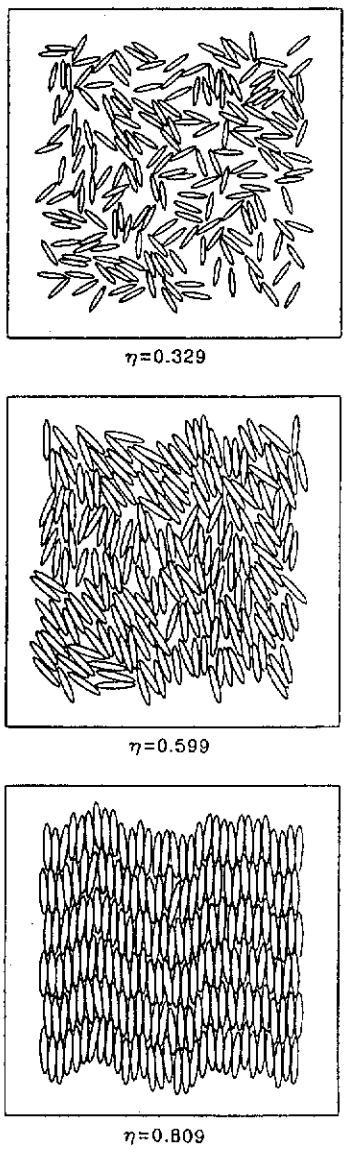

Figure 4.13. Snapshots of typical configurations of a system of hard ellipses in the isotropic phase ($\eta = 0.329$), near the estimated estimated isotropic–nematic transition (η=0.599) and in the high density phase ($\eta = 0.809$). Although the latter phase exhibits local solid-like ordering, it is not a true (two-dimensional) solid.

Yet it does clearly have a large amount of local order. The precise nature of this high density phase is currently under investigation.

V. STATIC PROPERTIES

A. Theory

This sections deals with the static properties of HCBs in the liquid-crystalline phase. Most of the scalar properties like the equation of state and the "vector" properties like the various correlation functions, that were discussed in Section I, are of course also relevant in this case. Only their definitions will have to adjusted to reflect the presence of long-range orientational and (partial) positional order that occurs. There are, however, also a few static properties that are unique to the liquid crystalline state, that is, the order parameters that describe the nature and degree of order, and the elastic constants that describe the response of the system to long wavelength distortions of the initially uniform field of preferred local orientations. Since it is basic to the whole discussion, we start by discussing the structure of the ODF in the LC phase, which leads us to the definitions of the order parameters. The other properties are then dealt with in turn.

1. Order Parameters

The ODF (one particle distribution function) $\rho^{(1)}$ was introduced in Section III, but its explicit form was left undetermined. This makes sense in the context of density functional theory where it plays the role of the basic variable as a single unit. In practice, however, we need to describe the ODF in more detail, even if only to be able to approximate it numerically. The most natural way to obtain such a description is to expand it into a complete set of functions that are in fact the irreducible representations of the original, unbroken symmetry group of the low density phase. In our case this is the group $G_0 = T \otimes O_3$ of the translation group T and the full three-dimensional orthogonal group O_3 . The basis functions in this expansion are just products of plane waves and irreducible rotation-group matrix elements. [252] A side product of this approach is the fact that the expansion coefficients will turn out to be order parameters not only in the intuitive sense that they will be zero in the disordered phase and nonzero in the ordered one but also in the formal sense of the Landau theory of phase transitions, that is, they themselves transform as irreducible basis sets of the unbroken symmetry group. [253] In the most general case, we can thus write

$$\rho(\mathbf{r}, \Omega) = \frac{1}{V} \sum_{\mathbf{k}}{}' \sum_{\ell,m,n} \frac{(2\ell+1)}{8\pi^2} a_{\mathbf{k},\ell,m,n} e^{i\mathbf{k}\cdot\mathbf{r}} D^{\ell}_{m,n}(\Omega) \tag{5.1}$$

where the prime on the first summation indicates a restriction to **k**-vectors in the first Brillioun zone.

For the typical system studied this expansion expansion reduces to a much simpler one. Consider, for example, a nematic phase formed by uniaxially symmetric molecules with inversion symmetry. In this case, we have no dependence on position and dependence on the orientation only through the angle θ the major molecular axis makes with the z-axis of an arbitrary reference frame. A systematic way of deducing the correct expansion is then to average Eq. (5.1) over the extra symmetries introduced. For the example of the nematic, we thus average over the system volume (no positional order) , the azimuthal angle ϕ of the lab frame (uniaxial symmetry of the phase), the angle ψ around the molecular symmetry axis and the inversion operation applied to the molecular frame. The result is the expansion

$$\rho(\mathbf{r}, \Omega)_{\text{nem}} \equiv nf(\theta) = n \sum_{\ell=\text{even}} \frac{(2\ell + 1)}{2} a_\ell P_\ell(\cos \theta) \tag{5.2}$$

The second expansion coefficient

$$a_2 = \langle P_2 \rangle = \int d \cos \theta f(\theta) P_2(\theta) \tag{5.3}$$

is, of course, the well known Maier–Saupe order parameter. [254]

In some cases it is preferable to work with the basis set generated by the so-called irreducible Cartesian tensors [255] rather than the rotation matrices. The uniaxial component of the second rank irreducible tensor is known as the de Gennes order parameter

$$\mathbf{S} = \frac{1}{2} (3\hat{\mathbf{n}} \otimes \hat{\mathbf{n}} - \mathbf{1}) \tag{5.4}$$

The unit vector $\hat{\mathbf{n}}$ is the so-called nematic director, which is actually defined up to a sign, reflecting the inversion symmetry of the phase. In a frame where **S** is diagonal, that is, the director is along the z-axis of the lab frame, the component S_{zz} is actually equal to the Maier–Saupe order parameter.

2. *Correlation Functions*

The usual method of the defining equilibrium distribution functions in a disordered fluid phase uses the explicit representation of the full N-particle distribution defined in terms of the system Hamiltonian. In a phase with any kind of long-range order, this method breaks down, since it cannot deal with the occurrence of spontaneous order which is an effect associated with the thermodynamic limit, $N \to \infty$, where the finite N

representation is meaningless. As mentioned in the previous chapter, these difficulties can be bypassed using the density functional formalism. The various correlation functions are then defined through their relation to the direct correlation functions which are obtained directly from the density functional itself. Recalling Eq. (4.5) from Section IV, we find for the two-particle direct correlation function

$$c^{(2)}(\xi_1, \xi_2) = \frac{\delta^2 \Phi[\rho^{(1)}]}{\delta\rho^{(1)}(\xi_1)\delta\rho^{(1)}(\xi_2)} \tag{5.5}$$

where we have used the shorthand $\xi = (\mathbf{r}, \Omega)$. From here, we can go to the usual two-particle distribution function $\rho^{(2)}$ via the generalized Ornstein–Zernike equation [152]

$$\rho^{(2)}(\xi_1, \xi_2) - \rho^{(1)}(\xi_1)\rho^{(1)}(\xi_2) = \rho^{(1)}(\xi_1)\rho^{(1)}(\xi_2)c^{(2)}(\xi_1, \xi_2) \tag{5.6}$$
$$+\rho^{(1)}(\xi_2) \int d\xi_3 \left(\rho^{(2)}(\xi_1, \xi_3) - \rho^{(1)}(\xi_1)\rho^{(1)}(\xi_3)\right) \rho^{(1)}(\xi_3)c^{(2)}(\xi_3, \xi_2)$$

3. *Equation of State*

In the context of density functional theory, the equation of state is probably best obtained directly from its definition in terms of the equilibrium free energy.

$$P = -\left(\frac{\partial F}{\partial V}\right)_{N,T}, \qquad F = \mathcal{F}[\rho^{(1)}{}_{\text{eq}}] \tag{5.7}$$

Lacking any substantial theory for the correlation function themselves, the traditional virial (cf. Eq. 2.10) and compressibility relations (cf. Eq. 2.27) are of limited use in an ordered phase.

4. *Frank Elastic Constants*

We consider here the effect of long wavelength distortions of the local preferred direction in a nematic liquid. Such a distortion is most conveniently described by introducing the director field $\hat{\mathbf{n}}(\mathbf{r})$ specifying the *direction* of the local preferred molecular orientation with respect to a fixed lab frame. The derivation of the macroscopic free energy of distortion is then an exercise in the construction of the relevant second order rotational invariants constructed from $\hat{\mathbf{n}}(\mathbf{r})$ and its derivatives. We quote here the well known result[2]

$$F_d = \tfrac{1}{2}K_1(\nabla \cdot \hat{\mathbf{n}})^2 + \tfrac{1}{2}K_2(\hat{\mathbf{n}} \cdot \nabla \wedge \hat{\mathbf{n}})^2 + \tfrac{1}{2}K_3(\hat{\mathbf{n}} \wedge (\nabla \wedge \hat{\mathbf{n}}))^2 \tag{5.8}$$

which introduces the Frank elastic constants: K_1 (splay), K_2 (twist) and K_3 (bend). The distortions of the director field associated with each of

the three constants are depicted in Fig. 5.1 It is now the task of statistical mechanics to come up with microscopic expressions for the Frank constants. For hard particles this question was first addressed by Priest [256] and Straley.[257] The first to derive an essentially exact formulation on the basis of density functional theory were Poniewierski and Stecki. [258–260] Here we present a slightly adapted version of their results. [261]

Consider a nematic phase of uniaxially symmetric molecules. The undistorted ODF has the form $\rho^{(1)}(\mathbf{r}, \hat{\mathbf{u}}) = nf(\hat{\mathbf{n}} \cdot \hat{\mathbf{u}})$, where n is the number density, $\hat{\mathbf{n}}$ the (constant) director and $\hat{\mathbf{u}}$ a unit vector along the molecular symmetry axis. We now allow the director to vary spatially with typical wavelengths much larger than the molecular scale. In this case, we can assume that the local orientational distribution function retains the same functional form as in the undistorted bulk, that is, the only thing that varies is the direction of the preferred orientation. In other words, if the orientational distribution in the undistorted bulk is given by $f_0(\hat{\mathbf{n}} \cdot \hat{\mathbf{u}})$, then the position dependent orientational distribution of the distorted system is given by $f(\mathbf{r}, \hat{\mathbf{u}}) = f_0(\hat{\mathbf{n}}(\mathbf{r}) \cdot \hat{\mathbf{u}})$, where $\hat{\mathbf{n}}(\mathbf{r})$ is the director at $\mathbf{r}$. If the distortions are not too large we can functionally expand the free energy functional in terms of the difference $\Delta f(\mathbf{r}, \hat{\mathbf{u}}) = f(\mathbf{r}, \hat{\mathbf{u}}) - f_0(\hat{\mathbf{n}} \cdot \hat{\mathbf{u}})$, yielding to second order

$$\beta \Delta \mathcal{F}[\Delta f] = -\tfrac{1}{2} n^2 \int d\mathbf{r}\, d\hat{\mathbf{u}} \int d\mathbf{r}'\, d\hat{\mathbf{u}}' \Delta f(\mathbf{r}, \hat{\mathbf{u}}) \Delta f(\mathbf{r}', \hat{\mathbf{u}}') c^{(2)}(\mathbf{r}, \hat{\mathbf{u}}, \mathbf{r}', \hat{\mathbf{u}}', [f_0]) \tag{5.9}$$

There are no first order terms in this expansion because the undistorted phase is stable, so that its first order variation with respect to arbitrary changes in the ODF vanishes (cf. Eq. 4.11). As we assumed only long wavelength distortions, we will make a gradient expansion of the difference

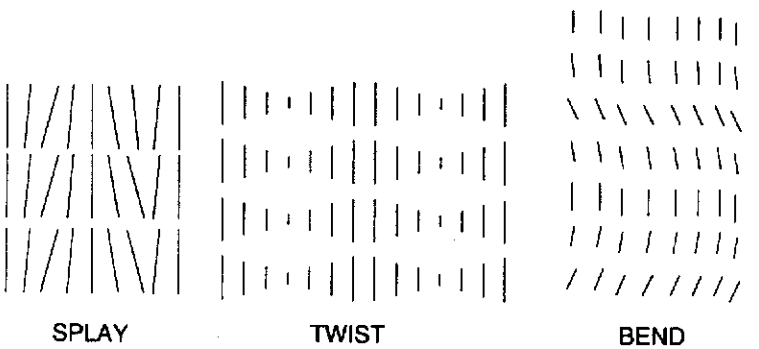

Figure 5.1. Distortions of the director in the nematic phase: from left to right: splay, twist and bend.

in the orientation distribution functions. To this end we first choose a more convenient reference system for the two-particle integration, defining the center-of-mass coordinates $\mathbf{R} = \frac{1}{2}(\mathbf{r} + \mathbf{r}')$ and the relative separation $\Delta\mathbf{r} = \mathbf{r} - \mathbf{r}'$. The distribution function at $\mathbf{r}$ and $\mathbf{r}$ can then be related to the one in the center of mass through the Taylor expansion

$$f(\hat{\mathbf{n}}(\mathbf{R} \pm \tfrac{1}{2}\Delta\mathbf{r}) = f_0(\hat{\mathbf{n}}(\mathbf{R}) \cdot \hat{\mathbf{u}}) \pm \frac{(\Delta\mathbf{r} \cdot \nabla_{\mathbf{R}})}{2} f_0(\hat{\mathbf{n}}(\mathbf{R}) \cdot \hat{\mathbf{u}}) + \tfrac{1}{2}\frac{(\Delta\mathbf{r} \cdot \nabla_{\mathbf{R}})}{2}\frac{(\Delta\mathbf{r} \cdot \nabla_{\mathbf{R}})}{2} f_0(\hat{\mathbf{n}}(\mathbf{R}) \cdot \hat{\mathbf{u}}) \pm \mathcal{O}(\Delta^3\mathbf{r}) \tag{5.10}$$

Inserting this into Eq. (5.9) and performing a partial integration, we find

$$\beta\Delta\mathcal{F}[\Delta f] = \frac{1}{4}n^2 \int d\mathbf{R}\, d\Delta\mathbf{r}\, d\hat{\mathbf{u}}\, d\hat{\mathbf{u}}' \dot{f}_0(\hat{\mathbf{n}}(\mathbf{R}) \cdot \hat{\mathbf{u}}) \dot{f}_0(\hat{\mathbf{n}}(\mathbf{R}) \cdot \hat{\mathbf{u}}') \times \left[(\Delta\mathbf{r} \cdot \nabla_{\mathbf{R}})\hat{\mathbf{n}}(\mathbf{R}) \cdot \hat{\mathbf{u}}\right] \left[(\Delta\mathbf{r} \cdot \nabla_{\mathbf{R}})\hat{\mathbf{n}}(\mathbf{R}) \cdot \hat{\mathbf{u}}'\right] c^{(2)}(\Delta\mathbf{r}, \hat{\mathbf{u}}, \hat{\mathbf{u}}', [f_0]) \tag{5.11}$$

where the dot on the distribution functions denotes differentiation with respect to their single argument, that is, $\hat{\mathbf{n}} \cdot \hat{\mathbf{u}}$.

The elastic constants can now be deduced by imposing infinitesimal distortion patterns corresponding to the three fundamental "modes" discussed earlier

$$\begin{aligned} \hat{\mathbf{n}}(\mathbf{R}) &= \hat{\mathbf{e}}_z + \epsilon X \hat{\mathbf{e}}_x \quad \text{(splay)} \\ \hat{\mathbf{n}}(\mathbf{R}) &= \hat{\mathbf{e}}_z + \epsilon X \hat{\mathbf{e}}_y \quad \text{(twist)} \\ \hat{\mathbf{n}}(\mathbf{R}) &= \hat{\mathbf{e}}_z + \epsilon Z \hat{\mathbf{e}}_x \quad \text{(bend)} \end{aligned} \tag{5.12}$$

Inserting these one by one into Eq. (5.11) one can simply read off the relevant constants

$$\begin{aligned} \beta K_1 &= \tfrac{1}{2}Nn \int d\Delta r\, d\hat{\mathbf{u}}\, d\hat{\mathbf{u}}' \dot{f}_0(\hat{\mathbf{n}} \cdot \hat{\mathbf{u}}) \dot{f}_0(\hat{\mathbf{n}} \cdot \hat{\mathbf{u}}') (\Delta x)^2 u_x u'_x c^{(2)}(\Delta\mathbf{r}, \hat{\mathbf{u}}, \hat{\mathbf{u}}', [f_0]) \\ \beta K_2 &= \tfrac{1}{2}Nn \int d\Delta r\, d\hat{\mathbf{u}}\, d\hat{\mathbf{u}}' \dot{f}_0(\hat{\mathbf{n}} \cdot \hat{\mathbf{u}}) \dot{f}_0(\hat{\mathbf{n}} \cdot \hat{\mathbf{u}}') (\Delta x)^2 u_y u'_y c^{(2)}(\Delta\mathbf{r}, \hat{\mathbf{u}}, \hat{\mathbf{u}}', [f_0]) \\ \beta K_3 &= \tfrac{1}{2}Nn \int d\Delta r\, d\hat{\mathbf{u}}\, d\hat{\mathbf{u}}' \dot{f}_0(\hat{\mathbf{n}} \cdot \hat{\mathbf{u}}) \dot{f}_0(\hat{\mathbf{n}} \cdot \hat{\mathbf{u}}') (\Delta z)^2 u_x u'_x c^{(2)}(\Delta\mathbf{r}, \hat{\mathbf{u}}, \hat{\mathbf{u}}', [f_0]) \end{aligned} \tag{5.13}$$

Of course, the major obstacle in the application of such formulas is, yet again, the lack of any hard facts about the direct correlation function of the nematic phase. Explicit predictions have therefore been given mainly for the Onsager approximation, where the direct correlation is at least known (cf. Eq. 4.39). The results of this approximation, which assumes

that the direct correlation is independent of both the density and the bulk phase of the system, can at best be of a rather qualitative nature.

Poniewierski and Stecki [260] have also shown how microscopic expressions for the Frank constants can also be derived from hydrodynamic fluctuation theory. [262] This formulation, although no more convenient from the purely theoretical point of view, has the distinct advantage of relating the elastic constants to properties more easily measurable in simulations. In order to give their results we need to define the Ursell function $U^{(2)}$

$$U^{(2)}(\mathbf{r}, \hat{\mathbf{u}}, \mathbf{r}', \hat{\mathbf{u}}') \equiv \rho^{(2)}(\mathbf{r}, \hat{\mathbf{u}}, \mathbf{r}', \hat{\mathbf{u}}') - \rho^{(1)}(\mathbf{r}, \hat{\mathbf{u}})\rho^{(1)}(\mathbf{r}', \hat{\mathbf{u}}') \tag{5.14}$$

Note that in the nematic phase this quantity is translationally invariant. The Frank constants are then given by

$$\begin{aligned}
\frac{n < P_2 >}{\beta K_1} &= \lim_{q_x \to 0} \lim_{q_z \to 0} q_x^2 \int d\hat{\mathbf{u}}\, d\hat{\mathbf{u}}' u_x u_x' u_z u_z' \hat{U}^{(2)}(\mathbf{q}, \hat{\mathbf{u}}, \hat{\mathbf{u}}') \\
\frac{n < P_2 >}{\beta K_2} &= \lim_{q_y \to 0} \lim_{q_z \to 0} q_y^2 \int d\hat{\mathbf{u}}\, d\hat{\mathbf{u}}' u_y u_y' u_z u_z' \hat{U}^{(2)}(\mathbf{q}, \hat{\mathbf{u}}, \hat{\mathbf{u}}') \\
\frac{n < P_2 >}{\beta K_3} &= \lim_{q_z \to 0} \lim_{q_x \to 0} q_z^2 \int d\hat{\mathbf{u}}\, d\hat{\mathbf{u}}' u_x u_x' u_z u_z' \hat{U}^{(2)}(\mathbf{q}, \hat{\mathbf{u}}, \hat{\mathbf{u}}')
\end{aligned} \tag{5.15}$$

B. Simulations

The detection of different kinds of orientational and translational order in a computer simulation requires special care. For instance, the structural information that is contained in the familiar radial distribution function, $g(r)$, is insufficient to distinguish between different kinds of (liquid-) crystalline ordering. Hence, other functions that probe the relevant forms of translational and orientational order must be introduced. Below, we describe the different structural probes that can be used to probe (liquid-) crystalline order in computer simulations.

1. Orientational Order Parameters

In an isotropic molecular liquid, the one-particle distribution function ρ_1 is a constant. In an ordered system, such as a liquid crystal, ρ_1 depends on the molecular orientation $\mathbf{\Omega}$ and possibly also on the center of mass coordinate $\mathbf{r}$. In a nematic, ρ_1 is a function of $\mathbf{\Omega}$ only.

Although knowledge of ρ_1 suffices to determine the nature and degree of ordering in a liquid crystal, it is often convenient to be able to quantify the liquid-crystalline order with a few numbers rather than with a continuous function. The quantities a_ℓ with $\ell \geq 2$, defined in Section V.A.1 can be used as a measure of the nematic order. Often the quantity $a_2 \equiv < P_2(\cos\theta) >$ is referred to as *the* nematic order parameter, and is

denoted by S. Similarly, it is possible to define order parameters that quantify smectic and columnar order by expanding the spatial variation of the single particle density function ρ_1 in Fourier components. The amplitude of the Fourier component with the lowest nonzero wave vector that is commensurate with the periodicity of the density modulation is a measure for the smectic (columnar) order.

From a computational point of view, the definition of the nematic order parameters in Eq. (5.2) is not entirely satisfactory for the following reason: a_ℓ is defined as the average of $P_\ell(\cos\theta)$, where θ is the angle between the molecular orientation vector $\hat{\mathbf{u}}$ (for convenience we consider axially symmetric molecules) and the nematic director $\hat{\mathbf{n}}$. But the director is defined as the average alignment direction of the molecules in a nematic. In the absence of external forces the direction of $\hat{\mathbf{n}}$ is not known a priori. Hence Eq. (5.2) suggests that in order to measure the order parameter, we should first determine the preferred alignment (i.e., we should already know if the sample is in the nematic phase) and only then can we measure the degree of nematic order.

Fortunately, it is possible to give a definition of S that does not presuppose knowledge of $\hat{\mathbf{n}}$. To see this, consider the expression for $< P_2(\hat{\mathbf{u}}\cdot\hat{\mathbf{e}}) >$, where $\hat{\mathbf{e}}$ is an arbitrary unit vector:

$$< P_2(\hat{\mathbf{u}}\cdot\hat{\mathbf{e}}) > = \frac{1}{N}\sum_{i=1}^{N} \hat{\mathbf{e}}\cdot\left(\frac{3\hat{\mathbf{u}}^i\hat{\mathbf{u}}^i - \mathbf{I}}{2}\right)\cdot\hat{\mathbf{e}} \qquad (5.16)$$
$$\equiv \hat{\mathbf{e}}\cdot\mathbf{Q}\cdot\hat{\mathbf{e}}$$

where $\mathbf{I}$ is the second-rank unit tensor and the last line of Eq. (5.16) defines the tensor order parameter $\mathbf{Q}$. $\mathbf{Q}$ is a traceless, symmetric second-rank tensor. Its eigenvalues correspond to the expectation values of $S_\alpha \equiv < P_2(\hat{\mathbf{u}}\cdot\hat{\mathbf{e}}_\alpha) >$ for the three orthonormal eigenvectors $\hat{\mathbf{e}}_\alpha$. We now *define* the director $\hat{\mathbf{n}}$ to be the eigenvector of $\mathbf{Q}$ that has the largest eigenvalue S. In a uniaxial nematic, the other two eigenvalues must be equal. If we combine this with the fact that $\mathbf{Q}$ is traceless, it follows that the latter eigenvalues must be equal to $-S/2$. In the nematic phase, we can therefore rewrite the tensor order parameter $\mathbf{Q}$ as

$$\mathbf{Q} = S\frac{3\hat{\mathbf{n}}\hat{\mathbf{n}} - \mathbf{I}}{2} \qquad (5.17)$$

In a numerical simulation, it is quite simple to determine the eigenvalues and eigenvectors of $\mathbf{Q}$. The nematic order parameter is then simply the largest eigenvalue of this second-rank tensor. Although this definition of S is indeed convenient to measure order *in the nematic phase*, it is less

convenient to detect the isotropic–nematic transition. The reason is that the largest eigenvalue of $\mathbf{Q}$ is, by construction, positive. Hence, even in the isotropic phase it does not fluctuate around zero, but remains positive. In Appendix B.B, we show that, in the isotropic phase, the largest eigenvalue of $\mathbf{Q}$ only vanishes as $1/\sqrt{N}$. If, in contrast we define the nematic order parameter as -2 times the *middle* eigenvalue of $\mathbf{Q}$, then we find that this quantity *does* fluctuate around zero in the isotropic phase. Its average value has a much weaker system size dependence, viz. as $1/N$. For details, see Appendix B.B.

2. *Correlation Functions*

a. Orientational Correlation Functions. A convenient probe, both of the long-range orientational order in liquid crystalline phases, and of the *local* orientational order in the isotropic phase, is provided by the orientational correlation functions $g_\ell(r)$, defined as

$$g_\ell(r) = \langle P_\ell(\hat{\mathbf{u}}(0) \cdot \hat{\mathbf{u}}(r)) \rangle \tag{5.18}$$

where $P_\ell(x)$ is the ℓ^{th} Legendre polynomial and $\hat{\mathbf{u}}(r)$ is a unit vector along the axis of the molecule at distance r from the reference molecule. In the nematic phase, all $g_\ell(r)$ with even ℓ are long-ranged. In the isotropic phase, they typically decay to zero within one molecular diameter, except very close to the isotropic–nematic transition. It is straightforward to verify that, in a phase with long-ranged orientational order, the following equality must hold

$$\lim_{r \to \infty} g_\ell(r) = S_\ell^2$$

where a_ℓ $(= S_\ell)$ is the ℓth orientational order parameter, defined in Eq. (5.2). In a simulation, we can only study orientational correlations for interparticle separations less than $L/2$, where L is the diameter of the periodic simulation box. Hence, in practice, we will use the approximate estimate

$$S_\ell \approx \sqrt{g_\ell(r = L/2)}$$

For ℓ=2, the above estimate of the nematic order agrees well with the value obtained using Eq. (5.16).

b. Translational Correlation Functions. In order to characterize (liquid-) crystalline phases with partial translational order, it is convenient to define correlation functions that probe this kind of ordering. Simplest among these functions is the longitudinal density correlation function denoted by $g_{\parallel}(r)$. This function measures the amplitude of density correlations in the direction of the alignment of the molecules. We can also define correlation

functions that probe density correlations in the directions perpendicular to the molecular alignment axis. The simplest function to measure such correlations is denoted by $g(r_\perp)$. Here, $r_\perp$ is defined as the component of the distance between two particles perpendicular to the molecular alignment axis. $g(r_\perp)$ can, for instance, be used to distinguish a columnar phase, where the ordering of columns in a two-dimensional crystal lattice creates a strong modulation of $g(r_\perp)$, from a nematic phase, where $g(r_\perp)$ is rather featureless. A detailed description of these, and other probes of partial translational order in liquid crystals can be found in Ref. [81]

3. *Frank Elastic Constants*

As discussed earlier, the Frank elastic constants determine the response of the system to any external perturbation causing an orientational deformation. In the simplest case of the nematic phase, the free energy of deformation may be written as in Eq. (5.8), which essentially defines the elastic constants K_1, K_2 and K_3.

In simulations, the elastic quantities are most conveniently computed from equilibrium orientational fluctuations. The necessary equations have been summarized by Forster. [262] We assume, for simplicity, that the molecules are axially symmetric, with a unit vector $\hat{\mathbf{e}}_i = (e_{ix}, e_{iy}, e_{iz})$ along the axis of each molecule i. The center of mass of molecule i is at position $\mathbf{r}_i$. Then the ordering tensor in reciprocal space, for N molecules in volume V, is defined as

$$\hat{Q}_{\alpha\beta}(\mathbf{k}) = \frac{V}{N}\sum_{i=1}^{N}\frac{3}{2}\left(e_{i\alpha}e_{i\beta} - \frac{1}{3}\delta_{\alpha\beta}\right)\exp(i\mathbf{k}\cdot\mathbf{r}_i) \tag{5.19}$$

Here $\delta_{\alpha\beta}$ is the Kronecker delta, $\alpha, \beta = x, y, z$,and $\mathbf{k}$ is the wave vector. This is the Fourier transform of the real space orientation density

$$Q_{\alpha\beta}(\mathbf{r}) \equiv \frac{1}{V}\sum_{\mathbf{k}}\hat{Q}_{\alpha\beta}(\mathbf{k})\exp(-i\mathbf{k}\cdot\mathbf{r}) \tag{5.20}$$

In an unperturbed system, the orientation density is independent of position:

$$\langle\mathbf{Q}(\mathbf{r})\rangle_0 = \langle\mathbf{Q}\rangle_0 = \langle\hat{\mathbf{Q}}(\mathbf{0})\rangle_0/V = \text{constant} \tag{5.21}$$

As discussed earlier, the order parameter $\overline{P}_2$ is the highest eigenvalue of $\langle\mathbf{Q}\rangle_0$, and $\hat{\mathbf{n}}$ is the corresponding eigenvector. If we choose $\hat{\mathbf{n}} = (0, 0, 1)$, then $\langle\mathbf{Q}\rangle_0$ is diagonal with

$$\langle Q_{xx}\rangle_0 = \langle Q_{yy}\rangle_0 = -\frac{1}{2}\overline{P}_2 \tag{5.22}$$

$$\langle Q_{zz} \rangle_0 = \overline{P_2} \tag{5.23}$$

Fluctuations of $\hat{\mathbf{Q}}$ are related to the elastic constants as follows:

$$\left\langle \hat{Q}_{xz}(\mathbf{k}) \hat{Q}_{xz}(-\mathbf{k}) \right\rangle_0 = \frac{9}{4} \left(\frac{\overline{P}_2^2 V k_B T}{K_1 k_x^2 + K_3 k_z^2} \right) \tag{5.24}$$

$$\left\langle \hat{Q}_{yz}(\mathbf{k}) \hat{Q}_{yz}(-\mathbf{k}) \right\rangle_0 = \frac{9}{4} \left(\frac{\overline{P}_2^2 V k_B T}{K_2 k_x^2 + K_3 k_z^2} \right) \tag{5.25}$$

where the wave vector $\mathbf{k} = (k_x, 0, k_z)$ is chosen in the xz plane. Just as the elastic constants are defined for long wavelength director fluctuations, so the above equations are valid only in the limit of small k. In practical applications, it is necessary to extrapolate to $k = 0$. Particular attention must be paid to this, since in a small simulation box, there will be only a limited range of wave vectors accessible.

It should be emphasized that these fluctuation expressions are exactly equivalent to the forms involving the direct correlation function $c^{(2)}$, as discussed in Section V.A. This correspondence is made clear in the work of Poniewierski and Stecki, [260] Somoza and Tarazona [263] and others. It is also worth stressing that the Frank constants for hard-particle liquid crystals exist and are well behaved. The free energy for these systems is entirely entropic in origin: a deformation of the director field changes the entropy through its effect on molecular freedom and packing. The appropriate thermodynamic derivative is the Frank elastic constant. In a similar way, the hard-sphere crystal elastic constants are well known and well behaved (except in the limit of close packing).

Attempts to calculate elastic constants have been made for hard ellipsoids and spherocylinders. [264,265] Typical system sizes are in the range $125 \leq N \leq 600$. For these system sizes, the accessible range of k is limited, and deviations from the ideal equations (5.24,5.25) can be seen. Nonetheless, the $k \to 0$ extrapolation is practicable, and results reliable to about 15% can be obtained. These are shown for two different ellipsoid shapes in Figs. 5.2, 5.3. The density functional theories of Section V.A [63] are also depicted in the figure, and it can be seen that theory generally underestimates the simulation results. A similar comparison has been carried out for spherocylinders by Somoza and Tarazona, [208] using the results of Allen and Frenkel. [264,265] Once more, the theory generally underestimates the results of simulation. Recall that these same theories are comparatively successful in reproducing the transition density and order parameter variation. This discrepancy is presumably due to the sensitivity of the elastic constants to the variation of the direct correlation function $c^{(2)}$ at larger r_{ij}, outside the hard core overlap region. A more detailed

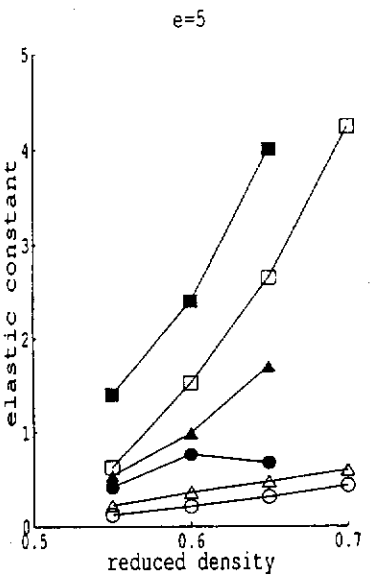

Figure 5.2. Elastic constants for prolate hard ellipsoids with $e = 5$ as a function of reduced density ρ/ρ_{cp}. We show K_1 (△), K_2 (○) and K_3 (□), with simulation results denoted by filled symbols, and the theory of Tjipto-Margo and Evans [63] by open symbols.

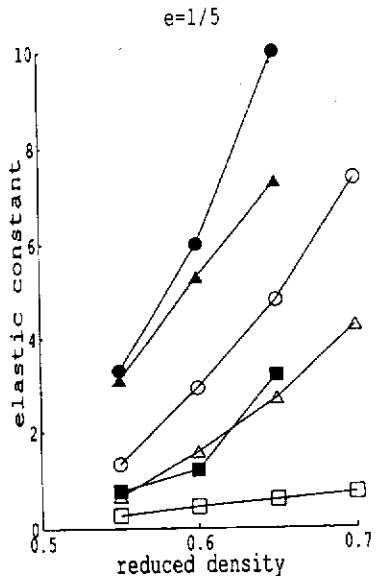

Figure 5.3. Elastic constants for oblate hard ellipsoids with $e = 1/5$ as a function of reduced density ρ/ρ_{cp}. Notation as for Fig. 5.2.

knowledge of the form of $c^{(2)}$ for both isotropic and nematic molecular liquids would be helpful.

Very recently, a more direct approach has been made [266] to calculate the twist elastic constant K_2, by directly measuring the torque density in a system of molecules in twisted periodic boundary conditions. For a cuboidal simulation box of dimensions $L_x = L_y \neq L_z$, periodic replicas in the $\pm z$ direction are rotated by, respectively, $\pm\pi/2$ about the z axis relative to the original. This rotation is applied to center of mass coordinates as well as molecular orientations, but for a nematic fluid the distortion of the positional degrees of freedom is inconsequential. A uniformly twisted nematic director field, with the director everywhere perpendicular to the z axis, of wave vector $k_z = \pi/2L_z$, is stabilized in these boundaries, as shown in Fig. 5.4. The torque density associated with this deformation is [2]

$$\tau/V \equiv -V^{-1}\partial F_d/\partial k_z = -K_2 k_z \tag{5.26}$$

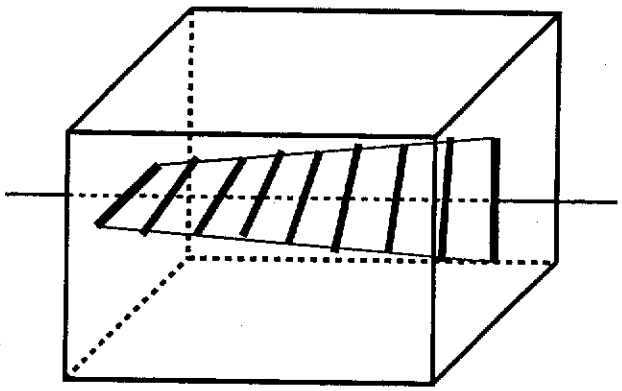

Figure 5.4. Director field stabilized in a cuboidal simulation box with twisted periodic boundary conditions applied. Neighboring boxes in the direction of the helix axis have all position and orientation vectors rotated by $\pm\pi/2$ about the axis.

where V is the volume of the box. The torque is measured as a sum of pairwise contributions

$$\tau/V = \frac{1}{2V}\left\langle \sum_i \sum_{j>i} (\tau_{ij}^z - \tau_{ji}^z) z_{ij} \right\rangle \tag{5.27}$$

where τ_{ij}^z is the z component of the torque on i exerted by j, and τ_{ji}^z the corresponding torque exerted on j by i. Further work is needed to establish the range of applicability of this technique, and to assess its value as a cross-check of the fluctuation expression approach discussed above.

VI. DYNAMIC PROPERTIES

In the nematic phase, two separate diffusion coefficients $D_\parallel$ and $D_\perp$ describe translation parallel and perpendicular to the director, respectively . Each is the time integral

$$D_\parallel = \int_0^\infty \mathrm{d}t\, c_\parallel(t) \tag{6.1}$$

$$D_\perp = \int_0^\infty \mathrm{d}t\, c_\perp(t) \tag{6.2}$$

of an appropriate component of the center of mass velocity autocorrelation function

$$c_\parallel(t) = \langle v_\parallel(0) v_\parallel(t) \rangle \tag{6.3}$$

$$c_\perp(t) = \langle v_\perp(0) v_\perp(t) \rangle \tag{6.4}$$

Here $v_\perp$ is either of the two Cartesian components perpendicular to the director (say, v_x, if the director is parallel to the z-axis) while $v_\parallel$ lies along it. Note that the chosen units of temperature and mass imply that $c_\perp(0) = c_\parallel(0) = 1$, that is, the correlation functions are normalized.

Diffusion in the nematic phase has been studied for ellipsoids of revolution. [267] For highly elongated prolate ellipsoids an unusual increase with density is seen for $D_\parallel$ just above the I→N transition; for very flat oblate ellipsoids a similar effect is observed for $D_\perp$. Examples are shown in Figs. 6.1 and 6.2. This seems to be associated with the rapid variation in order parameter close to the transition; physically the increasing order of the environment surrounding a molecule promotes slow decay of the velocity correlations, offsetting the general damping influence of an increasing collision rate. The correlations persist for many tens of collision times; these effects are illustrated in Figs. 6.3 and 6.4.

The most striking feature of these velocity correlations is the very slow long-time decay, extending to many tens of single particle collision times, of the more persistent component ($c_\parallel(t)$ for the prolate case, $c_\perp(t)$ for the oblate). We tentatively attribute this to coupling of the velocity with slow molecular reorientation, *not* to coupling with the hydrodynamic vortex

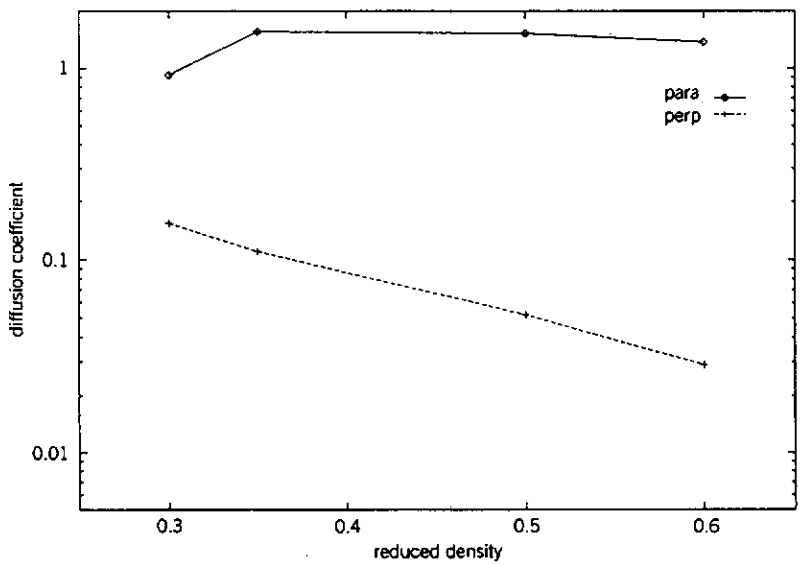

Figure 6.1. Diffusion coefficients parallel and perpendicular to the director (log scale) as functions of reduced density ρ/ρ_{cp} for prolate ellipsoids with $e = 10$.

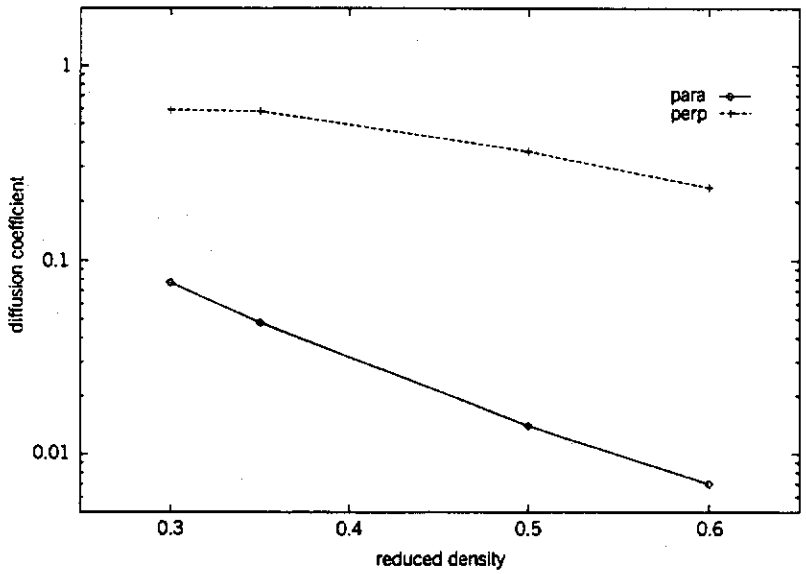

Figure 6.2. Diffusion coefficients parallel and perpendicular to the director (log scale) as functions of reduced density ρ/ρ_{cp} for oblate ellipsoids with $e = 1/10$.

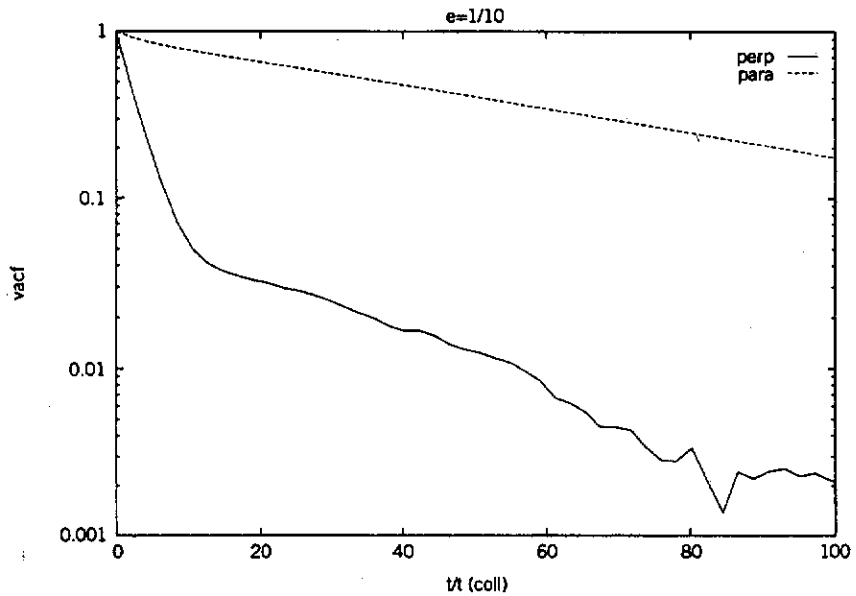

Figure 6.3. Translational velocity autocorrelation function (log scale), parallel and perpendicular to the director, for prolate ellipsoids with $e = 10$ at a reduced density $\rho/\rho_{cp} = 0.35$. Time is measured in units of the mean time between collisions per particle.

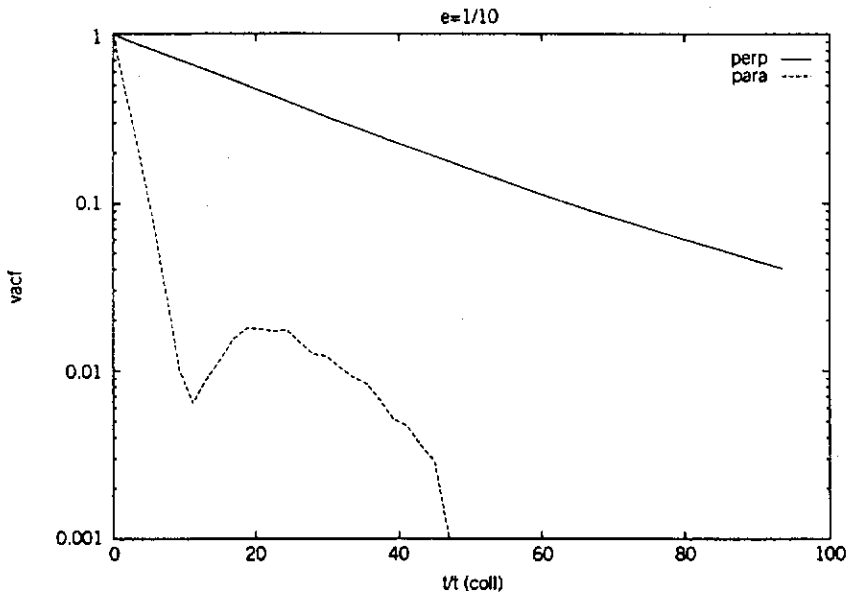

Figure 6.4. Translational velocity autocorrelation function (log scale), parallel and perpendicular to the director, for oblate ellipsoids with $e = 1/10$ at a reduced density $\rho/\rho_{cp} = 0.35$. Time is measured in units of the mean time between collisions per particle.

mode which gives rise to algebraic $t^{-3/2}$ long-time tails. [139–141] The long-time decay seems to be exponential, not algebraic. Yet, although we see no evidence for algebraic decay, we have no reason to doubt that the latter effect should be present at sufficiently long times. For shorter times, it is apparently masked by other effects.

Hess [268] has developed a theory based on relating the highly ordered system of ellipsoids to a reference system of hard spheres, by affine transformation. For perfect alignment (order parameter $S = 1$) a scaling of all the coordinates and ellipsoid shapes by a factor $1/e$ converts each ellipsoid configuration into an equivalent configuration of hard spheres. However, the scaling cannot simply be applied to the velocities as well, so there is not a one-to-one correspondence for dynamical properties. Nonetheless, it is possible to apply the scaling to the diffusion equation, and moreover to generalize the result to cater for imperfect orientational ordering ($S < 1$). The principal result of this analysis is an equation relating the anisotropy of diffusion to the order parameter S and the elongation e:

$$\Delta \equiv \frac{D_{\parallel} - D_{\perp}}{D_{\parallel} + 2D_{\perp}} = S\left(\frac{e^2 - 1}{e^2 + 2}\right) \tag{6.5}$$

In the limit of high ordering the anisotropy Δ is predicted to be substantial: for example, as $S \to 1$, $\Delta \to 0.97$ for $e = 10$, and $\Delta \to 0.89$ for $e = 5$. A previous theory, due to Chu and Moroi [269], when applied to ellipsoids yields a slightly different formula:

$$\Delta \equiv \frac{D_{\parallel} - D_{\perp}}{D_{\parallel} + 2D_{\perp}} = S\left(\frac{e-1}{e+2}\right). \tag{6.6}$$

Predicted values of Δ are rather lower than for Eq. (6.5): as $S \to 1$, $\Delta \to 0.75$ for $e = 10$, and $\Delta \to 0.57$ for $e = 5$.

Remarkably, the simulation results agree very well (see Fig. 6.5) with the universal affine-transformation prediction, Eq. (6.5), for all the shapes studied. Much higher values of Δ are observed than can be explained by the original Chu and Moroi theory (Fig. 6.6). However, the relationships between $D_{\parallel}$, $D_{\perp}$ and the "equivalent" hard-sphere values are not explained so well by the affine transformation model.

The increase of $D_{\parallel}$ with density for rod-like molecules is reminiscent of the divergence of the longitudinal diffusion coefficient predicted by Doi and Edwards [270–273] and tested by simulation of the *isotropic* hard needle fluid [142–144]. The Doi–Edwards theory applies in the semi-dilute regime, and their idea of "tube dilation" associated with orientational ordering may be valid here, although a detailed comparison for the orientationally ordered fluid in the prolate ellipsoid case is not valid.

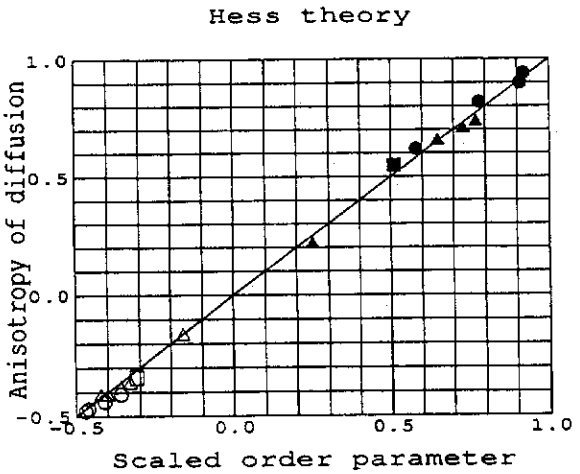

Figure 6.5. Test of the Hess theory for diffusion in the nematic phase. We plot the anisotropy of diffusion Δ versus the shape-scaled order parameter according to Eq. (6.5). Results for $e = 10$ (●), $e = 5$ (▲), $e = 3$ (■), $e = \frac{1}{3}$ (□), $e = \frac{1}{5}$ (△), and $e = \frac{1}{10}$ (○) are shown.

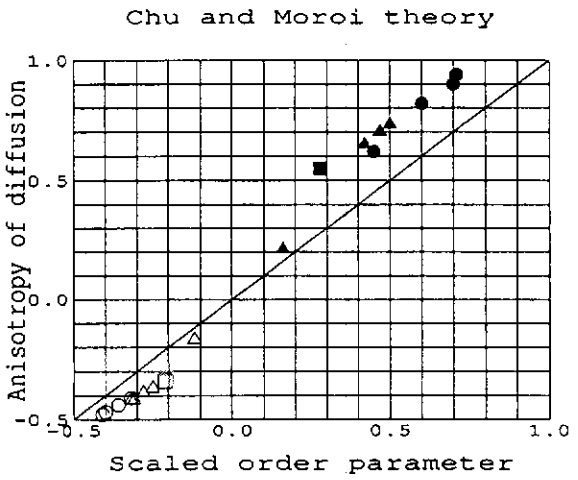

Figure 6.6. Test of the Chu and Moroi theory for diffusion in the nematic phase. We plot the anisotropy of diffusion Δ versus the shape-scaled order parameter according to Eq. (6.6). Notation as for Fig. 6.5.

Very recently, Tang and Evans [S. Tang and G.T. Evans, J. Chem. Phys., to appear] have formulated the kinetic theory in a way that explains the two-exponential decay very well. Using a projection operator formalism, they separate the decay rates of $c_{\parallel}(t)$ and $c_{\perp}(t)$ into components for different relative orientations of molecular axis, director, and direction of motion. Without any adjustable parameters, and taking only the density and order parameter as input, the measured diffusion coefficients and correlation functions are predicted quite accurately. This approach also explains two- exponential decay in the isotropic phase (see Section III.E.1), in terms of an Enskog-like theory.

Finally, we discuss an extreme example of anistropic diffusion in the nematic phase, namely the diffusion of infinitely thin hard platelets. [145] The latter model can be considered as oblate ellipsoids, in the limit $a/b \to 0$.

This system orders into a nematic phase at a density $\rho B_2 \approx 4$ ($B_2 = d^3\pi^2/16$), [67] where d denotes the diameter of a platelet. For such platelets, this nematic phase is stable at all finite densities with $\rho B_2 \geq 4$ (and therefore its nematic order parameter can be made arbitrarily close to one), in contrast to molecules with finite proper volume which freeze at high enough densities.

For this rather extreme model system, we can use a simple scaling argument to predict that, in the nematic phase, the transverse diffusion constant *increases* with increasing density. Consider an assembly of smooth

hard platelets of diameter d at a density ρ in which the system is in the nematic phase. The transverse diffusion coefficient for such a system can be estimated from a knowledge of the initial slope of the velocity autocorrelation function (assuming that this function decays exponentially with time). This slope is given by

$$1/\tau_\perp = -\frac{\langle \mathbf{v}_\perp^i . \Delta\mathbf{v} . \Gamma \rangle}{\langle \mathbf{v}_\perp^i . \mathbf{v}_\perp^i \rangle} \tag{6.7}$$

where Γ is the rate at which molecule i suffers collisions and $\Delta\mathbf{v}$ is the velocity change per collision. Assume that the normal to the plane of molecule i is inclined at an angle θ from the nematic director. A simple geometrical construction shows that [67]

$$\theta \sim \frac{1}{\pi d^3 \rho} \tag{6.8}$$

Γ the collision frequency goes as

$$\Gamma \sim \rho v_c d^2 \tag{6.9}$$

where v_c is the average relative velocity of the platelets at contact. v_c contains contributions from the relative translations and rotations of the platelets. In the nematic phase, v_c is dominated by $v_\parallel$ and rotations, and is only weakly dependent on density. Also $\Delta\mathbf{v}_\perp \sim -\theta^2 v_\perp$, since the impulse imparted at a rim-platelet collision is always perpendicular to the plane of the platelet which suffers the collision. (Note that $v_\perp$ is the velocity *parallel* to the plane of the platelet). In other words

$$\langle v_\perp(0)\dot{v}_\perp(0^+)\rangle \sim -\langle v_\perp^2(0)\rangle \frac{1}{\rho^{*2}} \frac{\rho^*}{d} \tag{6.10}$$

where the reduced density $\rho^* = \rho d^3$ has been substituted in (7), and some numerical factors have been omitted. Hence integrating the velocity autocorrelation function over all time, we obtain

$$D_\perp \sim \rho^* \tag{6.11}$$

Thus we arrive at the remarkable conclusion that the diffusion coefficient diverges with density. Physically this divergence can be understood simply as a consequence of the fact that as the density increases, the efficiency with which collisions can transfer momentum decreases (owing to the increased nematic order), so that the platelets are able to slide past each other with greater and greater ease, while diffusion perpendicular to the molecular plane is effectively suppressed. Incidentally, a scaling argument

similar to the one sketched above has been applied to diffusion in an isotropic system of infinitely thin needles. In the latter case, the scaling theory predicts a divergence of D with $\sqrt{\rho^*}$. [142]

To test whether such peculiar behavior of the diffusion constant is indeed observed, Alavi and Frenkel [145] performed molecular dynamics calculations of hard platelets in the density range $5 \leq \rho B_2 \leq 12$, which corresponds to a regime with pronounced nematic order ($0.92 < S < 0.99$) The diffusion coefficients $D_\perp$ and $D_\parallel$ were determined by examining the long-time limit of the mean-square displacement curves.

In Figure 6.7, we have plotted the diffusion coefficient $D_\perp$ against ρB_2.

From this figure, it is clear that $D_\perp$ does indeed increase with density, as had been anticipated earlier by the scaling arguments. In contrast, $D_\parallel$ drops with increasing density. This feature highlights the fact that the overall increase in diffusion is associated with the greater ease with which platelets move parallel to their planes as the density (and hence the nematic order) increases. At densities beyond $\rho B_2 = 8$, $D_\perp$ apparently increases approximately linearly with ρB_2, a result also anticipated by the scaling argument.

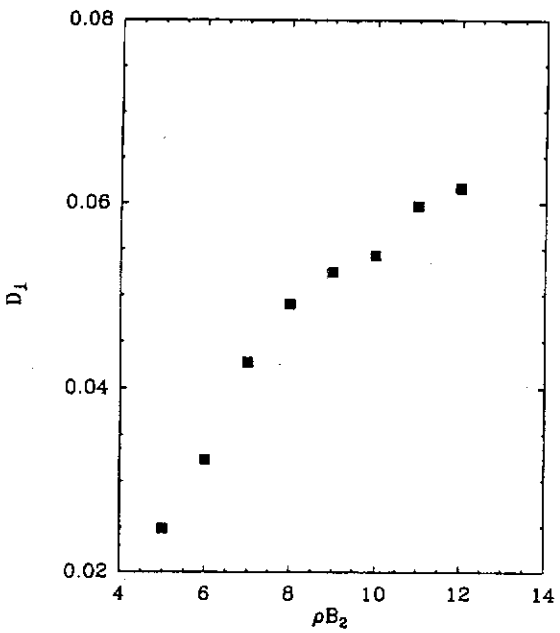

Figure 6.7. Density dependence of the diffusion coefficient $D_\perp$ of a system of infinitely thin, hard platelets in the nematic phase. The diffusion constant is expressed in reduced units $d\,(k_BT/M)^{1/2}$

VII. OUTLOOK

In this review, we have tried to summarize our current theoretical understanding of hard-convex body fluids. In view of the vast literature on this subject, this review is inevitably incomplete In fact, an up to date compilation of computer simulations on all kind of kind of models for molecular fluids can be found in the excellent review of Levesque and Weis. [274] It is clearly even more hazardous to make predictions about the future developments in this area. However, it seems clear that certain problems have received much more attention in the past than others. In particular, a vast amount of work has been reported on equations of state of pure HCB fluids in the isotropic phase. Much less is known, at present, about mixtures of HCBs. Yet, this seems to be an interesting topic because we may expect a much richer phase behavior in mixtures of nonspherical objects than in hard-sphere mixtures. If we then recall that, even for hard sphere mixtures, the presence or absence of a fluid–fluid phase separation is still a matter of debate, [275] it seems fair to say that the study of mixtures (binary, and, *a fortiori* polydisperse) of HCBs is a wide open area. It should also be stressed that there is also an "experimental" reason to try to understand the effect of polydispersity of the properties of hard-body fluids: the best experimental realizations of hard-body fluids are suspensions of nonspherical colloidal particles. These systems are hardly ever truly monodisperse and it seems likely that this polydispersity can effect the phase behavior of these colloidal suspensions in a nontrivial way. In fact, the recent numerical work of Stroobants on mixtures of hard parallel spherocylinders [244] is a case in point.

Next, let us consider transport properties. It is clear that our knowledge of the dynamics of HCB fluids is still quite limited. Most of what we know is limited to single particle properties ((rotational) diffusion) in the isotropic and, to a lesser extent, the nematic phase. Our knowledge of collective properties (viscosity, heat conductivity, collective orientational fluctuations) is quite limited for isotropic fluids and virtually nonexistent for the liquid-crystalline phases (see, however, Ref. [276]). As a consequence, the theories that describe the transport properties in isotropic molecular liquids remain largely untested. In the case of transport in liquid crystals, the situation is even more extreme as the corresponding "Enskog" expressions for the transport coefficients have not even been derived yet.

Finally, it is clear that, even if we stick to hard-core models, hard convex bodies are but a subclass of all model systems that we could consider. First of all, we could consider *rigid* nonconvex hard bodies (see, e.g., Refs. [65], [277,278]), and secondly, *flexible* hard molecules (see, e.g., Ref. [279]). Of course, very long-chain molecules have been studied extensively in

the context of polymer physics, but much less is known about short-chain molecules and the semi-flexible molecules ("worm-like chains"). Yet, flexibility is known to have a pronounced effect on the structure and phase behavior of hard-body fluids and, in particular, liquid crystals. Again, this area of research, and the study of dynamics in particular, appears wide open.

Of course, the study of highly idealized hard-core models cannot, and should not, replace the study of realistic models for molecular liquids and liquid crystals. Yet, for a fundamental understanding of real molecular systems, it is crucial to know how much of the behavior of such realistic models is already contained in simple hard-core models and how much of it is *truly* caused by other intermolecular interactions, such as dispersion forces, dipolar interactions or even many-body forces.

ACKNOWLEDGMENTS

We gratefully acknowledge the contributions of a large number of colleagues and collaborators. Special thanks are due to Dan Kivelson and Julian Talbot for their contribution to much of the work reported here. This research has been supported by the National Science Foundation (NSF), by the Petroleum Research Fund through grant PRF 18122-AC6 and by the Science and Engineering Research Council (SERC). The work of the FOM Institute is part of the research program of FOM and is supported by the Nederlandse Organisatie voor Wetenschappelijk Onderzoek (NWO). Computational facilities were provided at the John von Neumann Center for Scientific Computing at Princeton, NJ, at the University of Manchester Regional Computer Centre, and at the Amsterdam Computer Center (SARA), funded by NSF, SERC and WGS, respectively. International travel was made possible by a travel award from NATO.

A. APPENDICES TO PART I

A. The Ideal Free Energy of Rigid Bodies

In this appendix, we briefly discuss the calculation of the kinetic contribution to the free energy for a system of rigid bodies.

Consider a particle whose degrees of freedom are described by a set of n generalized coordinates, denoted by the n-dimensional vector $\mathbf{q}$. The Lagrangian of the particle in the absence of external force fields is just given by the kinetic energy

$$L = T = \frac{1}{2}\dot{\mathbf{q}} \cdot \mathbf{K}(\mathbf{q}) \cdot \dot{\mathbf{q}} \tag{A.1}$$

The generalized momenta conjugate to $\mathbf{q}$ are given by

$$\mathbf{p} = \frac{\partial L}{\partial \dot{\mathbf{q}}} = \mathbf{K}(\mathbf{q}) \cdot \dot{\mathbf{q}} \tag{A.2}$$

Using this to eliminate the generalized velocities $\dot{\mathbf{q}}$ from the kinetic energy, we find

$$T = \mathbf{p} \cdot \mathbf{K}(\mathbf{q})^{-1} \cdot \mathbf{p} \tag{A.3}$$

The canonical partition function of an interacting N particle system is then given by

$$Z_N = \frac{1}{h^n N!} \int \prod_{i=1}^{N} d\mathbf{p}_i d\mathbf{q}_i \exp[-\beta \sum_{i=1}^{N} \mathbf{p}_i \cdot \mathbf{K}(\mathbf{q}_i)^{-1} \cdot \mathbf{p}_i] \exp -\beta V(\{\mathbf{q}_k\}) \tag{A.4}$$

where $V(\{\mathbf{q}_k\})$ is the configurational energy of the system. We now perform the integration over the canonical momenta using the well-known generalized Gaussian integral identity

$$\int d\mathbf{x} e^{-\frac{1}{2}\mathbf{x} \cdot \mathbf{A} \cdot \mathbf{x}} = \sqrt{\frac{(2\pi)^n}{\det(\mathbf{A})}} \tag{A.5}$$

where $\mathbf{A}$ is a real, symmetric and positive definite $n \times n$ matrix. The result is

$$Z_N = \frac{1}{N!} \int \left\{ \prod_{i=1}^{N} d\mathbf{q}_i \sqrt{\frac{(2\pi)^n \det(\mathbf{K}(\mathbf{q}_i))}{h^{2n}\beta^n}} \right\} e^{-\beta V(\{\mathbf{q}_k\})} \tag{A.6}$$

where we have used the fact that $\det(\mathbf{A}^{-1}) = (\det(\mathbf{A}))^{-1}$.

For three-dimensional rigid bodies, the generalized coordinates are taken to be $\mathbf{q} = (x, y, x, \phi, \theta, \psi)$, that is, the coordinates of the center of mass in a Cartesian reference frame and the Euler angles specifying the orientation of a preferred frame (one in which the moment of inertia tensor is diagonal) of the particle with respect to this frame. The kinetic energy of such a particle is given by

$$T = \frac{1}{2}\left(m\dot{x}^2 + m\dot{y}^2 + m\dot{z}^2 + I_x\omega_x^2 + I_y\omega_y^2 + I_z\omega_z^2\right) \tag{A.7}$$

where m is the mass of the particle and I_x, I_y, I_z the principal moments of inertia. The instantaneous angular velocities in the particle-fixed frame are given by [280]

$$\omega_x = \dot{\phi} \sin\theta \sin\psi + \dot{\theta} \cos\psi \tag{A.8}$$

$$\omega_y = \dot{\phi} \sin\theta \cos\psi - \dot{\theta} \sin\psi \tag{A.9}$$

$$\omega_z = \dot{\phi} \cos\theta + \dot{\psi} \tag{A.10}$$

Evaluating the determinant of the kinetic tensor $\mathbf{K}(\mathbf{q})$, we find

$$\det(\mathbf{K}(\mathbf{q})) = m^3 I_x I_y I_z \sin^2\theta \tag{A.11}$$

Introducing this into the expression for the partition function, we arrive at

$$Z_N = \frac{1}{N!\mathcal{V}_T^N} \int \prod_{i=1}^{N} d\mathbf{r}_i d\Omega_i e^{-\beta V(\{\mathbf{r}_k,\Omega_k\})} \tag{A.12}$$

where we have introduced de orientational volume element $d\Omega = \sin\theta\, d\phi\, d\theta\, d\psi$ and the thermal volume

$$\mathcal{V}_T = \sqrt{\frac{(2\pi)^6\hbar^{12}\beta^6}{m^3 I_x I_y I_z}} = \lambda^3 \gamma_x \gamma_y \gamma_z \tag{A.13}$$

which can be interpreted as the product of the translational thermal wavelength (one factor for each translational degree of freedom)

$$\lambda = \sqrt{\frac{2\pi\hbar^2\beta}{m}} \tag{A.14}$$

and the orientational thermal angular spreads

$$\gamma_k = \sqrt{\frac{2\pi\hbar^2\beta}{I_k}}, \quad k = x, y, z \tag{A.15}$$

Finally, we calculate the free energy per particle of a noninteracting gas of rigid particles in a volume V in the thermodynamic limit $N, V \to \infty$ at constant density $N/V = \rho$.

$$\beta F_N^{\mathrm{id}}/N = \log \rho\mathcal{V}_T - 1 - \log 8\pi^2 \tag{A.16}$$

B. Center to Center Vectors

Consider two convex bodies whose mass centers are located at space points $\mathbf{r}_1$ and $\mathbf{r}_2$. The relative position of body 2 with respect to body 1 is $\mathbf{r}$,

$$\mathbf{r}_{12}(\mathbf{s}) = \mathbf{r}_2 - \mathbf{r}_1 = \xi(\hat{\mathbf{s}}_1) + s\hat{\mathbf{s}}_1 - \xi(\hat{\mathbf{s}}_2) \tag{A.17}$$

Here $\xi(\hat{\mathbf{s}}_i)$ are the "radius" vectors for body i, emanating from its mass center and terminating at the point on its surface with surface normal $\hat{\mathbf{s}}_i$. Since the surface-to-surface distance, s, is measured along a common surface normal, which we take to point out of surface 1, then

$$\hat{\mathbf{s}}_1 = -\hat{\mathbf{s}}_2 = \hat{\mathbf{s}} \tag{A.18}$$

and so

$$\mathbf{r}_{12}(\mathbf{s}) = \xi(\hat{\mathbf{s}}) + s\hat{\mathbf{s}} - \xi(-\hat{\mathbf{s}}) \tag{A.19}$$

The radius vectors can be specified in terms of the support function of the convex body

$$h_i = \hat{\mathbf{s}}_i \cdot \xi(\hat{\mathbf{s}}_i) \tag{A.20}$$

We derive h by taking the derivative of h with respect to $\hat{\mathbf{s}}$,

$$\nabla_{\hat{\mathbf{S}}} h = (I - \hat{\mathbf{s}}\hat{\mathbf{s}}) \cdot \xi(\hat{\mathbf{s}}) + \hat{\mathbf{s}}\dot{\nabla}_{\hat{\mathbf{S}}}\xi(\hat{\mathbf{s}}) \tag{A.21}$$

and as $\nabla_{\hat{\mathbf{S}}}\xi(\hat{\mathbf{s}})$ is perpendicular to $\hat{\mathbf{s}}$, then

$$\xi(\hat{\mathbf{s}}) = \hat{\mathbf{s}}h + \nabla_{\hat{\mathbf{S}}} h = \hat{\mathbf{s}}h + \hat{\mathbf{s}}_\theta \partial_\theta h + (1/\sin\theta)\hat{\mathbf{s}}_\phi \partial_\phi h \tag{A.22}$$

Given the support function, one can then determine the radius vector which traces out the exterior of the hard body.

C. Support Functions

Ideally one would like to have a support function that could represent convex shapes ranging from ellipsoids to spherocylinders. Although there is no unique choice of function that provides this feature, one function with some of these characteristics is a composite body formed by the addition of a sphere to a ellipsoid

$$h_i = (1/2)\sigma + h_i^e \tag{A.23}$$

where σ is the sphere diameter and h_i^e the ellipsoid support function of body i.

The equation for the surface of a biaxial ellipsoid with (semi-) axis lengths of a, b and c is given by

$$\mathbf{R}^T \cdot [\hat{\mathbf{u}}_x\hat{\mathbf{u}}_x a^{-2} + \hat{\mathbf{u}}_y\hat{\mathbf{u}}_y c^{-2} + \hat{\mathbf{u}}_z\hat{\mathbf{u}}_z b^{-2}] \cdot \mathbf{R} = 1 \tag{A.24}$$

where $\mathbf{R}$ is a Cartesian vector with components (R_x, R_y, R_z) in the body fixed principal axes. This surface has a support function

$$h^e = \hat{\mathbf{s}} \cdot \mathbf{R} = [(ax)^2 + (cy)^2 + (bz)^2]^{1/2} \tag{A.25}$$

where x, y, z are the projections of $\hat{\mathbf{s}}$ along the principal body axes,

$$(x, y, z) = \hat{\mathbf{s}}y(\hat{\mathbf{u}}_x, \hat{\mathbf{u}}_y, \hat{\mathbf{u}}_z) \tag{A.26}$$

A uniaxial body arises when $a = c$,

$$h^e = [a^2 + (b^2 - a^2)z^2]^{1/2} \tag{A.27}$$

and a sphere when $a = b = c$, wherein

$$h^e = a \tag{A.28}$$

A chiral convex body may be formed by rotating the $\hat{\mathbf{u}}_x, \hat{\mathbf{u}}_y$ of the biaxial ellipsoid by an angle α which depends on R_z. The resulting surface is still a homogeneous quadratic form except that the principal axes, described by the unit vectors $\hat{\mathbf{u}}_x(\alpha), \hat{\mathbf{u}}_y(\alpha)$, depend on R_z

$$\begin{aligned} \hat{\mathbf{u}}_x(\alpha) &= \hat{\mathbf{u}}_x \cos \alpha + \hat{\mathbf{u}}_y \sin \alpha \\ \hat{\mathbf{u}}_y(\alpha) &= -\hat{\mathbf{u}}_x \sin \alpha + \hat{\mathbf{u}}_y \cos \alpha \end{aligned} \tag{A.29}$$

with $\alpha = cR_z/d$ and d being the intrinsic chiral period. For this twisted biaxial ellipsoid, $\mathbf{R}$ is given parametrically in terms of θ_p and ϕ_p by

$$\begin{aligned} R_x &= \sin \theta_p [a \cos \phi_p - c \sin \phi_p \cos \alpha] \\ R_y &= \sin \theta_p [c \cos \phi_p \cos \alpha + a \sin \phi_p \sin \alpha] \\ R_z &= b \cos \theta_p \end{aligned} \tag{A.30}$$

and the surface by

$$\mathbf{R}^T \cdot [\hat{\mathbf{u}}_x(\alpha)\hat{\mathbf{u}}_x(\alpha)a^{-2} + \hat{\mathbf{u}}_y(\alpha)\hat{\mathbf{u}}_y(\alpha)c^{-2} + \hat{\mathbf{u}}_z\hat{\mathbf{u}}_z b^{-2}] \cdot \mathbf{R} = 1 \tag{A.31}$$

A representative surface is shown in Fig A.1. The surface normal for the twisted biaxial ellipsoid is proportional to the gradient of the surface and this together with $\mathbf{R}$ suffices to determine h. In the limit of small twists, the twisted body is still convex. For large twists, the chiral body becomes a twisted ribbon and is no longer convex. By means of a perturbation analysis of the chiral correction to the support function, we find

$$h_1 = h_1^e + \delta h_1 \tag{A.32}$$

where h_1^e is the support function of the convex biaxial ellipsoid and δh_1 is the first order chiral correction to body 1

$$\delta h_1 = \ell x_1 y_1 z_1 (3(c/h_1^e)^2 - (1 + (c/a)^2 + (c/b)^2)) \tag{A.33}$$

and ℓ is a length

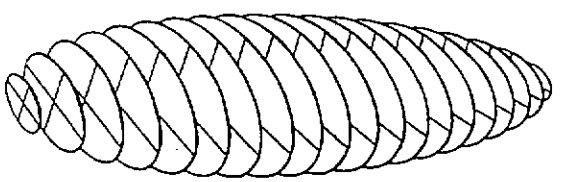

Figure A.1. The surface of a chiral particle as constructed by twisting a biaxial spheroid along its major axis.

$$\ell = (a^2 - c^2)b^2\pi/(c^2 d) \tag{A.34}$$

characterizing the extension of the surface due to chiral bulge.

At this point we can construct a variety of convex bodies: a sphere, a uniaxial ellipsoid, a biaxial ellipsoid and a twisted biaxial ellipsoidal body. By rolling a sphere over the exterior of these chosen bodies, we can flatten the sides of these bodies (which the exception, of course, of the sphere) to give shapes that approach spherocylinders, spheroplatelets, and twisted spheroplatelets but unlike the spherocylindric class of bodies, the composite bodies (sphere + ellipsoid) have a support function which is not defined piecewise. As an example, for two chiral bodies the support function for the pair is

$$h_{12} = h_1^e + h_2^e + \delta h_1 - \delta h_2 \tag{A.35}$$

whereas for a chiral body and a sphere of radius a,

$$h_{12} = a + h_1^e + \delta h_1 \tag{A.36}$$

If we choose to flatten either of these two shapes, we merely add to h_{12} a constant corresponding to the radius of the external sphere.

D. Jacobians

Typically, we shall require the Jacobian of the transformation from center to center coordinates to $\mathbf{s}$

$$d\mathbf{r}_{12} = |\partial \mathbf{r}_{12}/\partial \mathbf{s}| d\mathbf{s} \equiv S^{12}(\mathbf{s}) d\mathbf{s} \tag{A.37}$$

This determinant simplifies as $d\mathbf{r}_{12}/ds = \hat{\mathbf{s}}$ and so

$$S^{12}(\mathbf{s}) = |\hat{\mathbf{s}} \cdot \partial \mathbf{r}_{12}/\partial\theta \times \partial \mathbf{r}_{12}/\partial\phi| \tag{A.38}$$

When we take the θ and ϕ derivatives of $\mathbf{r}_{12}$, we obtain

$$\partial \mathbf{r}_{12}/\partial\theta = \hat{\mathbf{s}}_\theta [h + \partial_\theta^2 h] + \hat{\mathbf{s}}_\phi \partial_\theta [(1/\sin\theta)\partial_\phi h] \tag{A.39}$$

$$\partial \mathbf{r}_{12}/\partial\phi = \hat{\mathbf{s}}_\theta \partial_\theta [(1/\sin\theta)\partial_\phi h] \hat{\mathbf{s}}_\phi [h + \cot\theta \partial_\theta h + \partial_\theta^2 h] \tag{A.40}$$

and hence

$$S^{12} = (h + \partial_\theta^2 h)(h + \cot\theta \partial_\theta h + \partial_\theta^2 h) - (\partial_\theta [(1/\sin\theta)\partial_\phi h])^2 \tag{A.41}$$

In deriving these results, we have made use of the conventions that $\hat{\mathbf{s}}$ makes an anle θ and ϕ with respect to a space fixed (u_x, u_y, u_z) coordinate system. Further we have defined $\hat{\mathbf{s}}_\theta$ and $\hat{\mathbf{s}}_\phi$, the spherical polar unit vectors orthogonal to $\hat{\mathbf{s}}$.

$$\begin{aligned}
\hat{\mathbf{s}} &= \hat{\mathbf{u}}_z \cos\theta + \sin\theta[\hat{\mathbf{u}}_x \cos\phi + \hat{\mathbf{u}}_y \sin\phi] \\
&= \hat{\mathbf{s}}_\theta \times \hat{\mathbf{s}}_\phi = -(\partial\hat{\mathbf{s}}_\theta/\partial\theta) \\
\hat{\mathbf{s}}_\theta &= -\hat{\mathbf{u}}_z \sin\theta + \cos\theta[\hat{\mathbf{u}}_x \cos\phi + \hat{\mathbf{u}}_y \sin\phi] \\
&= \hat{\mathbf{s}}_\phi \times \hat{\mathbf{s}} = (\partial\hat{\mathbf{s}}/\partial\theta) \\
\hat{\mathbf{s}}_\phi &= -\hat{\mathbf{u}}_x \sin\phi + \hat{\mathbf{u}}_y \cos\phi
\end{aligned} \tag{A.42}$$

S^{12} is related to the orientation dependent second virial coefficient, $B_2(1,2)$ by

$$B_2(1,2) = (2\pi/3)h_{12}S^{12} \tag{A.43}$$

where h_{12} is the support functions for two bodies in contact. For two chiral bodies

$$h_{12} = h_1^e + h_2^e + \delta h_1 - \delta h_2 \tag{A.44}$$

whereas for a chiral body and a sphere of radius a,

$$h_{12} = a + h_1^e + \delta h_1 \tag{A.45}$$

Each of the four support functions directly above is expressed with respect to a common surface normal, $\hat{\mathbf{s}}$, emanating outward from the contact point on body 1.

B. APPENDICES TO PART II

A. Free Energy of Molecular Crystals

In this appendix, we discuss how the free energy of the solid phase of a given hard-core model system is related to the free energy of a known reference state. We use an artificial thermodynamic integration procedure to relate the free energy per particle, f_0, of the solid at a particular density ρ_0 to the free energy of an Einstein crystal of the same structure, at the same density. [229] The potential energy of this reference Einstein crystal is given by

$$U_E(\lambda_1,\lambda_2) = \lambda_1 \sum_{i=1}^{N} \Delta\mathbf{r}_i^2 + \lambda_2 \sum_{i=1}^{N} \sin^2\theta_i \tag{B.1}$$

where $\Delta\mathbf{r}_i \equiv \mathbf{r}_i - \mathbf{r}_i^0$ and θ_i denote, respectively, the translational and angular displacement of particle i from its equilibrium position and orientation. λ_1 and λ_2 are the coupling parameters which determine the strength of the harmonic force. The Einstein crystal is a convenient reference system, because its free energy per particle is known in closed form. For large

values of the coupling constants, the configurational part of this free energy is approximately given by

$$f_E \approx -\frac{k_B T}{N} \ln \left[N^{-3/2} \left(\frac{\pi}{\beta \lambda_1} \right)^{3/2(N-1)} \left(\frac{2\pi}{\beta \lambda_2} \right)^{N} \right] \quad (\lambda_{1,2} \to \infty) \qquad \text{(B.2)}$$

where we have imposed the additional constraint that the center of mass of the system is kept fixed. In order to construct a reversible path from the Einstein crystal to a hard-core crystal at the same density, we introduce a generalized potential energy function U_{λ_1,λ_2}

$$U_{\lambda_1,\lambda_2} = U_0 + U_E(\lambda_1, \lambda_2) \qquad \text{(B.3)}$$

where U_0 is the potential energy function of the hard-particle system in the absence of any harmonic springs. For sufficiently large values of λ_1 and λ_2, the free energy of this interacting Einstein crystal reduces to the free energy of the ideal Einstein crystal. This equality only holds if all configurations of the ideal Einstein crystal are also acceptable configurations of the interacting system. In practice, a small fraction, P_0, of the configurations of the ideal Einstein crystal would result in hard-core overlaps. However, it is easy correct for this effect. [229] In order to compute the free energy f_0 of the hard-particle crystal at the reference state ρ_0, we perform thermodynamic integration to compute the change in free energy as we slowly switch off the Einstein crystal coupling constants λ_1 and λ_2 from their maximum value $\lambda_{1,2}^{\max}$. The final expression that relates f_0 to the free energy of the ideal Einstein crystal is [229]

$$f_0 = f_E(\lambda_1^{\max}, \lambda_2^{\max}) + \frac{k_B T}{N} P_0 - k_B T \frac{\ln V}{N} - \int_0^{\lambda_1^{\max}} d\lambda_1 \langle \Delta r^2 \rangle_{\lambda_1,\lambda_2} - \int_0^{\lambda_2^{\max}} d\lambda_2 \langle \sin^2 \theta \rangle_{\lambda_1,\lambda_2} \qquad \text{(B.4)}$$

where $\langle \Delta r^2 \rangle_{\lambda_1,\lambda_2}$ is the mean-square displacement of a particle from its lattice site, at a given value of λ_1 and λ_2 and at fixed center of mass. The term $(-k_B T \ln V)/N$ corrects the free energy for this fixed center of mass constraint. Of course, the thermodynamic integration to the Einstein crystal must be performed at a density where the crystalline phase is at least mechanically stable. Once the absolute free energy of a phase is known at one density, we can use Eq. (4.69) to compute it at any other density that can be reached by reversible expansion or compression from the reference state.

B. System-Size Dependence of Nematic Order Parameter

When we determine the nematic order parameter in a numerical simulation, we find that the value of this quantity depends on the system size. It is, however, important to note that the different expressions for the the nematic order parameter that are used in the literature do not all have the same system-size dependence. In this section, we describe an approximate method to estimate the N-dependence of the different eigenvalues of the $\mathbf{Q}$ tensor

$$\mathbf{Q} = \frac{1}{N}\sum_i \left(\frac{3}{2}\hat{\mathbf{u}}_i\hat{\mathbf{u}}_i - \frac{\mathbf{I}}{2}\right) \tag{B.5}$$

(where $\hat{\mathbf{u}}_i$ is a unit vector specifying the orientation of molecule i; we assume cylindrically symmetric molecules). We consider an idealized model of an orientationally ordered fluid, namely one in which the $\mathbf{Q}$ tensors of different particles are uncorrelated, that is,

$$< \mathbf{Q}_i\mathbf{Q}_j > = < \mathbf{Q}_i >< \mathbf{Q}_j > \tag{B.6}$$

This situation will occur, for instance, in noninteracting gas of molecules in a magnetic field. Although in a real liquid crystal (or isotropic fluid) there are short-range orientational correlations the present analysis is still qualitatively valid in such a system if one reinterprets the $\mathbf{Q}_i$ not as molecular $\mathbf{Q}$ tensors but as the average $\mathbf{Q}$ tensor of a domain of size ξ^3, where ξ is the correlation length of order parameter fluctuations. The eigenvalue equation to be solved is

$$\mathbf{Q}\cdot\mathbf{v}_n = \lambda_n\mathbf{v}_n \tag{B.7}$$

where λ_n is the nth eigenvalue and $\mathbf{v}_n$ the nth eigenvector. It is convenient to study the equivalent problem of finding the eigenvalues of the tensor $\mathbf{M}$:

$$\mathbf{M} \equiv \frac{1}{N}\sum_i \hat{\mathbf{u}}_i\hat{\mathbf{u}}_i \tag{B.8}$$

The eigenvectors of $\mathbf{M}$ are the eigenvectors of $\mathbf{Q}$ and the eigenvalues μ of $\mathbf{M}$ are related to those of $\mathbf{Q}$ by $\mu_n = 2/3\lambda_n + 1/3$. The eigenvalue equation for $\mathbf{M}$ then becomes

$$\det|\mathbf{M} - \mu\mathbf{I}| = 0 \tag{B.9}$$

or

$$\begin{vmatrix} \frac{1}{N}\sum_i x_i x_i & \frac{1}{N}\sum_i x_i y_i & \frac{1}{N}\sum_i x_i z_i \\ \frac{1}{N}\sum_i y_i x_i & \frac{1}{N}\sum_i y_i y_i & \frac{1}{N}\sum_i y_i z_i \\ \frac{1}{N}\sum_i z_i x_i & \frac{1}{N}\sum_i z_i y_i & \frac{1}{N}\sum_i z_i z_i \end{vmatrix} = 0 \tag{B.10}$$

or

$$-\mu^3 + \mu^2 + c_1\mu + c_0 = 0 \tag{B.11}$$

where

$$c_1 = -\frac{1}{N^2}\sum_{i,j}\left[(x_i x_i y_j y_j - x_i y_i x_j y_j) + (x_i x_i z_j z_j - x_i z_i x_j z_j) + (y_i y_i z_j z_j - y_i z_i y_j z_j)\right] \tag{B.12}$$

$$c_0 = \frac{1}{N^3}\sum_{i,j,k}\left[(x_i x_i y_j y_j z_k z_k - x_i x_i y_j z_j y_k z_k - y_i y_i x_j z_j x_k z_k - z_i z_i x_j y_j x_k y_k) + 2x_i y_i y_k z_k z_j x_j\right] \tag{B.13}$$

Solving this equation yields μ_n as a function of all orientations:

$$\mu_n = f_n(x_1, y_1, z_1, \ldots, x_N, y_N, z_N) \tag{B.14}$$

where f_n is a *nonlinear* function of all orientations. To obtain $< \mu_n >$, one should average the roots of this nonlinear equation. This is in general not possible. We simplify this problem by solving the equation with the average coefficients $< c_1 >$ and $< c_0 >$. Of course, for a nonlinear problem, this is *not* equivalent to a procedure where the μ's are averaged after the equation has been solved. However, as discussed below, we have tested the quality of this approximation in a few specific cases and find that the pre-averaging has no noticeable effects on our qualitative or even, for that matter, quantitative conclusions.

The averaged equation for μ now reads

$$-\mu^3 + \mu^2 - \mu\frac{N-1}{N}\left(< x^2 > (< x^2 > + 2 < z^2 >)\right) + \frac{(N-1)(N-2)}{N^2} < x^2 >< y^2 >< z^2 > = 0 \tag{B.15}$$

where we have used a coordinate system such that the z-axis coincides with the axis of cylindrical symmetry. Moreover, we have used the fact that there is no short-range orientational correlation. Using the relation

$$< x^2 >=< y^2 >= (1 - S)/3$$
$$\text{and} \tag{B.16}$$
$$< z^2 >= (2S + 1)/3$$

where S is the nematic order parameter, we obtain the following equation for $\mu = 2/3\lambda + 1/3$:

$$\lambda^3 - \frac{3}{4}\lambda\frac{1 + S^2(N-1)}{N} - \left[S^3/4 + \frac{3(S^2 - S^3)}{4N} + \frac{1 - 3S^2 + 2S^3}{4N^2}\right] = 0 \tag{B.17}$$

This cubic equation can be solved in a closed form.

$$\lambda_n = r\cos(\phi_n + (n-1)\frac{2\pi}{3}), \quad n = -1, 0, 1 \tag{B.18}$$

with

$$r = \sqrt{\frac{1 + S^2(N-1)}{N}} \tag{B.19}$$

and

$$\phi = \frac{1}{3}\arccos\left(\frac{S^3 + 3(S^2 - S^3)/N + (1 - 3S^2 + 2S^3)/N^2}{r^3}\right) \tag{B.20}$$

Let us consider the isotropic case (S=0) first. In that case,

$$r = 1/\sqrt{N}$$
$$\text{and} \tag{B.21}$$
$$\phi = \tfrac{1}{3}\arccos\left(\tfrac{1}{\sqrt{N}}\right)$$

for N not too small (say $N > 20$),

$$\arccos\left(\frac{1}{\sqrt{N}}\right) \approx \frac{\pi}{2} - \frac{1}{\sqrt{N}} \tag{B.22}$$

and hence

$$\phi = \frac{\pi}{6} - \frac{1}{3\sqrt{N}} \tag{B.23}$$

The expressions for the eigenvalues λ_n then become

$$\begin{aligned}
\lambda_0 &= \tfrac{1}{\sqrt{N}}\cos\left(-\tfrac{\pi}{2} - \tfrac{1}{3\sqrt{N}}\right) &&\approx -\tfrac{1}{3N} \\
\lambda_+ &= \tfrac{1}{\sqrt{N}}\cos\left(-\tfrac{\pi}{6} - \tfrac{1}{3\sqrt{N}}\right) &&\approx -\tfrac{1}{\sqrt{N}}\left(\tfrac{\sqrt{3}}{2} + \tfrac{1}{6\sqrt{N}}\right) \\
\lambda_- &= \tfrac{1}{\sqrt{N}}\cos\left(-\tfrac{5\pi}{6} - \tfrac{1}{3\sqrt{N}}\right) &&\approx -\tfrac{1}{\sqrt{N}}\left(\tfrac{-\sqrt{3}}{2} + \tfrac{1}{6\sqrt{N}}\right)
\end{aligned} \tag{B.24}$$

We therefore arrive at the important conlusion that, although all eigenvalues vanish in the thermodynamic limit ($N \to \infty$), the largest (in absolute value) eigenvalues ($\lambda_\pm$) vanish as $1/\sqrt{N}$, whereas the middle eigenvalue (λ_0), vanishes as $1/N$. An example of the N-dependence of λ_-, λ_0 and λ_+ is shown in Fig. B.1. Next we consider the case $S \neq 0$. Then

$$\cos 3\phi = \left(\frac{S^3 + 3(S^2 - S^3)/N + (1 - 3S^2 + 2S^3)/N^2}{r^3} \right) \tag{B.25}$$

which, to leading order in $1/N$, is equal to

$$\cos 3\phi \approx 1 - \frac{3}{2N} + 3\frac{2S - 1}{2NS^2} \tag{B.26}$$

Clearly, for N and S not too small, we can expand the cosine to obtain the following expression for ϕ:

$$\phi^2 = \frac{1}{3N} + \frac{2S - 1}{3NS^2} \tag{B.27}$$

from which it follows that $\phi = \mathcal{O}(1/\sqrt{N})$. For $S \neq 0$, r is given by

$$r = \sqrt{S^2 + \frac{1 - S^2}{N}} = S + \frac{1 - S^2}{2NS} + \mathcal{O}(\frac{1}{N^2}) \tag{B.28}$$

Hence $r = S + \mathcal{O}(1/N)$. If we now look at λ_-, λ_0 and λ_+, we find that for $S \neq 0$,

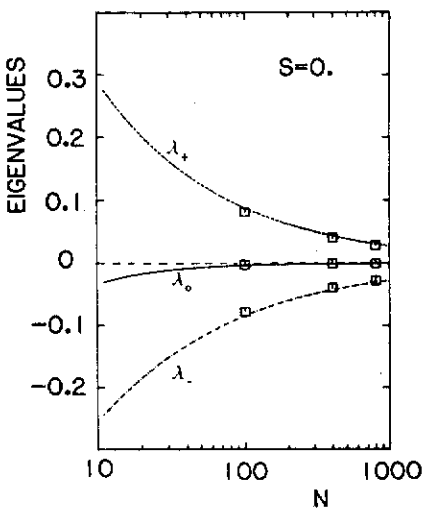

Figure B.1. System-size dependence of the three roots of the average **Q** tensor, as given by Eq. (B.16) for an isotropic fluid ($S = 0$) with no short-range correlations. In the same figure we have also indicated numerical results for an ideal isotropic gas for N= 100, 400 and 800 (OPEN SQUARES). Note that the numerical results agree quite well with the (approximate) analytical expressions.

$$\begin{aligned} \lambda_+ &= S + \mathcal{O}(\tfrac{1}{N}) \\ \lambda_0 &= -\tfrac{S}{2} + \mathcal{O}(\tfrac{1}{\sqrt{N}}) \\ \lambda_- &= -\tfrac{S}{2} + \mathcal{O}(\tfrac{1}{\sqrt{N}}) \end{aligned} \tag{B.29}$$

Hence, in the nematic phase, λ_- yields a better estimate of S than $-2\lambda_0$. Note that the fact that we find three different eigenvalues does not indicate a biaxial phase, because this result was derived assuming a uniaxial phase. The apparent biaxiality is a system size effect. The dependence of λ_-, λ_0 and λ_+ on S is shown in Fig. B.2.

Using the above analysis, we can give a simple "geometrical" interpretation to the fluctuations in the nematic order parameter. A graphical representation of the eigenvalues λ_-, λ_0 and λ_+ is shown in Fig. B.3. The three eigenvalues are equal to the projections of a triad of vectors of equal

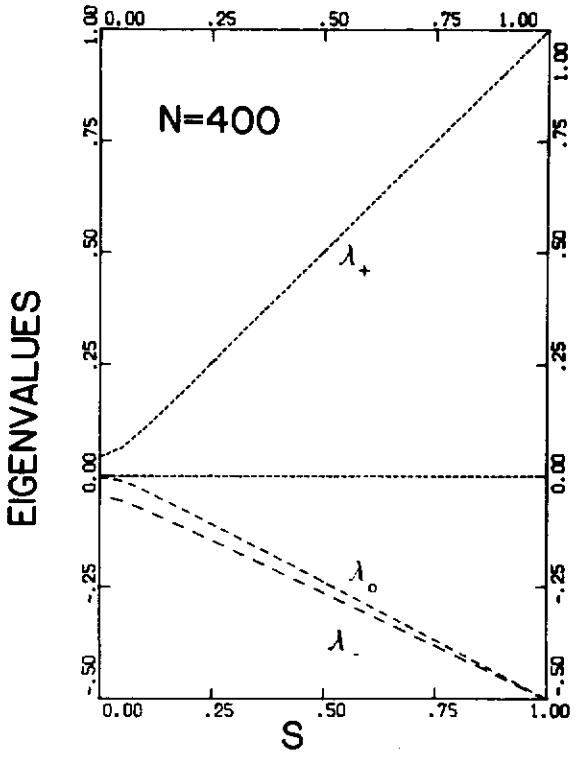

Figure B.2. Relation between the "real" (infinite system order parameter S, and the three roots of the average $\mathbf{Q}$ tensor, as computed using Eq. (B.16), for N=400. Note that at low values of S, λ_0 approaches zero more rapidly than either λ_+ or λ_-. At larger values of S, λ_+ approaches S.

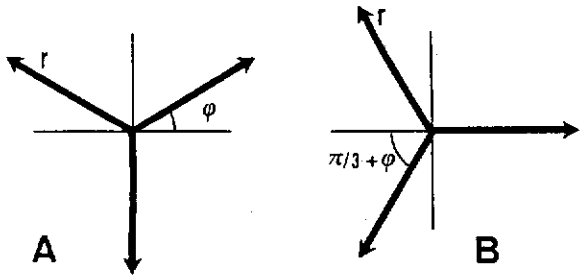

Figure B.3. Graphic representation of the computation of the eigenvalues of the **Q** tensor (Eq. B.16). The three eigenvalues are given by the projection of the three vectors on the horizontal axis. In the isotropic phase (a), $r=\mathcal{O}(1/\sqrt{N})$ while $\phi = \pi/6 - \mathcal{O}(1/\sqrt{N})$ In the nematic phase (b), $r=S + \mathcal{O}(1/N)$, while $\phi = \mathcal{O}(1/\sqrt{N})$. Fluctuations in the order parameter are caused by fluctuations in both r and ϕ.

length which make angles of 120° with one another. Fluctuations in the order parameters are driven by fluctuations in both the length of the vectors (r) and the angle (ϕ). It is important to note that the fluctuations in λ_0 contain both effects, that is, a contribution due to biaxial fluctuations (ϕ) and fluctuations in the size of the order parameter (r). As one approaches the isotropic–nematic transition, all fluctuations increase in magnitude and ϕ starts to rotate from $\pi/6$ to 0, while r grows from $1/\sqrt{N}$ to S. In the immediate vicinity of the I–N transition, all three eigenvalues of **Q** depend strongly on the size of the system.

Finally, we should return to the pre-averaging approximation that we made in order to solve Eq. (B.10). There we computed the eigenvalues of the averaged tensor order parameter, rather than the average of eigenvalues of the fluctuating tensor order parameter. It is of course interesting to know how seriously this averaging of a nonlinear equation affects the predicted average values of λ_n. To this end, we have carried out the following numerical test. We have generated the **Q** tensor for 10^4 configurations of a system of N ideal gas molecules (N = 100, 400, 800). In Fig. B.1 we compare the predicted eigenvalues computed from Eq. (B.16) with the average eigenvalues obtained by direct diagonalization of **Q** for all independent ideal gas configurations. Clearly, the agreement is quite good.

REFERENCES

[1] J.-P. Hansen and I. R. McDonald, *Theory of Simple Liquids*, 2nd edition, Academic Press, New York, (1986).

[2] P. G. de Gennes, *The Physics of Liquid Crystals*, Oxford University Press, (1974).

[3] L. Onsager, *Ann. N. Y. Acad. Sci.* **51**, 627 (1949).

[4] G. Ciccotti, D. Frenkel and I. R. McDonald, Eds., *Simulations of Liquids and Solids*, North-Holland, Amsterdam, (1987).
[5] J. Vieillard-Baron, *J. Chem. Phys.* **56**, 4729 (1972).
[6] J. Vieillard-Baron, *Mol. Phys.* **28**, 809 (1974).
[7] K. Mortensen, W. Brown and B. Nordén, *Phys. Rev. Lett.* **68**, 2340 (1992).
[8] J. W. Perram, M. S. Wertheim, J. L. Lebowitz and G. O. Williams, *Chem. Phys. Lett.* **105**, 277 (1984).
[9] J. W. Perram and M. S. Wertheim, *J. Comp. Phys.* **58**, 409 (1985).
[10] Ph. De Smedt, J. Talbot and J. L. Lebowitz, *Mol. Phys.* **59**, 625 (1986).
[11] M. P. Allen and D. J. Tildesley, *Computer Simulation of Liquids*, Clarendon Press, Oxford, (1987).
[12] T. Boublik and I. Nezbeda, *Collect. Czech. Chem. Comm.* **51**, 2301 (1986).
[13] D. A. McQuarrie, *Statistical Mechanics*, Harper and Row, New York, (1976).
[14] T. Boublik, *Mol. Phys.* **27**, 1415 (1974).
[15] T. Kihara, *Adv. Chem. Phys.* **5**, 147 (1963).
[16] B. Widom, *J. Chem. Phys.* **39**, 2808 (1963).
[17] R. S. C. She and G. T. Evans, *J. Chem. Phys.* **85**, 1513 (1986).
[18] W. A. Steele, *J. Chem. Phys.* **39**, 3197 (1963).
[19] L. Blum and A. J. Torruella, *J. Chem. Phys.* **56**, 303 (1972).
[20] L. Blum, *J. Chem. Phys.* **57**, 1862 (1972).
[21] L. Blum, *J. Chem. Phys.* **58**, 3295 (1973).
[22] Y. D. Chen and W. A. Steele, *J. Chem. Phys.* **50**, 1428 (1969).
[23] A. Perera, P. G. Kusalik and G. N. Patey, *J. Chem. Phys.* **87**, 1295 (1987).
[24] J. Talbot, A. Perera and G. N. Patey, *Mol. Phys.* **70**, 285 (1990).
[25] A. Perera, G. N. Patey, and J. J. Weis, *J. Chem. Phys.* **89**, 6941 (1987).
[26] W. B. Streett and D. J. Tildesley, *Proc. R. Soc. A* **348**, 485 (1976).
[27] P. A. Monson and M. Rigby, *Chem. Phys. Lett.* **58**, 1699 (1978).
[28] P. A. Monson and M. Rigby, *Mol. Phys.* **38**, 1699 (1979).
[29] V. N. Kabadi and W. A. Steele, *Ber. Bunsenges Phys. Chem.* **89**, 9 (1985).
[30] V. N. Kabadi, *Ber. Bunsenges Phys. Chem.* **90**, 332 (1985).
[31] V. N. Kabadi and W. A. Steele, *Ber. Bunsenges Phys. Chem.* **89**, 2 (1985).
[32] F. Gazi and M. Rigby, *Mol. Phys.* **62**, 1103 (1987).
[33] B. Kumar, C. James and G. T. Evans, *J. Chem. Phys.* **88**, 7071 (1988).
[34] J. Talbot, D. Kivelson, M. P. Allen, G. T. Evans and D. Frenkel, *J. Chem. Phys.* **92**, 3048 (1990).
[35] R. G. Cole and G. T. Evans, *Annu. Rev. Phys. Chem.* **37**, 106 (1986).
[36] D. Kivelson and P. A. Madden, *Annu. Rev. Phys. Chem.* **31**, 523 (1980).
[37] D. Frenkel, *J. Phys. Chem.* **91**, 4912 (1987).
[38] M. Rigby, *Mol. Phys.* **66**, 1261 (1989).
[39] M. Rigby, *Mol. Phys.* **68**, 686 (1989).
[40] P. A. Monson and M. Rigby, *Mol. Phys.* **35**, 1337 (1978).
[41] B. Tjipto-Margo and G. T. Evans, *J. Chem. Phys.* **93**, 4254 (1990).
[42] H. Reiss, H. L. Frisch, and J. L. Lebowitz, *J. Phys. Chem.* **31**, 369 (1959).

[43] E. Helfand, H. Reiss, H. L. Frisch, and J. L. Lebowitz, *J. Chem. Phys.* **33**, 1379 (1960).

[44] H. Reiss, *Statistical Mechanics and Statistical Methods in Theory and Applications: A Tribute To Elliott W. Montroll* Plenum Press, New York, (1976).

[45] H. Reiss, *J. Phys. Chem.* **96**, 4736 (1992).

[46] M. Wojcik and K. E. Gubbins, *Mol. Phys.* **53**, 397 (1984).

[47] K. H. Naumann and Y. P. Chen and T. W. Leland, *Ber. Bunsenges. Phys. Chem.* **85**, 1029 (1981).

[48] Y. Song and E. A. Mason, *Phys. Rev.* **41**, 3121 (1990).

[49] B. Barboy and W. M. Gelbart, *J. Chem. Phys.* **71**, 3053 (1979).

[50] B. Barboy and W. M. Gelbart, *J. Stat. Phys.* **22**, 685 (1980).

[51] B. Barboy and W. M. Gelbart, *J. Stat. Phys.* **22**, 709 (1980).

[52] J. K. Percus and G. J. Yevick, *Phys. Rev.* **110**, 1 (1958).

[53] N. F. Carnahan and K. E. Starling, *J. Chem. Phys.* **51**, 635 (1969).

[54] A. Isihara, *J. Chem. Phys.* **19**, 1142 (1951).

[55] B. M. Mulder, *Liq. Crys.* **1**, 539 (1986).

[56] B. Tjipto-Margo and G. T. Evans, *J. Chem. Phys.* **94**, 4546 (1991).

[57] R. S. C. She, C. James and G. T. Evans, *J. Chem. Phys.* **85**, 1525 (1986).

[58] D. M. Tully-Smith and H. Reiss, *J. Chem. Phys.* **53**, 4015 (1970).

[59] H. Reiss and R. V. Casberg, *J. Chem. Phys.* **61**, 1107 (1974).

[60] C. Gray and K. E. Gubbins, *Theory of Molecular Fluids*, Clarendon Press, Oxford, (1984).

[61] I. Nezbeda and S. Labik and A. Malijevsky, *Collect. Czech. Comm.* **54**, 1137 (1989).

[62] S. Labik and A. Malijevsky and W. R. Smith, *Mol. Phys.* **73**, 87 (1991).

[63] B. Tjipto-Margo, G. T. Evans, M. P. Allen and D. Frenkel, *J. Phys. Chem.* **96**, 3942 (1992).

[64] V. R. Bhethanabotla and W. Steele, *Mol. Phys.* **60**, 249 (1987).

[65] M. Whittle and A. J. Masters, *Mol. Phys.* **72**, 247 (1991).

[66] L. Verlet, *Phys. Rev.* **159**, 98 (1967).

[67] R. Eppenga and D. Frenkel, *Mol. Phys.* **52**, 1303 (1984).

[68] M. C. Duro and J. A. Martin-Pereda and L.M. Sesé, *Phys. Rev.* **A37**, 284 (1988).

[69] J. Vieillard-Baron, *These de Doctorat A637*, PhD thesis, Orsay, (1970).

[70] M. Weber, *Lehrbuch der Algebra I*, New York, (1962).

[71] W. H. Press and B. P. Flannery and S. A. Teukolsky and W. T. Vetterling, *Numerical Recipes: The Art of Scientific Computing*, Cambridge University Press, (1986).

[72] L. Qin, J. Wesemann and P. Siders, *Langmuir* **5**, 1358 (1989).

[73] M. He and P. Siders, *J. Phys. Chem.* **94**, 7280 (1990).

[74] J. W. Perram, We thank John Perram for sending us this material prior to publication.

[75] D. Frenkel and B. M. Mulder, *Mol. Phys.* **55**, 1171 (1985).

[76] F. H. Ree and W. G. Hoover, *J. Chem. Phys.* **40**, 939 (1964).

[77] M. P. Allen and D. Frenkel and J. Talbot, *Comp. Phys. Rep.* **9**, 301 (1989).

[78] W. W. Wood, *J. Chem. Phys.* **48**, 415 (1968).

[79] I. R. McDonald, *Mol. Phys.* **23**, 41 (1972).

[80] W. R. Cooney, S. M. Thompson and K. E. Gubbins, *Mol. Phys.* **66**, 1269 (1989).
[81] J. A. C. Veerman and D. Frenkel, *Phys. Rev.* **A45**, 5633 (1992).
[82] D. Frenkel, *J. Phys. Chem.* **91**, 4912 (1987).
[83] D. Frenkel, *J. Phys. Chem.* **92**, 5314 (1988); erratum to [82].
[84] D. Frenkel, *Mol. Phys.* **60**, 1 (1987).
[85] D. Frenkel, *Mol. Phys.* **65**, 493 (1988); erratum to [84].
[86] M. Wertheim and J. Talbot, We would like to thank Mike Wertheim and Julian Talbot for letting us use this unpublished material.
[87] C. F. Curtiss, *J. Chem. Phys.* **24**, 225 (1956).
[88] C. F. Curtiss and C. Muckenfuss, *J. Chem. Phys.* **26**, 1619 (1957).
[89] C. Muckenfuss and C. F. Curtiss, *J. Chem. Phys.* **29**, 1257 (1958).
[90] C. F. Curtiss and J. S. Dahler, *J. Chem. Phys.* **38**, 2352 (1963).
[91] N. F. Sather and J. S. Dahler, *J. Chem. Phys.* **35**, 2029 (1961).
[92] J. S. Dahler and N. F. Sather, *J. Chem. Phys.* **38**, 2363 (1963).
[93] S. I. Sandler and J. S. Dahler, *J. Chem. Phys.* **43**, 1750 (1965).
[94] S. I. Sandler and J. S. Dahler, *J. Chem. Phys.* **47**, 2621 (1967).
[95] D. K. Hoffman, *J. Chem. Phys.* **50**, 4823 (1969).
[96] D. K. Hoffman and J. S. Dahler, *J. Stat. Phys.* **1**, 521 (1969).
[97] S. Chapman and T. G. Cowling, *The Mathematical Theory of Non-Uniform Gases, 3rd edition*, Cambridge University Press, (1970).
[98] J. H. Ferziger and H. G. Kaper, *Mathematical Theory of Transport Processes of Gases*, North-Holland, Amsterdam, (1972).
[99] R. G. Cole and D. R. Evans and D. K. Hoffman, *J. Chem. Phys.* **82**, 2061 (1985).
[100] H. Mori, *Prog. Theor. Phys.* **33**, 423 (1965).
[101] G. T. Evans, *Mol. Phys.* **74**, 775 (1991).
[102] M. H. Ernst and J. R. Dorfman and E. G. D. Cohen, *Physica* **31**, 493 (1965).
[103] M. H. Ernst, J. R. Dorfman, W. R. Hoegy and J. M. J. van Leeuwen, *Physica* **45**, 127 (1969).
[104] M. H. Ernst, *Physica* **32**, 209 (1966).
[105] M. H. Ernst, *Physica* **32**, 273 (1966).
[106] J. R. Dorfman and H. van Beijeren, *Statistical Mechanics, Part B: Time Dependent Processes*, Plenum, New York, (1977).
[107] D. Forster, *Phys. Rev.* **A9**, 943 (1974).
[108] G. F. Mazenko, *Phys. Rev.* **A9**, 360 (1974).
[109] G. F. Mazenko and S. Yip, *Statistical Mechanics, Part B: Time Dependent Processes*, Plenum, New York, (1977).
[110] W. Sung and J. S. Dahler, *J. Chem. Phys.* **78**, 6264 (1983).
[111] W. Sung and J. S. Dahler, *J. Chem. Phys.* **78**, 6280 (1983).
[112] W. Sung and J. S. Dahler, *J. Chem. Phys.* **80**, 3025 (1984).
[113] G. T. Evans, *J. Chem. Phys.* **88**, 5035 (1988).
[114] G. T. Evans, *J. Chem. Phys.* **91**, 1252 (1989).
[115] T. Kagen and L. Maksimov, *Zh. Eksp. Teor. Fiz.* **51**, 5035 (1966).
[116] T. Kagen and L. Maksimov, *Sov. Phys. JETP* **24**, 1272 (1967).

[117] D. R. Evans, G. T. Evans and D. K. Hoffman, *J. Chem. Phys.* **93**, 8816 (1990).
[118] J. V. Sengers, *Phys. Fluids* **9**, 1333 (1966).
[119] J. V. Sengers, M. H. Ernst and D. T. Gillespie, *J. Chem. Phys.* **56**, 5583 (1972).
[120] J. R. Mehaffey and R. C. Desai and R. Kapral, *J. Chem. Phys.* **66**, 1665 (1977).
[121] S. R. deGroot and P. Mazur, *Non-Equilibrium Thermodynamics*, North-Holland, Amsterdam, (1962).
[122] M. Theodosopulu and J. S. Dahler, *J. Chem. Phys.* **60**, 3567 (1974).
[123] M. Theodosopulu and J. S. Dahler, *J. Chem. Phys.* **60**, 4048 (1974).
[124] J. S. Dahler and M. Theodosopulu, *Adv. Chem. Phys.* **31**, 155 (1975).
[125] S. Jagannathan and J. S. Dahler and W. Sung, *J. Chem. Phys.* **83**, 1808 (1985).
[126] R. G. Cole and D. K. Hoffman and G. T. Evans, *J. Chem. Phys.* **80**, 5365 (1984).
[127] H. Grad, *Pure Appl. Math.* **2**, 331 (1949).
[128] B. J. Berne and G. D. Harp, *Adv. Chem. Phys.* **17**, 63 (1970).
[129] P. Madden and G. T. Evans, *J. Chem. Phys.* **89**, 685 (1988).
[130] G. T. Evans and P. A. Madden, *Mol. Phys.* **74**, 1171 (1991).
[131] D. Kivelson and T. Keyes, *J. Chem. Phys.* **57**, 4599 (1972).
[132] G. T. Evans and R. G. Cole and D. K. Hoffman, *J. Chem. Phys.* **77**, 3209 (1982).
[133] G. Harrison, *The Dynamical Properties of Supercooled Liquids*, Academic Press, New York, (1976).
[134] R. A. MacPhail and D. Kivelson, *J. Chem. Phys.* **90**, 6555 (1989).
[135] S. Murad, D. P. Singh, H. J. M. Hanley and D. J. Evans, *Mol. Phys.* **72**, 487 (1991).
[136] G. T. Evans and D. Kivelson, *J. Chem. Phys.* **84**, 385 (1986).
[137] G. T. Evans and D. R. Evans, *J. Chem. Phys.* **81**, 6039 (1984).
[138] J. Talbot, M. P. Allen, G. T. Evans, D. Frenkel and D. Kivelson, *Phys. Rev.* **A39**, 4330 (1989).
[139] B. J. Alder, D. M. Gass and T. E. Wainwright, *J. Chem. Phys.* **53**, 3813 (1970).
[140] B. J. Alder and T. E. Wainwright, *J. Chem. Phys.* **31**, 459 (1959).
[141] B. J. Alder and T. E. Wainwright, *Phys. Rev.* **A1**, 18 (1970).
[142] D. Frenkel and J. F. Maguire, *Mol. Phys.* **49**, 503 (1983).
[143] J. J. Magda, H. T. Davis, and M. Tirrell, *J. Chem. Phys.* **85**, 6674 (1986).
[144] J. J. Magda, H. T. Davis, and M. Tirrell, *J. Chem. Phys.* **88**, 1207 (1988).
[145] A. Alavi and D. Frenkel, *Phys. Rev.* **A45**, 5355 (1992).
[146] M. P. Allen and D. Frenkel, *Phys. Rev. Lett.* **58**, 1748 (1987).
[147] T. Keyes and D. Kivelson, *J. Chem. Phys.* **56**, 1057 (1974).
[148] T. D. Gierke and W. H. Flygare, *J. Chem. Phys.* **61**, 2231 (1974).
[149] G. R. Alms, T. D. Gierke and W. H. Flygare, *J. Chem. Phys.* **61**, 4083 (1974).
[150] G. J. Vroege and H. N. W. Lekkerkerker, *Phase Transitions in Lyotropic Colloidal and Polymer Liquid Crystals*, *Rep. Prog. Phys.* **55**, 1241 (1992).
[151] H. Workman and M. Fixman, *J. Chem. Phys.* **58**, 5024 (1973).
[152] R. Evans, *Adv. Phys.* **28**, 143 (1979).
[153] T. Morita and K. Hiroike, *Prog. Theor. Phys.* **25**, 537 (1961).
[154] W. F. Saam and C. Ebner, *Phys. Rev.* **A15**, 2566 (1977).
[155] H. L. Frisch, N. River and D. Wyler, *Phys. Rev. Lett.* **54**, 2061 (1985).

[156] R. M. Gibbons, *Mol. Phys.* **17**, 81 (1969).
[157] G. Lasher, *J. Chem. Phys.* **53**, 4141 (1970).
[158] M. A. Cotter, *Phys. Rev.* **A10**, 625 (1974).
[159] K. M. Timling, *J. Chem. Phys.* **61**, 465 (1974).
[160] M. A. Cotter, *J. Chem. Phys.* **66**, 1098 (1977).
[161] B. M. Mulder and D. Frenkel, *Mol.Phys.* **55**, 1193 (1985).
[162] P. H. Fries and G. N. Patey, *J. Chem. Phys.* **82**, 429 (1985).
[163] R. Pynn, *Solid. State Comm.* **14**, 29 (1974).
[164] R. Pynn, *J. Chem. Phys.* **60**, 4579 (1974).
[165] F. Lado, *Mol. Phys.* **54**, 407 (1985).
[166] M. Baus, J.-L. Colot, X.-G. Wu and H. Xu, *Phys. Rev. Lett.* **59**, 2148 (1987).
[167] J.-L. Colot, X.-G. Wu, H. Xu and M. Baus, *Phys. Rev.* **A38**, 2022 (1988).
[168] P. Tarazona, *Mol. Phys.* **52**, 81 (1984).
[169] P. Tarazona and R. Evans, *Mol. Phys.* **52**, 847 (1985).
[170] W. A. Curtin and N. W. Ashcroft, *Phys. Rev.* **A32**, 2909 (1985).
[171] W. A. Curtin and N. W. Ashcroft, *Phys. Rev. Lett.* **56**, 2775 (1986).
[172] A. Poniewierski and R. Hołyst, *Phys. Rev. Lett.* **61**, 2461 (1988).
[173] R. Hołyst and A. Poniewierski, *Phys. Rev.* **A39**, 2742 (1989).
[174] A. M. Somoza and P. Tarazona, *J. Chem. Phys.* **91**, 517 (1989).
[175] A. M. Somoza and P. Tarazona, *Phys. Rev.* **A41**, 965 (1990).
[176] J. L. Lebowitz and J. W. Perram, *Mol. Phys.* **50**, 1207 (1983).
[177] L. Mederos and D. E. Sullivan, *Phys. Rev.* **A39**, 834 (1989).
[178] S. D. P. Flapper and G. Vertogen, *Phys Lett* **79A**, 87 (1980).
[179] S. D. P. Flapper and G. Vertogen, *Phys. Rev.* **A24**, 2089 (1981).
[180] S. D. Lee, *J. Chem. Phys.* **87**, 4972 (1987).
[181] S. D. Lee, *J. Chem. Phys.* **89**, 7036 (1988).
[182] J. D. Parsons, *Phys. Rev.* **A19**, 1225 (1979).
[183] D. Frenkel and B. M. Mulder, *Mol. Phys.* **55**, 1171 (1985).
[184] J. F. Marko, *Phys. Rev.* **A39**, 2050 (1989).
[185] U. P. Singh and Y. Singh, *Phys. Rev.* **A33**, 2725 (1986).
[186] U. P. Singh and U. Mohanty and Y. Singh, *Physica* **158A**, 817 (1989).
[187] G. J. Zarragoicoechea, D. Levesque and J. -J. Weis, *Mol. Phys.* **75**, 989 (1992).
[188] D. Frenkel, H. N. W. Lekkerkerker and A. Stroobants, *Nature* **332**, 822 (1988).
[189] M. Freiser, *Mol. Cryst. Liq. Cryst.* **14**, 165 (1971).
[190] R. Alben, J. R. McColl and C. S. Shih, *Solid State Comm.* **11**, 1081 (1972).
[191] C. S. Shih and R. Alben, *J. Chem. Phys.* **57**, 3055 (1972).
[192] R. Alben, *Phys. Rev. Lett.* **30**, 778 (1973).
[193] W. M. Gelbart and B. Barboy, *Acc. Chem. Res.* **13**, 290 (1980).
[194] B. M. Mulder, *Phys. Rev.* **A39**, 360 (1989).
[195] R. Hołyst and A. Poniewierski, *Mol. Phys.* **69**, 193 (1990).
[196] B. M. Mulder, *Liq. Cryst.* **8**, 527 (1990).
[197] M. P. Allen, *Liq. Cryst.* **8**, 499 (1990).

[198] G. T. Evans, *Mol. Phys.* (1992); in press.
[199] M. Hosino, H. Nakano and H. Kimura, *J. Phys. Soc. Jpn.* **46**, 1709 (1979).
[200] M. Hosino and H. Nakano and H. Kimura, *J. Phys. Soc. Jpn.* **47**, 740 (1979).
[201] A. Stroobants, H. N. W. Lekkerkerker and D. Frenkel, *Phys. Rev.* **A36**, 2929 (1987).
[202] B. M. Mulder, *Phys. Rev.* **A35**, 3095 (1987).
[203] X. Wen and R. B. Meyer, *Phys. Rev. Lett.* **59**, 1325 (1987).
[204] R. Hołyst and A. Poniewierski, *Mol. Phys.* **71**, 561 (1990).
[205] M. P. Taylor, R. Hentschke and J. Herzfeld, *Phys. Rev. Lett.* **62**, 800 (1989).
[206] J. M. Caillol and J. J. Weis, *J. Chem. Phys.* **90**, 7403 (1989).
[207] H. Xu, *Mol. Phys.* **77**, 311 (1992).
[208] A. M. Somoza and P. Tarazona, *Phys. Rev.* **A40**, 6069 (1989). At the time of publication the erratum of [265] had not appeared. This changes the comparison of simulation and theory in this paper.
[209] A. M. Somoza and P. Tarazona, *Phys. Rev.* **A40**, 4161 (1991).
[210] J. A. C. Veerman and D. Frenkel, *Phys. Rev.* **A43**, 4334 (1991).
[211] R. Hołyst, *Phys. Rev.* **A42**, 3438 (1990).
[212] A. Poniewierski and R. Hołyst, *Phys. Rev.* **A41**, 6871 (1990).
[213] A. Poniewierski and T. J. Sluckin, *Phys. Rev.* **A43**, 6837 (1991).
[214] A. M. Somoza and P. Tarazona, *Phys. Rev. Lett.* **61**, 2566 (1988).
[215] A. Poniewierski, *Phys. Rev.* **A45**, 5605 (1992).
[216] M. P. Taylor and J. Herzfeld, *Phys. Rev.* **A40**, 1678 (1989).
[217] G. T. Evans, *Mol. Phys.* **76**, 1359 (1992).
[218] R. Deblieck and H. N. W. Lekkerkerker, *J. Phys. Lett.* **41**, L-351 (1980).
[219] A. Stroobants and H. N. W. Lekkerkerker, *J. Phys. Chem.* **88**, 3699 (1984).
[220] R. Alben, *J. Chem. Phys.* **59**, 4299 (1973).
[221] Y. Rabin, W. E. McMullen and W. M. Gelbart, *Mol. Cryst. Liq. Cryst.* **89**, 67 (1982).
[222] P. Palffy-Muhoray, J. R. De Bruyn and D. A. Dunmur, *J. Chem. Phys.* **82**, 5294 (1985).
[223] J. A. Cuesta and D. Frenkel, *Phys. Rev.* **A42**, 2126 (1990).
[224] J. M. Kosterlitz and D. Thouless, *J. Phys. C* **6**, 1181 (1973).
[225] M. Romeiro, *J. Math. Phys.* **19**, 802 (1978).
[226] A. Z. Panagiotopoulos, *Mol. Phys.* **61**, 813 (1987).
[227] D. Frenkel, In G.Ciccotti and W.G.Hoover, eds., *Proc. 97th Int. School of Physics Enrico Fermi,* North-Holland, Amsterdam, 1986, pp. 151–188.
[228] W. G. Hoover and F. H. Ree, *J. Chem. Phys.* **47**, 4873 (1967).
[229] D. Frenkel and A. J. C. Ladd, *J. Chem. Phys.* **81**, 3188 (1984).
[230] E. J. Meijer, D. Frenkel, R. A. LeSar and A. J. C. Ladd, *J. Chem. Phys.* **92**, 7570 (1990).
[231] E. J. Meijer and D. Frenkel, *J. Chem. Phys.* **94**, 2269 (1991).
[232] J. S. van Duijneveldt and D. Frenkel, *J. Chem. Phys.* **96**, 4655 (1992).
[233] A. Stroobants, H. N. W. Lekkerkerker and D. Frenkel, *Phys. Rev. Lett.* **57**, 1452 (1986).

[234] J. A. C. Veerman and D. Frenkel, *Phys. Rev.* **A41**, 3237 (1990).
[235] W. G. T. Kranendonk and D. Frenkel, *Mol. Phys.* **72**, 699 (1991).
[236] W. G. Hoover and F. H. Ree, *J. Chem. Phys.* **49**, 3609 (1968).
[237] M. P. Allen and M. R. Wilson, *J. Computer Aided Molecular Design* **3**, 335 (1989).
[238] D. Frenkel, *Mol. Phys.* **54**, 145 (1985).
[239] H. Nakano, M. Hosino and H. Kimura, *J.Phys. Soc. Jpn* **46**, 1709 (1979).
[240] F. Dowell and D. E. Martire, *J. Chem. Phys.* **68**, 1088 (1978).
[241] F. Dowell and D. E. Martire, *J. Chem. Phys.* **68**, 1094 (1978).
[242] F. Dowell and D. E. Martire, *J. Chem. Phys.* **69**, 2322 (1978).
[243] F. Dowell, *Phys. Rev.* **A28**, 3526 (1983).
[244] A. Stroobants, *Phys. Rev. Lett.* **69**, 2388 (1992).
[245] T. E. Strzelecka, M. W. Davidson and R. L. Rill, *Nature* **331**, 457 (1988).
[246] F. Livolant, A. M. Levelut, J. Doucet and J. P. Benoit, *Nature* **339**, 724 (1989).
[247] D. Frenkel, *J. Phys. Chem.* **92**, 3280 (1988).
[248] D. Frenkel, *Liq. Cryst.* **5**, 929 (1989).
[249] H. Azzouz, J. M. Caillol, D. Levesque and J. J. Weis, *J. Chem. Phys.* **96**, 4551 (1992).
[250] D. Frenkel and R. Eppenga, *Phys. Rev.* **A31**, 1776 (1985).
[251] R. F. Kayser and H. J. Raveche, *Phys. Rev.* **A17**, 2067 (1978).
[252] Wu-Ki Tung, *Group Theory in Physics*, World Scientific, Singapore, (1985).
[253] J. C. Tolédano and P. Tolédano, *The Landau theory of Phase Transitions*, Lecture Notes in Physics, **Vol. 3**, World Scientific, Singapore, (1985).
[254] W. Maier and A. Saupe, *Z. Naturforsch.* **A13**, 564 (1958).
[255] M. Hammermesh, *Group Theory and its Applications to Physics*, Addison-Wesley, Reading, MA, (1962).
[256] R. G. Priest, *Phys. Rev.* **A7**, 720 (1973).
[257] J. P. Straley, *Phys. Rev.* **A8**, 2181 (1973).
[258] A. Poniewierski and J. Stecki, *Mol. Phys.* **38**, 1931 (1979).
[259] J. Stecki and A. Poniewierski, *Mol. Phys.* **41**, 1451 (1980).
[260] A. Poniewierski and J. Stecki, *Phys. Rev.* **A25**, 2368 (1982).
[261] D. Frenkel, In D. Levesque, J. P. Hansen, and J. Zinn-Justin, Eds., *Liquids, Freezing and the Glass Transition*, North-Holland, Amsterdam, 1991, Chapter 9,
[262] D. Forster, *Hydrodynamic Fluctuations, Broken Symmetry and Correlation Functions*, Frontiers in Physics, **Vol. 47**, Benjamin, Reading, MA, (1975).
[263] A. M. Somoza and P. Tarazona, *Mol. Phys.* **72**, 911 (1991).
[264] M. P. Allen and D. Frenkel, *Phys. Rev.* **A37**, 1813 (1988).
[265] M. P. Allen and D. Frenkel, *Phys. Rev.* **A42**, 3641 (1990); (Erratum).
[266] M. P. Allen and A. J. Masters, *Mol. Phys.* (1992). in press.
[267] M. P. Allen, *Phys. Rev. Lett.* **65**, 2881 (1990).
[268] S. Hess, D. Frenkel and M. P. Allen, *Mol. Phys.* **74**, 765 (1991).
[269] K.-S. Chu and D. S. Moroi, *J. Phys. Coll. C1* **36**, 99 (1975).
[270] M. Doi, *J. Phys.* **36**, 607 (1975).
[271] M. Doi and S. F. Edwards, *J. Chem. Soc., Faraday. Trans. 2* **74**, 568 (1978).

[272] M. Doi and S. F. Edwards, *J. Chem. Soc., Faraday. Trans. 2* **74**, 918 (1978).

[273] M. Doi and S. F. Edwards, *The Theory of Polymer Dynamics,* Clarendon Press, Oxford, (1986).

[274] D. Levesque and J. J. Weis, in K. Binder, ed., *The Monte Carlo Method in Condensed Matter Physics,* Springer Verlag, Berlin, 1992 Chapter 6

[275] T. Biben and J. P. Hansen, *Phys. Rev. Lett.* **66**, 2215 (1991).

[276] T. R. Kirkpatrick, *J. Chem. Phys.* **89**, 5020 (1988).

[277] M. D. Amos and G. Jackson, *Mol. Phys.* **74**, 191 (1991).

[278] A. L. Archer and G. Jackson, *Mol. Phys.* **73**, 881 (1991).

[279] G. Jackson, W. G. Chapman and K. E. Gubbins, *Mol. Phys.* **65**, 1 (1988).

[280] H. Goldstein, *Classical Mechanics, 2nd edition,* Addison-Wesley, Reading, MA, (1980).